Penalization and Bayesian numerical methods for multiscale inverse problems

Thèse N° 9360

Andrea DI BLASIO

2019

EPFL
ÉCOLE POLYTECHNIQUE
FÉDÉRALE DE LAUSANNE

To my family

Acknowledgements

Abstract

In this thesis we consider inverse problems involving multiscale elliptic partial differential equations. The name multiscale indicates that these models are characterized by the presence of parameters which vary on different spatial scales (macroscopic, microscopic, mesoscopic, etc.). The variations at the smallest scales make these equations very difficult to approximate also when considering forward problems, since classical numerical methods require a mesh resolution at the finest scales, hence a computational cost that is often prohibitive. For this reason one prefers to apply homogenization or effective methods which, neglecting what happens at the smallest scales, are able to provide accurate macroscopic solutions to the problem. For what concerns the solution of inverse problems, we propose then a new numerical algorithm based on homogenization techniques, model order reduction and regularization methods.

First, we consider elliptic operators whose tensor varies on a microscopic scale. Under the assumption that the nature of its micro structure is known, we aim at recovering a macroscopic parameterization of the tensor from measurements originating from the full multiscale model, using homogenization. Practical examples include multi-phase media whose constituents are known, but their respective volume fraction is unknown. We consider the Calderón's formulation of the inverse problem. We prove that, under some regularity assumptions on the fine scale tensor, the effective inverse problem, with observed data consisting of the homogenized Dirichlet to Neumann (DtN) map, is also well-posed. We then solve the problem by considering finite measurements of the multiscale DtN map and using Tikhonov regularization, and we establish a convergence result of the solution by means of G-convergence.

In a second stage, we consider a Bayesian approach which allows for uncertainty quantification of the results. We prove existence and well-posedness of the effective posterior probability measure, obtained by homogenization of the observation operator. By means of G-convergence we characterize the discrepancy between the fine scale and the homogenized model, and we prove convergence of the effective posterior towards the fine scale posterior in terms of the Hellinger distance. We also propose a numerical procedure to estimate the homogenization error statistics, which, if included in the inversion process, allow to account for approximation errors.

Finally, we deal with multiscale inverse problems for the linear elasticity equation. In this context we assume that the heterogeneity of the material is determined by its geometry

Abstract

rather than by the coefficients of the equation. In particular, we consider porous media with random perforations and, following the Bayesian approach, we solve the inverse problem of determining the elastic properties of an hypothetical isotropic material. We prove the existence and well-posedness of the effective posterior measure, as well as its convergence in the fine scale limit by means of G-convergence. We conclude by describing a new probabilistic numerical method which computes a new posterior measure that accounts for approximation errors and reveals the uncertainty intrinsic in the numerical method.

Key words: multiscale, homogenization, heterogeneous multiscale method, reduced basis, inverse problems, uncertainty quantification, penalization methods, Bayesian methods, probabilistic numerical method, linear elasticity.

Résumé

Dans cette thèse, nous examinons la solution de problèmes inverses pour des équations aux dérivées partielles multi-échelles de type elliptique. Le terme multi-échelles indique que ces modèles sont caractérisés par des paramètres présentant des variations à différentes échelles spatiales (macroscopique, microscopique, mésoscopique, etc.). Les variations aux plus petites échelles rendent l'approximation de ces équations difficile même dans le cas de problèmes directs, car les méthodes numériques classiques exigent une discrétisation spatiale assez fine pour capturer ces variations, nécessitant ainsi un coût de calcul prohibitif. Pour cette raison, il est souvent préférable de recourir à des méthodes dites d'homogénéisation ou effectives qui, tout en négligeant les caractéristiques du modèle aux plus fines échelles, sont capables de fournir des solutions macroscopiques au problème. Afin de résoudre les problèmes inverses dans le régime multi-échelles, nous proposons donc un nouvel algorithme numérique basé sur les techniques d'homogénéisation, de bases réduites, et les méthodes de régularisation.

Premièrement, nous considérons les opérateurs elliptiques dont le tenseur présente des variations à l'échelle microscopique. En supposant connaître la nature de sa structure microscopique, notre objectif est de déterminer une paramétrisation macroscopique du tenseur à partir d'observations provenant du modèle multi-échelles, mais en utilisant des méthodes d'homogénéisation. Un exemple typique est fourni par les matériaux composites, dont nous connaissons les constituants mais pas leur fraction volumétrique respective. Nous prenons en considération le problème inverse comme formulé par Calderón. Sous certaines hypothèses de régularité sur le tenseur multi-échelles, nous démontrons que le problème inverse effectif, où les observations sont représentées par l'opérateur Dirichlet to Neumann (DtN) homogénéisé, est bien posé. Nous résolvons le problème en considérant un nombre fini de mesures de l'opérateur DtN multi-échelle et en utilisant la méthode de Tikhonov pour sa régularisation, et nous établissons un résultat de convergence pour la solution en utilisant la G-convergence.

Dans un deuxième temps, nous considérons la méthode bayésienne qui permet de quantifier l'incertitude des résultats du problème inverse. Nous montrons que la mesure effective de probabilité a posteriori, obtenue par homogénéisation de l'opérateur d'observation, existe et est bien posée. En utilisant la G-convergence, nous caractérisons la différence entre les modèles multi-échelle et effectif. De plus, nous démontrons la convergence entre les deux mesures de probabilité a posteriori respectives en termes de distance de Hellinger. Nous proposons également un schéma numérique pour estimer a priori les statistiques de

Résumé

---

l'erreur d'homogénéisation, et nous observons numériquement que, si elles sont incluses dans le processus d'inversion, ces statistiques permettent de prendre en compte les erreurs d'approximation, qui pourraient sinon altérer les résultats.

Enfin, nous traitons des problèmes inverses multi-échelles pour l'équation de l'élasticité linéaire, en supposant que l'hétérogénéité du matériau est déterminée par sa géométrie plutôt que par les coefficients de l'équation. En particulier, nous considérons des materiaux poreux avec des vides répartis aléatoirement et, en utilisant la méthode bayésienne, nous résolvons le problème inverse pour déterminer les propriétés élastiques d'un matériau isotrope hypothétique. Nous montrons que la mesure effective de probabilité a posteriori existe et est bien posée et que, en utilisant la G-convergence, elle converge vers la mesure multi-échelle en termes de distance de Hellinger. Nous concluons en décrivant une nouvelle méthode numérique probabiliste permettant de calculer une nouvelle mesure effective a posteriori qui, en tenant compte des erreurs d'approximation, permet de révéler l'incertitude inhérente à la méthode numérique.

Mots clefs: multi-échelles, homogénéisation, méthode hétérogène multi-échelles, bases réduites, problèmes inverses, quantification de l'incertitude, méthodes de pénalisation, méthodes bayésiennes, méthodes numériques probabilistes, élasticité linéaire.

Contents

Contents

Notation

Problem setting

d	dimension of the problem, $d \in \{1,2,3\}$
ε	fine scale size of the two-scale model, $\varepsilon > 0$
D	macroscopic domain in $\mathbb{R}^d$
Y	unit cube in $\mathbb{R}^d$, $Y = (0,1)^d$
C	generic constant whose value can change at any occurrence

Abbreviations

PDE	partial differential equation
FE	finite element
FEM	finite element method
DOF	degree of freedom
HMM	heterogeneous multiscale method
RB	reduced basis
EIM	empirical interpolation method
DtN	Dirichlet to Neumann
KL	Karhunen-Loève
MCMC	Markov chain Monte Carlo
MH	Metropolis-Hastings

Common indices

mac	macro
mic	micro

Standard sets of numbers

$\mathbb{N}$	set of positive integers $\{1,2,\ldots\}$
$\mathbb{N}_0$	set of non-negative integers $\{0,1,2,\ldots\}$
$\mathbb{Z}$	set of integers
$\mathbb{R}$	set of real numbers

Functional spaces

$C^k(D)$	k-times continuously differentiable functions $D \to \mathbb{R}$, $0 \le k \le \infty$
$C_0^\infty(D)$	infinitely continuously differentiable functions $D \to \mathbb{R}$ with compact support on D
$C_{\text{per}}^k(Y)$	subset of Y-periodic functions in $C^k(D)$
$L^p(D)$	the usual Lebesgue space with $1 \le p \le \infty$
$W^{k,p}(D)$	the usual Sobolev space with $k \in \mathbb{N}$ and $p \in [1,\infty]$
$H^k(D)$	the Hilbert space $W^{k,2}(D)$
$H_0^1(D)$	subspace of $H^1(D)$ with a vanishing trace on ∂D
$H_\Gamma^1(D)$	subspace of $H^1(D)$ with a vanishing trace on $\Gamma \subset \partial D$
$H_{\text{per}}^1(Y)$	closure of $C_{\text{per}}^\infty(Y)$ in the norm $H^1(Y)$
X'	dual space of a vector space X
$\|\cdot\|_X$	standard norm in any normed linear space X
$\langle \cdot, \cdot \rangle_X$	standard inner product in any inner product space X

Finite element spaces

$\mathcal{T}_H$	a triangular or tetrahedral mesh consisting of elements $K \in \mathcal{T}_H$ the mesh size $H = \max_{K \in \mathcal{T}_H} \operatorname{diam}(K)$
$\mathcal{P}^n(K)$	vector space of polynomials in K of degree at most $n \in \mathbb{N}_0$
$S^n(D, \mathcal{T}_H)$	continuous finite element space in D on mesh $\mathcal{T}_H$ of degree n $S^n(D, \mathcal{T}_H) = \{q^H \in H^1(D): q^H|_K \in \mathcal{P}^n(K),\ \forall K \in \mathcal{T}_H\}$

Vectors and matrices

A_{ij}	coefficients of a matrix $A \in \mathbb{R}^{n \times m}$
$\|A\|_{\text{F}}$	Frobenius norm of a matrix $A \in \mathbb{R}^{n \times m}$
$\|A\|_\infty$	max norm of a matrix $A \in \mathbb{R}^{n \times m}$
b_i	elements of a vector $b \in \mathbb{R}^n$
$\|b\|_2$	Euclidean norm of a vector $b \in \mathbb{R}^n$
Sym_n	class of $n \times n$ real valued symmetric matrices
$\mathbf{e}^i$	the i-th canonical basis vector in $\mathbb{R}^n$
$M(\alpha, \beta, D)$	$\{A \in (L^\infty(D))^{n \times n}: \alpha|b|^2 \le A(x)b \cdot b,$ $|A(x)b| \le \beta|b|, \forall b \in \mathbb{R}^n,$ and a.e. on $D\}$

1 Introduction

Many applications in engineering and the sciences, such as heat conduction, geoscience and medical imaging [36, 65], require solving inverse problems involving partial differential equations (PDEs). In this thesis we are interested in inverse problems for PDEs that vary on a very fine scale describing, e.g., heterogeneity of the medium. Our goal is to find a parameter σ of a certain mathematical model, from a measurement z originating from the model itself. The problem to solve can be represented as

$$\text{given } z = G^\varepsilon(\sigma^*) \in V, \qquad \text{find } \sigma \in U \text{ such that } G^\varepsilon(\sigma) = z, \tag{1.1}$$

where U and V are two Banach spaces, σ^* is the exact solution, and $G^\varepsilon : U \to V$ is referred to as the observation or forward operator. The superscript ε emphasizes the multiscale nature of G^ε, which is assumed to be defined via a PDE whose inputs vary on a fine scale ε, much smaller than the size of the physical domain. Assuming that the nature of the micro structure in the model is known, we search for an unknown macroscopic parameterization of such a fine scale structure given measurements originating from the full multiscale model. A typical example is a multi-phase medium, whose constituents are known, but whose volume fraction or macroscopic orientation are unknown. Another example may come from a linear elasticity model defined on a multiscale porous medium, whose microscopic configuration is known, but whose elastic properties such as Young's modulus or Poisson's ratio are unknown. In all of the cases above, classical approaches such as the finite element method (FEM) or the finite difference method (FDM) would require the evaluation of the forward operator on a mesh resolving the finest scale ε. In addition, when solving inverse problems via penalization methods [50, 86] or Bayesian sampling [64, 84, 41], the repeated solution of such high dimensional problems represents a formidable computational challenge and is often not tractable in practice. The goal of the thesis is to show how one can overcome these computational issues for classes of multiscale problems by combining efficient inverse algorithm, coarse graining techniques and model order reduction.

Parameterized multiscale inverse elliptic problems.   We start by introducing the following multiscale scalar elliptic problem. Let $D \subset \mathbb{R}^d$, $d \leq 3$, be an open, bounded, connected set with sufficiently smooth boundary ∂D, and consider the problem of finding the weak solution $u^\varepsilon \in H^1(D)$ such that

$$
\begin{aligned}
-\nabla \cdot (A^\varepsilon_{\sigma^*} \nabla u^\varepsilon) &= 0 \qquad \text{in } D, \\
u^\varepsilon &= g \qquad\quad\; \text{on } \partial D,
\end{aligned}
\tag{1.2}
$$

where $g \in H^{1/2}(\partial D)$. The tensor $A^\varepsilon_{\sigma^*} = A^\varepsilon_{\sigma^*}(x)$, $x \in D$, belongs to the class of matrix functions $M(\alpha, \beta, D)$, where

$$
M(\alpha, \beta, D) = \left\{ A \in (L^\infty(D))^{d \times d} : \; \alpha|b|^2 \leq A(x)b \cdot b, |A(x)b| \leq \beta|b|, \forall b \in \mathbb{R}^d, \text{ and a.e. on } D \right\}.
$$

The tensor $A^\varepsilon_{\sigma^*}$ varies on a fine scale ε. In turn, the solution of (1.2) itself has variations on the same micro scale. Moreover, the subscript σ^* denotes the existence of a low dimensional parameter $\sigma^* : D \to \mathbb{R}$ such that $A^\varepsilon_{\sigma^*}(x) = A(\sigma^*(x), x/\varepsilon)$. An example of low dimensional parameterization of a multiscale tensor is given graphically in Figure 1.1.

The inverse problem we consider consists in recovering the coefficients of the tensor $A^\varepsilon_{\sigma^*}$ in D. A first rigorous formulation of this type of inverse problem (in the single scale setting) dates back to the 1980s, and is due to Calderón [26]. In Calderón's formulation of the inverse problem the question is if the knowledge of the Dirichlet to Neumann (DtN) map associated to (1.2), which is defined as the linear operator $\Lambda_{A^\varepsilon_{\sigma^*}} : H^{1/2}(\partial D) \to H^{-1/2}(\partial D)$ given by

$$
g \mapsto A^\varepsilon_{\sigma^*} \nabla u^\varepsilon \cdot \boldsymbol{\nu}|_{\partial D},
$$

where $\boldsymbol{\nu}$ denotes the exterior unit normal to ∂D, is sufficient to determine the conductivity tensor, i.e. $A^\varepsilon_{\sigma^*}$, in the domain's interior. This question gained great popularity in the recent decades and many authors have contributed to its analysis by providing results on uniqueness, continuity and stability of such problem [66, 85, 71, 20].

In this thesis we are mainly interested in a class of parameterized anisotropic multiscale tensors of the form $A^\varepsilon_{\sigma^*}(x) = A(\sigma^*(x), x/\varepsilon)$. We assume that the map $(t, x) \mapsto A(t, x/\varepsilon)$, $t \in \mathbb{R}$, is known and thus that only the function $\sigma^* : D \to \mathbb{R}$ has to be determined in order to recover the full tensor $A^\varepsilon_{\sigma^*}$. For tensors that do not exhibit a multiscale variation, i.e., for $(t, x) \mapsto A(t, x)$, uniqueness and stability at the boundary for the Calderón inverse problem were proved by G. Alessandrini and R. Gaburro [16], under some regularity assumptions on the map $(t, x) \mapsto A(t, x)$. This result is still valid for highly heterogeneous tensors, but the stability estimate depends then on a constant that scales as $\mathcal{O}(\varepsilon^{-1})$. Homogenization theory [21, 33, 63] guarantees the existence of an effective tensor $A^0_{\sigma^*}$ such that (up to a subsequence) the solution of (1.2) converges in a weak sense to a homogenized solution $u^0 \in H^1(D)$ satisfying the elliptic problem

$$
\begin{aligned}
-\nabla \cdot (A^0_{\sigma^*} \nabla u^0) &= 0 \qquad \text{in } D, \\
u^0 &= g \qquad\quad\; \text{on } \partial D.
\end{aligned}
\tag{1.3}
$$

In this work, we show how the homogenized model (1.3) can be exploited in order to retrieve a hidden macroscopic parameterization of $A_{\sigma*}^{\varepsilon}$, based on observations obtained from the full multiscale model (1.2).

Macroscopic parameter-
ization.

Multiscale conductivity.
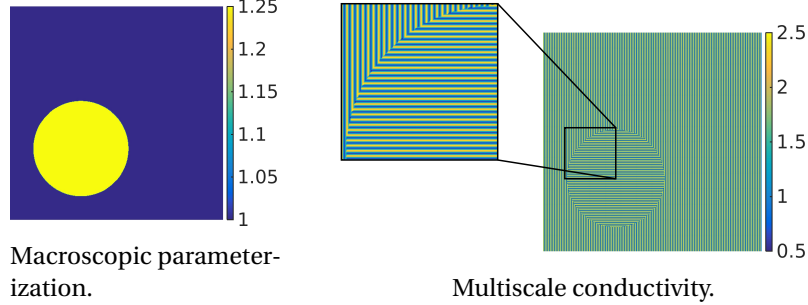
Figure 1.1: An example of a macroscopic spatial field controlling the orientation of the micro oscillations in the multiscale conductivity. This picture is taken from a numerical experiment in Chapter 4.

Application in linear elasticity with multiscale perforated domains. A natural extension of parameterized multiscale inverse problems associated to the scalar elliptic model of type (1.2) is given by inverse problems in linear elasticity with multiscale perforated domains. In this setting the multiscale nature of the problem is due to the computational domain rather than the elliptic operator. Given an open bounded set $D \subset \mathbb{R}^d$, $d \leq 3$, we consider a perforated domain $D^{\varepsilon} \subset D$, whose degree of fineness is inversely proportional to ε. We assume that D^{ε} is connected and that $\partial D \subset \partial D^{\varepsilon}$. A graphic representation of this setting can be found in Figure 1.2. Given $\Gamma_1 \subset \partial D$, $\Gamma_2 \subset \partial D$, such that $|\Gamma_1|, |\Gamma_2| > 0$, $\Gamma_1 \cap \Gamma_2 = \emptyset$, $\Gamma_1 \cup \Gamma_2 = \partial D$, $\mathbf{h} \in L^2(\Gamma_2)$, we consider the linear elasticity problem

$$
\begin{aligned}
-\frac{\partial}{\partial x_j}\left(A_{ijlm}\frac{\partial u_l^{\varepsilon}}{\partial x_m}\right) &= 0 && \text{in } D^{\varepsilon}\,, \\
\mathbf{u}^{\varepsilon} &= \mathbf{0} && \text{on } \Gamma_1\,, \\
A_{ijlm}\frac{\partial u_l^{\varepsilon}}{\partial x_m}\nu_j &= h_i && \text{on } \Gamma_2\,, \\
A_{ijlm}\frac{\partial u_l^{\varepsilon}}{\partial x_m}\nu_j &= 0 && \text{on } \partial D^{\varepsilon}\backslash\partial D\,,
\end{aligned}
\tag{1.4}
$$

for $i = 1,\dots,d$, where $\boldsymbol{\nu}$ is the unit outward normal at the boundary, and $A = \{A_{ijlm}\}_{1 \leq i,j,l,m \leq d}$, $A_{ijlm} \in \mathbb{R}$, is a constant fourth-order tensor. Note that the Einstein summation convention is used in (1.4). If the material is assumed to be isotropic the tensor A depends only on two scalar coefficients, e.g., the Young's modulus and the Poisson's ratio. In this work we assume that these two coefficients are unknown and we wish to estimate their values through the

knowledge of measurements coming from (1.4) and by employing the homogenized equation

$$-\frac{\partial}{\partial x_j}\left(A^0_{ijlm}\frac{\partial u^0_l}{\partial x_m}\right) = 0 \quad \text{in } D,$$

$$\mathbf{u}^0 = \mathbf{0} \qquad\qquad \text{on } \Gamma_1,$$

$$A^0_{ijlm}\frac{\partial u^0_l}{\partial x_m}\nu_j = h_i \qquad \text{on } \Gamma_2,$$

(1.5)

where $A^0 = \{A^0_{ijlm}\}_{1\le i,j,l,m\le d}$, $A^0_{ijlm} \in \mathbb{R}$, is the homogenized fourth-order tensor. The problem (1.5) is defined on a much simpler geometry and is a good approximation of (1.4) in the limit $\varepsilon \to 0$.
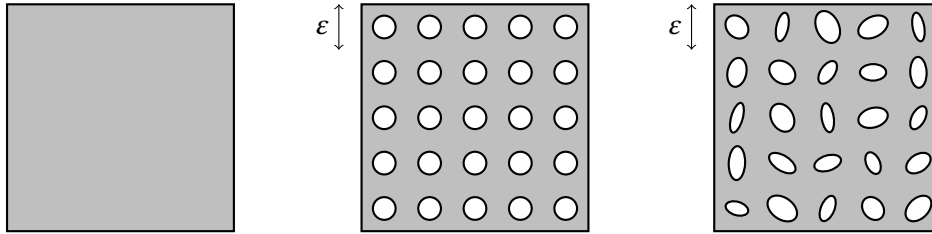
Figure 1.2: Domain D and two examples of multiscale perforated domains, one periodic and one random.

Tikhonov regularization of inverse problems. Having introduced the PDE models we will use in this thesis, we now return to the more abstract setting of (1.1) and briefly outline how homogenization techniques can enter into the solution of such problem. Consider the inverse problem introduced in (1.1) and let $G^0 : U \to V$ be the homogenized observation operator associated to G^ε. A coarse graining approach to the inverse problem (1.1) consists in solving the problem:

$$\text{given } z = G^\varepsilon(\sigma^*) \in V, \qquad \text{find } \sigma \in U \text{ such that } G^0(\sigma) = z.$$

(1.6)

Thanks to the homogeneous nature of G^0 this problem is often less computationally expensive than solving (1.1). However, it is typical of inverse problems as (1.1) or (1.6) to be ill-posed: their solution is neither guaranteed to exist, nor to be unique, nor to be stable with respect to the measurement z. Moreover, when solving (1.6) additional difficulties arise from the discrepancy between the model generating the data and the one used to reproduce them. In what follows we focus on the solution of the homogenized inverse problem (1.6). One approach to solve (1.6) is to consider the optimization problem of finding

$$\underset{\sigma \in U}{\arg\min} \|z - G^0(\sigma)\|^2_V.$$

However this minimization problem may possess minimizing sequences which do not converge, or even exhibit multiple minima. One way to ensure uniqueness and convergence of the solution is to consider the regularized Tikhonov minimization problem [88] which aims at finding

$$\arg\min_{\sigma \in W} \|z - G^0(\sigma)\|_V^2 + \|\sigma - \sigma_0\|_W^2,$$

where W is a Banach space compactly embedded into U and $\sigma_0 \in W$. This regularization strategy aims at producing a reasonable estimate of the quantity of interest based on the observations available, the space W and the point σ_0. However, in some cases a simple point estimate of the unknown could not be satisfactory. Moreover, the choice of the norms $\|\cdot\|_W$ and $\|\cdot\|_V$ and of the point σ_0 are arbitrary and in many cases difficult to establish a priori.

Bayesian regularization of inverse problems. An alternative technique for regularizing the inverse problems (1.1) and (1.6) is represented by the Bayesian approach [64, 84, 39, 40, 41]. In the Bayesian approach for inverse problems every quantity is treated as a random variable, and the solution of the problem consists of a probability distribution over the quantity of interest rather than a single point estimate. Let us assume that the space of the observations is finite dimensional, i.e., $V = \mathbb{R}^n$, and that the measurements are polluted by a source of noise $\zeta \in \mathbb{R}^n$ whose actual value is unknown, but which is distributed accordingly to a known probability measure. A typical example of the measurement model is given by

$$z = G^\varepsilon(\sigma^*) + \zeta, \quad \zeta \sim \mathcal{N}(0, C_\zeta), \tag{1.7}$$

where C_ζ is a given covariance matrix. Hence the probability distribution of z given σ is equal to $\mathcal{N}(G^\varepsilon(\sigma), C_\zeta)$ for any value $\sigma \in U$. Another essential assumption underlying Bayesian regularization is that all our prior knowledge about the parameters of interest can be encoded by a probability measure, the prior, which we denote by μ_{pr}. Then, Bayes' formula yields the probability measure of σ given the measurement z, which is denoted by $\mu^\varepsilon(\sigma|z)$ and referred to as the posterior measure, i.e., the posterior is related to the prior measure through the Radon-Nikodym derivative

$$\frac{\mathrm{d}\mu^\varepsilon(\sigma|z)}{\mathrm{d}\mu_{\mathrm{pr}}(\sigma)} \propto \exp\left(-\frac{1}{2}\|z - G^\varepsilon(\sigma)\|_{C_\zeta}^2\right), \tag{1.8}$$

where $\|\cdot\|_{C_\zeta}$ is the norm induced by the scalar product

$$\langle\cdot,\cdot\rangle_{C_\zeta} = \langle\cdot, C_\zeta^{-1}\cdot\rangle.$$

Since the proportionality constant in (1.8) is unknown, one needs to sample from the posterior measure through Markov chain Monte Carlo (MCMC) methods, which allow to obtain a Markov chain whose stationary distribution is given by $\mu^\varepsilon(\sigma|z)$. Obtaining a whole distribution instead of a single point estimate as for the Tikhonov regularization, allows for the

uncertainty quantification of the parameters of interest. However, we emphasize again that the dependence of μ^ε on the observation operator G^ε, which depends on a fine scale ε, implies a computational expense which in most cases could be not affordable. Hence, according to the coarse graining approach, we sample from the posterior measure defined by

$$\frac{\mathrm{d}\mu^0(\sigma|z)}{\mathrm{d}\mu_{\mathrm{pr}}(\sigma)} \propto \exp\left(-\frac{1}{2}\|z - G^0(\sigma)\|^2_{C_\zeta}\right). \tag{1.9}$$

This measure is independent of the small scale ε and can thus be approximated efficiently. However, we emphasize that the mismatch between multiscale and homogenized models gives rise to a source of error which can not be neglected far from the asymptotic regime $\varepsilon \to 0$. Let us furthermore remark that the observation operator can not be reproduced exactly and in practice is always replaced by an appropriate approximation (obtained by means of finite element methods (FEMs) or finite difference methods (FDMs) for example), which yields additional sources of errors that have to be taken into account in the inversion process. Even if such errors would converge asymptotically to zero as we refine the approximation, they can not be made arbitrarily small with a fixed computational budget. Thus, it can happen to have to face approximation errors which are relatively large, and that can propagate into the posterior measure and cause incorrect predictions. In the literature this problem has been treated in several studies and we recognize basically two different ways of proceeding. One approach is to try to empirically estimate the approximation error by a probability distribution and include it in the definition of the posterior measure to account for model discrepancy (see [28, 27]). Other works as [60, 38, 68, 12] illustrate how the use of probabilistic models (obtained considering a random space or time discretization for example) for solving inverse problems gives rise to a posterior measure which is more robust to failure and which better reflects the uncertainty in the solution due to the approximate model.

1.1 Literature overview

In the following we briefly review the literature related to this thesis. In particular we give an overview of the state-of-the-art in numerical multiscale methods and selected works which faced multiscale inverse problems.

Finite element multiscale heterogeneous multiscale method. The approach we suggest to solve multiscale inverse problems is based on homogenized models. Given a multiscale problem, an explicit form of the corresponding homogenized model is usually not known and can only be recovered at some points of the computational domain. This is the basic idea behind the heterogeneous multiscale method (HMM) which was introduced by E and Engquist [47] (see also [11] for a complete overview of the method). The method aims at recovering input data of the homogenized problem by relying only on the data defining the fine scale problem, which is achieved by solving appropriate micro problems on sampling domains.

When finite elements are used as macro and micro solvers the method goes under the name of finite element heterogeneous multiscale method (FE-HMM). This method introduces a macro and a micro finite element space, and given a macro quadrature formula, it proceeds by recovering the homogenized problem only on the given macro quadrature points. It has been applied to a large category of problems and applications, such as diffusion problems [47], parabolic problems [10], the wave equation [13], the Stokes equation [5] and linear elasticity problems [2, 49]. We also mention [61] for a description of the method when dealing with elliptic problems defined on multiscale and periodic perforated domains. A priori error estimates [1, 3, 48] guarantee theoretically the quality of the FE-HMM which makes it an extremely attractive method for multiscale PDEs.

Reduced basis finite element heterogeneous multiscale method. The main cost of the FE-HMM is represented by the solution of the micro problems, whose number and degrees of freedom increase as we refine both macro and micro discretizations. It is important to remark that such micro problems could be solved in parallel, since they are mutually independent. However, we can further reduce the computational cost by employing reduced basis (RB) techniques [80, 79] to obtain a small number of precomputed micro solutions which can then be appropriately interpolated when solving the forward problem. The combination of RB and the FE-HMM is developed in [4] for elliptic equations and in [5] for Stokes problems.

The main idea of the RB methodology is to approximate the solution of a parameter dependent problem by projecting it onto a low dimensional solution space, which is spanned by precomputed solutions of the original problem corresponding to a small set of parameter's values. In particular in the FE-HMM setting it is often the case that the micro problems are parameterized by the given macro quadrature points. The RB-FE-HMM is then based on two stages. At first, during what is called the offline stage, the method is trained on a set of different input locations and a small number of micro functions are selected to construct the reduced space by using a greedy algorithm. Then, this new small set of basis functions is used to obtain fast evaluations of micro problems during the online stage.

Multiscale inverse problems. Parameterized multiscale inverse conductivity problems of Calderón's type have first been introduced in [54], where it is assumed that the multiscale tensor is of the form $A^\varepsilon(\sigma^*(x), x/\varepsilon)$, and $\sigma^* : D \to \mathbb{R}$ has to be recovered. It is shown via numerical experiments that numerical homogenization can be used for the considered class of multiscale inverse problems by assuming that σ^* is parametrized by a small number of piecewise smooth coefficients. In Chapter 3 we generalize the applicability of the numerical homogenization to generic scalar fields and without any formal assumptions on the map $(t, x) \mapsto A(t, x/\varepsilon)$, $(t, x) \in \mathbb{R} \times D$. Hence, we provide a theoretical investigation of both the model problem and the computational approach for the coarse graining strategy. We mention also that inverse conductivity problems in the multiscale regime have been already treated in [73]. However there the problem's setting is different from the one we consider, as well

as the theoretical and numerical results. Indeed the authors, given some measurements of the fine scale solution u^ε, are interested in recovering the effective tensor rather than the full multiscale tensor, and, for this reason, no use of numerical homogenization is employed. In our setting numerical homogenization is instead necessary to retrieve the low dimensional parameters needed to recover the full multiscale tensor. We also mention the work [43], where a geometric framework for homogenization and inverse homogenization is introduced. The numerical method builds on harmonic coordinate transformations which require one to solve multiple fine scale problems over the whole domain. Again this setting differs from the one we propose in this thesis.

1.2   Main contributions and outline of the thesis

In this thesis we develop new numerical strategies based on homogenization and model order reduction to solve efficiently multiscale inverse problems. We consider both Tikhonov and Bayesian regularization of inverse problems. In what follows we outline the structure of the thesis and we highlight our main contributions.

In **Chapter 2** we recall homogenization theory and numerical methods for scalar elliptic multiscale problems. We give a detailed description of the FE-HMM and the RB-FE-HMM which will be used later in the thesis to build the numerical method we propose. A new numerical scheme to compute effective boundary fluxes is described, and a priori error estimates for this method are provided. In particular, this part of the chapter is based on results obtained in [9].

In **Chapter 3** we consider parameterized multiscale inverse problems of Calderón's type. We assume that the multiscale tensor is locally periodic and of the form $A^\varepsilon_{\sigma^*}(x) = A(\sigma^*(x), x/\varepsilon)$, where $\sigma^* : D \to \mathbb{R}$. By assuming that the fine scale problem is well-posed in the sense of [16], we show that the effective inverse problem, with observed data consisting of the homogenized DtN map, is also well-posed, and we establish stability results independent of the small scale ε. As the full DtN map is usually not available, we discuss a numerical strategy based on finite measurements of this map. The inverse problem requires regularization to be solved, and thus we opt for Tikhonov regularization. Moreover, by means of G-convergence we characterize the convergence of the solution of the effective inverse problem with multiscale observations as $\varepsilon \to 0$. Finally, we provide a new numerical strategy based on the HMM framework and RB techniques for solving the inverse problem. The convergence of the discrete optimization problem is established and various numerical results are presented to test our theoretical findings. The content of this chapter is essentially based on [9].

Departing from the preceding chapter, where in order to ensure well-posedness we solved the problem by means of Tikhonov regularization, we recast in **Chapter 4** the problem into a statistical framework, and develop a multiscale numerical method based on Bayesian techniques. The prohibitive cost of sampling from the multiscale posterior measure, forces us to introduce an effective forward operator and a related effective posterior measure. We give a

rigorous Bayesian formulation of the problem, and prove the well-posedness of the effective posterior measure, considering log-Gaussian and level set priors. We establish a link between the effective posterior measure and the fine scale model in terms of Hellinger distance, using G-convergence, to quantify the homogenization error introduced in this framework. The numerical method builds on the RB-FE-HMM. Inspired by [28] we provide an offline algorithm to approximate numerically the homogenization error distribution and to correct for the model discrepancy. Numerical experiments that illustrate our multiscale inverse method and confirm our theoretical conclusions are also presented. This chapter is based on [7].

In **Chapter 5** we give a rigorous formulation of the RB-FE-HMM for solving linear elasticity problems in multiscale perforated domains. In particular we consider random perforations. After having derived homogenization results for our model problem, by following ideas from [24] we describe how in practice the coefficients of the effective tensor are approximated. We provide a priori error estimates for the method and we conclude the chapter with some numerical experiments. The content of the chapter is based on [8].

In **Chapter 6** we consider inverse problems in linear elasticity with multiscale random perforated domains. We develop a method based on homogenization and Bayesian regularization. By extending the results obtained in Chapter 4 into the context of linear elasticity, we prove existence and well-posedness of the effective posterior measure. Using G-convergence, the convergence of the effective posterior measure towards the fine scale posterior is established in terms of the Hellinger distance. The numerical method is based on the RB-FE-HMM and since the multiscale model is randomly defined, we have to deal with an additional source of error which is inversely proportional to the size of the micro sampling domains. This error propagates into the effective posterior often leading to overconfident and misleading predictions. Therefore, we develop a probabilistic numerical method which allows to account for the impact of the modeling error in the forward solver and which gives rise to a new effective posterior measure which reflects the uncertainty in the approximate solution due to the numerical method. This new effective posterior measure converges nonetheless asymptotically with respect to the size of the micro domains. The content of this chapter is based on [6].

Finally we end with **Chapter 7**, where conclusions, future perspectives of research, and developments related to the topic of the thesis are discussed.

2 Homogenization and multiscale methods for elliptic equations

In this chapter we recall homogenization theory and numerical methods for the approximation of multiscale second order elliptic PDEs. Let D be an open bounded domain in $\mathbb{R}^d$, $d \leq 3$. Given $f \in H^{-1}(D)$ and $g \in H^{1/2}(\partial D)$, we are interested in finding the weak solution $u^\varepsilon \in H^1(D)$ which solves

$$
\begin{aligned}
-\nabla \cdot (A^\varepsilon \nabla u^\varepsilon) &= f && \text{in } D, \\
u^\varepsilon &= g && \text{on } \partial D,
\end{aligned}
\tag{2.1}
$$

where A^ε is a highly heterogeneous tensor which presents variations at a very fine scale $\varepsilon \ll 1$. To ensure the well-posedness of (2.1), we assume A^ε to be elliptic and bounded, i.e., $A^\varepsilon \in M(\alpha, \beta, D)$, where

$$
M(\alpha, \beta, D) = \left\{ A \in (L^\infty(D))^{d \times d} : \alpha |b|^2 \leq A(x) b \cdot b, |A(x)b| \leq \beta |b|, \forall b \in \mathbb{R}^d, \text{ and a.e. on } D \right\}.
$$

For simplicity, in what follows we will always assume A^ε to be symmetric and we will consider only Dirichlet conditions at the boundary. However the results presented can be generalized to non-symmetric tensors and other choices of boundary conditions.

Outline. The outline of the chapter is as follows. In Section 2.1 we recall homogenization results for elliptic scalar equations. In Section 2.2 we describe the finite element heterogeneous multiscale method (FE-HMM), and provide a priori error estimates. Moreover we introduce a numerical method based on the FE-HMM to approximate the homogenized flux at the boundary. We report partly the analysis of the method, which was obtained in [9]. In Section 2.3 we illustrate the reduced basis finite element heterogeneous multiscale method (RB-FE-HMM), which combines the FE-HMM and reduced basis techniques to reduce further the computational cost of the FE-HMM.

2.1   Homogenization of elliptic equations

Homogenization theory [21, 33, 63, 77, 87] aims at describing the asymptotic behavior of multiscale PDEs. Concerning (2.1), it is well-known that there exists an effective tensor A^0 such that the solution to problem (2.1) converges (in a weak sense) as $\varepsilon \to 0$ to a homogenized solution u^0, which solves the problem

$$
\begin{aligned}
-\nabla \cdot (A^0 \nabla u^0) &= f &&\text{in } D, \\
u^0 &= g &&\text{on } \partial D.
\end{aligned}
\tag{2.2}
$$

Locally periodic case.   One often assumes to have scale separation between the slow and the fast variables, i.e., the tensor can be written as

$$
A^{\varepsilon}(x) = A(x, x/\varepsilon),
$$

where x/ε denotes the fast variable. In the case of locally periodic tensors, i.e,

$$
A_{ij}(x, x/\varepsilon) = A_{ij}(x, y), \quad A_{ij}(x, \cdot) \text{ is } Y\text{-periodic}, \quad \forall x \in D, \forall i, j = 1, \dots, d,
$$

where $Y = (0,1)^d$ denotes the domain of periodicity, it is possible to give a formal expression for the coefficients of the homogenized matrix A^0. Indeed they are defined as

$$
A^0_{ij}(x) = \int_Y A(x, y) \mathbf{e}^i \cdot (\mathbf{e}^j - \nabla_y \chi^j) \, \mathrm{d}y, \quad \forall i, j = 1, \dots, d.
\tag{2.3}
$$

In (2.3), the micro functions χ^j, $j = 1, \dots, d$, are defined to be the unique solutions of the cell problems: find $\chi^j(x, \cdot) \in W^1_{\mathrm{per}}(Y)$ such that

$$
\int_Y A(x, y) \nabla_y \chi^j \cdot \nabla_y v \, \mathrm{d}y = \int_Y A(x, y) \mathbf{e}^j \cdot \nabla_y v \, \mathrm{d}y \quad \forall v \in W^1_{\mathrm{per}}(Y),
\tag{2.4}
$$

where $\{\mathbf{e}^j\}_{j=1}^d$ is the canonical basis of $\mathbb{R}^d$ and

$$
W^1_{\mathrm{per}}(Y) = \left\{ v \in H^1_{\mathrm{per}}(Y) : \int_Y v \, \mathrm{d}y = 0 \right\},
$$

and $H^1_{\mathrm{per}}(Y)$ is defined as the closure of $C^\infty_{\mathrm{per}}(Y)$ for the $H^1(Y)$-norm (where $C^\infty_{\mathrm{per}}(Y)$ denotes the subset of $C^\infty(\mathbb{R}^d)$ of periodic functions in Y). We recall that the quantity

$$
\| v \|_{W^1_{\mathrm{per}}(Y)} = \| \nabla v \|_{L^2(Y)}
$$

defines a norm on $W^1_{\mathrm{per}}(Y)$. From (2.3) and (2.4) one can show that the homogenized tensor A^0 is uniformly bounded and elliptic (see [33] for example). We remark that for globally

periodic tensors, i.e., $A^\varepsilon(x) = A(x/\varepsilon) = A(y)$ Y-periodic in the y variable, the corresponding homogenized tensor A^0 is constant on the whole domain.

For which concerns the convergence of u^ε towards u^0 it can be shown that (see [21, 81] for example)

$$u^\varepsilon \rightharpoonup u^0 \qquad \text{weakly in } H^1(D),$$
$$A^\varepsilon \nabla u^\varepsilon \rightharpoonup A^0 \nabla u^0 \quad \text{weakly in } (L^2(D))^d.$$

Extension to the non-periodic case. When considering non-periodic tensors, it is not possible to charcaterize formally the coefficients of the tensor A^0 as in (2.3). However, from the theoretical point of view we can rely on the concepts of G-convergence [83, 42] in the symmetric case, and H-convergence [70]. Let us recall the definition of G-convergence.

Definition 2.1.1. Let $\{A^\varepsilon\}_{\varepsilon>0}$ be a sequence of symmetric matrices in $M(\alpha, \beta, D)$. We say that $\{A^\varepsilon\}_{\varepsilon>0}$ G-converges to the symmetric matrix $A^0 \in M(\alpha, \beta, D)$ if and only if for every function $f \in H^{-1}(D)$, $g \in H^{1/2}(\partial D)$, the solution u^ε of

$$-\nabla \cdot (A^\varepsilon \nabla u^\varepsilon) = f \qquad \text{in } D,$$
$$u^\varepsilon = g \qquad \qquad \text{on } \partial D,$$

is such that

$$u^\varepsilon \rightharpoonup u^0 \quad \text{weakly in } H^1(D),$$

where u^0 is the unique solution of

$$-\nabla \cdot (A^0 \nabla u^0) = f \qquad \text{in } D,$$
$$u^0 = g \qquad \qquad \text{on } \partial D.$$

A consequence of G-convergence is the weak convergence of the flux

$$A^\varepsilon \nabla u^\varepsilon \rightharpoonup A^0 \nabla u^0 \quad \text{weakly in } (L^2(D))^d.$$

The G-convergence possesses the following main properties (see [33] for example).

1. The G-limit of a G-converging sequence $\{A^\varepsilon\}_{\varepsilon>0}$ in $M(\alpha, \beta, D)$ is unique.

2. Let $\{A^\varepsilon\}_{\varepsilon>0}$ and $\{B^\varepsilon\}_{\varepsilon>0}$ be two sequences of symmetric matrices in $M(\alpha, \beta, D)$ which G-converge respectively to A^0 and B^0. If for some subset $X \subset D$ one has

$$A^\varepsilon = B^\varepsilon \quad \text{in } X \quad \forall \varepsilon > 0,$$

then

$$A^0 = B^0 \quad \text{in } X.$$

3. Let $\{A^\varepsilon\}_{\varepsilon>0}$ be a sequence of symmetric matrices in $M(\alpha,\beta,D)$. Then there exists a subsequence $\{A^{\varepsilon'}\}_{\varepsilon'>0}$ and a matrix $A^0 \in M(\alpha,\beta,D)$ such that $\{A^{\varepsilon'}\}_{\varepsilon'>0}$ G-converges to A^0.

4. A sequence $\{A^\varepsilon\}_{\varepsilon>0}$ of symmetric matrices in $M(\alpha,\beta,D)$ G-converges if and only if all its G-converging subsequences have the same limit.

In practice the homogenized tensor is usually not known analytically (for both the locally periodic and non-periodic case) and therefore numerical homogenization is needed. The idea is to approximate the values of the homogenized tensor on given locations $x \in D$ by solving appropriate cell problems such as (2.4) on sampling domains. This is the strategy behind the FE-HMM which we will describe in next section.

2.2 Finite element heterogeneous multiscale method (FE-HMM)

Given $f \in H^{-1}(D)$ and $g \in H^{1/2}(\partial D)$, we consider the problem of finding the weak solution $u^\varepsilon \in H^1(D)$ such that

$$\begin{aligned} -\nabla \cdot (A^\varepsilon \nabla u^\varepsilon) &= f && \text{in } D, \\ u^\varepsilon &= g && \text{on } \partial D. \end{aligned} \tag{2.5}$$

If we denote $u^\varepsilon = \mathring{u}^\varepsilon + R_g$, where $\mathring{u}^\varepsilon \in H_0^1(D)$ and R_g is an appropriate Dirichlet lift of g, the variational formulation of problem (2.5) reads: find $\mathring{u}^\varepsilon \in H_0^1(D)$ such that

$$B_\varepsilon(\mathring{u}^\varepsilon, v) = F(v) - B_\varepsilon(R_g, v) \quad \forall v \in H_0^1(D), \tag{2.6}$$

where B_ε is the bilinear form defined as

$$B_\varepsilon(v,w) = \int_D A^\varepsilon \nabla v \cdot \nabla w \, dx,$$

and F is the continuous functional

$$F(v) = \langle f, v \rangle_{H^{-1}(D), H_0^1(D)}.$$

Lax-Milgram theorem ensures the existence of a family of solutions $\{u^\varepsilon\}_{\varepsilon>0}$, which is bounded in $H_0^1(D)$ independently of ε. Trying to approximate (2.6) by means of standard numerical techniques such as the finite element method (FEM) is prohibitive in terms of computational cost, since they require mesh resolution at the finest scale.

The FE-HMM is a numerical homogenization method which aims at approximating the effective solution u^0 corresponding to (2.5). It has been studied extensively in the literature
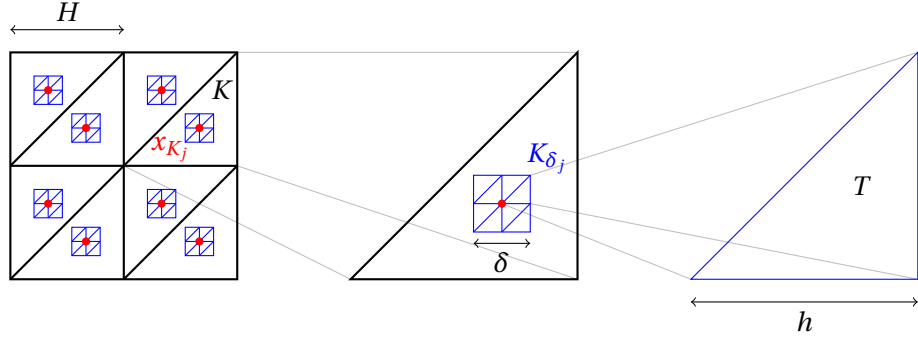
Figure 2.1: Macro and micro domains for the FE-HMM. Micro sampling domains K_{δ_j} located around the quadrature nodes x_{K_j} of the macro mesh.

and we refer the reader to [1, 3, 48, 74] for more details. The method is based on a macroscopic partition of the domain D, on which a macro quadrature formula is given. The idea is to approximate the values of the homogenized tensor only on the given macro quadrature points by solving PDEs on micro domains centered at the given macro quadrature points. Let us remark that even if we consider the model problem (2.5), the method can be applied to a large class of problems. Moreover it does not require particular structures in the oscillating tensor such as periodicity, and relies only on input data given by the fine scale model. However, we still assume to have scale separation between slow and fast variables so that $A^\varepsilon(x) = A(x, x/\varepsilon)$.

2.2.1 The numerical method

The FE-HMM is based on a macro finite element space $S_0^l(D, \mathcal{T}_H)$ defined as

$$S_0^l(D, \mathcal{T}_H) = \left\{ v^H \in H_0^1(D) : v^H|_K \in \mathcal{P}^l(K), \forall K \in \mathcal{T}_H \right\},$$

where $\mathcal{T}_H$ is a partition of D in simplicial or quadrilateral elements K of diameter H_K, and $\mathcal{P}^l(K)$ is the space of polynomials on K of total degree at most l if K is a simplicial element, while if K is a quadrilateral element $\mathcal{P}^l(K)$ is the space of polynomials on K of degree at most l in each variable. For the given mesh $\mathcal{T}_H$, we define

$$H = \max_{K \in \mathcal{T}_H} H_K,$$

and we allow H to be much larger than ε. We will always assume that the partition $\mathcal{T}_H$ is admissible and shape regular, i.e.,

- the intersection of two elements is either empty, exactly one vertex, or a common face, and $\cup_{K \in \mathcal{T}_H} K = \overline{D}$;

- $\forall K \in \mathcal{T}_H, \exists \kappa > 0$ such that $H_K / \rho_K \leq \kappa$, where ρ_K is the diameter of the largest sphere contained in K.

For each element $K \in \mathcal{T}_H$ we consider a reference element $\hat{K}$, such that $K = F_K(\hat{K})$, where F_K is a C^1-diffeomorphism. We assume that a quadrature formula $\{\hat{x}_j, \hat{\omega}_j\}_{j=1}^J$ on $\hat{K}$ is given, and that it satisfies $\hat{\omega}_j > 0$ and

$$\int_{\hat{K}} \hat{p}(\hat{x}) \, d\hat{x} = \sum_{j=1}^J \hat{\omega}_j \hat{p}(\hat{x}_j) \quad \forall \hat{p} \in \mathcal{P}^{l^*}(\hat{K}), \tag{2.7}$$

where $l^* = \max\{2l - 2, l\}$ if $\hat{K}$ is a simplicial element, or $l^* = \max\{2l - 1, l + 1\}$ if $\hat{K}$ is a quadrilateral element. Note that the transformation F_K induces a quadrature formula $\{x_{K_j}, \omega_{K_j}\}_{j=1}^J$ on K, such that $x_{K_j} = F_K(\hat{x}_j)$ and $\omega_{K_j} = \hat{\omega}_j |\det(\partial F_K)| > 0$, which satisfies

$$\int_K p(x) \, dx = \sum_{j=1}^J \omega_{K_j} p(x_{K_j}) \quad \forall p \in \mathcal{P}^{l^*}(K). \tag{2.8}$$

Given the macro finite element space $S_0^l(D, \mathcal{T}_H)$, one could think of applying directly the finite element method to the problem (2.2) by finding $u^{0,H} = \mathring{u}^{0,H} + R_g$, where $\mathring{u}^{0,H} \in S_0^l(D, \mathcal{T}_H)$ is the unique solution of

$$B_{0,H}(\mathring{u}^{0,H}, v^H) = F(v^H) - B_{0,H}(R_g, v^H) \quad \forall v^H \in S_0^l(D, \mathcal{T}_H), \tag{2.9}$$

where

$$B_{0,H}(v^H, w^H) = \sum_{K \in \mathcal{T}_H} \sum_{j=1}^J \omega_{K_j} A^0(x_{K_j}) \nabla v^H(x_{K_j}) \cdot \nabla w^H(x_{K_j}), \tag{2.10}$$

and R_g is a Dirichlet lift properly chosen. However, as already mentioned, the value of A^0 is usually not known. Then we introduce micro problems to evaluate the homogenized tensor on the macro quadrature points. To do so, for each macro element $K \in \mathcal{T}_H$, and for each macro quadrature point x_{K_j}, we define a micro domain $K_{\delta_j} = x_{K_j} + (-\delta/2, \delta/2)^d$, $\delta \geq \varepsilon$. Then, for a sampling domain K_{δ_j} we introduce the micro finite element space

$$S^q(K_{\delta_j}, \mathcal{T}_h) = \left\{ z^h \in W(K_{\delta_j}) : z^h|_T \in \mathcal{P}^q(T), \forall T \in \mathcal{T}_h \right\},$$

where

$$W(K_{\delta_j}) = W_{\mathrm{per}}^1(K_{\delta_j}) \tag{2.11}$$

in case of periodic coupling, or

$$W(K_{\delta_j}) = H_0^1(K_{\delta_j}) \tag{2.12}$$

for a coupling with Dirichlet boundary conditions. We define the bilinear form

$$B_H(v^H, w^H) = \sum_{K \in \mathcal{T}_H} \sum_{j=1}^{J} \frac{\omega_{K_j}}{|K_{\delta_j}|} \int_{K_{\delta_j}} A^\varepsilon(x) \nabla v_{K_j}^h \cdot \nabla w_{K_j}^h \, dx, \tag{2.13}$$

where $v_{K_j}^h$ (respectively $w_{K_j}^h$) denotes the solution to the micro problem: find $v_{K_j}^h$ such that $v_{K_j}^h - v_{\text{lin},j}^H \in S^q(K_{\delta_j}, \mathcal{T}_h)$ and

$$\int_{K_{\delta_j}} A^\varepsilon(x) \nabla v_{K_j}^h \cdot \nabla z^h \, dx = 0 \quad \forall z^h \in S^q(K_{\delta_j}, \mathcal{T}_h), \tag{2.14}$$

where $v_{\text{lin},j}^H(x) = v^H(x_{K_j}) + (x - x_{K_j}) \cdot \nabla v^H(x_{K_j})$. Finally the FE-HMM solution is given by $u^H = \mathring{u}^H + R_g$, where $\mathring{u}^H \in S_0^l(D, \mathcal{T}_H)$ is the unique solution of

$$B_H(\mathring{u}^H, v^H) = F(v^H) - B_H(R_g, v^H) \quad \forall v^H \in S_0^l(D, \mathcal{T}_H).$$

Reformulation of the FE-HMM. The values of the homogenized tensor can be computed during the assembly process by finding for $K \in \mathcal{T}_H$, $1 \le j \le J$, $1 \le i \le d$, $\hat{\chi}_{K_j}^{i,h} \in S^q(K_{\delta_j}, \mathcal{T}_h)$ such that

$$\int_{K_{\delta_j}} A^\varepsilon(x) \nabla \hat{\chi}_{K_j}^{i,h} \cdot \nabla z^h \, dx = \int_{K_{\delta_j}} A^\varepsilon(x) \mathbf{e}^i \cdot \nabla z^h \, dx \quad \forall z^h \in S^q(K_{\delta_j}, \mathcal{T}_h). \tag{2.15}$$

Once the functions $\hat{\chi}_{K_j}^{i,h}$ have been computed, the coefficients of the numerical homogenized tensor can be approximated as

$$A_{lm}^{0,h}(x_{K_j}) = \frac{1}{|K_{\delta_j}|} \int_{K_{\delta_j}} A^\varepsilon(x) \mathbf{e}^l \cdot (\mathbf{e}^m - \nabla \hat{\chi}_{K_j}^{m,h}) \, dx. \tag{2.16}$$

The bilinear form (2.13) can then be rewritten in the equivalent form [4]

$$B_H(v^H, w^H) = \sum_{K \in \mathcal{T}_H} \sum_{j=1}^{J} \omega_{K_j} A^{0,h}(x_{K_j}) \nabla v^H(x_{K_j}) \cdot \nabla w^H(x_{K_j}), \tag{2.17}$$

which reminds to the bilinear form (2.10), but differs from it since the unknown value of $A^0(x_{K_j})$ is replaced by its numerical approximation.

2.2.2 A priori error analysis

In this section we provide a priori estimates for the error between the exact homogenized solution u^0 of (2.2) and its approximation u^H obtained by means of the FE-HMM. A complete proof of the convergence rates is provided in [1, 3], while here we limit ourselves to reporting

the results given there.

Let us in introduce the semi-discrete bilinear form

$$\widetilde{B}_H(v^H, w^H) = \sum_{K \in \mathcal{T}_H} \sum_{j=1}^{J} \frac{\omega_{K_j}}{|K_{\delta_j}|} \int_{K_{\delta_j}} A^\varepsilon(x) \nabla v_{K_j} \cdot \nabla w_{K_j} \, dx, \qquad (2.18)$$

where v_{K_j} (respectively w_{K_j}) is the exact solution of (2.14) in the Sobolev space $W(K_{\delta_j})$. Hence we define $\widetilde{u}^H = \widetilde{\widetilde{u}}^H + R_g$, where $\widetilde{\widetilde{u}}^H \in S_0^l(D, \mathcal{T}_H)$ is the unique solution of

$$\widetilde{B}_H(\widetilde{\widetilde{u}}^H, v^H) = F(v^H) - \widetilde{B}_H(R_g, v^H) \quad \forall v^H \in S_0^l(D, \mathcal{T}_H).$$

Note that (2.18) can be rewritten in a similar form as (2.17)

$$\widetilde{B}_H(v^H, w^H) = \sum_{K \in \mathcal{T}_H} \sum_{j=1}^{J} \omega_{K_j} \widetilde{A}^0(x_{K_j}) \nabla v^H(x_{K_j}) \cdot \nabla w^H(x_{K_j}). \qquad (2.19)$$

In this case the coefficients of $\widetilde{A}^0$ are computed as in (2.16), with the difference that the micro functions $\hat{\chi}_{K_j}^{i,h} \in S^q(K_{\delta_j}, \mathcal{T}_h)$ are replaced by the exact solutions of (2.15) $\hat{\chi}_{K_j}^i \in W(K_{\delta_j})$.

Using the triangle inequality, we decompose the global error as

$$\|u^0 - u^H\|_{H^1(D)} \leq \|e_{\mathrm{mac}}\|_{H^1(D)} + \|e_{\mathrm{mod}}\|_{H^1(D)} + \|e_{\mathrm{mic}}\|_{H^1(D)}, \qquad (2.20)$$

where we have used the notation

$$e_{\mathrm{mac}} = u^0 - u^{0,H}, \quad e_{\mathrm{mod}} = u^{0,H} - \widetilde{u}^H, \quad e_{\mathrm{mic}} = \widetilde{u}^H - u^H.$$

Note that the function $u^{0,H}$ is the numerical solution obtained by applying the standard single scale finite element method to the problem (2.2), as defined in (2.9). Hence, the macro error e_{mac} can be bounded by using standard FEM error estimates [31]. Assume (2.7) holds and let $u^0 \in H^{l+1}(D)$ and $A_{ij}^0 \in W^{l+1,\infty}(D)$, $1 \leq i, j \leq d$. Then we have that

$$\|u^0 - u^H\|_{H^1(D)} \leq CH^l + \|e_{\mathrm{mod}}\|_{H^1(D)} + \|e_{\mathrm{mic}}\|_{H^1(D)},$$

where C is a generic constant independent of H, h, ε and δ. Note that from (2.10), (2.17) and (2.19) we get the following bounds for e_{mod} and e_{mic}:

$$\|e_{\mathrm{mod}}\|_{H^1(D)} \leq C \sup_{K \in \mathcal{T}_H} \sup_{1 \leq j \leq J} \|A^0(x_{K_j}) - \widetilde{A}^0(x_{K_j})\|_{\mathrm{F}},$$

$$\|e_{\mathrm{mic}}\|_{H^1(D)} \leq C \sup_{K \in \mathcal{T}_H} \sup_{1 \leq j \leq J} \|\widetilde{A}^0(x_{K_j}) - A^{0,h}(x_{K_j})\|_{\mathrm{F}},$$

where $\|\cdot\|_{\mathrm{F}}$ is the Frobenius norm. To estimate the quantity e_{mic} we need to make necessary assumptions about the regularity of $\hat{\chi}_{K_j}^i \in W(K_{\delta_j})$. In particular, we assume that $\hat{\chi}_{K_j}^i \in H^{q+1}(K_{\delta_j})$

and that

$$|\hat{\chi}^i_{K_j}|_{H^{q+1}(K_{\delta_j})} \le C\varepsilon^{-q}\sqrt{|K_{\delta_j}|},$$

where C is a constant independent of i, j, K, ε and δ (see Remark 4.6 in [11] for a justification of this assumption). Under these assumptions it can be proved that for both periodic and Dirichlet coupling we have

$$\|e_{\mathrm{mic}}\|_{H^1(D)} \le C\left(\frac{h}{\varepsilon}\right)^{2q}.$$

Finally, explicit error estimates for the modeling error can be provided in the case of locally periodic data, i.e.

$$A^\varepsilon(x) = A(x, x/\varepsilon),$$

and

$$A_{ij}(x, x/\varepsilon) = A_{ij}(x, y), \quad A_{ij}(x, \cdot) \text{ is } Y\text{-periodic}, \quad \forall x \in D, \forall i, j = 1, \dots, d.$$

By replacing $A^\varepsilon(x)$ with $A(x_{K_j}, x/\varepsilon)$ in (2.13), (2.14) we get [48, 14]

$$\|e_{\mathrm{mod}}\|_{H^1(D)} = 0 \quad \text{if } W(K_{\delta_j}) = W^1_{\mathrm{per}}(K_{\delta_j}) \text{ and } \frac{\delta}{\varepsilon} \in \mathbb{N},$$

$$\|e_{\mathrm{mod}}\|_{H^1(D)} \le C\frac{\varepsilon}{\delta} \quad \text{if } W(K_{\delta_j}) = H^1_0(K_{\delta_j}) \text{ and } \delta > \varepsilon.$$

Remark 2.2.1. Let us emphasize that for a given accuracy, the computational cost for solving the micro problems is independent of ε. Let N_{mac} and N_{mic} be the degrees of freedom in each direction for the macro domain and the micro domain respectively, so that

$$H = \mathcal{O}(N^{-1}_{\mathrm{mac}}), \quad h = \mathcal{O}(\delta N^{-1}_{\mathrm{mic}}).$$

Since $\delta = n\varepsilon$, $n \in \mathbb{N}$, $n > 0$, we obtain

$$\|e_{\mathrm{mic}}\| \le Ch^{2q},$$

where C is independent of ε. Then we obtain

$$\|u^0 - u^H\|_{H^1(D)} \le C(N^{-l}_{\mathrm{mac}} + N^{-2q}_{\mathrm{mic}}) + \|e_{\mathrm{mod}}\|_{H^1(D)}.$$

Hence, by choosing $N_{\mathrm{mac}} = N$, $N_{\mathrm{mic}} = N^{l/2q}$ for optimal convergence, the total complexity is $\mathcal{O}(N^{d(1+l/2q)}J)$, where J denotes the number of sampling domains per macro element $K \in \mathcal{T}_H$, for an accuracy of $\mathcal{O}(N^{-l})$. Finally, we emphasize that the micro problems are independent one from another and they can be solved in parallel. Hence the complexity of the method can be further reduced.

2.2.3 Approximation of the effective normal flux at the boundary

In this section we describe the numerical scheme to approximate the normal flux at the boundary for the homogenized PDE (2.2). We will denote the flux with the help of the Dirichlet to Neumann map associated to the tensor A^0, i.e.

$$\Lambda_{A^0} : g \in H^{1/2}(\partial D) \mapsto A^0 \nabla u^0 \cdot \boldsymbol{v}|_{\partial D} \in H^{-1/2}(\partial D),$$

where $\boldsymbol{v}$ denotes the exterior unit normal to ∂D. The method is based on a Galerkin projection [30], and is analyzed in detail in [78] in its classical finite element formulation. In particular, it allows us to obtain super-convergence of the approximate flux in the $L^2(\partial D)$-norm, and we aim at showing how such a super-convergence result can be extended in the context of the FE-HMM. In what follows we assume D to be a polygonal domain. The method is described and analyzed for the case of piecewise simplicial macro and micro finite elements. Moreover we consider locally periodic tensors of the form $A^\varepsilon(x) = A(x, x/\varepsilon)$,

$$A_{ij}(x, x/\varepsilon) = A_{ij}(x, y), \quad A_{ij}(x, \cdot) \text{ is } Y\text{-periodic}, \quad \forall x \in D, \forall i, j = 1, \dots, d,$$

and we assume to have periodic coupling for the micro problems. Under these assumptions it is possible to collocate the slow variable of $A^\varepsilon(x)$ at the macro quadrature points x_K. Hence the bilinear forms (2.10), (2.13), (2.18) respectively become

$$B_{0,H}(v^H, w^H) = \sum_{K \in \mathcal{T}_H} |K| A^0(x_K) \nabla v^H(x_K) \cdot \nabla w^H(x_K),$$

$$B_H(v^H, w^H) = \sum_{K \in \mathcal{T}_H} \frac{|K|}{|K_\delta|} \int_{K_\delta} A(x_K, x/\varepsilon) \nabla v_K^h \cdot \nabla w_K^h \, dx,$$

$$\widetilde{B}_H(v^H, w^H) = \sum_{K \in \mathcal{T}_H} \frac{|K|}{|K_\delta|} \int_{K_\delta} A(x_K, x/\varepsilon) \nabla v_K \cdot \nabla w_K \, dx,$$

where v_K (respectively w_K) is the exact solution to the micro problem (2.14) in the space of functions $W^1_{\mathrm{per}}(K_\delta)$ with $A^\varepsilon(x)$ and K_{δ_j} replaced by $A(x_K, x/\varepsilon)$ and K_δ respectively. Let us introduce the following subspaces of $S^1(D, \mathcal{T}_H)$:

$$S^1_c(D, \mathcal{T}_H) = \left\{ v^H \in S^1(D, \mathcal{T}_H) : v^H = 0 \text{ at the corners of } D \right\},$$

$$S^1_i(D, \mathcal{T}_H) = \left\{ v^H \in S^1_c(D, \mathcal{T}_H) : v^H = 0 \text{ at the interior nodes of } D \right\}.$$

Assume that the forcing term $f \in L^2(D)$ and that the flux is in $L^2(\partial D)$. Using integration by parts we have the following relation for the flux

$$\int_{\partial D} \Lambda_{A^0} g v \, ds = B_0(u^0, v) - \int_D f v \, dx \quad \forall v \in H^1(D), \tag{2.21}$$

where

$$B_0(v, w) = \int_D A^0 \nabla v \cdot \nabla w \, dx.$$

Let us denote by $S^1(\partial D, \mathcal{T}_H)$ the finite dimensional space of functions which are restrictions to the boundary of functions living in $S^1_c(D, \mathcal{T}_H)$. Hence by following [30, 78] we define the numerical flux by constructing a function $\Lambda^H_{A^{0,h}} g \in S^1(\partial D, \mathcal{T}_H)$ such that

$$\int_{\partial D} \Lambda^H_{A^{0,h}} g v^H \, ds = B_H(u^H, v^H) - \int_D f v^H \, dx \quad \forall v^H \in S^1_c(D, \mathcal{T}_H), \tag{2.22}$$

where the value of the flux at the corners of D is assumed to be known, as specified by direct calculations from the given Dirichlet conditions. Let us remark that u^H has already been computed, and so solving (2.22) reduces to solving a linear system whose unknowns are the values of the flux on the nodes of ∂D, except for the corners. To obtain an error estimate for the approximate flux, we recall the following inverse inequality, which relates the functions in $S^1_i(D, \mathcal{T}_H)$ to their traces on ∂D.

Lemma 2.2.2. *Let $X = X(D, \mathcal{T}_H)$ denote a strip of elements in $\mathcal{T}_H$, with each element having at least one vertex on ∂D, and let $v^H \in S^1_i(D, \mathcal{T}_H)$. Then*

$$\|\nabla v^H\|_{L^2(X)} \leq C H^{-1/2} \|v^H\|_{L^2(\partial D)}.$$

Lemma 2.2.3 (See [78])**.** *Consider a quasi-uniform family of macroscopic triangulations $\{\mathcal{T}_H\}_{H>0}$. Let the solution u^0 of the effective problem be in $H^3(D)$, $f \in H^2(D)$, $A^0 \in (W^{2,\infty}(D))^{d \times d}$. Let $v^H \in S^1_i(D, \mathcal{T}_H)$. Then*

$$|B_0(u^0, v^H) - B_{0,H}(u^{0,H}, v^H)| \leq C H^{3/2} (\|u^0\|_{H^3(D)} + \|f\|_{H^2(D)}) \|v^H\|_{L^2(\partial D)}.$$

Let $\mathscr{I}^H \Lambda_{A^0} g$ be the linear interpolation of $\Lambda_{A^0} g$ on ∂D.

Lemma 2.2.4. *Let $v^H \in S^1_i(D, \mathcal{T}_H)$. Then the following interpolation error estimate holds:*

$$\langle \Lambda_{A^0} g - \mathscr{I}^H \Lambda_{A^0} g, v^H \rangle_{L^2(\partial D)} \leq C H^{3/2} \|u^0\|_{H^3(D)} \|v^H\|_{L^2(\partial D)}.$$

Proof. A complete proof of this result is given in [78]. It is a consequence of the Bramble-Hilbert lemma, which yields

$$\|\Lambda_{A^0} g - \mathscr{I}^H \Lambda_{A^0} g\|_{L^2(\partial D)} \leq C H^{3/2} \|\Lambda_{A^0} g\|_{H^{3/2}(\partial D)}.$$

$\square$

Following [78], we can then obtain the following theorem, which establishes convergence rates for the numerical flux in the $L^2(\partial D)$-norm.

Theorem 2.2.5. *Consider a quasi-uniform family of macroscopic triangulations $\{\mathscr{T}_H\}_{H>0}$. Assume that the coupling between macro and micro meshes satisfies $H = \mathcal{O}(h/\varepsilon)$, and that the micro sampling domain has size $\delta = n\varepsilon$, where $n \in \mathbb{N}$, $n > 0$. Let the solution u^0 of the effective problem be in $H^3(D)$ and $A^0 \in (W^{2,\infty}(D))^{d \times d}$. Then the approximate boundary flux computed by means of* (2.22) *satisfies*

$$\|\Lambda_{A^0} g - \Lambda^H_{A^{0,h}} g\|_{L^2(\partial D)} \le C\left(H^{3/2} + \left(\frac{h}{\varepsilon}\right)^{3/2}\right),$$

where C is a constant independent on H, h, and ε.

Proof. Subtracting (2.22) from (2.21), we obtain

$$\langle \Lambda_{A^0} g - \Lambda^H_{A^{0,h}} g, v^H \rangle_{L^2(\partial D)} = B_0(u^0, v^H) - B_H(u^H, v^H) \quad \forall v^H \in S^1_c(D, \mathscr{T}_H). \tag{2.23}$$

Since for each function $v^H \in S^1_c(D, \mathscr{T}_H)$, there exist two functions $w^H \in S^1_0(D, \mathscr{T}_H)$ and $z^H \in S^1_i(D, \mathscr{T}_H)$ such that $v^H = w^H + z^H$, and hence (2.23) can be rewritten as

$$\langle \Lambda_{A^0} g - \Lambda^H_{A^{0,h}} g, v^H \rangle_{L^2(\partial D)} = I_1 + I_2 + I_3,$$

where

$$I_1 = B_0(u^0, z^H) - B_{0,H}(u^{0,H}, z^H),$$
$$I_2 = B_{0,H}(u^{0,H}, z^H) - \widetilde{B}_H(\widetilde{u}^H, z^H),$$
$$I_3 = \widetilde{B}_H(\widetilde{u}^H, z^H) - B_H(u^H, z^H).$$

From Lemma 2.2.3 we have that

$$|I_1| \le CH^{3/2}\|z^H\|_{L^2(\partial D)}.$$

On the other hand, it is well-known [1, 3] that

$$|I_3| \le C\left(\frac{h}{\varepsilon}\right)^2 \|\nabla u^H\|_{L^2(D)}\|\nabla z^H\|_{L^2(D)},$$

where C is a constant which is independent of δ and x_K. The term I_2 captures the modeling error, which vanishes under the assumptions that the locally periodic tensor admits explicit scale separation between slow and fast variables, that the slow variable is collocated at the quadrature point, and that $\delta = n\varepsilon$, with $n \in \mathbb{N}$, $n > 0$. Hence, from the bounds for I_1 and I_3, and using the fact that $I_2 = 0$ together with Lemma 2.2.2, we obtain that

$$\langle \Lambda_{A^0} g - \Lambda^H_{A^{0,h}} g, z^H \rangle_{L^2(\partial D)} \le C\left(H^{3/2} + \left(\frac{h}{\varepsilon}\right)^2 H^{-1/2}\right)\|z^H\|_{L^2(\partial D)} \qquad \forall z^H \in S^1_i(D, \mathscr{T}_H).$$

We note that

$$\langle \Lambda_{A^0} g - \Lambda_{A^{0,h}}^H g, z^H \rangle_{L^2(\partial D)} = \langle \Lambda_{A^0} g - \mathscr{I}^H \Lambda_{A^0} g, z^H \rangle_{L^2(\partial D)}$$
$$+ \langle \mathscr{I}^H \Lambda_{A^0} g - \Lambda_{A^{0,h}}^H g, z^H \rangle_{L^2(\partial D)},$$

where $\mathscr{I}^H$ is the linear interpolation operator which appears in Lemma 2.2.4. Then

$$\langle \mathscr{I}^H \Lambda_{A^0} g - \Lambda_{A^{0,h}}^H g, z^H \rangle_{L^2(\partial D)} = \langle \Lambda_{A^0} g - \Lambda_{A^{0,h}}^H g, z^H \rangle_{L^2(\partial D)}$$
$$+ \langle \mathscr{I}^H \Lambda_{A^0} g - \Lambda_{A^0} g, z^H \rangle_{L^2(\partial D)}.$$

By choosing $z^H = \mathscr{I}^H \Lambda_{A^0} g - \Lambda_{A^{0,h}}^H g$, thus we obtain that

$$\|\mathscr{I}^H \Lambda_{A^0} g - \Lambda_{A^{0,h}}^H g\|_{L^2(\partial D)} \le C\left(H^{3/2} + \left(\frac{h}{\varepsilon}\right)^2 H^{-1/2}\right).$$

Finally from the triangle inequality and the fact that $H = \mathscr{O}(h/\varepsilon)$ we conclude that

$$\|\Lambda_{A^0} g - \Lambda_{A^{0,h}}^H g\|_{L^2(\partial D)} \le C\left(H^{3/2} + \left(\frac{h}{\varepsilon}\right)^{3/2}\right). \tag{2.24}$$

$\square$

Remark 2.2.6. Again we emphasize that the computational cost for solving the micro problems is independent of ε, since the size of the micro domain $\delta \ge \varepsilon$ is proportional to ε. Let N_{mac} and N_{mic} be the degrees of freedom in one direction for the macro domain and the micro domain, respectively. Then (2.24) can be rewritten as

$$\|\Lambda_{A^0} g - \Lambda_{A^{0,h}}^H g\|_{L^2(\partial D)} \le C\left(N_{\mathrm{mac}}^{-3/2} + N_{\mathrm{mic}}^{-3/2}\right).$$

Hence, by choosing $N_{\mathrm{mac}} = N_{\mathrm{mic}} = N$ for optimal convergence, the total complexity is $\mathscr{O}(N^{2d})$ for an accuracy of $\mathscr{O}(N^{-3/2})$.

Numerical experiments. We perform some numerical experiments to test the convergence of the method and to observe how the micro error affects the approximate flux. We consider the elliptic problem

$$-\nabla \cdot (A^\varepsilon \nabla u^\varepsilon) = 0 \qquad \text{in } D,$$
$$u^\varepsilon = g \qquad\qquad \text{on } \partial D.$$

The domain D is defined as

$$D = \{x = (x_1, x_2) : 0 < x_1, x_2 < 1\},$$

while

$$g = \sin(\pi(x_1 + x_2)).$$

We perform two numerical tests for two different choices of A^ε. In the first experiment we consider the locally periodic tensor

$$A_{11}(x, x/\varepsilon) = (16(x_1^2 - x_1)(x_2^2 - x_2) + 1)\left(\cos^2\left(2\pi\frac{x_1}{\varepsilon}\right) + 1\right),$$

$$A_{22}(x, x/\varepsilon) = (16(x_1^2 - x_1)(x_2^2 - x_2) + 1)\left(\sin\left(2\pi\frac{x_2}{\varepsilon}\right) + 2\right),$$

$$A_{12}(x, x/\varepsilon) = A_{21}(x, x/\varepsilon) = 0.$$

We compute the approximate flux on the boundary nodes by means of the FE-HMM. We solve the problem for different choices of H and h/ε. To compute the error we use a reference solution computed with $H = h/\varepsilon = 1/64$. The size of the micro domain is such that $\delta = \varepsilon$. Numerical results are shown in Table 2.1 and Figure 2.2.

	$H = 1/4$	$H = 1/8$	$H = 1/16$	$H = 1/32$	$H = 1/64$
$h/\varepsilon = 1/4$	3.0276	1.0388	0.5654	0.4689	0.4485
$h/\varepsilon = 1/8$	2.6499	0.7069	0.1962	0.0715	0.0469
$h/\varepsilon = 1/16$	2.6154	0.6803	0.1700	0.0395	0.0093
$h/\varepsilon = 1/32$	2.6086	0.6751	0.1653	0.0346	0.0019
$h/\varepsilon = 1/64$	2.6069	0.6738	0.1642	0.0335	

Table 2.1: First experiment, error $\|\Lambda_{A^0}g - \Lambda_{A^{0,h}}^H g\|_{L^2(\partial D)}$ for different choices of H and h/ε ($\delta = \varepsilon$, $\|\Lambda_{A^0}g\|_{L^2(\partial D)} = 11.2655$).

Figure 2.2: First experiment, convergence of the error $\|\Lambda_{A^0}g - \Lambda_{A^{0,h}}^H g\|_{L^2(\partial D)}$ with respect to macro and micro discretizations ($\delta = \varepsilon$).

In the second experiment we consider the same setting, changing the tensor to

$$A_{11}(x, x/\varepsilon) = \left(\sqrt{\left(x_1^2 + \sin\left(2\pi\frac{x_1}{\varepsilon}\right) + 1.2\right)\left(x_1 x_2 + \sin\left(4\pi\frac{x_1}{\varepsilon}\right) + 1.5\right)}\right)^{-1},$$

$$A_{22}(x, x/\varepsilon) = \left(\left(x_1 x_2 + \sin\left(5\pi\frac{x_2}{\varepsilon}\right) + 1.2\right)\left(x_2^2 \cos\left(2\pi\frac{x_2}{\varepsilon}\right) + x_1 + 1.5\right)\right)^{-1},$$

$$A_{12}(x, x/\varepsilon) = A_{21}(x, x/\varepsilon) = 0.$$

As shown in Tables 2.1 and 2.2 and Figures 2.2 and 2.3, in both experiments the error converges quadratically as we decrease both H and h/ε. In particular, for the problems considered, the global error seems to depend more on the macro mesh. For the micro error we can observe quadratic convergence only for smaller values of H, while for larger values the micro error saturates due to the dominant macro error. This emphasizes that a simultaneous refinement of micro and macro meshes is needed for convergence. Finally, let us mention that the quadratic convergence was observed also in [30] for the FEM formulation of the method, suggesting that the error estimate obtained in [78] may not be sharp.

	$H = 1/4$	$H = 1/8$	$H = 1/16$	$H = 1/32$	$H = 1/64$
$h/\varepsilon = 1/4$	0.6143	0.1900	0.0956	0.0845	0.0841
$h/\varepsilon = 1/8$	0.5818	0.1613	0.0488	0.0251	0.0222
$h/\varepsilon = 1/16$	0.5743	0.1563	0.0420	0.0131	0.0080
$h/\varepsilon = 1/32$	0.5714	0.1545	0.0402	0.0096	0.0016
$h/\varepsilon = 1/64$	0.5707	0.1541	0.0399	0.0092	

Table 2.2: Second experiment, error $\|\Lambda_{A^0} g - \Lambda_{A^{0,h}}^H g\|_{L^2(\partial D)}$ for different choices of H and h/ε ($\delta = \varepsilon$, $\|\Lambda_{A^0} g\|_{L^2(\partial D)} = 2.8920$).
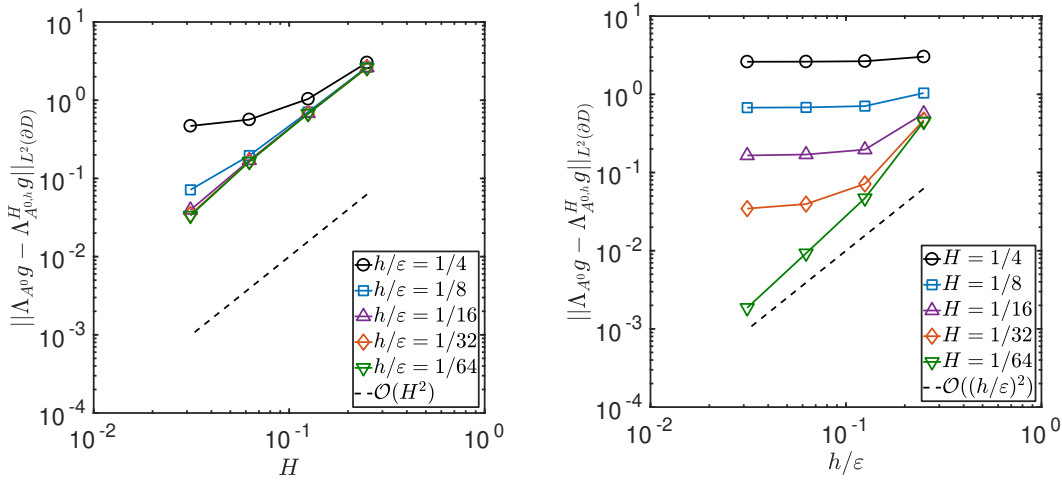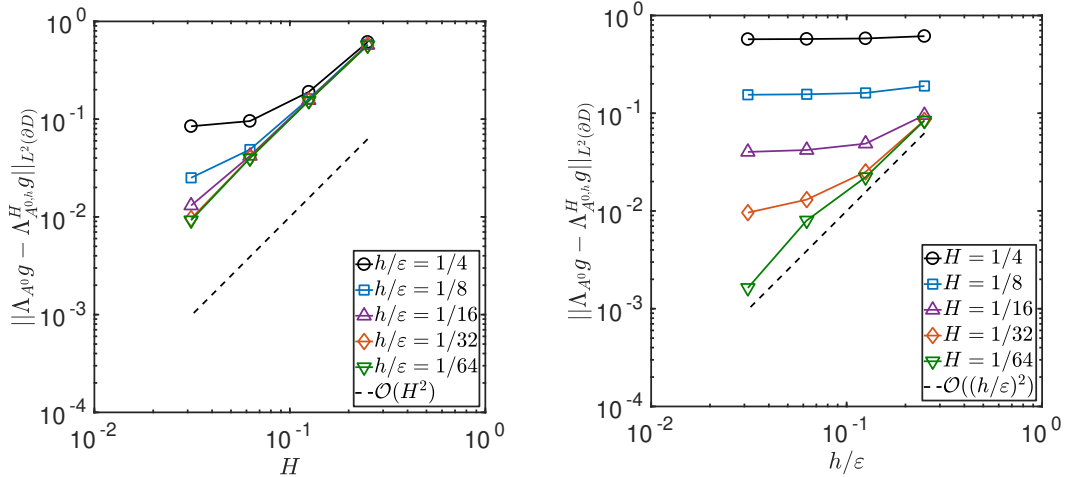

Figure 2.3: Second experiment, convergence of the error $\|\Lambda_{A^0} g - \Lambda_{A^{0,h}}^H g\|_{L^2(\partial D)}$ with respect to macro and micro discretizations ($\delta = \varepsilon$).

2.3 Reduced basis finite element heterogeneous multiscale method (RB-FE-HMM)

The FE-HMM introduced in the previous section is able to provide effective solutions to the problem (2.5) at a cost which is independent of ε which is already a great improvement with respect to classical FEMs. However, the repeated computation of micro problems for each macro element and each macro quadrature point, whose number and size increase as we refine both the macro and the micro meshes for an appropriate approximation of the effective solution, is still computationally very expensive. These cell problems vary on each macro element and are parameterized by the macro quadrature point. We note that the presence of repeated solutions of parameterized PDEs is the natural environment where to apply some model order reduction techniques. Hence, we combine reduced basis techniques with the FE-HMM, to design a new efficient method which drastically reduces the computational effort, by avoiding the repeated solutions of a large number of cell problems. The method goes under the name of reduced basis finite element heterogeneous multiscale method (RB-FE-HMM) and for a detailed analysis of the method we refer to [4].

2.3.1 Parameterized micro problems and model order reduction

Let us start with the following reformulation of the FE-HMM where we map the micro problems (2.15) into the reference cell $Y = (0,1)^d$. For each macro element $K \in \mathcal{T}_H$ and each macro quadrature point x_{K_j} we can map the sampling domain K_{δ_j} into the reference domain Y through $x = G_{x_{K_j}}(y) = x_{K_j} + \delta(y - 1/2)$. Hence for $K \in \mathcal{T}_H$, $1 \le j \le J$, $1 \le i \le d$, we consider the solution $\chi_{K_j}^{i,\hat{h}} \in S^q(Y, \mathcal{T}_{\hat{h}})$, where $\hat{h} = h/\delta$, such that

$$\int_Y A_{x_{K_j}}(y) \nabla \chi_{K_j}^{i,\hat{h}} \cdot \nabla z^{\hat{h}} \, dy = \int_Y A_{x_{K_j}}(y) \mathbf{e}^i \cdot \nabla z^{\hat{h}} \, dy \quad \forall z^{\hat{h}} \in S^q(Y, \mathcal{T}_{\hat{h}}), \qquad (2.25)$$

where we have used the notation $A_{x_{K_j}}(y) = A^\varepsilon(G_{x_{K_j}}(y))$. Note that the coefficients of the numerical homogenized tensor can be approximated now as

$$A_{lm}^{0,h}(x_{K_j}) = \int_Y A_{x_{K_j}}(y) \mathbf{e}^l \cdot (\mathbf{e}^m - \nabla \chi_{K_j}^{m,\hat{h}}) \, dy.$$

Having to solve (2.25) for each macro quadrature point can be prohibitively expensive. However, given this parameterization of the micro solutions, we can think now to apply model order reduction techniques to speed up the computation of the effective macroscopic tensor. The main idea is the following: instead of computing the micro solutions in each macro element at the given macro quadrature points, we select a small number of carefully precomputed micro solutions to construct a small subspace of functions living in $S^q(Y, \mathcal{T}_{\hat{h}})$. This is called the *offline stage*. Then in the *online stage* each micro solution is obtained as linear combination of the precomputed micro functions.
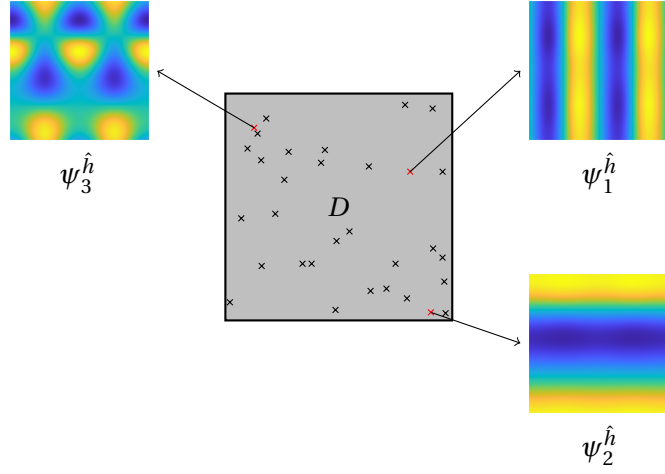
Figure 2.4: Representation of the first three iterations of the offline stage in the RB-FE-HMM. The training points are randomly distributed into the computational domain.

The offline stage. The variational problem (2.25) is parameterized by the macro variable $x_{K_j} \in D$ and the index i, $1 \le i \le d$. Therefore we define the space of parameters as $\Xi = D \times \{1, \dots, d\}$. Given an element $\xi = (x, i) \in \Xi$, we denote the corresponding micro function as $\chi_\xi^{\hat{h}}$ which satisfies the variational equation (2.25) associated to the mapping G_x, i.e.,

$$b(\chi_\xi^{\hat{h}}, z^{\hat{h}}; \xi) = f(z^{\hat{h}}; \xi) \quad \forall z^{\hat{h}} \in S^q(Y, \mathcal{T}_{\hat{h}}),$$

where

$$b(z^{\hat{h}}, w^{\hat{h}}; \xi) = \int_Y A_x(y) \nabla z^{\hat{h}} \cdot \nabla w^{\hat{h}} \, \mathrm{d}y,$$

and

$$f(z^{\hat{h}}; \xi) = \int_Y A_x(y) \mathbf{e}^i \cdot \nabla z^{\hat{h}} \, \mathrm{d}y.$$

In the offline stage, using a greedy procedure which will be described later in the section, we construct a reduced space of precomputed micro functions denoted by

$$S^N(Y) = \mathrm{span}\left\{ \psi_1^{\hat{h}}, \dots, \psi_N^{\hat{h}} \right\},$$

where $N \ll \dim(S^q(Y, \mathcal{T}_{\hat{h}}))$. Then, during the online stage, the problem (2.25) is projected and solved into the functions space $S^N(Y)$. For each $\xi \in \Xi$ we obtain a RB approximation of $\chi_\xi^{\hat{h}}$ by searching for $\chi_\xi^N \in S^N(Y)$ such that

$$b(\chi_\xi^N, \psi_n^{\hat{h}}; \xi) = f(\psi_n^{\hat{h}}; \xi) \quad \forall n = 1, \dots, N.$$

Before describing the greedy algorithm to identify the N reduced basis, we remark that a crucial assumption to deal efficiently with the problem is that the tensor $A_x(y) = A^\varepsilon(G_x(y))$ is available in the affine form

$$A_x(y) = \sum_{q=1}^{Q} \Theta^q(x) A^q(y), \quad \forall y \in Y, \tag{2.26}$$

where $\Theta^q : D \to \mathbb{R}$. If $A_x(y)$ is not directly available in the affine form (2.26), the empirical interpolation method (EIM) [57] can be applied to obtain an affine approximation of $A_x(y)$ of the type

$$A_x^M(y) = \sum_{m=1}^{M} \varphi_m(x) p_m(y).$$

The idea of EIM is to approximate $A_x(y)$ by a linear combination of snapshots $\{p_m(y)\}_{m=1}^{M}$. For an arbitrary $x \in D$, the approximation of A_x is based on the interpolation points $\{y_m\}_{m=1}^{M}$, $y_m \in Y$. The interpolation points and the snapshots are determined offline using a greedy algorithm controlled by an a posteriori error estimate. We refer to [57] for a detailed description of the method. In the online stage, given $x \in D$, $A_x(y)$ is approximated numerically by the following steps.

1. Evaluate $A_x(y)$ at the interpolation points $\{y_m\}_{m=1}^{M}$.

2. Solve the $M \times M$ linear system

$$\sum_{m=1}^{M} \varphi_m(x) p_m(y_m) = A_x(y_m)$$

   to determine the coefficients $\{\varphi_m(x)\}_{m=1}^{M}$.

The affine representation of the tensor is necessary to perform an efficient a posteriori error estimate during the offline stage while adding new basis functions to the reduced space. We refer to [80] for more details, while here we limit ourselves to a brief description of the main ideas. For a given $\xi \in \Xi$, let

$$\hat{e}_\xi^N = \chi_\xi^N - \chi_\xi^{\hat{h}}.$$

From (2.25) follows the identity

$$b(\hat{e}_\xi^N, z^{\hat{h}}; \xi) = b(\chi_\xi^N, z^{\hat{h}}; \xi) - f(z^{\hat{h}}; \xi) \quad \forall z^{\hat{h}} \in S^q(Y, \mathscr{T}_{\hat{h}}).$$

Hence by Riesz's theorem we know the existence of a unique $\overline{e}_\xi^N \in S^q(Y, \mathscr{T}_{\hat{h}})$ such that

$$\langle \overline{e}_\xi^N, z^{\hat{h}} \rangle_{W(Y)} = b(\hat{e}_\xi^N, z^{\hat{h}}; \xi) \quad \forall z^{\hat{h}} \in S^q(Y, \mathscr{T}_{\hat{h}}), \tag{2.27}$$

where $\langle \cdot, \cdot \rangle_{W(Y)}$, defined as

$$\langle z, w \rangle_{W(Y)} = \int_Y \nabla z \cdot \nabla w \, dy,$$

denotes the inner product in the space $W(Y)$ corresponding to (2.11) or (2.12). The error estimate $\overline{e}_\xi^N$ can be computed by solving (2.27). This can be done very efficiently thanks to the affine representation of the tensor $A_x(y)$, since it allows to decompose the right hand side of (2.27), which is parameter dependent, into several bilinear forms which are independent of x and i, and therefore can be precomputed. Finally the a posteriori error estimate is defined as

$$\Delta_\xi^N = \frac{\|\overline{e}_\xi^N\|_{W(Y)}}{\sqrt{\alpha_{\mathrm{LB}}}},$$

where α_{LB} is a lower bound for the coercivity constant of the bilinear form $b(\cdot, \cdot; \cdot)$.

In what follows we briefly list the several steps to perform the greedy offline stage. Input parameters are N_{Train} (the size of the training set), tol_{RB} (a prescribed tolerance used as stopping criterion), and N_{RB} (the maximum number of reduced basis functions allowed).

1. Randomly define (by a Monte Carlo method for example) the training set $\Xi_{\mathrm{Train}} \subset \Xi$

$$\Xi_{\mathrm{Train}} = \{\xi_n = (x_n, i_n) : 1 \le n \le N_{\mathrm{Train}}, x_n \in D, 1 \le i_n \le d\}.$$

2. Select randomly one element from Ξ_{Train}, i.e. ξ_1, and compute $\chi_{\xi_1}^{\hat{h}}$ such that

$$b(\chi_{\xi_1}^{\hat{h}}, z^{\hat{h}}; \xi_1) = f(z^{\hat{h}}; \xi_1) \quad \forall z^{\hat{h}} \in S^q(Y, \mathcal{T}_{\hat{h}}).$$

   Set

$$\psi_1^{\hat{h}} = \frac{\chi_{\xi_1}^{\hat{h}}}{\|\chi_{\xi_1}^{\hat{h}}\|_{W(Y)}},$$

   and initialize the space as $S^1(Y) = \mathrm{span}\left\{\psi_1^{\hat{h}}\right\}$.

3. For $2 \le j \le N_{\mathrm{RB}}$ perform the following steps.
   (a) For each $\xi_n \in \Xi_{\mathrm{Train}}$ compute the corresponding micro function $\chi_{\xi_n}^{j-1} \in S^{j-1}(Y)$ by solving

$$b(\chi_{\xi_n}^{j-1}, \psi_k^{\hat{h}}; \xi_n) = f(\psi_k^{\hat{h}}; \xi_n) \quad \forall k = 1, \ldots, j-1,$$

   and the corresponding residual $\Delta_{\xi_n}^{j-1}$.

(b) Select the new reduced basis by choosing

$$\xi_j = \max_{\xi_n \in \Xi_{\text{Train}}} \Delta_{\xi_n}^{j-1}.$$

(c) If $(\Delta_{\xi_j}^{j-1})^2 < tol_{\text{RB}}$ the algorithm ends, otherwise compute $\chi_{\xi_j}^{\hat{h}}$ such that

$$b(\chi_{\xi_j}^{\hat{h}}, z^{\hat{h}}; \xi_j) = f(z^{\hat{h}}; \xi_j) \quad \forall z^{\hat{h}} \in S^q(Y, \mathcal{T}_{\hat{h}}).$$

Set

$$\psi_j^{\hat{h}} = \frac{R_j^{\hat{h}}}{\|R_j^{\hat{h}}\|_{W(Y)}},$$

where

$$R_j^{\hat{h}} = \chi_{\xi_j}^{\hat{h}} - \sum_{k=1}^{j-1} \langle \chi_{\xi_j}^{\hat{h}}, \psi_k^{\hat{h}} \rangle_{W(Y)} \psi_k^{\hat{h}}.$$

(d) $S^j(Y) = S^{j-1}(Y) \cup \text{span}\left\{\psi_j^{\hat{h}}\right\}.$

The online stage. Having computed the reduced space $S^N(Y)$, we can now introduce a new macro bilinear form similar to (2.17) which reads

$$B_{H,\text{RB}}(v^H, w^H) = \sum_{K \in \mathcal{T}_H} \sum_{j=1}^{J} \omega_{K_j} A^{0,N}(x_{K_j}) \nabla v^H(x_{K_j}) \cdot \nabla w^H(x_{K_j}), \qquad (2.28)$$

where

$$A_{lm}^{0,N}(x_{K_j}) = \int_Y A_{x_{K_j}}(y) \mathbf{e}^l \cdot (\mathbf{e}^m - \nabla \chi_{K_j}^{m,N}) \, dy,$$

and $\chi_{K_j}^{m,N}$ is the solution of (2.25) in the reduced space $S^N(Y)$. Thanks to the affine representation of the tensor $A_x(y)$, computing each micro solution online reduces in solving a $N \times N$ linear system leading to a significant saving of computational effort. During the online stage indeed, given a new $\xi = (x, i) \in \Xi$ we need to solve the problem of finding $\chi_\xi^N \in S^N(Y)$ such that

$$\int_Y A_x(y) \nabla \chi_\xi^N \cdot \nabla \psi_n^{\hat{h}} \, dy = \int_Y A_x(y) \mathbf{e}^i \cdot \nabla \psi_n^{\hat{h}} \, dy \quad \forall n = 1, \dots, N. \qquad (2.29)$$

The function χ_ξ^N can be represented as

$$\chi_\xi^N = \sum_{n=1}^{N} a_n \psi_n^{\hat{h}},$$

where $a_n \in \mathbb{R}$, $1 \le n \le N$. Thanks to the affine representation of $A_x(y)$ solving (2.29) reduces in finding $(a_1, \dots, a_N)^\top \in \mathbb{R}^N$ such that

$$\sum_{q=1}^{Q} \sum_{n=1}^{N} \Theta^q(x) a_n \int_Y A^q(y) \nabla \psi_n^{\hat{h}} \cdot \nabla \psi_{n'}^{\hat{h}} \, dy = \sum_{q=1}^{Q} \Theta^q(x) \int_Y A^q(y) \mathbf{e}^i \cdot \nabla \psi_{n'}^{\hat{h}} \, dy \quad \forall n' = 1, \dots, N,$$

(2.30)

where the integrals in (2.30) are parameter independent and can then be precomputed. Finally the effective macro solution to the problem (2.5), computed by means of the RB-FE-HMM, is given by $u^{H,\mathrm{RB}} = \mathring{u}^{H,\mathrm{RB}} + R_g$, where $\mathring{u}^{H,\mathrm{RB}} \in S_0^l(D, \mathcal{T}_H)$ satisfies

$$B_{H,\mathrm{RB}}(\mathring{u}^{H,\mathrm{RB}}, v^H) = F(v^H) - B_{H,\mathrm{RB}}(R_g, v^H) \quad \forall v^H \in S_0^l(D, \mathcal{T}_H).$$

2.3.2 A priori error analysis

The reduced basis method approximates the solution manifold

$$\mathcal{M}(Y, \mathcal{T}_{\hat{h}}) = \left\{ \chi_\xi^{\hat{h}}, \xi \in \Xi \right\},$$

with linear subspaces of $S^q(Y, \mathcal{T}_{\hat{h}})$ of dimension N. The approximability of $\mathcal{M}(Y, \mathcal{T}_{\hat{h}})$ is described by what is referred to as the Kolmogorov N-width of $\mathcal{M}(Y, \mathcal{T}_{\hat{h}})$ defined as

$$d_N(\mathcal{M}) = \inf_{\substack{S^N \in S^q \\ \dim(S^N) = N}} \sup_{\chi_\xi^{\hat{h}} \in \mathcal{M}} \mathrm{dist}(\chi_\xi^{\hat{h}}, S^N),$$

where

$$\mathrm{dist}(\chi_\xi^{\hat{h}}, S^N) = \min_{\chi_{\xi'}^N \in S^N} \| \chi_\xi^{\hat{h}} - \chi_{\xi'}^N \|_{W(Y)}.$$

In [22] it is proved that for coercive problems, there exists $\gamma \in (0, 1]$ such that:

1. If there are two constants $C_1, a > 0$ such that $d_N(\mathcal{M}) \le C_1 N^{-a} \quad \forall N \ge 0$, then

$$\mathrm{dist}(\chi_\xi^{\hat{h}}, S^N) \le C_1 C_2 N^{-a},$$

where C_2 depends of γ and a only.

2. If there are $C_1, a, b > 0$ such that $d_N(\mathcal{M}) \leq C_1 \exp(-bN^a) \quad \forall N \geq 0$, then

$$\text{dist}(\chi_\xi^{\hat{h}}, S^N) \leq C_1 C_2 \exp(-cN^{a/(a+1)}),$$

where C_2 and c depend on γ and a only.

We are interested in the error due to the reduced basis approach with respect to N. Similarly to (2.20), the error between the exact homogenized solution u^0 and its approximation $u^{H,\text{RB}}$ obtained by means of the RB-FE-HMM can be decomposed as

$$\|u^0 - u^{H,\text{RB}}\|_{H^1(D)} \leq \|e_{\text{mac}}\|_{H^1(D)} + \|e_{\text{mod}}\|_{H^1(D)} + \|e_{\text{mic}}\|_{H^1(D)} + \|e_{\text{RB}}\|_{H^1(D)}.$$

The results obtained in Section 2.2.2 for e_{mac}, e_{mod} and e_{mic} are still valid, and to give a complete a priori error estimate for the RB-FE-HMM we need to consider the new error term $e_{\text{RB}} = u^H - u^{H,\text{RB}}$. From (2.17) and (2.28) we obtain that

$$\|e_{\text{RB}}\|_{H^1(D)} \leq C \sup_{K \in \mathcal{T}_H} \sup_{1 \leq j \leq J} \|A^{0,h}(x_{K_j}) - A^{0,N}(x_{K_j})\|_{\text{F}},$$

which can in turn be bounded by the decay of the Kolmogorov N-width of $\mathcal{M}(Y, \mathcal{T}_{\hat{h}})$. We can not give a priori estimate of the Kolmogorov N-width of the micro solutions manifold. However if it is decaying exponentially, so it will do the error due to the reduced basis approach.

3 Numerical method for solving multi-scale inverse problems via Tikhonov regularization

In this chapter we consider inverse conductivity problems for multiscale scalar elliptic partial differential equations. Let $D \subset \mathbb{R}^d$, $d \leq 3$, be an open, bounded, connected set with sufficiently smooth boundary ∂D and consider the problem of finding the weak solution $u^\varepsilon \in H^1(D)$ to

$$
\begin{aligned}
-\nabla \cdot (A_{\sigma^*}^\varepsilon \nabla u^\varepsilon) &= 0 && \text{in } D, \\
u^\varepsilon &= g && \text{on } \partial D,
\end{aligned}
\tag{3.1}
$$

where $g \in H^{1/2}(\partial D)$, and $A_{\sigma^*}^\varepsilon \in M(\alpha, \beta, D)$ is defined as

$$
A_{\sigma^*}^\varepsilon(x) = A(\sigma^*(x), x/\varepsilon),
$$

where $\sigma^* : D \to \mathbb{R}$ and

$$
A_{ij}(\sigma^*(x), x/\varepsilon) = A_{ij}(\sigma^*(x), y), \quad A_{ij}(\sigma^*(x), \cdot) \text{ is } Y\text{-periodic},
$$

$\forall x \in D$, $\forall i, j = 1, \dots, d$. The tensor $A_{\sigma^*}^\varepsilon$ is a highly oscillatory anisotropic tensor which varies on a microscopic scale ε, and which is parameterized by a scalar function $\sigma^* : D \to \mathbb{R}$. Moreover we assume $A_{\sigma^*}^\varepsilon$ to be symmetric.

In Chapter 2 we have introduced homogenization theory and multiscale methods to obtain in an efficient way effective macroscopic solutions to PDEs of the type as (3.1).

Now, we treat the inverse problem of determining $A_{\sigma^*}^\varepsilon$ from the knowledge of the Dirichlet to Neumann (DtN) map associated to the boundary value problem (3.1). The DtN map is defined as the linear operator $\Lambda_{A_{\sigma^*}^\varepsilon} : H^{1/2}(\partial D) \to H^{-1/2}(\partial D)$ given by

$$
g \mapsto A_{\sigma^*}^\varepsilon \nabla u^\varepsilon \cdot \boldsymbol{v}|_{\partial D},
$$

where $\boldsymbol{v}$ denotes the exterior unit normal to ∂D, and u^ε solves (3.1). The assumption we make is that the map $(t, x) \mapsto A(t, x/\varepsilon)$, $t \in \mathbb{R}$, $x \in D$, is known and σ^* has to be determined. Standard numerical approaches (such as FEM) for solving such problem would require multiple

evaluations of the model (3.1) with mesh resolution at the finest scale. Then, solving the inverse problem for small ε represents a formidable computational challenge and is often not tractable. Hence, in this chapter we propose a coarse graining strategy which relies on numerical homogenization and model order reduction to overcome this computational issue.

Outline. The outline of the chapter is as follows. In Section 3.1 we recall briefly results of uniqueness and stability for the class of inverse problems that we consider. In Section 3.2, assuming that the fine scale inverse problem is well-posed, we prove that the effective inverse problem, with observed data consisting of the homogenized Dirichlet to Neumann map, is also well-posed. In Section 3.3 we establish a convergence result for the solution to the inverse problem in the context of Tikhonov regularization. In Section 3.4 we describe how the multiscale inverse problem is solved numerically, and we provide a convergence analysis of the discrete solution of the inverse problem. In Section 3.5 we present some numerical results to test our theoretical findings and illustrate the viability of our numerical method. The content of this chapter is essentially taken from [9].

3.1 Stability and uniqueness results for inverse problems with parameterized tensors

Let D be an open bounded set in $\mathbb{R}^d$. We consider a multiscale tensor $A_{\sigma^*}^\varepsilon$ of the form $A_{\sigma^*}^\varepsilon(x) = A(\sigma^*(x), x/\varepsilon)$, where $\sigma^* : D \to \mathbb{R}$ is a scalar function with range in $[\sigma^-, \sigma^+]$. The problem we are interested in is to recover $A_{\sigma^*}^\varepsilon$ from measurements of the Dirichlet to Neumann map. The inverse conductivity problem was first introduced by Calderón [26], while inverse conductivity problems for special anisotropic tensors of the form $A_{\sigma^*}(x) = A(\sigma^*(x), x)$ are analyzed in details in [16]. In particular in [16] results on uniqueness and stability at the boundary for the inverse problem are proved in the case where some prior knowledge on the map $(t, x) \mapsto A(t, x)$ is assumed. The goal of this section is to recall such preliminary results, which will be then used to establish similar results for our problem of interest.

In [16] it is required that the tensor $A(t, x)$, $t \in [\sigma^-, \sigma^+]$, $x \in D$, belongs to some special class of matrix functions that we recall below. In what follows we will use the norms

$$\|A\|_{L^p(D)} = \left(\int_D \sum_{i=1}^d \sum_{j=1}^d |A_{ij}(x)|^p \, dx \right)^{1/p}, \quad 1 \le p < \infty,$$

$$\|A\|_{L^\infty(D)} = \max_{1 \le i,j \le d} \operatorname*{ess\,sup}_{x \in D} |A_{ij}(x)|, \qquad p = \infty.$$

for a matrix $A(x) = \{A_{ij}(x)\}_{1 \le i,j \le d}$, $x \in D$.

Definition 3.1.1 (Definition 2.2 in [16]). Given $p > d$, $\alpha, \beta, E_1 > 0$, and denoting by Sym_d the class of $d \times d$ real valued symmetric matrices, we say that $A : [\sigma^-, \sigma^+] \times D \to \mathrm{Sym}_d$ belongs to $\mathscr{H}$ if the following conditions hold for all $t \in [\sigma^-, \sigma^+]$.

1. $A \in W^{1,p}([\sigma^-, \sigma^+] \times D, \mathrm{Sym}_d)$.

2. $\partial_t A \in W^{1,p}([\sigma^-, \sigma^+] \times D, \mathrm{Sym}_d)$.

3. $\underset{t \in [\sigma^-, \sigma^+]}{\mathrm{ess\,sup}} (\|A(t,\cdot)\|_{L^p(D)} + \|\nabla_x A(t,\cdot)\|_{L^p(D)} + \|\partial_t A(t,\cdot)\|_{L^p(D)} + \|\partial_t \nabla_x A(t,\cdot)\|_{L^p(D)})$
   $\leq E_1$.

4. Condition of uniform ellipticity:

$$\alpha|b|^2 \leq A(t,x)b \cdot b, |A(t,x)b| \leq \beta|b|, \quad \text{for a.e. } x \in D$$
$$\text{and } \forall t \in [\sigma^-, \sigma^+], b \in \mathbb{R}^d.$$

5. Condition of monotonicity with respect to the variable t:

$$\partial_t A(t,x)b \cdot b \geq E_1^{-1}|b|^2, \quad \text{for a.e. } x \in D$$
$$\text{and } \forall t \in [\sigma^-, \sigma^+], b \in \mathbb{R}^d.$$

In [16] the following stability result at the boundary for the unknown function σ^* has been shown, in the case where $A_{\sigma^*}(x) = A(\sigma^*(x), x)$, $\sigma^* \in W^{1,p}(D)$, $A(\cdot, \cdot) \in \mathcal{H}$.

Theorem 3.1.2 (See Theorem 2.1 in [16]). *Given $p > d$, let D be a bounded domain with Lipschitz boundary. Given $E > 0$, let σ_1, σ_2 satisfy*

$$\sigma^- \leq \sigma_1(x), \sigma_2(x) \leq \sigma^+ \quad \text{for every } x \in D, \tag{3.2}$$

and

$$\|\sigma_1\|_{W^{1,p}(D)}, \|\sigma_2\|_{W^{1,p}(D)} \leq E. \tag{3.3}$$

Let $A_{\sigma_1}(x) = A(\sigma_1(x), x)$, $A_{\sigma_2}(x) = A(\sigma_2(x), x)$, and $A(\cdot, \cdot) \in \mathcal{H}$. Then we have

$$\|A_{\sigma_1} - A_{\sigma_2}\|_{L^\infty(\partial D)} \leq C\|\Lambda_{A_{\sigma_1}} - \Lambda_{A_{\sigma_2}}\|_{\mathscr{L}(H^{1/2}(\partial D), H^{-1/2}(\partial D))},$$

where C depends on σ^-, σ^+, E, E_1, p, and D.

A uniqueness result is also provided in [16].

Theorem 3.1.3 (See Theorem 2.4 in [16]). *Given $E > 0$, let σ_1 and σ_2 be two scalar functions satisfying (3.2) and (3.3) with $p = \infty$, and $A(\cdot, \cdot) \in \mathcal{H}$. Moreover, assume $A \in W^{1,\infty}([\sigma^-, \sigma^+] \times D, \mathrm{Sym}_d)$. In addition, suppose that D can be partitioned into a finite number of Lipschitz domains $\{D_j\}_{j=1}^N$ such that $\sigma_1 - \sigma_2$ is analytic on each $\overline{D}_j$. If*

$$\Lambda_{A(\sigma_1(x),x)} = \Lambda_{A(\sigma_2(x),x)}$$

then we have

$$A(\sigma_1(x), x) = A(\sigma_2(x), x) \quad \text{in } D.$$

The same results hold for matrix functions of the type $A^\varepsilon_{\sigma^*}(x) = A(\sigma^*(x), x/\varepsilon)$ for fixed ε. However, in this case the constant E_1 in Definition 3.1.1 scales as $1/\varepsilon$, and therefore, as $\varepsilon \to 0$, such results may become useless. Moreover, in numerical experiments, when ε is very small, trying to solve the problem numerically by using an approximation of (3.1) as model for inversion is prohibitive in terms of computational cost, and therefore a different strategy is preferred. Then the motivation for a coarse graining approach, which we obtain by using the framework of homogenization, becomes clear.

3.2 Stability and uniqueness results for the fine scale and the effective inverse problem

In Definition 3.1.1 we have listed the regularity properties that the map $(t, x) \mapsto A(t, x/\varepsilon)$ has to satisfy to ensure stability and uniqueness of the inverse problem. However, we already mentioned that for the class of problems we are interested in, results obtained in [16] are dependent on ε, and a new strategy based on homogenization is preferred. As first step we want to analyze under which conditions on $(t, x) \mapsto A(t, x/\varepsilon)$ the map $t \mapsto A^0(t)$ satisfies the regularity properties to ensure stability and uniqueness for the homogenized inverse problem. First, let us introduce as a corollary of Theorems 3.1.2 and 3.1.3 the conditions that $t \mapsto A^0(t)$ must satisfy to ensure stability and uniqueness.

Corollary 3.2.1. *Given $\alpha, \beta, E_2 > 0$ and $p > d$, let us consider a $d \times d$ symmetric matrix valued function $t \mapsto A(t)$, $t \in [\sigma^-, \sigma^+]$, satisfying the following conditions.*

$$|\partial_t A(t)| + |\partial_t^2 A(t)| \leq E_2, \qquad\qquad \forall t \in [\sigma^-, \sigma^+]. \qquad (3.4)$$

$$\alpha |b|^2 \leq A(t) b \cdot b, |A(t) b| \leq \beta |b|, \qquad\qquad \forall t \in [\sigma^-, \sigma^+], b \in \mathbb{R}^d. \qquad (3.5)$$

$$\partial_t A(t) b \cdot b \geq E_2^{-1} |b|^2, \qquad\qquad \forall t \in [\sigma^-, \sigma^+], b \in \mathbb{R}^d. \qquad (3.6)$$

Let σ_1 and σ_2 be two scalar functions satisfying (3.2) and (3.3). Let $A_{\sigma_1}(x) = A(\sigma_1(x))$ and $A_{\sigma_2}(x) = A(\sigma_2(x))$. Then we have the following results.

1. *The following estimate holds:*

   $$\|A_{\sigma_1} - A_{\sigma_2}\|_{L^\infty(\partial D)} \leq C \|\Lambda_{A_{\sigma_1}} - \Lambda_{A_{\sigma_2}}\|_{\mathscr{L}(H^{1/2}(\partial D), H^{-1/2}(\partial D))},$$

   where C depends on σ^-, σ^+, E, E_2, p, and D.

2. *Let σ_1 and σ_2 satisfy (3.2) and (3.3) with $p = \infty$. In addition, suppose that D can be partitioned into a finite number of Lipschitz domains $\{D_j\}_{j=1}^N$ such that $\sigma_1 - \sigma_2$ is analytic on each $\overline{D}_j$. If*

   $$\Lambda_{A(\sigma_1(x))} = \Lambda_{A(\sigma_2(x))}$$

then we have

$$A(\sigma_1(x)) = A(\sigma_2(x)) \quad in\, D.$$

We also mention the following lemma, which establishes a regularity result for the solutions of the cell problems with respect to the variable t [15].

Lemma 3.2.2. *Assume that $A(t, x/\varepsilon)$ is uniformly elliptic and the map $t \mapsto A(t, x/\varepsilon)$ is of class $C^1([\sigma^-, \sigma^+])$. Let $x/\varepsilon = y$, $y \in Y = (0,1)^d$. Consider the micro functions χ_t^j, $j = 1, \ldots, d$, unique solutions of the following problem: find $\chi_t^j \in W^1_{\mathrm{per}}(Y)$ such that*

$$\int_Y A(t, y)\nabla\chi_t^j \cdot \nabla v \, \mathrm{d}y = \int_Y A(t, y)\mathbf{e}^j \cdot \nabla v \, \mathrm{d}y \quad \forall v \in W^1_{\mathrm{per}}(Y). \tag{3.7}$$

Then the map $t \in [\sigma^-, \sigma^+] \mapsto \chi_t^j \in W^1_{\mathrm{per}}(Y)$ is of class $C^1([\sigma^-, \sigma^+])$ and satisfies

$$\partial_t \chi_t^j = \phi_t^j, \quad \partial_t \nabla\chi_t^j = \nabla\phi_t^j, \tag{3.8}$$

where $\phi_t^j \in W^1_{\mathrm{per}}(Y)$ satisfies

$$\int_Y A(t, y)\nabla\phi_t^j \cdot \nabla v \, \mathrm{d}y = \int_Y \partial_t A(t, y)(\mathbf{e}^j - \nabla\chi_t^j) \cdot \nabla v \, \mathrm{d}y \quad \forall v \in W^1_{\mathrm{per}}(Y). \tag{3.9}$$

Proof. Consider problem (3.7) for the tensors $A(t, y)$ and $A(t + \Delta t, y)$. We have that

$$\int_Y A(t, y)(\nabla\chi_{t+\Delta t}^j - \nabla\chi_t^j) \cdot \nabla v \, \mathrm{d}y$$
$$= \int_Y (A(t + \Delta t, y) - A(t, y))(\mathbf{e}^j - \nabla\chi_{t+\Delta t}^j) \cdot \nabla v \, \mathrm{d}y \quad \forall v \in W^1_{\mathrm{per}}(Y). \tag{3.10}$$

From Lax-Milgram theorem and the fact that $t \mapsto A(t, y)$ is of class $C^1([\sigma^-, \sigma^+])$, we obtain that $\|\chi_{t+\Delta t}^j - \chi_t^j\|_{H^1(Y)} \to 0$ as $\Delta t \to 0$. Now consider the identity (3.10), divide it by Δt, and subtract equation (3.9). We obtain

$$\frac{1}{\Delta t}\int_Y A(t, y)(\nabla\chi_{t+\Delta t}^j - \nabla\chi_t^j) \cdot \nabla v \, \mathrm{d}y - \int_Y A(t, y)\nabla\phi_t^j \cdot \nabla v \, \mathrm{d}y$$
$$= \frac{1}{\Delta t}\int_Y (A(t + \Delta t, y) - A(t, y))(\mathbf{e}^j - \nabla\chi_{t+\Delta t}^j) \cdot \nabla v \, \mathrm{d}y - \int_Y \partial_t A(t, y)(\mathbf{e}^j - \nabla\chi_t^j) \cdot \nabla v \, \mathrm{d}y.$$

By taking the limit $\Delta t \to 0$ we obtain (3.8). $\qquad\square$

Then we can establish the following theorem.

Theorem 3.2.3. *Let $x/\varepsilon = y$, $y \in Y = (0,1)^d$. Given $\alpha, \beta, E_1 > 0$, $p > d$, consider the class of $d \times d$ symmetric matrix functions $(t, y) \mapsto A(t, y)$, where A_{ij} is Y-periodic, $\forall i, j = 1, \ldots, d$, $t \in [\sigma^-, \sigma^+]$. Assume that A satisfies the following conditions.*

$$A \in W^{1,\infty}([\sigma^-, \sigma^+] \times Y, \mathrm{Sym}_d), \quad \partial_t A \in W^{1,\infty}([\sigma^-, \sigma^+] \times Y, \mathrm{Sym}_d), \tag{3.11}$$

$$\|A\|_{L^\infty([\sigma^-, \sigma^+]; L^\infty(Y))} + \|\partial_t A\|_{L^\infty([\sigma^-, \sigma^+]; L^\infty(Y))} + \|\partial_t^2 A\|_{L^\infty([\sigma^-, \sigma^+]; L^\infty(Y))} \leq E_1, \tag{3.12}$$

$$\alpha |b|^2 \leq A(t, y) b \cdot b, |A(x) b| \leq \beta |b|, \quad \text{for a.e. } y \in Y \text{ and } \forall t \in [\sigma^-, \sigma^+], b \in \mathbb{R}^d.$$

$$\partial_t A(t, y) b \cdot b \geq E_1^{-1} |b|^2, \quad \text{for a.e. } y \in Y \text{ and } \forall t \in [\sigma^-, \sigma^+], b \in \mathbb{R}^d. \tag{3.13}$$

Then the homogenized map $t \mapsto A^0(t)$ satisfies (3.4)*-*(3.6)*.*

Proof. We start by showing (3.4). Note that the homogenized coefficients can be rewritten in the form

$$A_{ij}^0(t) = \int_Y A(t, y)(\mathbf{e}^j - \nabla \chi_t^j) \cdot (\mathbf{e}^i - \nabla \chi_t^i) \, dy. \tag{3.14}$$

Differentiating (3.14) with respect to the variable t, we obtain after a straightforward calculation

$$\partial_t A_{ij}^0(t) = \int_Y (\partial_t A(t, y))(\mathbf{e}^j - \nabla \chi_t^j) \cdot (\mathbf{e}^i - \nabla \chi_t^i) \, dy. \tag{3.15}$$

Then from Hölder's inequality we get

$$\operatorname*{ess\,sup}_{t \in [\sigma^-, \sigma^+]} |\partial_t A_{ij}^0(t)|$$

$$\leq \operatorname*{ess\,sup}_{t \in [\sigma^-, \sigma^+]} \|\partial_t A(t, \cdot)\|_{L^\infty(Y)} \|\mathbf{e}^j - \nabla \chi_t^j\|_{L^2(Y)} \|\mathbf{e}^i - \nabla \chi_t^i\|_{L^2(Y)},$$

and by using Lax-Milgram theorem, the triangle inequality, and (3.12) we obtain

$$\operatorname*{ess\,sup}_{t \in [\sigma^-, \sigma^+]} |\partial_t A_{ij}^0(t)|$$

$$\leq \operatorname*{ess\,sup}_{t \in [\sigma^-, \sigma^+]} \|\partial_t A(t, \cdot)\|_{L^\infty(Y)} (1 + \alpha^{-1} \|A(t, \cdot) \cdot \mathbf{e}^j\|_{L^\infty(Y)})(1 + \alpha^{-1} \|A(t, \cdot) \cdot \mathbf{e}^i\|_{L^\infty(Y)})$$

$$\leq E_1 (1 + \alpha^{-1} E_1)^2 = C_1.$$

Now, let $t, s \in [\sigma^-, \sigma^+]$. From (3.15) and Hölder's inequality we have

$$
\begin{aligned}
&|\partial_t A_{ij}^0(t) - \partial_t A_{ij}^0(s)| \\
&\leq \|\partial_t A(t, \cdot) - \partial_t A(s, \cdot)\|_{L^\infty(Y)} \|\mathbf{e}^j - \nabla \chi_t^j\|_{L^2(Y)} \|\mathbf{e}^i - \nabla \chi_t^i\|_{L^2(Y)} \\
&\quad + \|\partial_t A(s, \cdot)\|_{L^\infty(Y)} \|\nabla(\chi_t^j - \chi_s^j)\|_{L^2(Y)} \|\mathbf{e}^i - \nabla \chi_t^i\|_{L^2(Y)} \\
&\quad + \|\partial_t A(s, \cdot)\|_{L^\infty(Y)} \|\mathbf{e}^j - \chi_s^j\|_{L^2(Y)} \|\nabla(\chi_t^i - \chi_s^i)\|_{L^2(Y)}.
\end{aligned}
$$

Now, from the weak definition of the solution of the micro problems, we derive for each $i = 1, \ldots, d$, $s, t \in [\sigma^-, \sigma^+]$, $\forall v \in W_{\mathrm{per}}^1(Y)$

$$
\begin{aligned}
\int_Y A(t, y) \nabla(\chi_t^i - \chi_s^i) \cdot \nabla v \, dy &= \int_Y (A(t, y) - A(s, y)) \mathbf{e}^i \cdot \nabla v \, dy \\
&\quad + \int_Y (A(s, y) - A(t, y)) \nabla \chi_s^i \cdot \nabla v \, dy.
\end{aligned}
$$

By choosing $v = \chi_t^i - \chi_s^i$, using Hölder's inequality and (3.12) we obtain

$$
\begin{aligned}
\|\nabla(\chi_t^i - \chi_s^i)\|_{L^2(Y)} &\leq \alpha^{-1} \|\partial_t A\|_{L^\infty([\sigma^-, \sigma^+]; L^\infty(Y))} (1 + \alpha^{-1} \|A(s, \cdot)\mathbf{e}^i\|_{L^\infty(Y)}) |t - s| \\
&\leq \alpha^{-1} E_1 (1 + \alpha^{-1} E_1) |t - s| \\
&= C_2 |t - s|.
\end{aligned}
$$

Using this latter result and (3.12) gives

$$
\begin{aligned}
|\partial_t A_{ij}^0(t) - \partial_t A_{ij}^0(s)| &\leq (C_1 + 2E_1(1 + \alpha^{-1} E_1) C_2) |t - s| \\
&= C_1(1 + 2\alpha^{-1} E_1)|t - s| = C_3 |t - s|,
\end{aligned}
$$

and (3.4) follows.

The condition of uniform ellipticity, namely

$$
\alpha |b|^2 \leq A^0(t) b \cdot b, |A^0(t) b| \leq \beta |b|, \quad \text{for a.e. } t \in [\sigma^-, \sigma^+], b \in \mathbb{R}^d,
$$

follows from a well-known property of the homogenized tensor (see for example Theorem 6.1 in [33]).

Finally we show that the condition of monotonicity with respect to the variable t holds. From (3.15), by using the notation $\varphi^i = (\mathbf{e}^i - \nabla \chi_t^i)$, $i = 1, \ldots, d$, we have that

$$
\partial_t A_{ij}^0(t) = \int_Y \partial_t A(t, y) \varphi^j \cdot \varphi^i \, dy.
$$

Since $\partial_t A(t, y)$ is symmetric, $\partial_t A^0(t)$ is also symmetric. Then, given $b \in \mathbb{R}^d$,

$$
\begin{aligned}
\partial_t A^0(t) b \cdot b &= b^\top \partial_t A^0(t) b \\
&= \int_Y \sum_{j=1}^d \sum_{i=1}^d b_i {\varphi^i}^\top \partial_t A(t, y) b_j \varphi^j \, \mathrm{d}y \\
&= \int_Y \left(\sum_{i=1}^d b_i \varphi^i \right)^\top \partial_t A(t, y) \left(\sum_{i=1}^d b_i \varphi^i \right) \mathrm{d}y \\
&\geq E_1^{-1} \int_Y \left| \sum_{i=1}^d b_i \varphi^i \right|^2 \mathrm{d}y \geq 0, \quad \text{for any } b \in \mathbb{R}^d.
\end{aligned}
$$

In particular this inequality implies that

$$
\partial_t A^0(t) b \cdot b > 0, \quad \text{for any } b \in \mathbb{R}^d, \, b \neq 0, \tag{3.16}
$$

as can be shown by contradiction using a simple argument. Indeed, if this was not true, one would have some $b \neq 0$ such that

$$
\left| \sum_{i=1}^d b_i \varphi^i \right| = \left| \sum_{i=1}^d b_i (\mathbf{e}^i - \nabla \chi_t^i) \right| = 0.
$$

This means that

$$
\sum_{i=1}^d b_i (y_i - \chi_t^i) = \text{constant},
$$

and then

$$
\sum_{i=1}^d b_i y_i = \sum_{i=1}^d b_i \chi_t^i + \text{constant},
$$

which is impossible since the right hand side is periodic by definition and $b \neq 0$. From (3.16) we easily derive (3.6), and the proof is complete. $\qquad\square$

Theorem 3.2.3 shows that under appropriate regularity assumptions on $(t, x) \mapsto A(t, x/\varepsilon)$, the homogenized real valued tensor $t \mapsto A^0(t)$ satisfies the assumptions of Corollary 3.2.1. Hence, we established stability and uniqueness for the inverse conductivity problem in the case where the measurements at the boundary consist of the homogenized Dirichlet to Neumann map. However, as already mentioned in the introduction to this chapter, this is not the case we are interested in, since we aim at solving the inverse problem when the data consist of the multiscale Dirichlet to Neumann map $\Lambda_{A^\varepsilon_{\sigma*}}$. Moreover, in real experiments we do not have full knowledge of the map $\Lambda_{A^\varepsilon_{\sigma*}}$. Indeed, we would have to know the results of all possible boundary measurements for any Dirichlet boundary condition g, which is impossible. In practice, we consider a set of L experiments, described by a finite set of Dirichlet conditions

$\{g_l\}_{l=1}^{L} \in H^{1/2}(\partial D)$, and for each of them we measure the corresponding boundary flux. Let us define

$$U = \left\{ \sigma \in W^{1,\infty}(D) : \sigma^- \leq \sigma(x) \leq \sigma^+ \right\},$$

$$U_{\text{ad}} = \left\{ \sigma \in U : \|\sigma\|_{W^{1,\infty}(D)} \leq E, E > 0 \right\}.$$

Then we would like to solve the following minimization problem

$$\inf_{\sigma \in U_{\text{ad}}} \sum_{l=1}^{L} \|\Lambda_{A_{\sigma^*}^{\varepsilon}} g_l - \Lambda_{A_{\sigma}^0} g_l\|_{H^{-1/2}(\partial D)}^2,$$

subject to

$$\begin{aligned} -\nabla \cdot (A_{\sigma}^0 \nabla u^0) &= 0 && \text{in } D, \\ u^0 &= g_l && \text{on } \partial D, \end{aligned} \tag{3.17}$$

where $A_{\sigma}^0(x) = A^0(\sigma(x))$ is the homogenized tensor corresponding to $A_{\sigma}^{\varepsilon}(x) = A(\sigma(x), x/\varepsilon)$. It is important to remark that G-convergence of $A(\sigma^*(x), x/\varepsilon)$ to $A^0(\sigma^*(x))$ does not imply convergence of the corresponding fluxes at the boundary in the $H^{-1/2}(\partial D)$-norm, but only weak* convergence, as stated in the following lemma.

Lemma 3.2.4. *Let us consider a sequence of symmetric tensors $\{A_{\sigma}^{\varepsilon}\}_{\varepsilon>0}$ in $M(\alpha, \beta, D)$ which G-converges to $A_{\sigma}^0 \in M(\alpha, \beta, D)$ as $\varepsilon \to 0$. Then $\{\Lambda_{A_{\sigma}^{\varepsilon}} g\}_{\varepsilon>0}$ converges weakly* to $\Lambda_{A_{\sigma}^0} g$ in $H^{-1/2}(\partial D)$ for all $g \in H^{1/2}(\partial D)$ as $\varepsilon \to 0$.*

Proof. From the definition of G-convergence we have that, for any $\psi \in H^1(D)$,

$$\int_D (A_{\sigma}^{\varepsilon} \nabla u^{\varepsilon} - A_{\sigma}^0 \nabla u^0) \cdot \nabla \psi \, dx \to 0 \quad \text{as } \varepsilon \to 0.$$

Then, using integration by parts, we obtain that

$$\langle \Lambda_{A_{\sigma}^{\varepsilon}} g - \Lambda_{A_{\sigma}^0} g, \psi \rangle_{H^{-1/2}(\partial D), H^{1/2}(\partial D)} \to 0 \quad \text{as } \varepsilon \to 0,$$

for each $g, \psi \in H^{1/2}(\partial D)$. Then

$$\Lambda_{A_{\sigma}^{\varepsilon}} g \rightharpoonup \Lambda_{A_{\sigma}^0} g \quad \text{weakly* in } H^{-1/2}(\partial D).$$

$\square$

3.3 Tikhonov regularization: multiscale and coarse grained minimizers

Due to the difficulties of working with fractional-order Sobolev spaces when performing numerical experiments, we will consider the $L^2(\partial D)$-norm to evaluate the distance between data and numerical results produced by the homogenized model.

Assumption 3.3.1. We assume that the boundary conditions g_l of problem (3.17) satisfy $g_l \in H^{3/2}(\partial D)$ for $l = 1, \ldots, L$ and that the corresponding solution $u^0(\sigma, \cdot) \in H^2(D)$ for any $\sigma \in U$.

Let $\Phi^\varepsilon : U \to \mathbb{R}$ be defined as

$$\Phi^\varepsilon(\sigma) = \sum_{l=1}^{L} \|\Lambda_{A_{\sigma^*}^\varepsilon} g_l - \Lambda_{A_\sigma^0} g_l\|_{L^2(\partial D)}^2,$$

and let us consider the minimization problem

$$\overline{\Phi^\varepsilon} = \inf_{\sigma \in U_{\text{ad}}} \Phi^\varepsilon(\sigma). \tag{3.18}$$

Since U_{ad} is a closed, convex and bounded set in $W^{1,\infty}(D)$, it is possible to prove that any minimizing sequence $\{\sigma_n^\varepsilon\}_{n>0}$ for (3.18) contains a subsequence which weakly converges in $H^1(D)$ to $\overline{\sigma}^\varepsilon$, for which we have $\overline{\Phi^\varepsilon} = \Phi^\varepsilon(\overline{\sigma}^\varepsilon)$. This follows from the fact that $H^1(D)$ embeds compactly into $L^r(D)$, $r < \infty$ in two dimensions, $r < 6$ in three dimensions, and that $\Phi^\varepsilon : U \to \mathbb{R}^+$ is continuous with respect to the $L^r(D)$-norm. This continuity result is stated in the Lemma 3.3.3. Before proving such a lemma, let us recall Meyer's theorem on regularity of elliptic problems.

Theorem 3.3.2 (N. G. Meyers, 1963, [69, 55]). *Let $D \in \mathbb{R}^d$ be a bounded open set, with a Lipschitz continuous boundary. Let $A \in M(\alpha, \beta, D)$. There exists a constant $q_1 > 2$, depending on d, D, α, and β only, such that if u is the unique weak solution of*

$$-\nabla \cdot (A \nabla u) = f \qquad \text{in } D,$$
$$u = g \qquad\qquad \text{on } \partial D,$$

and $f \in W^{-1,q'}(D)$, $g \in W^{1/q,q}(\partial D)$, $1/q' + 1/q = 1$, $q \in [2, q_1)$, then $u \in W^{1,q}(D)$ and there exists a constant C_1, depending on d, D, α, β, and q only, such that

$$\|u\|_{W^{1,q}(D)} \leq C_1 (\|R_g\|_{W^{1,q}(D)} + \|f\|_{W^{-1,q'}(D)}),$$

where R_g denotes the extension of g onto $W^{1,q}(D)$.

Lemma 3.3.3. *Let $A^0(\cdot) \in W^{1,\infty}([\sigma^-, \sigma^+], \text{Sym}_d)$ and satisfy (3.4)-(3.5). If a sequence $\{\sigma_n\}_{n>0}$ in U converges to some $\sigma \in U$ in $L^r(D)$, $r \geq 1$, then the sequence $\{\Lambda_{A_{\sigma_n}^0} g\}_{n>0}$ converges to $\Lambda_{A_\sigma^0} g$ in $H^{-1/2}(\partial D)$. Under Assumption 3.3.1, the sequence $\{\Lambda_{A_{\sigma_n}^0} g\}_{n>0}$ converges to $\Lambda_{A_\sigma^0} g$ in $L^2(\partial D)$.*

Proof. It follows from the weak formulation of $u^0(\sigma_n)$ and $u^0(\sigma)$ that, $\forall v \in H_0^1(D)$, we have

$$\int_D (A_\sigma^0 \nabla u^0(\sigma) - A_{\sigma_n}^0 \nabla u^0(\sigma_n)) \cdot \nabla v \, dx = 0.$$

Then

$$\int_D A^0_{\sigma_n}(\nabla u^0(\sigma) - \nabla u^0(\sigma_n)) \cdot \nabla v \, dx = \int_D (A^0_{\sigma_n} - A^0_\sigma)\nabla u^0_\sigma \cdot \nabla v \, dx.$$

By choosing $v = u^0(\sigma) - u^0(\sigma_n) \in H^1_0(D)$, and using Hölder's inequality, we obtain

$$\begin{aligned}
\|\nabla u^0(\sigma) - \nabla u^0(\sigma_n)\|_{L^2(D)} &\le \alpha^{-1}C_1 \|A^0_\sigma - A^0_{\sigma_n}\|_{L^p(D)}\|R_g\|_{W^{1,q}(D)} \\
&\le \alpha^{-1}C_1 E_1\|\sigma - \sigma_n\|_{L^p(D)}\|R_g\|_{W^{1,q}(D)} \quad (3.19) \\
&\le C_2\|\sigma - \sigma_n\|_{L^p(D)},
\end{aligned}$$

where $q \in [2, q_1)$, C_1 comes from Theorem 3.3.2, and p satisfies $1/p + 1/q = 1/2$. We then set $w = A^0_\sigma \nabla u^0(\sigma) - A^0_{\sigma_n}\nabla u^0(\sigma_n)$ and obtain

$$\begin{aligned}
\int_D |w|^2 \, dx &= \int_D A^0_{\sigma_n}(\nabla u^0(\sigma) - \nabla u^0(\sigma_n)) \cdot w \, dx \\
&\quad + \int_D (A^0_\sigma - A^0_{\sigma_n})\nabla u^0(\sigma) \cdot w \, dx \\
&\le \|A^0_{\sigma_n}\|_{L^\infty(D)}\|\nabla u^0(\sigma) - \nabla u^0(\sigma_n)\|_{L^2(D)}\|w\|_{L^2(D)} \\
&\quad + \|A^0_\sigma - A^0_{\sigma_n}\|_{L^p(D)}\|\nabla u^0(\sigma)\|_{L^q(D)}\|w\|_{L^2(D)},
\end{aligned}$$

and hence, by using (3.19) we get

$$\begin{aligned}
\|A^0_\sigma \nabla u^0(\sigma) - A^0_{\sigma_n}\nabla u^0(\sigma_n)\|_{L^2(D)} &\le (E_1 + \alpha)C_2\|\sigma - \sigma_n\|_{L^p(D)} \\
&\le C_4\|\sigma - \sigma_n\|_{L^p(D)}. \quad (3.20)
\end{aligned}$$

Observing that $w \in H(D, \mathrm{div})$ and using the continuity of the map $w \in H(D, \mathrm{div}) \mapsto w \cdot \boldsymbol{\nu} \in H^{-1/2}(\partial D)$, we can finally conclude that

$$\|\Lambda_{A^0_\sigma}g - \Lambda_{A^0_{\sigma_n}}g\|_{H^{-1/2}(\partial D)} \le C_3 C_4\|\sigma - \sigma_n\|_{L^p(D)}.$$

The desired assertion follows immediately if $r \ge p$. Otherwise, if $r < p$, we can exploit the $L^\infty(D)$ bound of the set U, i.e., for any $\sigma \in U$ we have

$$\int_D |\sigma|^p \, dx \le (\sigma^+)^{p-r}\int_D |\sigma|^r \, dx.$$

Assume $u^0 \in H^2(D)$. Then, due to the regularity assumptions on $A^0(t)$, the admissible set U, and u^0, we have that the sequence $\{A^0_{\sigma_n}\nabla u^0(\sigma_n)\}_{n>0}$ is uniformly bounded in $(H^1(D))^d$. Then, there exists a subsequence $\{A^0_{\sigma_{n'}}\nabla u^0(\sigma_{n'})\}_{n'>0}$ such that

$$A^0_{\sigma_{n'}}\nabla u^0(\sigma_{n'}) \rightharpoonup q \quad \text{weakly in } (H^1(D))^d$$

for some $q \in (H^1(D))^d$, and hence

$$A^0_{\sigma_{n'}} \nabla u^0(\sigma_{n'}) \to q \quad \text{strongly in } (L^2(D))^d.$$

But from (3.20) all subsequences $\{A^0_{\sigma_{n'}} \nabla u^0(\sigma_{n'})\}_{n'>0}$ must converge to the same limit, hence

$$A^0_{\sigma_n} \nabla u^0(\sigma_n) \rightharpoonup A^0_\sigma \nabla u^0(\sigma) \quad \text{weakly in } (H^1(D))^d,$$

hence

$$A^0_{\sigma_n} \nabla u^0(\sigma_n) \cdot \boldsymbol{v} \rightharpoonup A^0_\sigma \nabla u^0(\sigma) \cdot \boldsymbol{v} \quad \text{weakly in } H^{1/2}(\partial D),$$

or

$$\Lambda_{A^0_{\sigma_n}} g \rightharpoonup \Lambda_{A^0_\sigma} g \quad \text{weakly in } H^{1/2}(\partial D).$$

Finally, the compact injection $H^{1/2}(\partial D) \subset L^2(\partial D)$ yields

$$A^0_{\sigma_n} \nabla u^0(\sigma_n) \cdot \boldsymbol{v} \to A^0_\sigma \nabla u^0(\sigma) \cdot \boldsymbol{v} \quad \text{strongly in } L^2(\partial D),$$

or

$$\Lambda_{A^0_{\sigma_n}} g \to \Lambda_{A^0_\sigma} g \quad \text{strongly in } L^2(\partial D).$$

$\square$

Let us return to the problem (3.18). In numerical experiments we may prefer to adopt indirect methods to ensure stability of the inverse problem instead of directly imposing a constraint during the minimization procedure. Among the possible methods to regularize inverse problems, we choose Tikhonov regularization (see for example [50, 53]). Tikhonov regularization ensures well-posedness by adding to the cost functional a convex variational penalty, so that the new minimization problem reads

$$\overline{\Psi^\varepsilon} = \inf_{\sigma \in U} \Psi^\varepsilon(\sigma), \tag{3.21}$$

where

$$\Psi^\varepsilon(\sigma) = \Phi^\varepsilon(\sigma) + \gamma R(\sigma),$$

where γ is the regularization parameter, and R is the penalty term. Such penalty term induces a priori knowledge on expected conductivity. In what follows we consider $R(\sigma) = \|\sigma - \sigma_0\|^2_{H^1(D)}$, where σ_0 is a prior guess of σ^*. The regularization parameter controls the trade-off between the Φ^ε and R, and has to be properly chosen. The choice of γ represents a problem of considerable interest and will affect how much oscillation is allowed in any minimizing sequence. As the

regularization parameter γ varies, we obtain different regularized solutions having properties that vary with γ. However, how to choose γ is not the main subject of study of this particular work. For the sake of completeness we mention that several methods have been proposed in the literature, such as the Morozov's discrepancy principle [64, 82] or the L-curve method [58, 59]. Let us introduce the functional $\Psi^0 : U \to \mathbb{R}$, such that

$$\overline{\Psi^0} = \inf_{\sigma \in U} \Psi^0(\sigma), \tag{3.22}$$

where

$$\Psi^0(\sigma) = \Phi^0(\sigma) + \gamma \|\sigma - \sigma_0\|_{H^1(D)}^2,$$

and

$$\Phi^0(\sigma) = \sum_{l=1}^{L} \|\Lambda_{A_{\sigma^*}^0} g_l - \Lambda_{A_{\sigma}^0} g_l\|_{L^2(\partial D)}^2.$$

Remark 3.3.4. From the non-negativity of $\Psi^\varepsilon(\sigma)$ and $\Psi^0(\sigma)$, it follows that $\Psi^\varepsilon(U)$ and $\Psi^0(U)$ are subsets of $\mathbb{R}^+$, and therefore there exist minimizing sequences $\{\sigma_n^\varepsilon\}_{n>0}$ and $\{\sigma_n^0\}_{n>0}$ such that

$$\overline{\Psi^\varepsilon} = \liminf_{n \to \infty} \Psi^\varepsilon(\sigma_n^\varepsilon) = \inf_{\sigma \in U} \Psi^\varepsilon(\sigma),$$
$$\overline{\Psi^0} = \liminf_{n \to \infty} \Psi^0(\sigma_n^0) = \inf_{\sigma \in U} \Psi^0(\sigma).$$

The following lemma is an adaptation of a classical result in non-linear Tikhonov regularization theory (see [52] for example).

Lemma 3.3.5. *Under Assumption 3.3.1 consider a minimizing sequence $\{\sigma_n^0\}_{n>0}$ for (3.22). Then it contains a weakly convergent subsequence in $H^1(D)$ with limit $\overline{\sigma}^0 \in U$ which attains the infimum, i.e., $\overline{\Psi^0} = \Psi^0(\overline{\sigma}^0)$.*

Proof. The set U is a non-empty closed convex subset of $H^1(D)$, hence sequentially weakly closed. From the minimizing property of $\{\sigma_n^0\}_{n>0}$ and the non-negativity of $\Phi^0(\sigma)$ it follows that $\{\sigma_n^0\}_{n>0}$ is bounded in $H^1(D)$. Indeed if this is not the case, there exists a subsequence $\{\sigma_{n'}^0\}_{n'>0}$ such that $\|\sigma_{n'}^0\|_{H^1(D)} \to \infty$ as $n' \to \infty$, hence

$$\Psi^0(\sigma_{n'}^0) \geq \gamma \|\sigma_{n'}^0 - \sigma_0\|_{H^1(D)}^2 \to \infty,$$

and therefore $\overline{\Psi^0} = \infty$. Then $\{\sigma_n^0\}_{n>0}$ admits a subsequence $\{\sigma_{n'}^0\}_{n'>0}$ such that $\sigma_{n'}^0 \rightharpoonup \overline{\sigma}^0$ weakly in $H^1(D)$. Since $\Phi^0 : L^r(D) \cap U \to \mathbb{R}^+$ is continuous (Lemma 3.3.3) and the $H^1(D)$-norm

is weakly lower semi-continuous we have that

$$\Psi^0(\overline{\sigma}^0) \le \liminf_{n'\to\infty} \Psi^0(\sigma^0_{n'}) = \overline{\Psi^0}.$$

Since $\Psi^0(\overline{\sigma}^0) \ge \overline{\Psi^0}$, the result follows. $\qquad\square$

Using the same arguments, we can prove the following lemma.

Lemma 3.3.6. *Consider $u^\varepsilon(\sigma^*) \in H^2(D)$ for each g_l, $l = 1,\dots,L$. Under Assumption 3.3.1 consider a minimizing sequence $\{\sigma^\varepsilon_n\}_{n>0}$ for (3.21). Then it contains a weakly convergent subsequence in $H^1(D)$ with limit $\overline{\sigma}^\varepsilon \in U$ which attains the infimum, i.e., $\overline{\Psi^\varepsilon} = \Psi^\varepsilon(\overline{\sigma}^\varepsilon)$.*

We now state the main result, which quantifies (in a weak sense) the link between the minimization problem (3.21) involving the fine scale Dirichlet to Neumann map $\Lambda_{A^\varepsilon_{\sigma^*}}$ and the homogenized map $\Lambda_{A^0_\sigma}$, and problem (3.22) involving only homogenized maps.

Theorem 3.3.7. *Let the assumptions of Theorem 3.2.3 and Assumption 3.3.1 hold. Consider the sequence of minimization problems of type (3.21) for $\varepsilon \to 0$. Then the sequence of minimizers $\{\overline{\sigma}^\varepsilon\}_{\varepsilon>0}$, such that $\overline{\Psi^\varepsilon} = \Psi^\varepsilon(\overline{\sigma}^\varepsilon)$ for all $\varepsilon > 0$, contains a weakly convergent subsequence $\{\overline{\sigma}^{\varepsilon'}\}_{\varepsilon'>0}$ in $H^1(D)$ with limit $\overline{\sigma} \in U$ which attains the infimum, i.e., $\overline{\Psi^0} = \Psi^0(\overline{\sigma})$. Moreover any weakly convergent subsequence $\{\overline{\sigma}^{\varepsilon'}\}_{\varepsilon'>0}$ in $H^1(D)$ with limit $\overline{\sigma} \in U$ satisfies $\overline{\Psi^0} = \Psi^0(\overline{\sigma})$.*

Proof. The minimizing property of $\{\overline{\sigma}^\varepsilon\}_{\varepsilon>0}$ and the non-negativity of $\Phi^\varepsilon(\sigma)$ imply that the sequence $\{\overline{\sigma}^\varepsilon\}_{\varepsilon>0}$ is bounded in $H^1(D)$. Indeed we have that for each $\varepsilon > 0$, $\Psi^\varepsilon(\overline{\sigma}^\varepsilon)$ is bounded by $\Psi^\varepsilon(\sigma^*)$, which is in turn bounded with respect to ε. From calculations similar to those in the proof of Lemma 3.3.3 we obtain

$$\Psi^\varepsilon(\sigma^*) = \sum_{l=1}^{L} \|\Lambda_{A^\varepsilon_{\sigma^*}} g_l - \Lambda_{A^0_{\sigma^*}} g_l\|^2_{L^2(\partial D)} + \gamma\|\sigma^* - \sigma_0\|^2_{H^1(D)}$$

$$\le \sum_{l=1}^{L} 2\beta^2 \|g_l\|^2_{H^{3/2}(\partial D)} + \gamma\|\sigma^* - \sigma_0\|^2_{H^1(D)}. \tag{3.23}$$

Then $\{\overline{\sigma}^\varepsilon\}_{\varepsilon>0}$ admits a subsequence $\{\overline{\sigma}^{\varepsilon'}\}_{\varepsilon'>0}$ which converges weakly in $H^1(D)$ to some $\overline{\sigma} \in U$. For any subsequence $\{\overline{\sigma}^{\varepsilon'}\}_{\varepsilon'>0}$ which converges weakly in $H^1(D)$ to some $\overline{\sigma} \in U$ we have that

$$\Psi^{\varepsilon'}(\overline{\sigma}^{\varepsilon'}) \le \Psi^{\varepsilon'}(\overline{\sigma}^0) \quad \forall\varepsilon' > 0. \tag{3.24}$$

Moreover, for each $\sigma \in U$ and $\varepsilon > 0$ the following identity holds:

$$\begin{aligned}
\Psi^\varepsilon(\sigma) =& \Phi^\varepsilon(\sigma^*) + \Phi^0(\sigma) + \gamma\|\sigma - \sigma_0\|^2_{H^1(D)} \\
&+ 2\sum_{l=1}^{L} \langle \Lambda_{A^\varepsilon_{\sigma^*}} g_l - \Lambda_{A^0_{\sigma^*}} g_l, \Lambda_{A^0_{\sigma^*}} g_l - \Lambda_{A^0_\sigma} g_l \rangle_{L^2(\partial D)}.
\end{aligned} \tag{3.25}$$

Inserting (3.25) into (3.24), we obtain

$$\Psi^0(\overline{\sigma}^{\varepsilon'}) \le \Psi^0(\overline{\sigma}^0) + 2\sum_{l=1}^{L} \langle \Lambda_{A_{\sigma^*}^{\varepsilon'}} g_l - \Lambda_{A_{\sigma^*}^0} g_l, \Lambda_{A_{\overline{\sigma}^{\varepsilon'}}^0} g_l - \Lambda_{A_{\overline{\sigma}^0}^0} g_l \rangle_{L^2(\partial D)}.$$

From Lemma 3.3.3 and the weak lower semi-continuity of the $H^1(D)$-norm we have that

$$\begin{aligned}
\Psi^0(\overline{\sigma}) &\le \liminf_{\varepsilon'\to 0} \Psi^0(\overline{\sigma}^{\varepsilon'}) \\
&\le \liminf_{\varepsilon'\to 0} \left(\Psi^0(\overline{\sigma}^0) + 2\sum_{l=1}^{L} \langle \Lambda_{A_{\sigma^*}^{\varepsilon'}} g_l - \Lambda_{A_{\sigma^*}^0} g_l, \Lambda_{A_{\overline{\sigma}^{\varepsilon'}}^0} g_l - \Lambda_{A_{\overline{\sigma}^0}^0} g_l \rangle_{L^2(\partial D)} \right) \\
&\le \Psi^0(\overline{\sigma}^0) \\
&\quad + \limsup_{\varepsilon'\to 0} 2\sum_{l=1}^{L} \langle \Lambda_{A_{\sigma^*}^{\varepsilon'}} g_l - \Lambda_{A_{\sigma^*}^0} g_l, \Lambda_{A_{\overline{\sigma}^{\varepsilon'}}^0} g_l \rangle_{L^2(\partial D)} \\
&\quad + \limsup_{\varepsilon'\to 0} 2\sum_{l=1}^{L} \langle \Lambda_{A_{\sigma^*}^{\varepsilon'}} g_l - \Lambda_{A_{\sigma^*}^0} g_l, -\Lambda_{A_{\overline{\sigma}^0}^0} g_l \rangle_{L^2(\partial D)}.
\end{aligned}$$

Using G-convergence of $A(\sigma^*(x), x/\varepsilon)$ to $A^0(\sigma^*(x))$, we obtain that

$$\begin{aligned}
\Psi^0(\overline{\sigma}) &\le \Psi^0(\overline{\sigma}^0) \\
&\quad + \limsup_{\varepsilon'\to 0} 2\sum_{l=1}^{L} \langle \Lambda_{A_{\sigma^*}^{\varepsilon'}} g_l - \Lambda_{A_{\sigma^*}^0} g_l, \Lambda_{A_{\overline{\sigma}^{\varepsilon'}}^0} g_l \rangle_{L^2(\partial D)} \\
&\le \Psi^0(\overline{\sigma}^0) \\
&\quad + \limsup_{\varepsilon'\to 0} 2\sum_{l=1}^{L} \langle \Lambda_{A_{\sigma^*}^{\varepsilon'}} g_l - \Lambda_{A_{\sigma^*}^0} g_l, \Lambda_{A_{\overline{\sigma}}^0} g_l \rangle_{L^2(\partial D)} \\
&\quad + \limsup_{\varepsilon'\to 0} 2\sum_{l=1}^{L} \langle \Lambda_{A_{\sigma^*}^{\varepsilon'}} g_l - \Lambda_{A_{\sigma^*}^0} g_l, \Lambda_{A_{\overline{\sigma}^{\varepsilon'}}^0} g_l - \Lambda_{A_{\overline{\sigma}}^0} g_l \rangle_{L^2(\partial D)} \\
&\le \Psi^0(\overline{\sigma}^0) \\
&\quad + \limsup_{\varepsilon'\to 0} 4\sum_{l=1}^{L} \beta \|g_l\|_{H^{3/2}(\partial D)} \|\Lambda_{A_{\overline{\sigma}^{\varepsilon'}}^0} g_l - \Lambda_{A_{\overline{\sigma}}^0} g_l\|_{L^2(\partial D)} \\
&= \Psi^0(\overline{\sigma}^0) = \overline{\Psi^0}.
\end{aligned}$$

Since $\Psi^0(\overline{\sigma}) \ge \overline{\Psi^0}$, the result follows. $\qquad\square$

As a consequence we then have that $\Psi^0(\overline{\sigma}^{\varepsilon}) \to \Psi^0(\overline{\sigma}^0)$ up to a subsequence when $\varepsilon \to 0$. Hence we have established a link between the solutions to the multiscale problem (3.21) and the solutions to the coarse grained minimization problem (3.22).

3.4 Reduced basis method for the solution of the regularized multi-scale inverse problem

This section is devoted to illustrating how the problem (3.21) is solved numerically. The multiscale method we define is based on the numerical homogenization methods introduced in the previous chapter (FE-HMM and RB-FE-HMM) and a suitable optimization scheme. Given $\sigma \in U$, we have to be able to evaluate numerically $\Psi^\varepsilon(\sigma)$, and hence the following steps are required.

1. Solve for $1 \le l \le L$

$$
\begin{aligned}
-\nabla \cdot (A_\sigma^0 \nabla u^0) &= 0 && \text{in } D, \\
u^0 &= g_l && \text{on } \partial D,
\end{aligned}
\tag{3.26}
$$

   where A_σ^0 is the homogenized tensor corresponding to the locally periodic tensor $A_\sigma^\varepsilon(x) = A(\sigma(x), x/\varepsilon)$.

2. Compute the normal fluxes at the boundary $\Lambda_{A_\sigma^0} g_l$ for $1 \le l \le L$.

FE-HMM setting. In the FE-HMM framework, we discretize the domain by using simplicial elements, and we approximate both macro and micro finite element spaces with piecewise linear polynomials. Hence we introduce

$$
S_0^1(D, \mathcal{T}_H) = \left\{ v^H \in H_0^1(D) : v^H|_K \in \mathcal{P}^1(K), \forall K \in \mathcal{T}_H \right\},
$$

where $\mathcal{T}_H$ is a partition of D in simplicial elements K of diameter H_K, and $\mathcal{P}^1(K)$ is the space of linear polynomials on K. For each macro element, an approximation of the homogenized tensor on each integration point x_K is needed. Such approximation is obtained by solving a micro problem defined on the sampling domains $K_\delta = x_K + (-\delta/2, \delta/2)^d$, with $\delta \ge \varepsilon$. For a sampling domain K_δ we define a micro finite element space

$$
S^1(K_\delta, \mathcal{T}_h) = \left\{ z^h \in W_{\text{per}}^1(K_\delta) : z^h|_T \in \mathcal{P}^1(T), \forall T \in \mathcal{T}_h \right\},
$$

where

$$
W_{\text{per}}^1(K_\delta) = \left\{ z \in H_{\text{per}}^1(K_\delta) : \int_{K_\delta} z \, dx = 0 \right\}.
$$

Let u_l^H be the approximate solution to the effective PDE (3.26) for some l. It is computed by finding $u_l^H = \mathring{u}_l^H + R_{g_l}$, where $\mathring{u}_l^H \in S_0^1(D, \mathcal{T}_H)$ satisfies

$$
B_H(\mathring{u}_l^H, v^H) = -B_H(R_{g_l}, v^H) \quad \forall v^H \in S_0^1(D, \mathcal{T}_H),
$$

where R_{g_l} is a suitable Dirichlet lift of g_l, and

$$B_H(v^H, w^H) = \sum_{K \in \mathcal{T}_H} \frac{|K|}{|K_\delta|} \int_{K_\delta} A(\sigma(x_K), x/\varepsilon) \nabla v_K^h \cdot \nabla w_K^h \, \mathrm{d}x. \tag{3.27}$$

In (3.27) v_K^h (respectively w_K^h) denotes the solution to the micro problem: find v_K^h such that $v_K^h - v^H \in S^1(K_\delta, \mathcal{T}_h)$ and

$$\int_{K_\delta} A(\sigma(x_K), x/\varepsilon) \nabla v_K^h \cdot \nabla z^h \, \mathrm{d}x = 0 \quad \forall z^h \in S^1(K_\delta, \mathcal{T}_h). \tag{3.28}$$

Note that since the multiscale tensor is assumed to be locally periodic and admits explicit scale separation, the slow variable of the tensor $A_\sigma^\varepsilon(x)$ has been collocated at the macro quadrature point in (3.27), (3.28), so that the modeling error vanishes. Let

$$S_c^1(D, \mathcal{T}_H) = \left\{ v^H \in S^1(D, \mathcal{T}_H) : v^H = 0 \text{ at the corners of } D \right\},$$

and $S^1(\partial D, \mathcal{T}_H)$ the finite dimensional space of functions which are restrictions to the boundary of functions living in $S_c^1(D, \mathcal{T}_H)$. The numerical flux is computed by constructing a function $\Lambda_{A_\sigma^{0,h}}^H g_l \in S^1(\partial D, \mathcal{T}_H)$ such that

$$\int_{\partial D} \Lambda_{A_\sigma^{0,h}}^H g_l v^H \, \mathrm{d}s = B_H(u^H, v^H) \quad \forall v^H \in S_c^1(D, \mathcal{T}_H),$$

where the value of the flux at the corners of D is assumed to be known, as specified by direct calculations from the given Dirichlet conditions. Let

$$U^H = \left\{ \sigma^H \in S^1(D, \mathcal{T}_H) : \sigma^- \leq \sigma^H \leq \sigma^+ \right\}$$

be the admissible set for the discrete solution to the inverse problem, where

$$S^1(D, \mathcal{T}_H) = \left\{ v^H \in H^1(D) : v^H|_K \in \mathcal{P}^1(K), \forall K \in \mathcal{T}_H \right\}.$$

Given the set of boundary values

$$g_l \qquad 1 \leq l \leq L,$$

the discrete minimization problem reads as follows: find $\overline{\sigma}^{\varepsilon, H} \in U^H$ such that

$$\Psi_{H,h}^\varepsilon(\overline{\sigma}^{\varepsilon, H}) = \inf_{\sigma^H \in U^H} \Psi_{H,h}^\varepsilon(\sigma^H), \tag{3.29}$$

where

$$\Psi_{H,h}^\varepsilon(\sigma^H) = \sum_{l=1}^L \|\Lambda_{A_{\sigma^*}^\varepsilon} g_l - \Lambda_{A_{\sigma^H}^{0,h}}^H g_l\|_{L^2(\partial D)}^2 + \gamma\|\sigma^H - \sigma_0\|_{H^1(D)}^2$$
$$= \Phi_{H,h}^\varepsilon(\sigma^H) + \gamma\|\sigma^H - \sigma_0\|_{H^1(D)}^2.$$

Optimization scheme. The minimization problem is solved by means of the interior point algorithm (see for example [25]). Let N_H be the number of macro DOFs associated to the finite element space $S^1(D, \mathcal{T}_H)$. The unknown variable σ_H can be then represented as

$$\sigma^H(x) = \sum_{i=1}^{N_H} \sigma_i \varphi_i(x), \tag{3.30}$$

where $\boldsymbol{\sigma} = (\sigma_1, \ldots, \sigma_{N_h})^\top \in \mathbb{R}^{N_H}$ is the vector containing the unknown coefficients, and φ_i, $1 \le i \le N_H$, are the Lagrange basis functions for the space $S^1(D, \mathcal{T}_H)$. The minimization problem (3.29) can be then rewritten in the equivalent form

$$\inf_{\boldsymbol{\sigma}\in\mathbb{R}^{N_H}} \Psi_{H,h}^\varepsilon(\sigma^H) \quad \text{such that } c(\boldsymbol{\sigma}) \le 0, \tag{3.31}$$

where $c(\boldsymbol{\sigma}) = (c_1(\boldsymbol{\sigma}), c_2(\boldsymbol{\sigma}))$, $c_1, c_2 : \mathbb{R}^{N_H} \to \mathbb{R}^{N_H}$ are defined as

$$c_1(\boldsymbol{\sigma}) = \sigma^- - \boldsymbol{\sigma}, \quad c_2(\boldsymbol{\sigma}) = \boldsymbol{\sigma} - \sigma^+.$$

Following [25] we consider the approximate minimization problem

$$\inf_{\boldsymbol{\sigma}\in\mathbb{R}^{N_H}, \mathbf{s}\in\mathbb{R}^M} \Psi_{H,h}^\varepsilon(\sigma^H) - \mu \sum_{i=1}^M \ln(s_i) \quad \text{such that } c(\boldsymbol{\sigma}) + \mathbf{s} = 0, \tag{3.32}$$

where $M = 2N_H$ is the number of inequality constraints in (3.31). The logarithmic term is referred to as barrier function, the coefficient $\mu > 0$ is the barrier parameter, and the variable $\mathbf{s} = (s_1, \ldots, s_M)^\top$ is assumed to be larger than zero, so that $\ln(s_i)$ remains bounded $\forall i$, $1 \le i \le M$. We have transformed the inequality constrained problem (3.31) into an equality constrained problem. Note that if we let $\mu \to 0$ the solution of problem (3.32) should converge to the solution of problem (3.31). The idea is then to solve problem (3.32) for a sequence of barrier parameters $\{\mu_1, \ldots, \mu_N\}$, so that $\mu_n > \mu_{n+1}$ $\forall n$, $\mu_N = 0$. To characterize the solution of (3.32) we introduce the corresponding Lagrangian

$$\mathcal{L}(\boldsymbol{\sigma}, \mathbf{s}, \boldsymbol{\lambda}) = \Psi_{H,h}^\varepsilon(\sigma^H) - \mu \sum_{i=1}^M \ln(s_i) + \boldsymbol{\lambda}^\top(c(\boldsymbol{\sigma}) + \mathbf{s}),$$

where $\boldsymbol{\lambda} \in \mathbb{R}^M$ is the vector of Lagrange multipliers. The Karush-Kuhn-Tucker (KKT) optimality conditions for the problem (3.32) lead to solving the following system of equations

$$\nabla_{\boldsymbol{\sigma}} \mathcal{L}(\boldsymbol{\sigma}, \mathbf{s}, \boldsymbol{\lambda}) = \nabla_{\boldsymbol{\sigma}} \Psi_{H,h}^{\varepsilon}(\sigma^H) + J_{\boldsymbol{\sigma}}^c(\boldsymbol{\sigma})^\top \boldsymbol{\lambda} = 0,$$
$$\nabla_{\mathbf{s}} \mathcal{L}(\boldsymbol{\sigma}, \mathbf{s}, \boldsymbol{\lambda}) = -\mu \operatorname{diag}(\mathbf{s})^{-1} \mathbf{e} + \boldsymbol{\lambda} = 0,$$
$$\nabla_{\boldsymbol{\lambda}} \mathcal{L}(\boldsymbol{\sigma}, \mathbf{s}, \boldsymbol{\lambda}) = c(\boldsymbol{\sigma}) + \mathbf{s} = 0,$$

where $J_{\boldsymbol{\sigma}}^c$ is the Jacobian matrix of c computed with respect to $\boldsymbol{\sigma}$, and $\mathbf{e} = (1,\dots,1)^\top \in \mathbb{R}^M$. A Newton iteration on the KKT conditions leads to the following linear system

$$\begin{pmatrix} \nabla_{\boldsymbol{\sigma\sigma}}^2 \mathcal{L}(\boldsymbol{\sigma}_k, \boldsymbol{\lambda}_{\text{old}}) & 0 & (J_{\boldsymbol{\sigma}}^c(\boldsymbol{\sigma}_k))^\top \\ 0 & \mu \operatorname{diag}(\mathbf{s}_k)^{-2} & \mathbf{I} \\ J_{\boldsymbol{\sigma}}^c(\boldsymbol{\sigma}_k) & \mathbf{I} & 0 \end{pmatrix} \begin{pmatrix} \Delta\boldsymbol{\sigma} \\ \Delta\mathbf{s} \\ \boldsymbol{\lambda}_{\text{new}} \end{pmatrix} = \begin{pmatrix} -\nabla_{\boldsymbol{\sigma}} \Psi_{H,h}^{\varepsilon}(\sigma_k^H) \\ \mu \operatorname{diag}(\mathbf{s}_k)^{-1} \mathbf{e} \\ -c(\boldsymbol{\sigma}_k) - \mathbf{s}_k \end{pmatrix},$$

$(\boldsymbol{\sigma}_{k+1}, \mathbf{s}_{k+1}) = (\boldsymbol{\sigma}_k + \Delta\boldsymbol{\sigma}, \mathbf{s}_k + \Delta\mathbf{s})$, where $\nabla_{\boldsymbol{\sigma\sigma}}^2 \mathcal{L}$ denotes the Hessian matrix of $\mathcal{L}$ with respect to the variable $\boldsymbol{\sigma}$. In order to measure the optimality conditions we introduce the merit function

$$F(\boldsymbol{\sigma}, \mathbf{s}; \mu) = \max\{\|\nabla_{\boldsymbol{\sigma}} \mathcal{L}(\boldsymbol{\sigma}, \mathbf{s}, \boldsymbol{\lambda})\|_2, \|\nabla_{\mathbf{s}} \mathcal{L}(\boldsymbol{\sigma}, \mathbf{s}, \boldsymbol{\lambda})\|_2, \|\nabla_{\boldsymbol{\lambda}} \mathcal{L}(\boldsymbol{\sigma}, \mathbf{s}, \boldsymbol{\lambda})\|_2\}.$$

Then, given a starting point $(\boldsymbol{\sigma}_0, \mathbf{s}_0)$, a sequence of barrier parameters $\{\mu_1,\dots,\mu_N\}$, so that $\mu_n > \mu_{n+1} \; \forall n$, $\mu_N = 0$, and corresponding tolerances $\{tol_{\mu_1},\dots,tol_{\mu_N}\}$, $tol_{\mu_n} > tol_{\mu_{n+1}} \; \forall n$, the algorithm is given by the following steps.

1. For $1 \le n \le N$ perform the following operations.
    (a) Starting from $\boldsymbol{\sigma}_0 \in \mathbb{R}^{N_H}$, $\mathbf{s}_0 \in \mathbb{R}^M$, use Newton to find $\overline{\boldsymbol{\sigma}} \in \mathbb{R}^{N_H}$, $\overline{\mathbf{s}} \in \mathbb{R}^M$ such that

$$F(\overline{\boldsymbol{\sigma}}, \overline{\mathbf{s}}; \mu_n) \le tol_{\mu_n}.$$

    (b) Set $\boldsymbol{\sigma}_0 = \overline{\boldsymbol{\sigma}}$, $\mathbf{s}_0 = \overline{\mathbf{s}}$.
2. Set $\overline{\boldsymbol{\sigma}}^\varepsilon = \overline{\boldsymbol{\sigma}}$.

Finally accordingly to (3.29) and (3.30) we define the discrete solution to the inverse problem as

$$\overline{\sigma}^{\varepsilon,H}(x) = \sum_{i=1}^{N_H} \overline{\sigma}_i^\varepsilon \varphi_i(x),$$

where $\overline{\boldsymbol{\sigma}}^\varepsilon = (\overline{\sigma}_1^\varepsilon,\dots,\overline{\sigma}_{N_H}^\varepsilon)^\top \in \mathbb{R}^{N_H}$.

Convergence analysis with respect to macro and micro discretization. The set U^H is finite dimensional and uniformly bounded. Thus the existence of a minimizer $\overline{\sigma}^{\varepsilon,H} \in U^H$ to the discrete optimization problem (3.29) is ensured for any $H > 0$ by compactness and continuity of $\Psi_{H,h}^\varepsilon$. One question we would like to answer, is whether the sequence $\{\overline{\sigma}^{\varepsilon,H}\}_{H>0}$ of discrete

solutions converges to a minimizer $\overline{\sigma}^\varepsilon$ of the continuous problem as we refine the mesh. To this end we first state a discrete analogue of Lemma 3.3.3.

Lemma 3.4.1. *Suppose the assumptions of Theorem 2.2.5 and Lemma 3.3.3 hold, and let the sequence $\{\sigma^H\}_{H>0}$ in $U^H \subset U$ converge in $L^r(D)$, $r \geq 1$, to some $\sigma \in U$ as $H \to 0$. Then the sequence of approximations $\{\Lambda^H_{A^{0,h}_{\sigma^H}} g\}_{H>0}$ converges to $\Lambda_{A^0_\sigma} g$ in $L^2(\partial D)$ as $H \to 0$.*

Proof. The desired assertion easily follows from Lemma 3.3.3 and the estimate (2.24). $\square$

Now, thanks to Lemma 3.4.1 we can state the convergence of the discrete approximate solutions $\{\overline{\sigma}^{\varepsilon,H}\}_{H>0}$. Let $\overline{\sigma}^\varepsilon$ be a solution of the regularized inverse problem in the infinite dimension, so that

$$\Psi^\varepsilon(\overline{\sigma}^\varepsilon) = \inf_{\sigma \in U} \Psi^\varepsilon(\sigma), \tag{3.33}$$

where

$$\Psi^\varepsilon(\sigma) = \sum_{l=1}^{L} \|\Lambda_{A^\varepsilon_{\sigma*}} g_l - \Lambda_{A^0_\sigma} g_l\|^2_{L^2(\partial D)} + \gamma \|\sigma - \sigma_0\|^2_{H^1(D)}$$

$$= \Phi^\varepsilon(\sigma) + \gamma \|\sigma - \sigma_0\|^2_{H^1(D)}.$$

Theorem 3.4.2. *Suppose the assumptions of Theorem 2.2.5 hold, and consider the sequence of minimization problems of type (3.29) for $H \to 0$. The sequence of minimizers $\{\overline{\sigma}^{\varepsilon,H}\}_{H>0}$ contains a subsequence that converges weakly in $H^1(D)$ to a minimizer $\hat{\sigma}^\varepsilon$ of problem (3.33) as $H \to 0$.*

Proof. Our proof is inspired from [56]. Here we briefly sketch the main steps to obtain the desired result. Let $\mathscr{I}^H = U \to U^H$ be the linear interpolation operator. We start by noting that the minimizing properties of $\{\overline{\sigma}^{\varepsilon,H}\}_{H>0}$ imply that for each $H, h > 0$, $\Psi^\varepsilon_{H,h}(\overline{\sigma}^{\varepsilon,H})$ is bounded by $\Psi^\varepsilon_{H,h}(\mathscr{I}^H \overline{\sigma}^\varepsilon)$, which, thanks to (3.23) is in turn bounded independently of H and h. Then, $\{\overline{\sigma}^{\varepsilon,H}\}_{H>0}$ admits a subsequence $\{\overline{\sigma}^{\varepsilon,H'}\}_{H'>0}$ which weakly converges to some $\hat{\sigma}^\varepsilon$ in $H^1(D)$. It remains now to show that $\hat{\sigma}^\varepsilon$ is indeed a minimizer of problem (3.33). Since $C^\infty(\overline{D})$ is dense in $H^1(D)$, we have that for any $\sigma \in U$ there exists a sequence $\{\sigma_n\}_{n>0}$ in $C^\infty(\overline{D}) \cap U$ such that

$$\lim_{n \to \infty} \|\sigma_n - \sigma\|_{H^1(D)} = 0. \tag{3.34}$$

The minimizing properties of $\{\overline{\sigma}^{\varepsilon,H'}\}_{H'>0}$ imply that

$$\Psi^\varepsilon_{H',h}(\overline{\sigma}^{\varepsilon,H'}) \leq \Psi^\varepsilon_{H',h}(\mathscr{I}^H \sigma_n) \quad \forall n > 0.$$

Letting $H' \to 0$, we obtain from the approximation properties of $\mathscr{I}^H$ and Lemma 3.4.1 that

$$\Psi^\varepsilon(\hat{\sigma}^\varepsilon) \leq \Psi^\varepsilon(\sigma_n) \quad \forall n > 0.$$

3.4. Reduced basis method for the solution of the regularized multiscale inverse problem

By letting $n \to \infty$, we deduce from (3.34) and Lemma 3.3.3 that

$$\Psi^\varepsilon(\hat{\sigma}^\varepsilon) \leq \Psi^\varepsilon(\sigma) \quad \forall \sigma \in U,$$

and the desired assertion follows. $\qquad\square$

Model order reduction. Having to solve (3.29) requires a large number of evaluations of the function $\Psi^\varepsilon_{H,h}$, and so multiple computations of micro solutions, for each macro element and each macro quadrature point. If we map each micro problem into the reference cell $Y = (0, 1)^d$ through $x = G_{x_K}(y) = x_K + \delta(y - 1/2)$, with $\delta = n\varepsilon$, $n \in \mathbb{N}$, $n > 0$, we can define an alternative version of (3.27) as

$$B_H(v^H, w^H) = \sum_{K \in \mathscr{T}_H} |K| A^{0,h}(\sigma(x_K)) \nabla v^H(x_K) \cdot \nabla w^H(x_K),$$

where

$$A^{0,h}_{ij}(\sigma(x_K)) = \int_Y A(\sigma(x_K), y) \mathbf{e}^i \cdot (\mathbf{e}^j - \nabla \chi_K^{j,\hat{h}}) \, \mathrm{d}y,$$

where $\hat{h} = h/\delta$, and $\chi_K^{j,\hat{h}} \in S^1(Y, \mathscr{T}_{\hat{h}})$ is the solution of

$$\int_Y A(\sigma(x_K), y) \nabla \chi_K^{j,\hat{h}} \cdot \nabla z^{\hat{h}} \, \mathrm{d}y = \int_Y A(\sigma(x_K), y) \mathbf{e}^j \cdot \nabla z^{\hat{h}} \, \mathrm{d}y \quad \forall z^{\hat{h}} \in S^1(Y, \mathscr{T}_{\hat{h}}). \tag{3.35}$$

We note that each micro solution $\chi_K^{j,\hat{h}}$ is parameterized by the value of $\sigma(x_K)$, and so, in the spirit of Section 2.3, we build during an offline stage a reduced space of precomputed micro functions, to perform fast evaluations of the micro problems when solving the inverse problem online. Similarly to Section 2.3 we define the space of parameters as $\Xi = [\sigma^-, \sigma^+] \times \{1, \ldots, d\}$. Given an element $\xi = (t, i) \in \Xi$, the corresponding micro solution is denoted by $\chi_\xi^{\hat{h}}$ and satisfies

$$b(\chi_\xi^{\hat{h}}, z^{\hat{h}}; \xi) = f(z^{\hat{h}}; \xi) \quad \forall z^{\hat{h}} \in S^1(Y, \mathscr{T}_{\hat{h}}),$$

where

$$b(z^{\hat{h}}, \hat{w}^{\hat{h}}; \xi) = \int_Y A(t, y) \nabla z^{\hat{h}} \cdot \nabla \hat{w}^{\hat{h}} \, \mathrm{d}y,$$

and

$$f(z^{\hat{h}}; \xi) = \int_Y A(t, y) \mathbf{e}^i \cdot \nabla z^{\hat{h}} \, \mathrm{d}y.$$

Then starting from a training set randomly defined

$$\Xi_{\text{Train}} = \left\{ \xi_n = (t_n, i_n) : 1 \le n \le N_{\text{Train}}, t_n \in [\sigma^-, \sigma^+], 1 \le i_n \le d \right\},$$

we perform the greedy offline stage described in Section 2.3 to build the reduced space

$$S^N(Y) = \text{span}\left\{ \psi_1^{\hat{h}}, \dots, \psi_N^{\hat{h}} \right\}.$$

We make the assumption that the tensor $A(t, y)$ is available in the affine form

$$A(t, y) = \sum_{q=1}^{Q} \Theta_q(t) A_q(y), \quad \forall y \in Y,$$

where $\Theta_q : \mathbb{R} \to \mathbb{R}$. Otherwise, we apply the empirical interpolation method to obtain an affine approximation of $A(t, y)$. Once the offline stage is concluded, we can define the new macro bilinear form

$$B_{H,\text{RB}}(v^H, w^H) = \sum_{K \in \mathscr{T}_H} A^{0,N}(\sigma(x_K)) \nabla v^H(x_K) \cdot \nabla w^H(x_K),$$

where

$$A_{ij}^{0,N}(\sigma(x_K)) = \int_Y A(\sigma(x_K), y) \mathbf{e}^i \cdot (\mathbf{e}^j - \nabla \chi_K^{j,N}) \, dy,$$

and $\chi_K^{j,N}$ is the solution of (3.35) computed on the reduced space $S^N(Y)$. Hence the approximated macro solution of problem (3.26) computed by means of the RB-FE-HMM is given by $u_l^{H,\text{RB}} = \mathring{u}_l^{H,\text{RB}} + R_{g_l}$, where $\mathring{u}_l^{H,\text{RB}} \in S_0^1(D, \mathscr{T}_H)$ satisfies

$$B_{H,\text{RB}}(\mathring{u}_l^{H,\text{RB}}, v^H) = -B_{H,\text{RB}}(R_{g_l}, v^H) \quad \forall v^H \in S_0^1(D, \mathscr{T}_H),$$

where R_{g_l} is a Dirichlet lift of g_l properly chosen. The corresponding normal flux at the boundary is given by $\Lambda_{A_\sigma^{0,N}}^H g_l \in S^1(\partial D, \mathscr{T}_H)$ such that

$$\int_{\partial D} \Lambda_{A_\sigma^{0,N}}^H g_l v^H \, ds = B_{H,\text{RB}}(u_l^{H,\text{RB}}, v^H) \quad \forall v^H \in S_c^1(D, \mathscr{T}_H).$$

Remark 3.4.3. In the RB-FE-HMM framework the discrete inverse problem we need to solve is

$$\Psi_{H,N}^\varepsilon(\overline{\sigma}^{\varepsilon,H}) = \inf_{\sigma^H \in U^H} \Psi_{H,N}^\varepsilon(\sigma^H) \tag{3.36}$$

where

$$\Psi_{H,N}^{\varepsilon}(\sigma^H) = \sum_{l=1}^{L} \|\Lambda_{A_{\sigma^*}^{\varepsilon}} g_l - \Lambda_{A_{\sigma^H}^{0,N}}^{H} g_l\|_{L^2(\partial D)}^2 + \gamma \|\sigma^H - \sigma_0\|_{H^1(D)}^2$$

$$= \Phi_{H,N}^{\varepsilon}(\sigma^H) + \gamma \|\sigma^H - \sigma_0\|_{H^1(D)}^2.$$

The convergence results established in Lemma 3.4.1 and Theorem 3.4.2 still hold. In the convergence analysis we need to take into account the error due to the model order reduction. This error is based on the distance between the reduced space $S^N(Y)$ and the space $S^1(Y, \mathcal{T}_{\hat{h}})$. Such distance can be quantified by means of the notion of Kolmogorov N-width (see Chapter 2).

Summary of the multiscale method to solve the inverse problem. The numerical method to solve the discrete inverse problem (3.36) can be summarized as follows.

1. During the offline stage construct a reduced space of micro functions $S^N(Y)$.

2. For each new guess $\sigma^H \in U^H$ in order to evaluate $\Psi_{H,N}^{\varepsilon}(\sigma^H)$ while performing the interior point algorithm, for $1 \le l \le L$ we do the following operations.

   (a) Find $u_l^{H,\mathrm{RB}} = \mathring{u}_l^{H,\mathrm{RB}} + R_{g_l}$, where $\mathring{u}_l^{H,\mathrm{RB}} \in S_0^1(D, \mathcal{T}_H)$ satisfies

   $$B_{H,\mathrm{RB}}(\mathring{u}_l^{H,\mathrm{RB}}, v^H) = -B_{H,\mathrm{RB}}(R_{g_l}, v^H) \quad \forall v^H \in S_0^1(D, \mathcal{T}_H),$$

   where R_{g_l} is a Dirichlet lift of g_l properly chosen, and

   $$B_{H,\mathrm{RB}}(v^H, w^H) = \sum_{K \in \mathcal{T}_H} A^{0,N}(\sigma^H(x_K)) \nabla v^H(x_K) \cdot \nabla w^H(x_K),$$

   where

   $$A_{ij}^{0,N}(\sigma^H(x_K)) = \int_Y A(\sigma^H(x_K), y) \mathbf{e}^i \cdot (\mathbf{e}^j - \nabla \chi_K^{j,N}) \, dy,$$

   and $\chi_K^{j,N}$ is a micro solution computed on the reduced space $S^N(Y)$.

   (b) Find $\Lambda_{A_{\sigma^H}^{0,N}}^{H} g_l \in S^1(\partial D, \mathcal{T}_H)$ such that

   $$\int_{\partial D} \Lambda_{A_{\sigma^H}^{0,N}}^{H} g_l v^H \, ds = B_{H,\mathrm{RB}}(u_l^{H,\mathrm{RB}}, v^H) \quad \forall v^H \in S_c^1(D, \mathcal{T}_H).$$

3.5 Numerical experiments

In this section we present numerical experiments that illustrate the behavior of the proposed numerical method for solving inverse problems. We first explain how we define the Dirichlet

conditions $\{g_l\}_{l=1}^L$ and how we collect multiscale observations. Then, we solve the inverse problem for two different types of macroscopic parameterizations: an affine parameterization which controls the amplitude of the micro oscillations characterizing $A_{\sigma^*}^\varepsilon$, and a non-affine parameterization controlling their orientation. In particular, for the first parameterization, we perform different numerical tests to observe the sensitivity of the results with respect to the several parameters involved (γ, ε, H, L) and assess our theoretical findings. For the second parameterization, we fix the values of such parameters and we report the solution obtained by means of the proposed algorithm for solving multiscale inverse problems. To conclude, we remark that the forward homogenized problem is computed by means of the RB-FE-HMM, and the offline stage is performed for the following choice of the parameters: $h/\varepsilon = 1/64$, $\delta = \varepsilon$, $tol_{\mathrm{RB}} = 10^{-11}$, where tol_{RB} is the prescribed tolerance used as stopping criterion for the greedy process we use to select the micro basis functions.

3.5.1 Setup

The setup of the numerical experiments is as follows. The domain D is defined as

$$D = \{x = (x_1, x_2) : 0 < x_1, x_2 < 1\} .$$

We then compute the multiscale fluxes $\Lambda_{A_{\sigma^*}^\varepsilon}^{h_{\mathrm{obs}}} g_l$ for different Dirichlet conditions $\{g_l\}_{l=1}^L$ by means of FEM, using a mesh size $h_{\mathrm{obs}} \ll \varepsilon$. In particular we take $\{g_l\}_{l=1}^L = \{\sqrt{\lambda_l}\varphi_l\}_{l=1}^L$, where $\{(\lambda_l, \varphi_l)\}_{l=1}^L$ are the L eigenpairs corresponding to the smallest L eigenvalues of the one dimensional discrete Laplacian operator. Each g_l is then interpolated on the boundary ∂D to define the respective Dirichlet condition. This procedure ensures that the functions $\{g_l\}_{l=1}^L$ are smooth and orthonormal, so that each contribution is independent from the others. Moreover $\|\nabla g_l\|_{L^2(\partial D)} < C$, where C is a constant independent of L. In Figure 3.1 the first five g_l functions are shown.
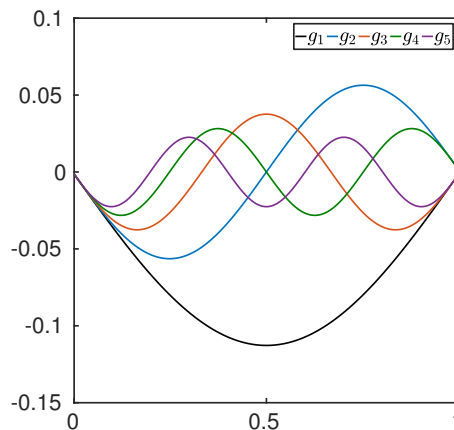

Figure 3.1: First five Dirichlet conditions used for the numerical experiments.

3.5.2 A 2D affinely parameterized tensor

For the first parameterization we consider a tensor $A_{\sigma^*}^{\varepsilon}$ given by

$$A_{11}(\sigma^*(x), x/\varepsilon) = \sigma^*(x)\left(\cos^2\left(2\pi\frac{x_1}{\varepsilon}\right) + 1\right) + \cos^2\left(2\pi\frac{x_2}{\varepsilon}\right),$$

$$A_{22}(\sigma^*(x), x/\varepsilon) = \sigma^*(x)\left(\sin\left(2\pi\frac{x_2}{\varepsilon}\right) + 2\right) + \cos^2\left(2\pi\frac{x_1}{\varepsilon}\right),$$

$$A_{12}(\sigma^*(x), x/\varepsilon) = A_{21}(\sigma^*(x), x/\varepsilon) = 0,$$

where

$$\sigma^*(x) = 16(x_1^2 - x_1)(x_2^2 - x_2) + 1.$$

For this first set of numerical experiments σ^* is a simple smooth parabola, and its profile, together with that of $A_{\sigma^*}^{\varepsilon}$, is shown in Figure 3.2.
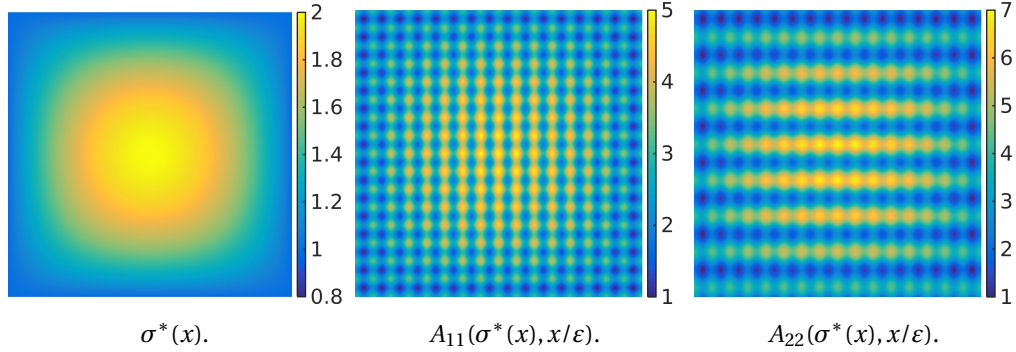
$\sigma^*(x)$. $\qquad\qquad A_{11}(\sigma^*(x), x/\varepsilon)$. $\qquad\qquad A_{22}(\sigma^*(x), x/\varepsilon)$.

Figure 3.2: The true field σ^* and the two components $A_{11}(\sigma^*(x), x/\varepsilon)$ and $A_{22}(\sigma^*(x), x/\varepsilon)$ of the multiscale tensor ($\varepsilon = 1/8$).

Sensitivity with respect to γ. We start by observing how the solution to the problem

$$\Psi_{H,N}^{\varepsilon}(\overline{\sigma}^{\varepsilon,H}) = \inf_{\sigma^H \in U^H} \Psi_{H,N}^{\varepsilon}(\sigma^H)$$

$$= \inf_{\sigma^H \in U^H} \sum_{l=1}^{L} \|\Lambda_{A_{\sigma^*}^{\varepsilon}}^{h_{\text{obs}}} g_l - \mathscr{I}^{h_{\text{obs}}} \Lambda_{A_{\sigma^H}^{0,N}}^{H} g_l\|_{L^2(\partial D)}^2 + \gamma \|\sigma^H - \sigma_0\|_{H^1(D)}^2,$$

behaves as we vary the regularization parameter γ, where $\mathscr{I}^{h_{\text{obs}}} \Lambda_{A_{\sigma^H}^{0,N}}^{H} g_l$ is the linear extension of $\Lambda_{A_{\sigma^H}^{0,N}}^{H} g_l$ on $S^1(\partial D, \mathscr{T}_{h_{\text{obs}}})$. We set $\sigma_0 = 1$, while σ^- and σ^+ are chosen to be equal to 0.5 and 2.5 respectively. We fix $\varepsilon = 1/64$, $H = 1/16$, $L = 20$, and we solve the problem for different values of γ. The optimization problem is solved by means of the interior point method, with initial guess equal to σ_0. The relative error we obtain is shown in Figure 3.3 for different norms and different values of γ. As it can been observed, the approximated solutions we obtain have different properties which vary with the regularization parameter γ. The larger is γ, the more

regularized is the inverse problem. Thus, if γ is too large, the solution is too regularized, and it can be far from the true scalar field we want to retrieve. On the other hand, when γ becomes too small, the problem becomes more unstable, and many more oscillations are allowed in the reconstructed scalar field. For our problem we observe that the $L^2(D)$-error is minimum when $\gamma \in [2.5 \times 10^{-4}, 5 \times 10^{-4}]$.
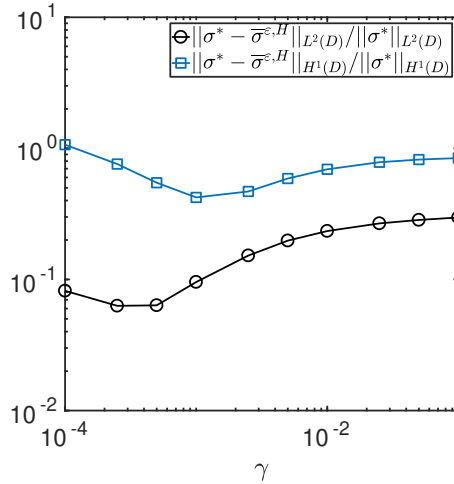

Figure 3.3: Error behavior with respect to the regularization parameter γ.

Convergence with respect to ε.   In this other numerical test we set $\gamma = 5 \times 10^{-4}$, and we verify the statement of Theorem 3.3.7. Moreover, we check the convergence of the approximated solution towards $\overline{\sigma}^{0,H}$, which is the approximated solution of the discrete version of problem (3.22). Other parameters such as H and L are the same as in the previous numerical test. From Figure 3.4 we can see that the error $|\Psi^0_{H,N}(\overline{\sigma}^{0,H}) - \Psi^0_{H,N}(\overline{\sigma}^{\varepsilon,H})|$ converges to zero as $\varepsilon \to 0$, as expected from Theorem 3.3.7. Relative errors between $\overline{\sigma}^{0,H}$ and $\overline{\sigma}^{\varepsilon,H}$ are also shown in Figure 3.4 for both $L^2(D)$- and $H^1(D)$-norms. We can observe convergence of $\overline{\sigma}^{\varepsilon,H}$ to $\overline{\sigma}^{0,H}$ as $\varepsilon \to 0$, in agreement with Theorem 3.3.7. For relatively large values of ε, namely $\varepsilon > H$, the error we obtain is relatively large and no convergence is observed. This is due to the fact that, since $\varepsilon > H$, the approximate homogenized flux, which approximates at best the multiscale flux, is capable of capturing its typical oscillations. Hence, such oscillations will affect the retrieved solution as well.

Convergence with respect to H.   To verify convergence with respect to discretization, we fix $\gamma = 5 \times 10^{-4}$, $\varepsilon = 1/64$, $L = 20$ and use the discrete minimizer $\overline{\sigma}^{\varepsilon,H}$ obtained on the finest discretization as reference solution. In Figure 3.5 we show the numerical errors obtained, and the picture agrees with what is stated in Theorem 3.4.2.
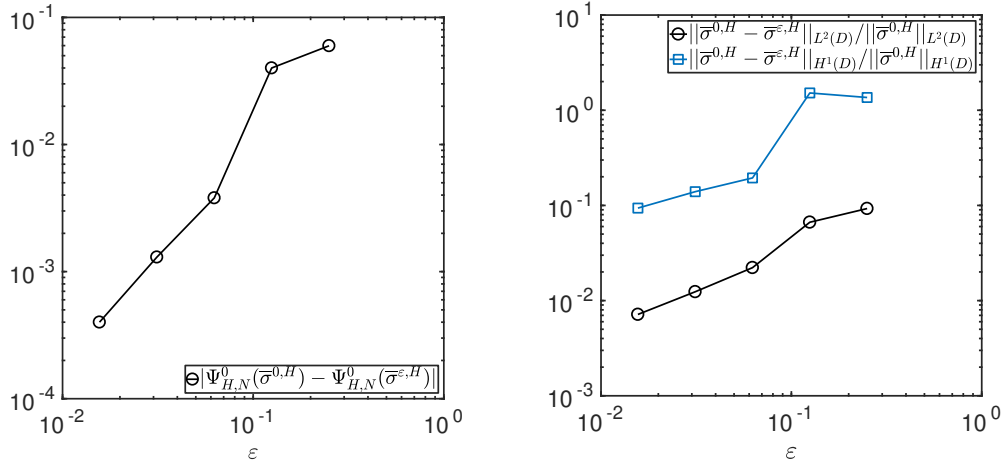
Figure 3.4: Error convergence as $\varepsilon \to 0$.
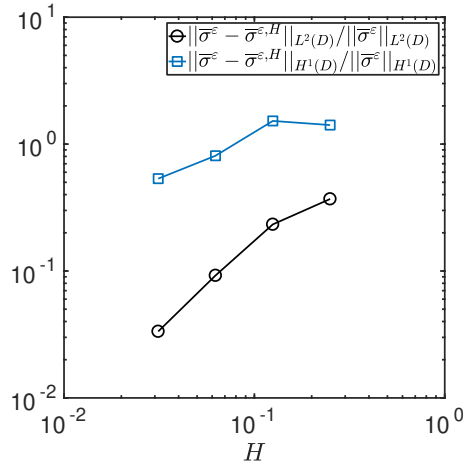
Figure 3.5: Error convergence as $H \to 0$.

Sensitivity with respect to L. Finally we let vary the number L of different Dirichlet conditions used to define the inverse problem, and check if a larger value of L leads to a better approximated solution. For this experiment $\gamma = 5 \times 10^{-4}$, $\varepsilon = 1/64$, $H = 1/16$, while we allow L to vary between 1 and 20. We can observe in Figure 3.6 that the relative error between the exact function σ^* and our approximation decreases as L becomes larger. However, it is also important to mention that as L increases, we should decrease H since the functions g_l becomes more and more oscillating as $L \to \infty$, and therefore we need a small mesh size to approximate them well. This could also be the reason why the $H^{(}D)1$-error increases for the last larger values of L.

Finally in Figure 3.7 we show the conductivity tensor we retrieve with $\varepsilon = 1/64$, $\gamma = 5 \times 10^{-4}$, $H = 1/16$, $L = 20$. It is important to remark that the results showed in Figure 3.2 are obtained for $\varepsilon = 1/64$ (hence we obtain $\overline{\sigma}^{\varepsilon,H}$, $\varepsilon = 1/64$). However, in order to visualize the results well
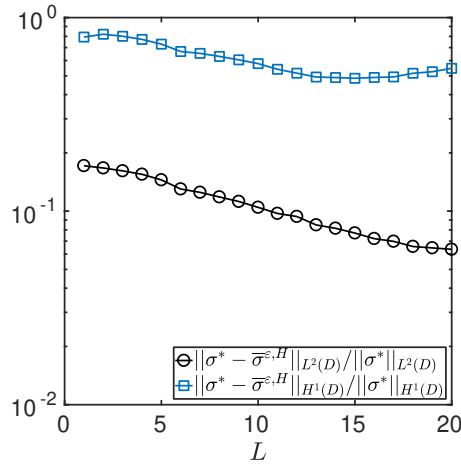
Figure 3.6: Error behavior with respect of the number of Dirichlet conditions L.

and compare the profile of the multiscale tensor with the one shown in Figure 3.2, we plot $A(\overline{\sigma}^{\varepsilon,H}(x), x/\varepsilon')$, where $\varepsilon' = 1/8$. We can see a good agreement between our solution shown in Figure 3.7 and the true tensor shown in Figure 3.2.

$\overline{\sigma}^{\varepsilon,H}(x)$. $\quad\quad A_{11}(\overline{\sigma}^{\varepsilon,H}(x), x/\varepsilon')$. $\quad\quad A_{22}(\overline{\sigma}^{\varepsilon,H}(x), x/\varepsilon')$.
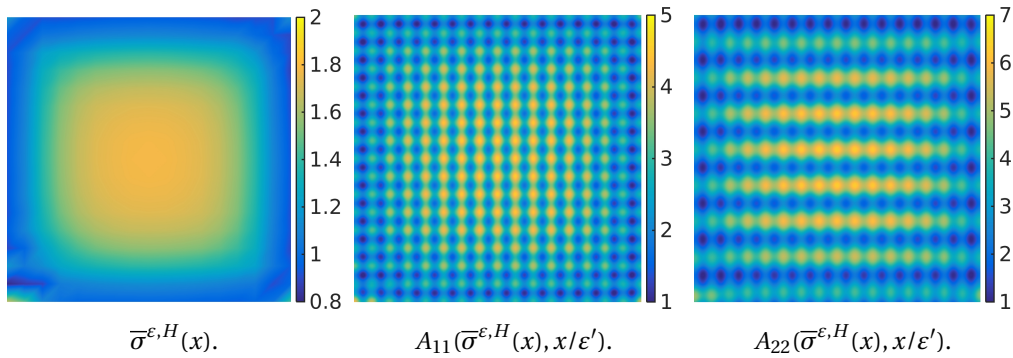
Figure 3.7: The approximated solution $\overline{\sigma}^{\varepsilon,H}$ and the two components $A_{11}(\overline{\sigma}^{\varepsilon,H}, x/\varepsilon')$ and $A_{22}(\overline{\sigma}^{\varepsilon,H}, x/\varepsilon')$ of the multiscale tensor ($H = 1/16$, $\varepsilon = 1/64$, $\varepsilon' = 1/8$).

3.5.3 A 2D non-affinely parameterized tensor

For the second experiment we consider a non-affine parameterization of the multiscale tensor. In this case the function σ^* controls the orientation of the oscillations of the full tensor $A_{\sigma^*}^{\varepsilon}$,

which is defined as follows,

$$A_{11}(\sigma^*(x), x/\varepsilon) = 4\left(\sin\left(\frac{2\pi\mathbf{e}^{1\top}Qx}{\varepsilon}\right) + 1.5\right),$$

$$A_{22}(\sigma^*(x), x/\varepsilon) = 4\left(\cos\left(\frac{2\pi\mathbf{e}^{1\top}Qx}{\varepsilon}\right) + 1.5\right),$$

$$A_{12}(\sigma^*(x), x/\varepsilon) = A_{21}(\sigma^*(x), x/\varepsilon) = 0,$$

where $Q = Q(\sigma^*(x))$ is a rotation matrix depending on σ^* and is defined as

$$Q = \begin{pmatrix} \cos(2\pi\sigma^*(x)) & \sin(2\pi\sigma^*(x)) \\ -\sin(2\pi\sigma^*(x)) & \cos(2\pi\sigma^*(x)) \end{pmatrix},$$

with

$$\sigma^*(x) = 1.05 + 0.15x_1.$$

Let us remark that for this parameterization the monotonicity assumption (3.13) in Theorem 3.2.3 does not hold. However, Theorem 3.3.7 and Theorem 3.4.2 are still valid. The exact function σ^*, and the components of $A_{\sigma^*}^\varepsilon$ are shown in Figure 3.8, for $\varepsilon = 1/8$. For solving the
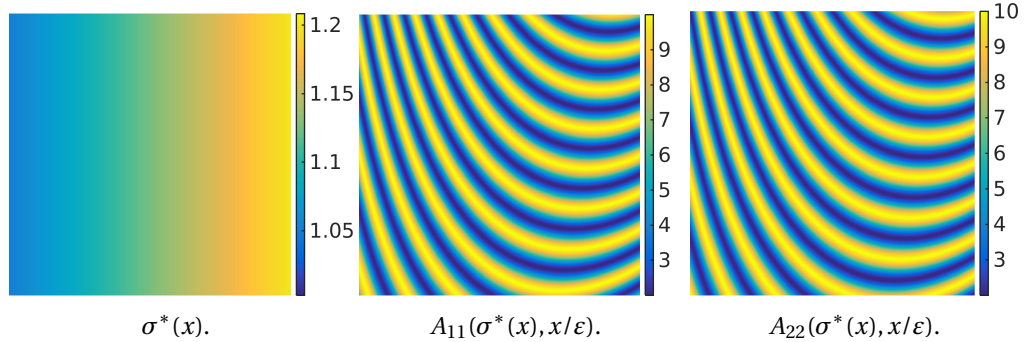
$\sigma^*(x)$. $\quad$ $A_{11}(\sigma^*(x), x/\varepsilon)$. $\quad$ $A_{22}(\sigma^*(x), x/\varepsilon)$.

Figure 3.8: The true field σ^* and the two components $A_{11}(\sigma^*(x), x/\varepsilon)$ and $A_{22}(\sigma^*(x), x/\varepsilon)$ of the multiscale tensor for the non-affine parameterization ($\varepsilon = 1/8$).

problem we set $\varepsilon = 1/64$, $H = 1/16$, $L = 8$, $\sigma^- = 1$, $\sigma^+ = 1.25$, $\sigma_0 = 1.05$. For this experiment we slightly modify the regularization term. The exact field we want to retrieve changes only with respect to the variable x_1. Then we assume to know this qualitative property of the unknown and we define the regularization term such that variations with respect to the x_2 direction are more penalized than variations with respect to the x_1 direction. Observe that

$$\|\sigma - \sigma_0\|_{H^1(D)}^2 = \|\sigma - \sigma_0\|_{L^2(D)}^2 + \|\partial_{x_1}(\sigma - \sigma_0)\|_{L^2(D)}^2 + \|\partial_{x_2}(\sigma - \sigma_0)\|_{L^2(D)}^2. \tag{3.37}$$

Then, instead of multiplying the three addends on the right hand side of (3.37) by the same parameter γ, we use different weights for each of the three addends. The new penalty term is

then defined as

$$\gamma_1 \|\sigma - \sigma_0\|^2_{L^2(D)} + \gamma_2 \|\partial_{x_1}(\sigma - \sigma_0)\|^2_{L^2(D)} + \gamma_3 \|\partial_{x_2}(\sigma - \sigma_0)\|^2_{L^2(D)},$$

and for the experiment we are considering we adopt $\gamma_1 = 0.1$, $\gamma_2 = 0.1$, $\gamma_3 = 4$. Let us remark that all the theoretical conclusions are still valid under this regularization term, since it represents a norm equivalent to the $H^1(D)$-norm. As the parameterization is non-affine, in the offline stage we apply the empirical interpolation method (EIM) to obtain an affine approximation of the tensor, using $tol_{\text{EIM}} = 10^{-14}$, where tol_{EIM} is a prescribed tolerance used as stopping criterion for the a posteriori error control in the EIM algorithm. In Figure 3.9 we show convergence of the residuals in the EIM approximation, and for the reduced basis approximation. In total we get 21 affine terms for A^ε_{11}, and 20 affine terms for A^ε_{22}, while the reduced space is spanned by $N = 47$ precomputed micro solutions. Therefore for each new value of the unknown, approximating the new homogenized tensor at a macro quadrature point reduces in solving a 47×47 linear system instead of a 4096×4096 linear system, leading to a great saving of computational time. In Figure 3.10 we show the approximated solution we get
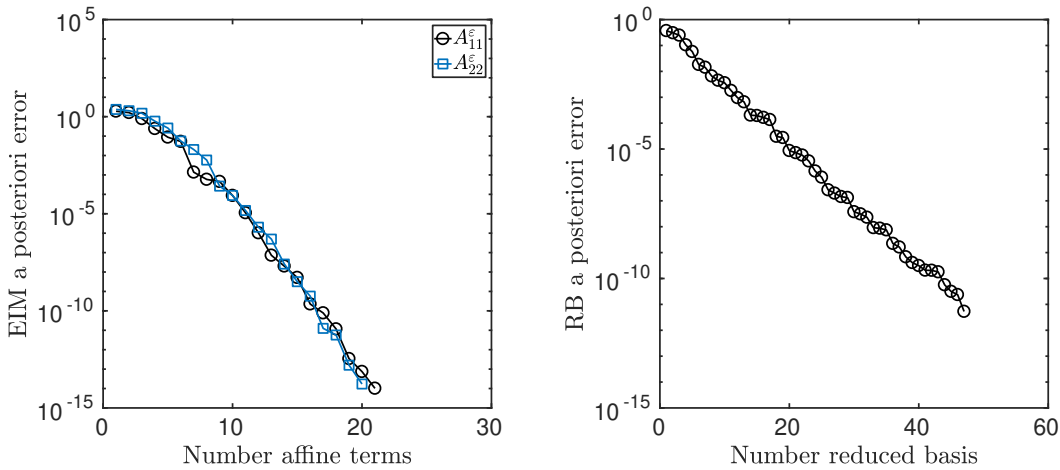
Figure 3.9: Residuals for the a posteriori error control in the offline stage.

using our proposed method. Again we note that we show the conductivity tensor we retrieve when $\varepsilon = 1/64$ (hence we obtain $\overline{\sigma}^{\varepsilon,H}$, $\varepsilon = 1/64$). However, in order to better visualize the results and compare the profile of the multiscale tensor to the one shown in Figure 3.8, we plot $A(\overline{\sigma}^{\varepsilon,H}(x), x/\varepsilon')$, where $\varepsilon' = 1/8$. We can notice that the orientation of the micro oscillations is well captured for most part of the computational domain. As an additional measure of accuracy we also mention that the relative error between the two corresponding homogenized tensors, i.e., $A^0(\sigma^*)$ and $A^0(\overline{\sigma}^{\varepsilon,H})$, is about 6%.

$\overline{\sigma}^{\varepsilon,H}(x)$. $A_{11}(\overline{\sigma}^{\varepsilon,H}(x), x/\varepsilon')$. $A_{22}(\overline{\sigma}^{\varepsilon,H}(x), x/\varepsilon')$.
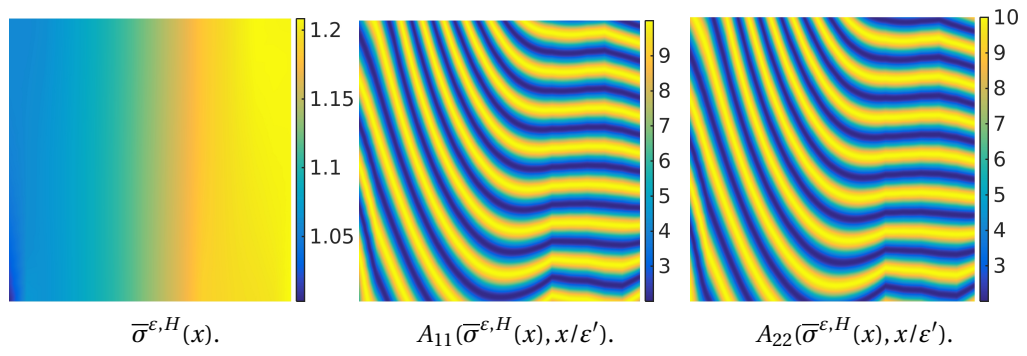
Figure 3.10: The approximated solution $\overline{\sigma}^{\varepsilon,H}$ and the two components $A_{11}(\overline{\sigma}^{\varepsilon,H}, x/\varepsilon')$ and $A_{22}(\overline{\sigma}^{\varepsilon,H}, x/\varepsilon')$ of the multiscale tensor for the non-affine parameterization ($H = 1/16$, $\varepsilon = 1/64$, $\varepsilon' = 1/8$).

4 Numerical method for solving multi-scale inverse problems via Bayesian techniques

In Chapter 4 we consider the same class of parameterized multiscale inverse problems treated in the preceding chapter, but we recast them into a statistical framework, and develop an efficient multiscale numerical method based on homogenization and Bayesian techniques. We still deal with elliptic inverse problems for a class of parameterized multiscale symmetric tensors $A^\varepsilon_{\sigma^*}$ of the form

$$A^\varepsilon_{\sigma^*}(x) = A(\sigma^*(x), x/\varepsilon),$$

where $\sigma^* : D \to \mathbb{R}$ and

$$A_{ij}(\sigma^*(x), x/\varepsilon) = A_{ij}(\sigma^*(x), y), \quad A_{ij}(\sigma^*(x), \cdot) \text{ is } Y\text{-periodic},$$

$\forall x \in D, \forall i, j = 1, \dots, d$.

Given the PDE

$$\begin{aligned} -\nabla \cdot (A^\varepsilon_{\sigma^*} \nabla u^\varepsilon) &= 0 && \text{in } D, \\ u^\varepsilon &= g && \text{on } \partial D, \end{aligned} \tag{4.1}$$

and assuming that the map $(t, x) \mapsto A(t, x/\varepsilon)$ is known, the goal is to determine the macroscopic parameterization $\sigma^* : D \to \mathbb{R}$ based on the knowledge of the Dirichlet to Neumann map $\Lambda_{A^\varepsilon_{\sigma^*}} : H^{1/2}(\partial D) \to H^{-1/2}(\partial D)$ defined as

$$g \mapsto A^\varepsilon_{\sigma^*} \nabla u^\varepsilon \cdot \boldsymbol{v}|_{\partial D}, \tag{4.2}$$

where $\boldsymbol{v}$ denotes the exterior unit normal to ∂D. Since standard numerical techniques which require mesh resolution at the finest scale are not appropriate to approximate (4.1), we describe a coarse graining strategy based on numerical homogenization and model order reduction. Moreover, in order to ensure well-posedness, we solve the problem following the Bayesian approach.

Outline.   The outline of the chapter is as follows. In Section 4.1 we describe our setting for the inverse problem and we recall some useful tools for the Bayesian approach to inverse problems. Our main results are presented in Section 4.2. We state some preliminary results on well-posedness of the posterior measure and we introduce two types of prior measures that we will use throughout the work. Hence, we prove existence and well-posedness of the effective posterior, and establish the convergence of the Hellinger distance between the effective posterior and the posterior measure based on the full fine scale model. In Section 4.3 we give a brief survey on the algorithm used to sample from the posterior distribution, which is based on Markov chain Monte Carlo (MCMC) methods. In Section 4.4 we explain how to solve the problem numerically by means of RB-FE-HMM. Numerical experiments that illustrate our multiscale inverse method and confirm our theoretical findings are presented in Section 4.5. The content of this chapter is essentially taken from [7].

4.1   An elliptic multiscale inverse problem with finite observations

Let D be an open and bounded set in $\mathbb{R}^d$. We consider a class of parameterized multiscale locally periodic tensors of the type $A_{\sigma^*}^\varepsilon(x) = A(\sigma^*(x), x/\varepsilon)$, where $\sigma^* : D \to \mathbb{R}$. Given $g \in H^{1/2}(\partial D)$, our aim is to recover $A_{\sigma^*}^\varepsilon$ from measurements originating from the model

$$
\begin{aligned}
-\nabla \cdot (A_{\sigma^*}^\varepsilon \cdot \nabla u^\varepsilon) &= 0 \qquad \text{in } D, \\
u^0 &= g \qquad\qquad \text{on } \partial D.
\end{aligned}
$$

Our unknown is represented by σ^*, while we assume to know the map $(t, y) \mapsto A(t, y)$, $t \in \mathbb{R}$, $y \in Y$, where $y = x/\varepsilon$, $y \in Y = (0,1)^d$ and Y is the periodicity cell. In this chapter we will consider the family of parameterized tensors $(t, y) \mapsto A(t, y)$ such that, for any $0 < \sigma^- < \sigma^+ < \infty$, $t \mapsto A(t, y)$ is of class $C^1([\sigma^-, \sigma^+])$ and there exist $\alpha_{[\sigma^-,\sigma^+]}, \beta_{[\sigma^-,\sigma^+]} > 0$ such that

$$
\alpha_{[\sigma^-,\sigma^+]}|b|^2 \le A(t, y)b \cdot b, \quad |A(t, y)b| \le \beta_{[\sigma^-,\sigma^+]}|b|, \quad \text{for a.e. } y \in Y \text{ and } \forall\, t \in [\sigma^-, \sigma^+], \, b \in \mathbb{R}^d.
$$

$$\tag{4.3}$$

Hence, we say that a macroscopic function $\sigma : D \to \mathbb{R}$ will be admissible if there exist two constants σ^- and σ^+, $0 < \sigma^- < \sigma^+ < \infty$, such that

$$
\sigma^- \le \sigma(x) \le \sigma^+ \quad \forall\, x \in D.
$$

In what follows we will denote as U the set of all such functions. We consider $J \in \mathbb{N}$ boundary portions of ∂D, and we denote them as $\Gamma_j \subset \partial D$, $j = 1,\ldots,J$, $\Gamma_i \cap \Gamma_j = \emptyset$ for $i \ne j$. These portions of the boundary represent the locations at which the measurements are carried out. Moreover, the same experiment is reproduced for $L \in \mathbb{N}$ different Dirichlet data, which we denote by g_l, $l = 1,\ldots,L$. Hence we have $J \times L$ observations. Then, we may introduce the

forward operator $F^\varepsilon : U \to \mathbb{R}^{JL}$, $F^\varepsilon(\sigma) = \text{vec}(\{f^\varepsilon_{jl}(\sigma)\}_{\substack{1 \le j \le J \\ 1 \le l \le L}})$,

$$f^\varepsilon_{jl}(\sigma) = \langle \Lambda_{A^\varepsilon_\sigma} g_l, \phi_j \rangle_{H^{-1/2}(\partial D), H^{1/2}(\partial D)}, \quad j = 1, \dots, J, l = 1, \dots, L, \tag{4.4}$$

where $\Lambda_{A^\varepsilon_\sigma}$ is the Dirichlet to Neumann map (4.2) associated to the tensor $A^\varepsilon_\sigma(x) = A(\sigma(x), x/\varepsilon)$, and $\phi_j \in H^{1/2}(\partial D)$ such that $\text{supp}(\phi_j) \subseteq \Gamma_j$ for all $j = 1, \dots, J$. In the following setting, we
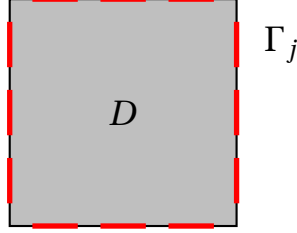

Figure 4.1: Picture representing the computational domain D and the boundary portions Γ_j used to compute the observations.

assume to dispose of a finite number of observations, corrupted by some noise, so that

$$z = F^\varepsilon(\sigma^*) + \zeta, \quad \zeta \sim \mathcal{N}(0, C_\zeta), \tag{4.5}$$

where C_ζ is a given covariance matrix. Based on these measurements we would like to recover σ^*. Let X be a Banach space, and P some map $P : \theta \in X \mapsto \sigma \in U$. The introduction of X and P will be useful later on to build different kind of prior measures on the admissible set U. Introducing this abstract framework is also useful to perform a rigorous analysis about the validity of our approach, which will be carried out in Section 4.2. Let us define the potential function $\Phi^\varepsilon : X \times \mathbb{R}^{JL} \to \mathbb{R}$, which measures the distance between the observed data and the values produced by the observation model for some $\theta \in X$ as

$$\begin{aligned}
\Phi^\varepsilon(\theta, z) &= \frac{1}{2} \| z - G^\varepsilon(\theta) \|^2_{C_\zeta} \\
&= \frac{1}{2} \langle z - G^\varepsilon(\theta), z - G^\varepsilon(\theta) \rangle_{C_\zeta} \\
&= \frac{1}{2} (z - G^\varepsilon(\theta))^\top C_\zeta^{-1} (z - G^\varepsilon(\theta)),
\end{aligned} \tag{4.6}$$

where $G^\varepsilon = F^\varepsilon \circ P$. Simply trying to minimize (4.6) leads to an ill-posed problem. To ensure well-posedness we may add some regularization term (e.g. Tikhonov regularization) or recast the problem into a statistical framework, where all the quantities involved are treated as random variables (Bayesian approach). Differently from standard regularization techniques, which produce as solution a single point estimate of the unknown, with the statistical approach the solution is represented by a probability measure, so called the posterior probability measure. The posterior measure can then be used to infer about the parameter values and quantify their uncertainties. In Bayesian theory, it is assumed that all the prior information we dispose about the unknown we are seeking for, can be described by what is called the prior measure, which

we denote here as μ_{pr}. Using (4.5) and applying Bayes' formula we obtain that the posterior measure of θ given z, denoted by $\mu^{\varepsilon}(\theta|z)$, is related to μ_{pr} through the Radon-Nikodym derivative

$$\frac{\mathrm{d}\mu^{\varepsilon}(\theta|z)}{\mathrm{d}\mu_{\mathrm{pr}}(\theta)} \propto \exp(-\Phi^{\varepsilon}(\theta,z)). \tag{4.7}$$

Unfortunately trying to explore $\mu^{\varepsilon}(\theta|z)$ via sampling techniques as Markov chain Monte Carlo (MCMC) methods is infeasible, due to the high computational effort needed to evaluate the model G^{ε} even for few realizations of $\theta \in X$. Hence, to drastically reduce the computational cost, we combine the inverse problem with a coarse graining strategy.

Using homogenization theory, we may introduce the operator $F^0 : U \to \mathbb{R}^{JL}$, defined as $F^0(\sigma) = \mathrm{vec}(\{f_{jl}^0(\sigma)\}_{\substack{1 \le j \le J \\ 1 \le l \le L}})$,

$$f_{jl}^0(\sigma) = \langle \Lambda_{A_{\sigma}^0} g_l, \phi_j \rangle_{H^{-1/2}(\partial D), H^{1/2}(\partial D)}, \quad j = 1,\ldots,J, l = 1,\ldots,L,$$

where $\Lambda_{A_{\sigma}^0}$ is the Dirichlet to Neumann map associated to the tensor A_{σ}^0, the homogenized tensor corresponding to A_{σ}^{ε}. Then, we can define a new potential function $\Phi^0 : X \times \mathbb{R}^{JL} \to \mathbb{R}$ as

$$\Phi^0(\theta,z) = \frac{1}{2}\|z - G^0(\theta)\|_{C_{\zeta}}^2, \tag{4.8}$$

where $G^0 : F^0 \circ P$, and P is a map such that $P : X \to U$. As for the full fine scale model, we can invoke Bayes' formula to define a posterior measure $\mu^0(\theta|z)$ associated to the potential function (4.8) which satisfies

$$\frac{\mathrm{d}\mu^0(\theta|z)}{\mathrm{d}\mu_{\mathrm{pr}}(\theta)} \propto \exp(-\Phi^0(\theta,z)). \tag{4.9}$$

We note that this new measure is much easier to explore via sampling techniques since the homogenized forward model $F^0 : U \to \mathbb{R}^{JL}$ can be approximated efficiently and independently of ε.

4.2   Well-posedness and convergence of the effective posterior measure

We recall some theoretical results about existence and well-posedness of the posterior measure. It is important to underline that existence and well-posedness of the posterior measure is typically determined from continuity properties of the forward operator entering in the definition of the potential function. Then, it is necessary to build prior measures such that every proposal lies in the function space on which the continuity properties of the forward operator are satisfied. Hence, some analysis on regularity properties of the forward operator is needed. This is carried on in what follows. We assume to have a prior Gaussian measure

$\mu_{\mathrm{pr}} = \mathcal{N}(\theta_{\mathrm{pr}}, C_{\mathrm{pr}})$ defined on a Banach space X, such that $\mu_{\mathrm{pr}}(X) = 1$. Let $\mu^0(\theta|z)$ be a posterior measure that we assume as in Section 4.1 to satisfy

$$\frac{\mathrm{d}\mu^0(\theta|z)}{\mathrm{d}\mu_{\mathrm{pr}}(\theta)} = \frac{1}{C^0(z)} \exp(-\Phi^0(\theta, z)), \tag{4.10}$$

where $\Phi^0(\theta, z)$ is the potential defined in (4.8) and $C^0(z)$ is the normalization constant

$$C^0(z) = \int_X \exp(-\Phi^0(\theta, z)) \mu_{\mathrm{pr}}(\mathrm{d}\theta),$$

so that $\mu^0(\theta|z)$ is actually a probability measure.

Definition 4.2.1. Let μ^1 and μ^2 be two probability measures on a Banach space X. Assume that μ^1 and μ^2 are both absolutely continuous with respect to a common reference measure μ, defined on the same measure space. Then the Hellinger distance between μ^1 and μ^2 is defined as

$$d_{\mathrm{Hell}}^2(\mu^1, \mu^2) = \frac{1}{2} \int_X \left(\sqrt{\frac{\mathrm{d}\mu^1}{\mathrm{d}\mu}} - \sqrt{\frac{\mathrm{d}\mu^2}{\mathrm{d}\mu}} \right)^2 \mathrm{d}\mu.$$

The next theorem gives sufficient conditions on $\Phi^0 : X \times \mathbb{R}^{JL} \to \mathbb{R}$ and μ_{pr} for the posterior measure defined in (4.10) to be well-defined. We refer to [84] and [41] for a complete overview of the Bayesian approach to inverse problems. For a rigorous Bayesian formulation of the inverse conductivity problem, known also as electrical impedance tomography (EIT), we also mention [46].

Theorem 4.2.2 (See [84] or [41])**.** *Assume that μ_{pr} is a Gaussian measure on the Banach space X such that $\mu_{\mathrm{pr}}(X) = 1$. In addition, assume that the function $\Phi^0 : X \times \mathbb{R}^{JL} \to \mathbb{R}$ and the measure μ_{pr} satisfy the following properties:*

1. *For every $r > 0$ there is a $K = K(r)$ such that for all $\theta \in X$ and for all $z \in \mathbb{R}^{JL}$ such that $\max\{\|\theta\|_X, \|z\|_{C_\zeta}\} < r$*

$$0 \le \Phi^0(\theta, z) \le K.$$

2. *For any fixed $z \in \mathbb{R}^{JL}$ the function $\Phi^0(\cdot, z) : X \to \mathbb{R}$ is continuous μ_{pr}-almost surely.*

3. *For $z_1, z_2 \in \mathbb{R}^{JL}$ with $\max\{\|z_1\|_{C_\zeta}, \|z_2\|_{C_\zeta}\} < r$ and for every $\theta \in X$, there is $M = M(r, \|\theta\|_X)$, $M : \mathbb{R}^+ \times \mathbb{R}^+ \to \mathbb{R}^+$, monotonic non-decreasing, such that*

$$|\Phi^0(\theta, z_1) - \Phi^0(\theta, z_2)| \le M(r, \|\theta\|_X) \|z_1 - z_2\|_{C_\zeta}.$$

Then the posterior measure μ^0 given by (4.10) is a well-defined probability measure.

4. *Moreover, if*

$$M(r, \|\cdot\|_X) \in L^2_{\mu_{\mathrm{pr}}}(X),$$

then μ^0 is Lipschitz in the data z, with respect to the Hellinger distance: if $\mu^0(\theta|z_1)$ and $\mu^0(\theta|z_2)$ are two measures corresponding to data z_1 and z_2, then there is a constant $C = C(r) > 0$ such that, for all z_1, z_2 with $\max\{\|z_1\|_{C_\zeta}, \|z\|_{C_\zeta}\} < r$,

$$d_{Hell}(\mu^0(\theta|z_1), \mu^0(\theta|z_2)) \le C\|z_1 - z_2\|_{C_\zeta}.$$

We consider the case where μ_{pr} is a Gaussian probability measure on the Banach space $X = C^0(\overline{D})$, and we will show that the assumptions of Theorem 4.2.2 are satisfied by μ_{pr} and Φ^0 given in (4.8), with $G^0 = F^0 \circ P$, where $P : \theta \in C^0(\overline{D}) \mapsto \sigma \in U$ is some map such that if $\|\theta - \theta_n\|_{L^\infty(D)} \to 0$, then $P(\theta_n) \to P(\theta)$ either uniformly or in measure. In particular, we consider two different definitions of P, which we denote by P_1 and P_2, described in what follows.

Log-Gaussian prior. The map P_1 is simply defined as $P_1(\theta) = \exp(\theta)$. We note that for any $\sigma = \exp(\theta), \theta \in C^0(\overline{D})$, we have that

$$\exp(-\|\theta\|_{L^\infty(D)}) \le \sigma(x) \le \exp(\|\theta\|_{L^\infty(D)}) \quad \forall x \in D.$$

Hence P_1 does map into the admissible set U. In the conditions (4.3) we can take $\sigma^- = \exp(-\|\theta\|_{L^\infty(D)})$ and $\sigma^+ = \exp(\|\theta\|_{L^\infty(D)})$. We can hence note that the quantities $\alpha_{[\sigma^-,\sigma^+]}^{-1}$ and $\beta_{[\sigma^-,\sigma^+]}$ can be described as monotonic non-decreasing functions of $\|\theta\|_{L^\infty(D)}$, and we will use the notation

$$\alpha_{[\sigma^-,\sigma^+]} = \alpha_{\|\theta\|_{L^\infty(D)}}, \quad \beta_{[\sigma^-,\sigma^+]} = \beta_{\|\theta\|_{L^\infty(D)}}. \tag{4.11}$$

Finally, we remark that from continuity of P_1 we see that if $\theta \in C^0(\overline{D})$ and $\{\theta_n\}_{n>0}$ is a sequence in $C^0(\overline{D})$ such that $\|\theta - \theta_n\|_{L^\infty(D)} \to 0$, then $\|P_1(\theta) - P_1(\theta_n)\|_{L^\infty(D)} \to 0$. Let us also remark that since θ is distributed according to a Gaussian measure, $P_1(\theta)$ is distributed according to a log-Gaussian measure.

Level set prior. The map P_2, which in [62] is referred to as level set prior, is defined instead in the following way. Let $n \in \mathbb{N}$ and fix constants $-\infty = c_0 < \ldots < c_n = \infty$. Given $\theta : D \to \mathbb{R}$, we define $D_i \subseteq D$ as

$$D_i = \{x \in D : c_{i-1} \le \theta(x) < c_i\}, \quad i = 1, \ldots, n,$$

so that $\overline{D} = \cup_{i=1}^{n} \overline{D}_i$ and $D_i \cap D_j = \emptyset$ for $i \neq j$. Let us also define the level sets

$$D_i^0 = \overline{D}_i \cap \overline{D}_{i+1} = \{x \in D : \theta(x) = c_i\}, \quad i = 1 \ldots, n-1.$$

Now given some strictly positive functions $f_1, \ldots, f_n \in C^0(\overline{D})$, we define the map $P_2 : C^0(\overline{D}) \to U$ as

$$P_2(\theta) = \sum_{i=1}^{n} f_i \mathbb{1}_{D_i}.$$

In particular we will consider f_i which are constant on D. Hence, each $\sigma = P_2(\theta)$ will be uniformly bounded below and above, and so also the quantities $\alpha_{[\sigma^-,\sigma^+]}$ and $\beta_{[\sigma^-,\sigma^+]}$ are uniformly bounded with respect to θ. For the continuity of the map P_2, we have the following proposition given in [62] (we denote by $|D_j|$ the measure of D_j).

Proposition 4.2.3 (See Proposition 2.6 and Proposition 2.8 in [62])**.** *Let $\{\theta_n\}_{n>0} \subset C^0(\overline{D})$ converge to some $\theta \in C^0(\overline{D})$ uniformly. Then $\{P_2(\theta_n)\}_{n>0}$ converges to $P_2(\theta)$ in $L^q(D)$, $1 \le q < \infty$, if and only if $|D_i^0| = 0$ for all $i = 1, \ldots, n-1$. Let μ_{pr} be a Gaussian probability measure on $C^0(\overline{D})$ and let $\theta \sim \mu_{\mathrm{pr}}$. Then $|D_i^0| = 0$ μ_{pr}-almost surely for $i = 1, \ldots, n-1$.*

4.2.1 Well-posedness of the effective posterior measure

In what follows we study the continuity of the forward operator $G^0 : C^0(\overline{D}) \to \mathbb{R}^{JL}$.

Lemma 4.2.4. *Let $x/\varepsilon = y$, $y \in Y = (0,1)^d$. Consider the class of $d \times d$ symmetric matrix functions $(t, y) \mapsto A(t, y)$, where $A_{ij}(t, \cdot)$ is Y-periodic, $\forall i, j = 1, \ldots, d$, $t \in [\sigma^-, \sigma^+]$, $0 < \sigma^- < \sigma^+ < \infty$. Assume that the map $t \mapsto A(t, y)$ is of class $C^1([\sigma^-, \sigma^+])$ and that there exist $\alpha_{[\sigma^-,\sigma^+]}$ and $\beta_{[\sigma^-,\sigma^+]} > 0$ such that (4.3) holds. Then the homogenized map $t \mapsto A^0(t)$ satisfies*

$$\alpha_{[\sigma^-,\sigma^+]}|b|^2 \le A^0(t)b \cdot b, \quad |A^0(t)b| \le \beta_{[\sigma^-,\sigma^+]}|b|, \quad \forall t \in [\sigma^-, \sigma^+], b \in \mathbb{R}^d, \tag{4.12}$$

and there exists a constant $E_{[\sigma^-,\sigma^+]} > 0$ such that

$$|\partial_t A(t)| \le E_{[\sigma^-,\sigma^+]}, \quad \forall t \in [\sigma^-, \sigma^+]. \tag{4.13}$$

Proof. The statement of the lemma is contained in what stated by Theorem 3.2.3. Therefore see Theorem 3.2.3 for the proof. $\qquad\square$

Lemma 4.2.5. *Let the assumptions of Lemma 4.2.4 be satisfied. Let $\sigma \in U$ and the sequence $\{\sigma_n\}_{n>0}$ in U be such that:*

1. *Either $\{\sigma_n\}_{n>0}$ converges to σ uniformly.*

2. *Or $\{\sigma_n\}_{n>0}$ converges to σ in the Lebesgue measure and there exist σ^- and σ^+, with $0 < \sigma^- < \sigma^+ < \infty$, such that $\sigma^- \le \sigma_n(x) \le \sigma^+$ for all $x \in \overline{D}$ and for all $n > 0$.*

Then the sequence $\{\Lambda_{A_{\sigma_n}^0} g\}_{n>0}$ converges to $\Lambda_{A_\sigma^0} g$ in $H^{-1/2}(\partial D)$.

Proof. The first part of the result has been proved in Lemma 3.3.3. For convenience we briefly recall the arguments. Let us define $w = A_\sigma^0 \nabla u^0(\sigma) - A_{\sigma_n}^0 \nabla(\sigma_n)$. Observing that $w \in H(D, \mathrm{div})$ and using the continuity of the map $w \in H(D, \mathrm{div}) \mapsto w \cdot \boldsymbol{\nu} \in H^{-1/2}(\partial D)$ we know that

$$\| w \cdot \boldsymbol{\nu} \|_{H^{-1/2}(\partial D)} \le \| w \|_{L^2(D)}.$$

Note that if $\{\sigma_n\}_{n>0}$ converges to $\sigma \in U$ uniformly, then we have that there exist σ^- and σ^+ such that for every n sufficiently large $\sigma^- \le \sigma_n(x) \le \sigma^+$ $\forall x \in D$, and so $\alpha_{[\sigma^-,\sigma^+]}$, $\beta_{[\sigma^-,\sigma^+]}$, $E_{[\sigma^-,\sigma^+]}$ are uniformly bounded with respect to n. The same is true for sequences converging in the Lebesgue measure since they are uniformly bounded by assumption. Hence in what follows we will just refer to such quantities as α, β, E. Using Cauchy-Schwarz inequality and (4.13)-(4.12) we obtain

$$\begin{aligned}
\int_D |w|^2 \, \mathrm{d}x &= \int_D A_{\sigma_n}^0 (\nabla u^0(\sigma) - \nabla u^0(\sigma_n)) \cdot w \, \mathrm{d}x \\
&\quad + \int_D (A_\sigma^0 - A_{\sigma_n}^0) \nabla u^0(\sigma) \cdot w \, \mathrm{d}x \\
&\le \beta \| \nabla u^0(\sigma) - \nabla u^0(\sigma_n) \|_{L^2(D)} \| w \|_{L^2(D)} \\
&\quad + E \left(\int_D |\sigma - \sigma_n|^2 |\nabla u^0(\sigma)|^2 \, \mathrm{d}x \right)^{1/2} \| w \|_{L^2(D)}.
\end{aligned} \tag{4.14}$$

It follows from the weak formulation of $u^0(\sigma)$ and $u^0(\sigma_n)$ that, for all $v \in H_0^1(D)$, we have that

$$\int_D (A_\sigma^0 \nabla u^0(\sigma) - A_{\sigma_n}^0 \nabla u^0(\sigma_n)) \cdot \nabla v \, \mathrm{d}x = 0.$$

Then

$$\int_D A_\sigma^0 (\nabla u^0(\sigma) - \nabla u^0(\sigma_n)) \cdot \nabla v \, \mathrm{d}x = \int_D (A_{\sigma_n}^0 - A_\sigma^0) \nabla u^0(\sigma_n) \cdot \nabla v \, \mathrm{d}x \quad \forall v \in H_0^1(D).$$

By choosing $v = u^0(\sigma) - u^0(\sigma_n) \in H_0^1(D)$, using Cauchy-Schwarz inequality, (4.13) and (4.12), we obtain

$$\| \nabla u^0(\sigma) - \nabla u^0(\sigma_n) \|_{L^2(D)} \le \alpha^{-1} E \left(\int_D |\sigma - \sigma_n|^2 |\nabla u^0(\sigma_n)|^2 \, \mathrm{d}x \right)^{1/2}. \tag{4.15}$$

Inserting (4.15) into (4.14) we obtain

$$\| w \|_{L^2(D)} \le E(1 + \alpha^{-1}\beta) \left(\int_D |\sigma - \sigma_n|^2 |\nabla u^0(\sigma)|^2 \, \mathrm{d}x \right)^{1/2}, \tag{4.16}$$

and by using Holder's inequality and Lax-Milgram we finally obtain

$$
\begin{aligned}
\|w\|_{L^2(D)} &\le E(1 + \alpha^{-1}\beta)\|\sigma - \sigma_n\|_{L^\infty(D)}\|\nabla u^0(\sigma)\|_{L^2(D)} \\
&\le E\alpha^{-1}\beta(1 + \alpha^{-1}\beta)\|g\|_{H^{1/2}(\partial D)}\|\sigma - \sigma_n\|_{L^\infty(D)}.
\end{aligned}
\tag{4.17}
$$

Now, if $\|\sigma - \sigma_n\|_{L^\infty(D)} \to 0$ the result follows from (4.17). On the other hand if $|\sigma - \sigma_n| \to 0$ in measure, since $|D| < \infty$ and $\nabla u^0(\sigma) \in (L^2(D))^d$, we have also that the integrand of (4.16) $|\sigma - \sigma_n|^2|\nabla u^0(\sigma)|^2 \to 0$ in measure (see Corollary 2.2.6 in [23] for example). Now, since $|\sigma - \sigma_n|$ is uniformly bounded by assumptions, the whole integrand is bounded by a scalar multiple of $|\nabla u^0(\sigma)|^2$. Therefore by applying the Lebesgue's dominated convergence theorem, we obtain that $|\sigma - \sigma_n|^2|\nabla u^0(\sigma)|^2 \to 0$ in $L^1(D)$, and the result follows. $\qquad\square$

Remark 4.2.6. The Lebesgue's dominated convergence theorem is stated for sequences converging almost everywhere. However, convergence almost everywhere can be replaced in this case by convergence in measure, since $|D| < \infty$.

By using the results given in Lemma 4.2.4 and Lemma 4.2.5 we can deduce the following lemma that establishes the continuity of the effective forward operator $F^0 : U \to \mathbb{R}^{JL}$.

Lemma 4.2.7. *Let the assumptions of Lemma 4.2.5 be satisfied. Then the sequence $\{F^0(\sigma_n)\}_{n>0}$ converges to $F^0(\sigma)$.*

Proof. We have that

$$
\begin{aligned}
\|F^0(\sigma) - F^0(\sigma_n)\|_{C_\zeta} &\le C \sum_{j=1}^{J}\sum_{l=1}^{L} |\langle (\Lambda_{A_\sigma^0} - \Lambda_{A_{\sigma_n}^0})g_l, \phi_j\rangle_{H^{-1/2}(\partial D), H^{1/2}(\partial D)}| \\
&\le C \sup_l \|(\Lambda_{A_\sigma^0} - \Lambda_{A_{\sigma_n}^0})g_l\|_{H^{-1/2}(\partial D)} \sup_j \|\phi_j\|_{H^{1/2}(\partial D)},
\end{aligned}
$$

and the result follows from Lemma 4.2.5. $\qquad\square$

Hence, we can establish that the posterior measure (4.10) based on the potential function Φ^0 is well-defined and Lipschitz continuous in the data with respect to the Hellinger distance.

Theorem 4.2.8. *Let the assumptions of Lemma 4.2.4 be satisfied. Let μ_{pr} be a Gaussian probability measure on $C^0(\overline{D})$, and let $P : \theta \in C^0(\overline{D}) \mapsto \sigma \in U$ be defined as P_1 or P_2 previously introduced. Then, the function $\Phi^0 : C^0(\overline{D}) \times \mathbb{R}^{JL} \to \mathbb{R}$ defined in (4.8), with $G^0 = F^0 \circ P : C^0(\overline{D}) \to \mathbb{R}^{JL}$, satisfies assumptions 1-3 of Theorem 4.2.2. In case where $P = P_2$ also assumption 4 of Theorem 4.2.2 is satisfied. In the case where $P = P_1$, assumption 4 holds if*

$$
\beta_{\|\cdot\|_{L^\infty(D)}}^2 \alpha_{\|\cdot\|_{L^\infty(D)}}^{-1} \in L^2_{\mu_{\mathrm{pr}}}(C^0(\overline{D})).
\tag{4.18}
$$

Proof. Let σ be an admissible functions in U. We have that

$$
\begin{aligned}
\|F^0(\sigma)\|_{C_\zeta} &\le C \sum_{j=1}^{J} \sum_{l=1}^{L} |\langle \Lambda_{A_\sigma^0} g_l, \phi_j \rangle_{H^{-1/2}(\partial D), H^{1/2}(\partial D)}| \\
&\le C \sup_l \|\Lambda_{A_\sigma^0} g_l\|_{H^{-1/2}(\partial D)} \| \sup_j \|\phi_j\|_{H^{1/2}(\partial D)} \\
&\le C \beta_{[\sigma^-,\sigma^+]}^2 \alpha_{[\sigma^-,\sigma^+]}^{-1} \sup_l \|g_l\|_{H^{1/2}(\partial D)} \\
&\le C \beta_{[\sigma^-,\sigma^+]}^2 \alpha_{[\sigma^-,\sigma^+]}^{-1}.
\end{aligned}
$$

In case where $P = P_1$ then $\sigma = \exp(\theta)$, where $\theta \in C^0(\overline{D})$, and $\beta_{[\sigma^-,\sigma^+]}^2 \alpha_{[\sigma^-,\sigma^+]}^{-1}$ is a positive and monotonic non-decreasing functions of $\|\theta\|_{L^\infty(D)}$ (see (4.11)). Thus we obtain

$$
\|G^0(\theta)\|_{C_\zeta} \le \beta_{\|\theta\|_{L^\infty(D)}}^2 \alpha_{\|\theta\|_{L^\infty(D)}}^{-1}.
$$

If $P = P_2$, $\|G^0(\theta)\|_{C_\zeta}$ is bounded by a constant $\forall \theta \in C^0(\overline{D})$ since P_2 is uniformly bounded. Using the triangle inequality we have that

$$
\Phi^0(\theta, z) \le C(\|z\|_{C_\zeta}^2 + \|G^0(\theta)\|_{C_\zeta}^2),
$$

and therefore assumption 1 follows. To fulfill assumption 3 we note that we have

$$
\begin{aligned}
|\Phi^0(\theta, z_1) - \Phi^0(\theta, z_2)| &= \frac{1}{2} |\langle z_1 + z_2 - 2G^0(\theta), z_1 - z_2 \rangle_{C_\zeta}| \\
&\le C(\|z_1\|_{C_\zeta} + \|z_2\|_{C_\zeta} + 2\|G^0(\theta)\|_{C_\zeta}) \|z_1 - z_2\|_{C_\zeta}.
\end{aligned}
$$

Let r such that $\max\{\|z_1\|_{C_\zeta}, \|z_2\|_{C_\zeta}\} < r$. Hence we obtain

$$
\begin{aligned}
|\Phi^0(\theta, z_1) - \Phi^0(\theta, z_2)| &\le C(2r + 2\|G^0(\theta)\|_{C_\zeta}) \|z_1 - z_2\|_{C_\zeta} \\
&\le M(r, \|\theta\|_{L^\infty(D)}) \|z_1 - z_2\|_{C_\zeta},
\end{aligned}
$$

with

$$
M(r, \|\theta\|_{L^\infty(D)}) = C(2r + 2\|G^0(\theta)\|_{C_\zeta}).
$$

If $P = P_2$, $M(r, \|\theta\|_{L^\infty(D)})$ is positive and monotonic non-decreasing, and uniformly bounded with respect to $\|\theta\|_{L^\infty(D)}$. Hence, assumptions 3 and 4 follow. In the case $P = P_1$ we have that

$$
M(r, \|\theta\|_{L^\infty(D)}) = C(2r + 2\beta_{\|\theta\|_{L^\infty(D)}}^2 \alpha_{\|\theta\|_{L^\infty(D)}}^{-1}).
$$

We note that $M(r, \|\theta\|_{L^\infty(D)})$ is positive and monotonic non-decreasing, hence assumption 3 follows. Moreover if

$$
\beta_{\|\cdot\|_{L^\infty(D)}}^2 \alpha_{\|\cdot\|_{L^\infty(D)}}^{-1} \in L_{\mu_{\mathrm{pr}}}^2(C^0(\overline{D})),
$$

then

$$M(r, \|\cdot\|_{L^\infty(D)}) \in L^2_{\mu_{\mathrm{pr}}}(C^0(\overline{D})).$$

It remains to show that assumption 2 is also satisfied. Assume that $P = P_1$. If $\|\theta - \theta_n\|_{L^\infty(D)} \to 0$ then $P(\theta_n) \to P(\theta)$ uniformly. Then by Lemma 4.2.7 we have that $G^0 = F^0 \circ P$ is continuous at θ. Assume now $P = P_2$. If $\|\theta - \theta_n\|_{L^\infty(D)} \to 0$, then by Proposition 4.2.3 $P(\theta_n) \to P(\theta)$ in $L^q(D)$, $1 \le q < \infty$, at the points where the level sets have measure zero. However since we are assuming $\theta \sim \mu_{\mathrm{pr}}$ and μ_{pr} is a Gaussian probability measure on $C^0(\overline{D})$, it follows from Proposition 4.2.3 that θ has μ_{pr}-almost surely this property. Finally since $P_2(\theta_n(x))$ is uniformly bounded for all $x \in \overline{D}$ and all $n > 0$, by Lemma 4.2.5 we have that assumption 2 is satisfied also in the case where $P = P_2$. $\qquad\square$

Remark 4.2.9. The result in Lemma 4.2.7 can be proved in a similar way also for the sequence $\{\Lambda_{A^\varepsilon_{\sigma_n}} g\}_{n>0}$. It can also be proved that when $P = P_1$ also for $G^\varepsilon(\theta)$ we have that

$$\|G^\varepsilon(\theta)\|_{C_\zeta} \le C\beta^2_{\|\theta\|_{L^\infty(D)}} \alpha^{-1}_{\|\theta\|_{L^\infty(D)}},$$

while when $P = P_2$, $\|G^\varepsilon(\theta)\|_{C_\zeta}$ is bounded by a constant independent of θ. Hence, under the assumptions of Theorem 4.2.8 the posterior measure (4.7) based on the potential function Φ^ε is also well-defined and Lipschitz continuous in the data with respect to the Hellinger distance.

4.2.2 Convergence of the fine scale posterior towards the effective posterior

Before moving to the numerical aspects of the problem, an investigation of the validity of our approach is necessary. First we observe that (4.5) can be rewritten as

$$z = F^0(\sigma^*) + \zeta^\varepsilon(\sigma^*) + \zeta, \quad \zeta \sim \mathcal{N}(0, C_\zeta), \tag{4.19}$$

where

$$\zeta^\varepsilon(\sigma^*) = F^\varepsilon(\sigma^*) - F^0(\sigma^*).$$

The quantity $\zeta^\varepsilon(\sigma^*)$ represents the homogenization error capturing the mismatch between the full multiscale model and the homogenized one. In particular, (4.19) suggests that the observed data originating from the full multiscale model can be seen as data originating from the homogenized model, which are affected by two sources of errors: the noise and the homogenization error. Both sources of errors can affect our predictions and we must take them into account when solving inverse problems to obtain good approximations of the unknown, especially when ε is relatively large. For the homogenization error we can show that we have in our case that $\zeta^\varepsilon(\sigma) \to 0$ as $\varepsilon \to 0$ for every $\sigma \in U$, as stated in the following theorem.

Theorem 4.2.10. *Let σ be a function in U and let $\{A^\varepsilon_\sigma\}_{\varepsilon>0}$ be a sequence of symmetric matrices*

in $M(\alpha_{[\sigma^-,\sigma^+]}, \beta_{[\sigma^-,\sigma^+]}, D)$ which G-converges to the matrix $A_\sigma^0 \in M(\alpha_{[\sigma^-,\sigma^+]}, \beta_{[\sigma^-,\sigma^+]}, D)$, and let $\zeta^\varepsilon(\sigma) = \mathrm{vec}(\{\widetilde{\zeta}_{jl}^\varepsilon(\sigma)\}_{\substack{1 \le j \le J \\ 1 \le l \le L}})$, where

$$\widetilde{\zeta}_{jl}^\varepsilon(\sigma) = \langle (\Lambda_{A_\sigma^\varepsilon} - \Lambda_{A_\sigma^0}) g_l, \phi_j \rangle_{H^{-1/2}(\partial D), H^{1/2}(\partial D)}, \quad j = 1,\ldots,J, l = 1,\ldots,L,$$

where $\Gamma_j \subset \partial D$ for all $j = 1,\ldots,L$, $\Gamma_i \cap \Gamma_j = \emptyset$ for $i \ne j$, and $\phi_j, g_l \in H^{1/2}(\partial D)$ for all $j = 1,\ldots,J$, $supp(\phi_j) \subseteq \Gamma_j$ for all $j = 1,\ldots,J$. Then $\|\zeta^\varepsilon(\sigma)\|_{C_\zeta} \to 0$ as $\varepsilon \to 0$.

Proof. We have that for arbitrary j and l and $\forall \sigma \in U$

$$\widetilde{\zeta}_{jl}^\varepsilon(\sigma) = \langle (\Lambda_{A_\sigma^\varepsilon} - \Lambda_{A_\sigma^0}) g_l, \phi_j \rangle_{H^{-1/2}(\partial D), H^{1/2}(\partial D)}.$$

Using integration by parts we have that

$$\widetilde{\zeta}_{jl}^\varepsilon(\sigma) = \int_D (A_\sigma^\varepsilon \nabla u^\varepsilon - A_\sigma^0 \nabla u^0) \cdot \nabla \widetilde{\phi}_j \, \mathrm{d}x, \tag{4.20}$$

where $\widetilde{\phi}_j$ is some function in $H^1(D)$ whose trace is ϕ_j. From G-convergence of A_σ^ε to A_σ^0 we know that (4.20) converges to zero as $\varepsilon \to 0$. $\qquad\square$

Theorem 4.2.11. *Let μ^ε and μ^0 be defined as in (4.7) and (4.9) respectively. Let the assumptions of Theorem 4.2.8 be satisfied, together with (4.18). Then we have that*

$$\lim_{\varepsilon \to 0} d_{\mathrm{Hell}}(\mu^0, \mu^\varepsilon) = 0.$$

Proof. From the definition of the Hellinger distance we have that

$$2d_{\mathrm{Hell}}^2(\mu^0, \mu^\varepsilon) = \int_{C^0(\overline{D})} \left(\sqrt{\frac{\mathrm{d}\mu^0}{\mathrm{d}\mu_{\mathrm{pr}}}} - \sqrt{\frac{\mathrm{d}\mu^\varepsilon}{\mathrm{d}\mu_{\mathrm{pr}}}} \right)^2 \mu_{\mathrm{pr}}(\mathrm{d}\theta)$$

$$= \int_{C^0(\overline{D})} \left(\frac{1}{\sqrt{C^0}} \exp\left(-\frac{1}{2}\Phi^0(\theta, z)\right) - \frac{1}{\sqrt{C^\varepsilon}} \exp\left(-\frac{1}{2}\Phi^\varepsilon(\theta, z)\right) \right)^2 \mu_{\mathrm{pr}}(\mathrm{d}\theta), \tag{4.21}$$

where C^0 and C^ε are the two normalization constants such that $\mu^0(\theta|z)$ and $\mu^\varepsilon(\theta|z)$ are probability measures, i.e.,

$$C^0 = \int_{C^0(\overline{D})} \exp(-\Phi^0(\theta, z)) \mu_{\mathrm{pr}}(\mathrm{d}\theta), \quad C^\varepsilon = \int_{C^0(\overline{D})} \exp(-\Phi^\varepsilon(\theta, z)) \mu_{\mathrm{pr}}(\mathrm{d}\theta).$$

Let us notice that

$$
\begin{aligned}
|C^0 - C^\varepsilon| &\leq \int_{C^0(\overline{D})} \left| \exp(-\Phi^0(\theta, z)) - \exp(-\Phi^\varepsilon(\theta, z)) \right| \mu_{\mathrm{pr}}(\mathrm{d}\theta) \\
&\leq \int_{C^0(\overline{D})} \left| \Phi^0(\theta, z) - \Phi^\varepsilon(\theta, z) \right| \mu_{\mathrm{pr}}(\mathrm{d}\theta).
\end{aligned}
\tag{4.22}
$$

From (4.21) we get that

$$
2 d_{\mathrm{Hell}}^2(\mu^0, \mu^\varepsilon) \leq I_1 + I_2,
$$

where

$$
I_1 = \frac{1}{C^0} \int_{C^0(\overline{D})} \left(\exp\left(-\frac{1}{2}\Phi^0(\theta, z)\right) - \exp\left(-\frac{1}{2}\Phi^\varepsilon(\theta, z)\right) \right)^2 \mu_{\mathrm{pr}}(\mathrm{d}\theta),
$$

$$
I_2 = \left(\frac{1}{\sqrt{C^0}} - \frac{1}{\sqrt{C^\varepsilon}} \right)^2 C^\varepsilon.
$$

We have that

$$
I_1 \leq \frac{1}{4C^0} \int_{C^0(\overline{D})} (\Phi^0(\theta, z) - \Phi^\varepsilon(\theta, z))^2 \mu_{\mathrm{pr}}(\mathrm{d}\theta),
$$

and

$$
\begin{aligned}
I_2 &\leq \frac{1}{4} \max\left\{ (C^0)^{-3}, (C^\varepsilon)^{-3} \right\} (C^0 - C^\varepsilon)^2 \\
&\leq C \int_{C^0(\overline{D})} (\Phi^0(\theta, z) - \Phi^\varepsilon(\theta, z))^2 \mu_{\mathrm{pr}}(\mathrm{d}\theta),
\end{aligned}
$$

where we have used (4.22). Using the definition of Φ^0 and Φ^ε we find

$$
\begin{aligned}
2 d_{\mathrm{Hell}}^2(\mu^0, \mu^\varepsilon) &\leq C \int_{C^0(\overline{D})} (\Phi^0(\theta, z) - \Phi^\varepsilon(\theta, z))^2 \mu_{\mathrm{pr}}(\mathrm{d}\theta) \\
&\leq C \int_{C^0(\overline{D})} (2\|z\|_{C_\zeta} + \|G^0(\theta)\|_{C_\zeta} + \|G^\varepsilon(\theta)\|_{C_\zeta})^2 \|G^0(\theta) - G^\varepsilon(\theta)\|_{C_\zeta}^2 \mu_{\mathrm{pr}}(\mathrm{d}\theta).
\end{aligned}
$$

From Theorem 4.2.10 we have that $\lim_{\varepsilon \to 0} \|G^0(\theta) - G^\varepsilon(\theta)\|_{C_\zeta} = 0$. We also have that (see Theorem 4.2.8) if $P = P_1$, then $\|G^0(\theta)\|_{C_\zeta}$ (respectively $\|G^\varepsilon(\theta)\|_{C_\zeta}$) is bounded by some scalar multiple of $\beta^2_{\|\theta\|_{L^\infty(D)}} \alpha^{-1}_{\|\theta\|_{L^\infty(D)}}$ which is square integrable with respect to μ_{pr}. Otherwise if $P = P_2$ both $\|G^0(\theta)\|_{C_\zeta}$ and $\|G^\varepsilon(\theta)\|_{C_\zeta}$ are bounded by a constant since P_2 is uniformly bounded, and again square integrability follows. Then by the Lebesgue's dominated convergence theorem it follows that $d_{\mathrm{Hell}}(\mu^0, \mu^\varepsilon) \to 0$ as $\varepsilon \to 0$. $\qquad\square$

Offline approximation of the homogenization error distribution. The interpretation of the result is that when ε is small we can neglect the homogenization error, since it will be close to zero, and we do not need to take into account its probability distribution in the inversion process. However, for larger values of ε, the mismatch between the observations and the data produced by the homogenized model might not be negligible, and using the coarse graining approach without taking into account the homogenization error distribution may lead to bad predictions. In order to avoid that, we can correct the likelihood function, by approximating the probability distribution of the homogenization error. In [28] a strategy for approximating the first two moments of the distribution of the discretization error caused by FEM is proposed. Hence, by following [28], we derive an algorithm which aims at approximating the mean $\overline{\zeta}^{\varepsilon}$ and the covariance $C_{\zeta^{\varepsilon}}$ of the homogenization error distribution. Given the prior measure μ_{pr} on $C^0(\overline{D})$, the map $P : C^0(\overline{D}) \to U$, and a sample size M, the numerical procedure is given by the following steps.

1. Draw from the prior measure a sample of realizations $S = \{\theta_1, \ldots, \theta_M\}$.

2. For $1 \le i \le M$ compute

$$\zeta_i^{\varepsilon} = G^{\varepsilon}(\theta_i) - G^0(\theta_i) = F^{\varepsilon}(P(\theta_i)) - F^0(P(\theta_i)).$$

3. $\overline{\zeta}^{\varepsilon} = \dfrac{1}{M} \sum_{i=1}^{M} \zeta_i^{\varepsilon}.$

4. $C_{\zeta^{\varepsilon}} = \dfrac{1}{M} \sum_{i=1}^{M} (\overline{\zeta}^{\varepsilon} - \zeta_i^{\varepsilon})(\overline{\zeta}^{\varepsilon} - \zeta_i^{\varepsilon})^{\top}.$

We assume a Gaussian distribution for the homogenization error, so that $\zeta^{\varepsilon} \sim \mathcal{N}(\overline{\zeta}^{\varepsilon}, C_{\zeta^{\varepsilon}})$ for all σ, and we can rewrite (4.19) as

$$z = F^0(\sigma^*) + \zeta^*, \quad \zeta^* \sim \mathcal{N}(\overline{\zeta}^{\varepsilon}, C_{\zeta} + C_{\zeta^{\varepsilon}}). \tag{4.23}$$

We emphasize that the homogenization error distribution is approximated offline. Only M evaluations of the full multiscale model are needed. Hence, we use this approximation to modify the potential function as in (4.24), and sample from the posterior by evaluating only the coarse homogenized model. We note that in (4.23) to apply the Bayesian framework for inverse problem, we still assume the independence of ζ^* and θ, despite the introduction of the homogenization error in ζ^*. Nevertheless, the practical uselfulness of such algorithm has been shown in numerous works (see [19, 28]). Then, we may define the new likelihood as

$$\Phi^0(\theta, \overline{z}) = \frac{1}{2} \|\overline{z} - G^0(\theta)\|_{C_{\zeta} + C_{\zeta^{\varepsilon}}}^2, \tag{4.24}$$

where $\overline{z} = z - \overline{\zeta}^{\varepsilon}$. Note that conclusions about existence and well-posedness of the posterior measure are still valid under this definition of the potential function, which is equivalent to the one in (4.8), apart from the fact that observations z are shifted by $\overline{\zeta}^{\varepsilon}$, and the covariance matrix is given by $C_{\zeta} + C_{\zeta^{\varepsilon}}$.

4.3 Sampling from the effective posterior measure

The output of the Bayesian approach consists in the posterior measure. However, in practice numerical sampling is needed to approximate the distribution, in order to obtain some meaningful information (such as expected value and variance of the unknown, or confidence intervals). We consider as prior a Gaussian measure $\mu_{\mathrm{pr}} = \mathcal{N}(\theta_{\mathrm{pr}}, C_{\mathrm{pr}})$ on the Hilbert space $L^2(D)$. The random variable $\theta \sim \mathcal{N}(\theta_{\mathrm{pr}}, C_{\mathrm{pr}})$ can be written using the Karhunen-Loève expansion as

$$\theta(x) = \theta_{\mathrm{pr}}(x) + \sum_{k=1}^{\infty} \sqrt{\lambda_k}\eta_k \varphi_k(x),$$

where $\{\varphi_k, \lambda_k\}_{k=1}^{\infty}$ is an orthonormal set of eigenfunctions and eigenvalues of C_{pr}, and $\{\eta_k\}_{k=1}^{\infty}$ is an i.i.d. sequence with $\eta_1 \sim \mathcal{N}(0,1)$. Since we defined the push forward maps as $P_i : C^0(\overline{D}) \to U$, $i = 1, 2$, we may ask which condition the prior measure has to satisfy so that each sample from μ_{pr} is in $C^0(\overline{D})$. For the Matérn covariance operator that we will use in the numerical examples, we will ensure that draws from $\mathcal{N}(\theta_{\mathrm{pr}}, C_{\mathrm{pr}})$ are continuous (see Section 4.5.1).

In numerical experiments to reduce the dimension of the unknown we use a truncated Karhunen-Loève expansion

$$\theta^K(x) = \theta_{\mathrm{pr}}(x) + \sum_{k=1}^{K} \sqrt{\lambda_k}\eta_k \varphi_k(x),$$

where $\{\varphi_k, \lambda_k\}_{k=1}^{K}$ is the orthonormal set of eigenfunctions and eigenvalues of C_{pr} corresponding to the K largest eigenvalues. The unknown parameter is then parameterized by the K coefficients $\{\eta_k\}_{k=1}^{K}$, which are a priori i.i.d. as $\mathcal{N}(0,1)$. In what follows, we will denote sometimes the unknown parameter as $\theta_{\boldsymbol{\eta}}^K$ to emphasize its dependence on $\boldsymbol{\eta} = (\eta_1, \ldots, \eta_K)^\top$. Hence, the inverse problem consists in approximating the posterior distribution of the K coefficients by sampling from the posterior density $\pi^0(\boldsymbol{\eta}|z)$ which is given by

$$\pi^0(\boldsymbol{\eta}|z) \propto \exp\left(-\frac{1}{2}\|z - G^0(\theta_{\boldsymbol{\eta}}^K)\|_{C_\zeta}^2 - \frac{1}{2}\|\theta_{\boldsymbol{\eta}}^K - \theta_{\mathrm{pr}}\|_{C_{\mathrm{pr}}}^2\right), \qquad (4.25)$$

where $\|\cdot\|_{C_{\mathrm{pr}}}$ is the norm induced by the scalar product

$$\langle\cdot,\cdot\rangle_{C_{\mathrm{pr}}} = \langle C_{\mathrm{pr}}^{-1/2}(\cdot), C_{\mathrm{pr}}^{-1/2}(\cdot)\rangle_{L^2(D)},$$

and for any $\theta \in L^2(D)$ and any $\alpha \in \mathbb{R}$ we have that

$$C_{\mathrm{pr}}^{\alpha}(\theta) = \sum_{k=1}^{\infty} \lambda_k^{\alpha}\langle\theta, \varphi_k\rangle_{L^2(D)}\varphi_k.$$

It easy to obtain that (4.25) reduces to

$$\pi^0(\boldsymbol{\eta}|z) \propto \exp\left(-\frac{1}{2}\|z - G^0(\theta_{\boldsymbol{\eta}}^K)\|_{C_\zeta}^2 - \frac{1}{2}\boldsymbol{\eta}^\top\boldsymbol{\eta}\right). \tag{4.26}$$

To sample from the posterior density we employ the Markov chain Monte Carlo (MCMC) techniques. Many algorithms belonging to the family of MCMC sampling methods are available in the literature. We decide to use the Metropolis-Hastings (MH) algorithm, which we illustrate just below. With this approach, at each iteration we generate a new candidate $\boldsymbol{\eta} \in \mathbb{R}^K$ from a proposal density $q(\boldsymbol{\eta}^j, \boldsymbol{\eta})$, $q : \mathbb{R}^K \times \mathbb{R}^K \to \mathbb{R}^+$, where $\boldsymbol{\eta}^j$ is the current value of the variable. This new candidate is accepted with probability

$$a(\boldsymbol{\eta}^j, \boldsymbol{\eta}) = \min\left\{1, \frac{\pi^0(\boldsymbol{\eta}|z)\,q(\boldsymbol{\eta}, \boldsymbol{\eta}^j)}{\pi^0(\boldsymbol{\eta}^j|z)\,q(\boldsymbol{\eta}^j, \boldsymbol{\eta})}\right\}. \tag{4.27}$$

Otherwise, the candidate is rejected and the chain remains at the current position $\boldsymbol{\eta}^j$. Note that if the proposal density is symmetric, i.e. $q(\boldsymbol{\eta}^j, \boldsymbol{\eta}) = q(\boldsymbol{\eta}, \boldsymbol{\eta}^j)$, (4.27) reduces to

$$a(\boldsymbol{\eta}^j, \boldsymbol{\eta}) = \min\left\{1, \frac{\pi^0(\boldsymbol{\eta}|z)}{\pi^0(\boldsymbol{\eta}^j|z)}\right\}.$$

In our experiments we consider the random walk proposal distribution to explore the density. Then

$$q(\boldsymbol{\eta}^j, \boldsymbol{\eta}) = \frac{1}{\sqrt{(2\pi s^2)^K}} \exp\left(-\frac{1}{2s^2}(\boldsymbol{\eta} - \boldsymbol{\eta}^j)^\top(\boldsymbol{\eta} - \boldsymbol{\eta}^j)\right), \tag{4.28}$$

which is symmetric, and leads to the following algorithm. Given the target distribution $\pi^0(\boldsymbol{\eta}|z)$, a starting point $\boldsymbol{\eta}^1 \in \mathbb{R}^K$, a desired number of samples N_{sample}, and a symmetric proposal density $\mathcal{N}(0, s^2 I)$, we perform the following steps.

1. Set $j = 1$, $\mathscr{S} = \boldsymbol{\eta}^1$.

2. For $2 \le j \le N_{\text{sample}}$ perform the following operations.
   (a) $\boldsymbol{\eta} = \boldsymbol{\eta}^j + sw$, $w \sim \mathcal{N}(0, I)$.
   (b) $a(\boldsymbol{\eta}^j, \boldsymbol{\eta}) = \min\left\{1, \dfrac{\pi^0(\boldsymbol{\eta}|z)}{\pi^0(\boldsymbol{\eta}^j|z)}\right\}$.
   (c) Draw $u \sim \mathcal{U}([0,1])$, and if $a(\boldsymbol{\eta}^j, \boldsymbol{\eta}) > u$ accept $\boldsymbol{\eta}$ and set $\boldsymbol{\eta}^{j+1} = \boldsymbol{\eta}$. Otherwise reject the proposed step and set $\boldsymbol{\eta}^{j+1} = \boldsymbol{\eta}^j$.
   (d) $\mathscr{S} = \mathscr{S} \cup \boldsymbol{\eta}^{j+1}$.

3. Return $\mathscr{S}$.

The approximation of the target distribution improves as the number of samples N_{sample} increases, and asymptotic convergence is guaranteed as $N_{\text{sample}} \to \infty$ under certain regularity properties of the target distribution and the proposal density. Therefore, the results may be strongly dependent on the number of samples required, but also on the proposal density. In

particular, it is a difficult task to establish when a sample is large enough. At the same time, another general issue for the MH algorithm is the choice of s in (4.28), whose magnitude affects the speed at which the posterior distribution is explored and the number of rejected realizations. We can easily deduce that if s is too small, the probability distribution will be explored very slowly, and we might need a large number of samples to have a good approximation. On the other hand, if s is larger we may explore the distribution faster, but at each iteration the probability to have to reject a new realization will be higher. In particular, multiple rejections of some candidate are undesirable, since they may increase the autocorrelation between the realized paths, and reduce the efficiency of the algorithm. To find an optimal value for s we could perform some pilot simulations for different values of s, and hence observe for which value we have a good sampling of the target distribution.

4.4 A reduced basis method for the solution of the Bayesian multiscale inverse problem

In order to sample from the posterior density defined in (4.26), we need an efficient numerical method to compute $G^0(\theta_{\boldsymbol{\eta}}^K)$, where $\boldsymbol{\eta}$ is a proposed step by the MH algorithm. Let us recall that $G^0 = F^0 \circ P$, where $P : C^0(\overline{D}) \to U$ is one of the maps introduced in Section 4.2. Then, the following operations are required.

1. Solve for $1 \le l \le L$

$$
\begin{aligned}
-\nabla \cdot (A_\sigma^0 \nabla u^0) &= 0 && \text{in } D, \\
u^0 &= g_l && \text{on } \partial D,
\end{aligned}
\tag{4.29}
$$

where $\sigma = P(\theta_{\boldsymbol{\eta}}^K)$, and A_σ^0 is the homogenized tensor corresponding to the locally periodic tensor $A_\sigma^\varepsilon(x) = A(\sigma(x), x/\varepsilon)$.

2. Compute the normal fluxes at the boundary $\Lambda_{A_\sigma^0} g_l$ for $1 \le l \le L$, and evaluate $F^0(\sigma)$.

To do so we rely on RB-FE-HMM which has been extensively described in Chapter 2. As for the Tikhonov inverse problem, we choose to use macro and micro piecewise linear simplicial elements. In this setting the RB-FE-HMM for parameterized PDEs of type (4.29) has been discussed in Section 3.4.

Convergence analysis.   It is interesting to analyze how the numerical error intrinsic in the forward model affects the numerical posterior. To this end we will assume the forward model is approximated using FE-HMM (no model order reduction). In this case the numerical flux is given by $\Lambda_{A_\sigma^{0,h}}^H g_l \in S^1(\partial D, \mathcal{T}_H)$ where

$$
\int_{\partial D} \Lambda_{A_\sigma^{0,h}}^H g_l v^H \, ds = B_H(u_l^H, v^H) \quad \forall v^H \in S_c^1(D, \mathcal{T}_H).
$$

Hence, we define the operator $F^{H,h} : U \to \mathbb{R}^{JL}$, $F^{H,h}(\sigma) = \text{vec}(\{f_{jl}^{H,h}(\sigma)\}_{\substack{1 \le j \le J, \\ 1 \le l \le L}})$,

$$f_{jl}^{H,h}(\sigma) = \langle \Lambda_{A_\sigma^h}^H g_l, \phi_j \rangle_{H^{-1/2}(\partial D), H^{1/2}(\partial D)}, \quad j = 1, \dots, J, l = 1, \dots, L,$$

and the corresponding potential function $\Phi^{H,h} : C^0(\overline{D}) \times \mathbb{R}^{JL} \to \mathbb{R}$ given by

$$\Phi^{H,h}(\theta, z) = \frac{1}{2} \|z - G^{H,h}(\theta)\|_{C_\zeta}^2,$$

where $G^{H,h} : F^{H,h} \circ P$, and P is one of the map introduced in Section 4.2. We denote by $\mu^{H,h}(\theta|z)$ the numerical posterior given by

$$\frac{\mathrm{d}\mu^{H,h}(\theta|z)}{\mathrm{d}\mu_{\mathrm{pr}}(\theta)} \propto \exp(-\Phi^{H,h}(\theta, z)). \tag{4.30}$$

The following theorem establishes the convergence rate of the numerical posterior towards the true posterior $\mu^0(\theta|z)$ in the Hellinger metric. In particular, the rate is the same as the one for the error in the approximated forward model. Since convergence rates for the forward model are available only in the case where $\sigma \in W^{1,\infty}(\overline{D})$, we assume in what follows that each draw from the prior μ_{pr} is in $W^{1,\infty}(\overline{D})$, and that $P : \theta \mapsto \sigma$ is $P_1(\cdot) = \exp(\cdot)$.

Theorem 4.4.1. *Let μ^0 and $\mu^{H,h}$ be defined as in* (4.10) *and* (4.30) *respectively. Let the assumptions of Theorem 4.2.8 be satisfied together with* (4.18). *Assume that $A^0(P(\theta(\cdot))) \in W^{1,\infty}(D, \text{Sym}_d)$, and $P(\theta) = P_1(\theta) = \exp(\theta)$. Furthermore, assume that $\mu_{\mathrm{pr}}(W^{1,\infty}(\overline{D})) = 1$, and that $u^0 \in H^2(D)$ for each $l = 1, \dots, L$. Then we have that*

$$d_{\mathrm{Hell}}(\mu^0, \mu^{H,h}) \le C \left(H + \left(\frac{h}{\varepsilon} \right)^2 \right),$$

where C is a constant independent of H, h, and ε.

Proof. From the definition of the Hellinger distance we have that

$$2d_{\mathrm{Hell}}^2(\mu^0, \mu^{H,h}) = \int\limits_{W^{1,\infty}(\overline{D})} \left(\sqrt{\frac{\mathrm{d}\mu^0}{\mathrm{d}\mu_{\mathrm{pr}}}} - \sqrt{\frac{\mathrm{d}\mu^{H,h}}{\mathrm{d}\mu_{\mathrm{pr}}}} \right)^2 \mu_{\mathrm{pr}}(\mathrm{d}\theta)$$

$$= \int\limits_{W^{1,\infty}(\overline{D})} \left(\frac{1}{\sqrt{C^0}} \exp\left(-\frac{1}{2}\Phi^0(\theta, z)\right) - \frac{1}{\sqrt{C^{H,h}}} \exp\left(-\frac{1}{2}\Phi^{H,h}(\theta, z)\right) \right)^2 \mu_{\mathrm{pr}}(\mathrm{d}\theta),$$

where C^0 and $C^{H,h}$ are the two normalization constants such that $\mu^0(\theta|z)$ and $\mu^{H,h}(\theta|z)$ are probability measures, i.e.,

$$C^0 = \int\limits_{W^{1,\infty}(\overline{D})} \exp(-\Phi^0(\theta, z))\mu_{\mathrm{pr}}(\mathrm{d}\theta), \quad C^{H,h} = \int\limits_{W^{1,\infty}(\overline{D})} \exp(-\Phi^{H,h}(\theta, z))\mu_{\mathrm{pr}}(\mathrm{d}\theta).$$

4.4. A reduced basis method for the solution of the Bayesian multiscale inverse problem

By computations similar to the ones in the proof of Theorem 4.2.11 we obtain that

$$2d_{\text{Hell}}^2(\mu^0, \mu^{H,h}) \leq C \int\limits_{W^{1,\infty}(\overline{D})} (\Phi^0(\theta, z) - \Phi^{H,h}(\theta, z))^2 \mu_{\text{pr}}(\mathrm{d}\theta)$$

$$\leq C \int\limits_{W^{1,\infty}(\overline{D})} (2\|z\|_{C_\zeta} + \|G^0(\theta)\|_{C_\zeta} + \|G^{H,h}(\theta)\|_{C_\zeta})^2 \|G^0(\theta) - G^{H,h}(\theta)\|_{C_\zeta}^2 \mu_{\text{pr}}(\mathrm{d}\theta).$$

$$(4.31)$$

We know that (see Theorem 4.2.8) if $P = P_1$, $\|G^0(\theta)\|_{C_\zeta}$ and $\|G^{H,h}(\theta)\|_{C_\zeta}$ are bounded by some scalar multiple of $\beta_{\|\theta\|_{L^\infty(D)}}^2 \alpha_{\|\theta\|_{L^\infty(D)}}^{-1}$, which is square integrable with respect to μ_{pr}. Moreover, we also have that

$$\|G^0(\theta) - G^{H,h}(\theta)\|_{C_\zeta} \leq C \sum_{j=1}^J \sum_{l=1}^L |\langle (\Lambda_{A_{P_1(\theta)}^0} - \Lambda_{A_{P_1(\theta)}^{0,h}}^H) g_l, \phi_j \rangle_{H^{-1/2}(\partial D), H^{1/2}(\partial D)}.$$

Using integration by parts together with Cauchy-Schwarz inequality we get

$$\|G^0(\theta) - G^{H,h}(\theta)\|_{C_\zeta} \leq C \sup_l \|A^0(P_1(\theta))\nabla u^0 - A^{0,h}(P_1(\theta))\nabla u^H\|_{L^2(D)} \sup_j \|\nabla \widetilde{\phi}_j\|_{L^2(D)},$$

where $\widetilde{\phi}_j$ is some function in $H^1(D)$ whose trace is ϕ_j. Using standard FE-HMM a priori error estimates (see [1] for example) we obtain

$$\|G^0(\theta) - G^{H,h}(\theta)\|_{C_\zeta} \leq C \left(H + \left(\frac{h}{\varepsilon}\right)^2 \right),$$

$$(4.32)$$

where C is independent of H, h, and ε. Hence, using (4.31) and (4.32) together with the Lebesgue's dominated convergence theorem the result follows. $\qquad\square$

Corollary 4.4.2. *Let $A^0(P(\theta(\cdot))) \in W^{2,\infty}(D, \text{Sym}_d)$, $P(\theta) = P_1(\theta) = \exp(\theta)$, $\mu_{\text{pr}}(W^{2,\infty}(\overline{D})) = 1$, and $u^0 \in H^3(D)$ for each $l = 1, \ldots, L$. Then, we can establish a faster convergence rate for the Hellinger distance between the two measures by using the error estimate for the $L^2(\partial D)$-norm of the boundary flux obtained in [9], namely*

$$d_{\text{Hell}}(\mu^0, \mu^{H,h}) \leq C \left(H^{3/2} + \left(\frac{h}{\varepsilon}\right)^{3/2} \right).$$

Remark 4.4.3. If the forward model is approximated by means of the RB-FE-HMM, the error due to the micro discretization is usally negligible as the reduced space is built with precomputed micro functions computed on a very fine discretization. However, a new error enters into the estimate, namely the error due to the model order reduction. This error is based on the distance between the reduced space $S^N(Y)$ and $S^1(Y, \mathcal{T}_{\hat{h}})$. Such distance can be quantified by means of the notion of Kolmogorov N-width (see Chapter 2).

Summary of the numerical scheme. Let us give a brief summary of the numerical scheme. We denote by $\mathcal{T}_H$ the macro triangulation, and as N_H the number of macro DOFs. In the discrete setting, the prior measure $\mu_{\mathrm{pr}} = \mathcal{N}(\theta_{\mathrm{pr}}, C_{\mathrm{pr}})$ is replaced by $\mathcal{N}(\theta_{\mathrm{pr}}^H, C_{\mathrm{pr}}^H)$, where $\theta_{\mathrm{pr}}^H = \mathscr{I}^H \theta_{\mathrm{pr}}$, $\mathscr{I}^H$ is the linear interpolation operator, and $C_{\mathrm{pr}}^H \in \mathbb{R}^{N_H \times N_H}$ is a symmetric positive matrix which approximate the covariance operator C_{pr}. We denote by $\{\varphi_k^H, \lambda_k^H\}_{k=1}^{N_H}$ the orthonormal set of eigenvectors and eigenvalues of C_{pr}^H. Each $\theta^H \sim \mathcal{N}(\theta_{\mathrm{pr}}^H, C_{\mathrm{pr}}^H)$ can be then represented as

$$\theta^H(x) = \theta_{\mathrm{pr}}^H(x) + \sum_{k=1}^{N_H} \sqrt{\lambda_k^H} \eta_k \varphi_k^H(x),$$

where $\{\eta_k\}_{k=1}^{N_H}$ is an i.i.d. sequence with $\eta_1 \sim \mathcal{N}(0,1)$. If we truncate the KL expansion at the K largest eigenvalues we obtain

$$\theta^{H,K}(x) = \theta_{\mathrm{pr}}^H(x) + \sum_{k=1}^{K} \sqrt{\lambda_k^H} \eta_k \varphi_k^H(x).$$

In what follows, we will use the notation $\theta_{\boldsymbol{\eta}}^{H,K}$ to emphasize the dependence on the vector $\boldsymbol{\eta} = (\eta_1, \ldots, \eta_K)^\top$. Given the perturbed observations $z \in \mathbb{R}^{JL}$, the numerical scheme for solving the Bayesian multiscale inverse problem can be then summarized as follows.

1. Compute in an offline stage a reduced space of micro functions $S^N(Y)$ as described in Section 3.4.

2. Compute in an offline stage the set $\{\varphi_k^H, \lambda_k^H\}_{k=1}^{K}$ of eigenvectors and eigenvalues of the prior covariance C_{pr}^H, so that for a point $\boldsymbol{\eta} \in \mathbb{R}^K$ we have that

$$\theta_{\boldsymbol{\eta}}^{H,K}(x) = \theta_{\mathrm{pr}}^H(x) + \sum_{k=1}^{K} \sqrt{\lambda_k^H} \eta_k \varphi_k^H(x).$$

3. Sample online from the posterior distribution using the MH algorithm. In particular, for a new realization $\boldsymbol{\eta} \in \mathbb{R}^K$, in order to evaluate $\pi^0(z|\boldsymbol{\eta})$, for $1 \le l \le L$ the following steps are required.

  (a) Find $u_l^{H,\mathrm{RB}} = \mathring{u}_l^{H,\mathrm{RB}} + R_{g_l}$, where $\mathring{u}_l^{H,\mathrm{RB}} \in S_0^1(D, \mathcal{T}_H)$ satisfies

$$B_{H,\mathrm{RB}}(\mathring{u}_l^{H,\mathrm{RB}}, v^H) = -B_{H,\mathrm{RB}}(R_{g_l}, v^H) \quad \forall v^H \in S_0^1(D, \mathcal{T}_H),$$

where R_{g_l} is a Dirichlet lift of g_l properly chosen, and

$$B_{H,\mathrm{RB}}(v^H, w^H) = \sum_{K \in \mathcal{T}_H} A^{0,N}(\sigma(x_K)) \nabla v^H(x_K) \cdot \nabla w^H(x_K),$$

where

$$A_{ij}^{0,N}(\sigma(x_K)) = \int_Y A(\sigma(x_K), y) \mathbf{e}^i \cdot (\mathbf{e}^j - \nabla \chi_K^{j,N}) \, dy,$$

where $\sigma = P(\theta_{\boldsymbol{\eta}}^{H,K})$, $P : C^0(\overline{D}) \to U$ is one of the maps introduced in Section 4.2, and $\chi_K^{j,N}$ is a micro solution computed on the reduced space $S^N(Y)$.

(b) Find $\Lambda_{A_\sigma^{0,N}}^H g_l \in S^1(\partial D, \mathscr{T}_H)$ such that

$$\int_{\partial D} \Lambda_{A_\sigma^{0,N}}^H g_l v^H \, \mathrm{d}s = B_{H,\mathrm{RB}}(u_l^{H,\mathrm{RB}}, v^H) \quad \forall v^H \in S_c^1(D, \mathscr{T}_H).$$

4.5 Numerical experiments

In this section we will present some numerical experiments to illustrate our multiscale Bayesian algorithm for inverse problems. We start by explaining how observed data are collected. We then solve the inverse problem for different macroscopic parameterizations. At first, we consider an affine parameterization of the form $A^\varepsilon(x) = \sigma^*(x)B^\varepsilon(x) = \sigma^*(x)B(x/\varepsilon)$, so that the function σ^* controls the amplitude of the characteristic micro oscillations. Let us point out that, for this choice, we have that $A^0(x) = \sigma^*(x)B^0$, and thus the use of reduced basis methods for solving the forward problem is not required. This simple problem allows us to perform numerous tests to quantify the sensitivity of the method with respect to the several parameters involved in the approximation, such as ε, the size of the microscopic oscillations, K, the number of terms in the truncated Karhunen-Loève expansion, and L, the number Dirichlet data. Then, we will consider two different non-affine macroscopic parameterizations, one controlling the orientation of the micro oscillations, the other the volume fraction of a hypothetical layered material. For these problems, we make the following choice of parameters for the RB-FE-HMM offline stage: $h/\varepsilon = 1/64$, $\delta = \varepsilon$, $tol_{\mathrm{RB}} = 10^{-11}$, where tol_{RB} is a prescribed tolerance used as stopping criterion for the greedy algorithm employed to select the reduced basis functions.

4.5.1 Setup

The computational domain is the unit square

$$D = \{x = (x_1, x_2) : 0 < x_1, x_2 < 1\}.$$

We approximate the solution to problem (4.1) by means of the finite element method (FEM) using a very fine discretization $h_{\mathrm{obs}} \ll \varepsilon$. The forward homogenized problem is instead computed using a macro mesh size $H = 1/64$. The problem is solved for different Dirichlet conditions $\{g_l\}_{l=1}^L$. In particular we take $\{g_l\}_{l=1}^L = \{\sqrt{\lambda_l}\varphi_l\}_{l=1}^L$, where $\{(\lambda_l, \varphi_l)\}_{l=1}^L$ are the L eigenpairs corresponding to the L smallest eigenvalues associated to the one dimensional discrete Laplacian operator. Each g_l is then projected on the boundary ∂D to define the corresponding Dirichlet condition. This procedure ensures that the functions $\{g_l\}_{l=1}^L$ are smooth and orthonormal, so that each experiment contributes differently one from another. Moreover $\|\nabla g_l\|_{L^2(\partial D)} < C$, where C is a constant independent of L. Finally, we consider

$J = 12$ boundary portions $\Gamma_j \subset \partial D$, three for each side of the computational domain as shown in Figure 4.1. Each Γ_j has length equal to 0.2. The functions ϕ_j appearing in (4.4) are hat functions with $\mathrm{supp}(\phi_j) = \Gamma_j$, and which take value one at the midpoint of each Γ_j. Once the observed data have been computed, they are perturbed by the noise given by $\zeta = 10^{-4} w$, $w \sim \mathcal{N}(0, I)$. Let p_i and p_j be two nodes of the macro triangulation $\mathcal{T}_H$, and let N_H the total number of nodes defining $\mathcal{T}_H$. Note that $N_H = H^{-2}$. The covariance matrix in the prior measure $\mu_{\mathrm{pr}} = \mathcal{N}(\theta_{\mathrm{pr}}^H, C_{\mathrm{pr}}^H)$ is then $C_{\mathrm{pr}}^H \in \mathbb{R}^{N_H \times N_H}$ defined as

$$(C_{\mathrm{pr}}^H)_{ij} = \gamma \exp\left(-\frac{\|p_i - p_j\|_2}{\lambda} \right), \quad \gamma, \lambda \in \mathbb{R}^+, \tag{4.33}$$

while the prior mean is $\theta_{\mathrm{pr}}^H = \mathcal{I}^H \theta_{\mathrm{pr}}$, where θ_{pr} is some function in $C^0(\overline{D})$. We set different values for γ, λ and θ_{pr}, depending on the macroscopic parameterization we want to retrieve. In particular, $\lambda > 0$ is a correlation length that describes how the values at different positions of the functions supported by the prior measure are related, while $\gamma > 0$ is the amplitude scaling factor. Let us point out that the covariance matrix C_{pr}^H belongs to the family of Matérn covariances. In particular, we have that each draw from $\mathcal{N}(\theta_{\mathrm{pr}}^H, C_{\mathrm{pr}}^H)$ with C_{pr}^H defined as in (4.33) is a.s. s-Hölder continuous with $0 < s < 1/2$ for θ_{pr}^H sufficiently regular (see [72] for more details).

4.5.2   A 2D affinely parameterized tensor (amplitude of micro oscillations)

In this first set of numerical experiments we consider the tensor $A_{\sigma^*}^\varepsilon$ given by

$$A_{11}(\sigma^*(x), x/\varepsilon) = \sigma^*(x) \left(\cos^2\left(\frac{2\pi x_1}{\varepsilon} \right) + 1 \right),$$

$$A_{22}(\sigma^*(x), x/\varepsilon) = \sigma^*(x) \left(\sin\left(\frac{2\pi x_2}{\varepsilon} \right) + 2 \right),$$

$$A_{12}(\sigma^*(x), x/\varepsilon) = A_{21}(\sigma^*(x), x/\varepsilon) = 0,$$

where

$$\sigma^*(x) = 1.3 + 0.3 \mathbb{1}_{\tilde{D}_1} - 0.4 \mathbb{1}_{\tilde{D}_2},$$

and

$$\tilde{D}_1 = \left\{ x = (x_1, x_2) : (x_1 - 5/16)^2 + (x_2 - 11/16)^2 \le 0.025 \right\},$$

$$\tilde{D}_2 = \left\{ x = (x_1, x_2) : (x_1 - 11/16)^2 + (x_2 - 5/16)^2 \le 0.025 \right\}.$$

The task of the problem is to retrieve the function σ^*, which is shown together with the component A_{11}^ε of the tensor, $\varepsilon = 1/64$, in Figure 4.2.

Sensitivity with respect to ε.   We start by studying how different choices of ε can affect our predictions. The computations are reported in Figure 4.4. We briefly describe the setting.

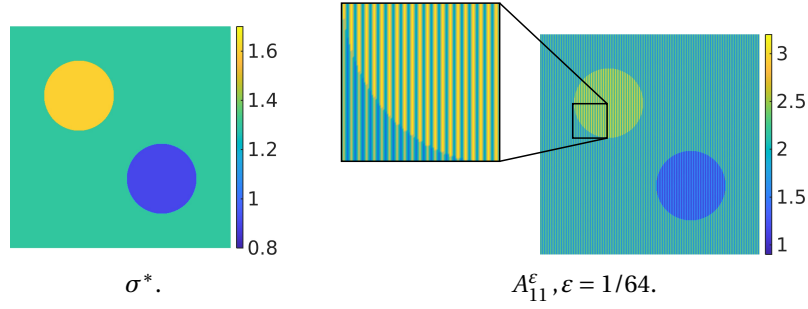σ^*. $\hspace{4cm}$ $A_{11}^\varepsilon, \varepsilon = 1/64$.

Figure 4.2: Representation of the true spatial field σ^* and the first component of the highly oscillating tensor for the problem considered in Section 4.5.2.

We compute numerically by means of a resolved FEM synthetic observations for different values of $\varepsilon = \{1/4, 1/8, 1/16, 1/8, 1/64\}$, for $L = 6$ different Dirichlet conditions. We consider a truncated Karhunen-Loève expansion with $K = 60$. The only assumption we make on σ^* is the one of σ^* be positive. hence we consider a log-Gaussian prior for this first set of numerical tests. We remark that the condition (4.18) holds under the choice made for $(t, y) \mapsto A(t, y)$. The prior measure μ_{pr} on $\theta \in C^0(\overline{D})$ is $\mathcal{N}(\theta_{\mathrm{pr}}^H, C_{\mathrm{pr}}^H)$, with $\theta_{\mathrm{pr}} = \log 1.3$ and C_{pr}^H defined in (4.33) with $\gamma = 0.05$ and $\lambda = 0.5$. In particular, the choice of $\theta_{\mathrm{pr}} = \log 1.3$ is such that the resulting log-Gaussian distribution on the admissible set U has median 1.3. We then push each draw θ into the admissible set through the function $P_1 : \theta \mapsto \exp(\theta)$. Example of realizations from the log-Gaussian prior are shown in Figure 4.3. We draw then 2×10^5 samples from the posterior
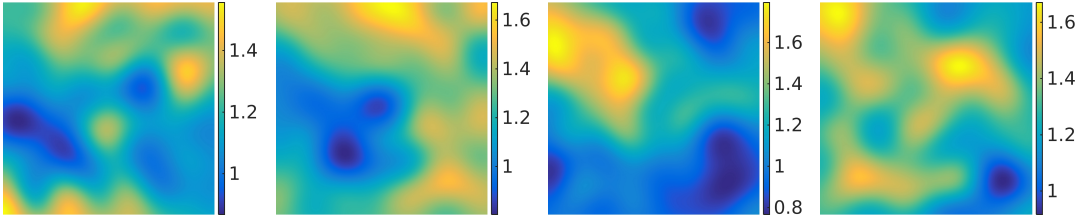

Figure 4.3: Four samples from the prior density used in the problem considered in Section 4.5.2.

distribution (4.26) using the MH algorithm. The parameter s is set to 0.01. The starting point is $\boldsymbol{\eta}^1 = 0 \in \mathbb{R}^K$. With this choice of the parameters we obtain an acceptance rate of about 27% for all choices of ε. In Figure 4.4 we plot for each ε the quantities $P_1(\mathbb{E}[\theta^{H,K}])$, $\mathbb{E}[P_1(\theta^{H,K})]$, and the variance $\mathrm{Var}[P_1(\theta^{H,K})]$. The first quantity is produced by computing first the mean on the Banach space $C^0(\overline{D})$ and then pushing it into the admissible set U through $P_1 : C^0(\overline{D}) \to U$. Moreover, we also show the approximation of the posterior density for the first three coefficients in the truncated Karhunen-Loève expansion. We can observe that as ε gets smaller, these densities stabilize and converge to the same posterior. We notice that with $\varepsilon = 1/4$ we get inaccurate predictions about the quantity of interest, while already with $\varepsilon = 1/8$ the approximation of the posterior mean is in good agreement with Figure 4.2. The source of error for large ε comes from the discrepancy between the multiscale model from where the

observations are obtained and the homogenized model used for solving the inverse problem.

Approximation of the homogenization error distribution.   As seen in Figure 4.4 for large values of ε the homogenization error (the discrepancy between the fine scale and the homogenized problems) pollutes the posterior prediction. Therefore, we perform again the same experiment for $\varepsilon = 1/4$, but taking into account the homogenization error as described in Section 4.2.2. We approximate the homogenization error distribution, by computing its mean and covariance offline as explained in Section 4.2.2, and we include these quantities into the posterior density definition according to (4.24). We perform the experiment for various number of sample sizes M to approximate the homogenization error distribution, namely $M = \{5, 10, 20\}$. The parameters such as K and L are identical to the previous numerical test. Numerical results are shown in Figure 4.5. In particular we can observe how already with $M = 5$ we can manage to significantly improve the results reported in Figure 4.4 for $\varepsilon = 1/4$.

Sensitivity with respect to L (number of Dirichlet data).   Next, we investigate the sensitivity of the approximated solution with respect to the parameter L, denoting the number of different Dirichlet conditions used to produce the observations. The setting is the same as in the previous numerical experiments, except that ε is fixed and equal to $1/64$, while $L = \{2, 4, 6\}$. Numerical results are shown in Figure 4.6. We notice that for $L = 2$ the variance is significantly larger than for $L = 4$ or $L = 6$, which indicates more uncertainty about the approximated solution. This is also visible from the approximation of the posterior density obtained for the three first coefficients of the Karhunen-Loève expansion.

Sensitivity with respect to K (number of terms in the truncated KL expansion).   Finally, we examine how the size of the truncated Karhunen-Loève expansion affects our predictions. We perform experiments for $K = \{10, 20, 30, 40, 50, 60\}$, while L and ε are fixed, set to 6 and $1/64$ respectively. The results shown in Figure 4.7 illustrate that by increasing the number of eigenvalues/eigenfunctions we obtain a better sampling of the quantity of interest. However we note that for smaller K, a coarser mesh can be used for the forward discrete problem, leading to a significant saving of the computational cost. Hence, we suggest the possibility of investigating the implementation of a Metropolis-Hastings algorithm on multiple levels, with an approximation of the distribution of the lowest modes on a coarse mesh, while performing fewer samples for the highest modes on a finer mesh to guarantee a proper sample of the posterior density, as described in [44].
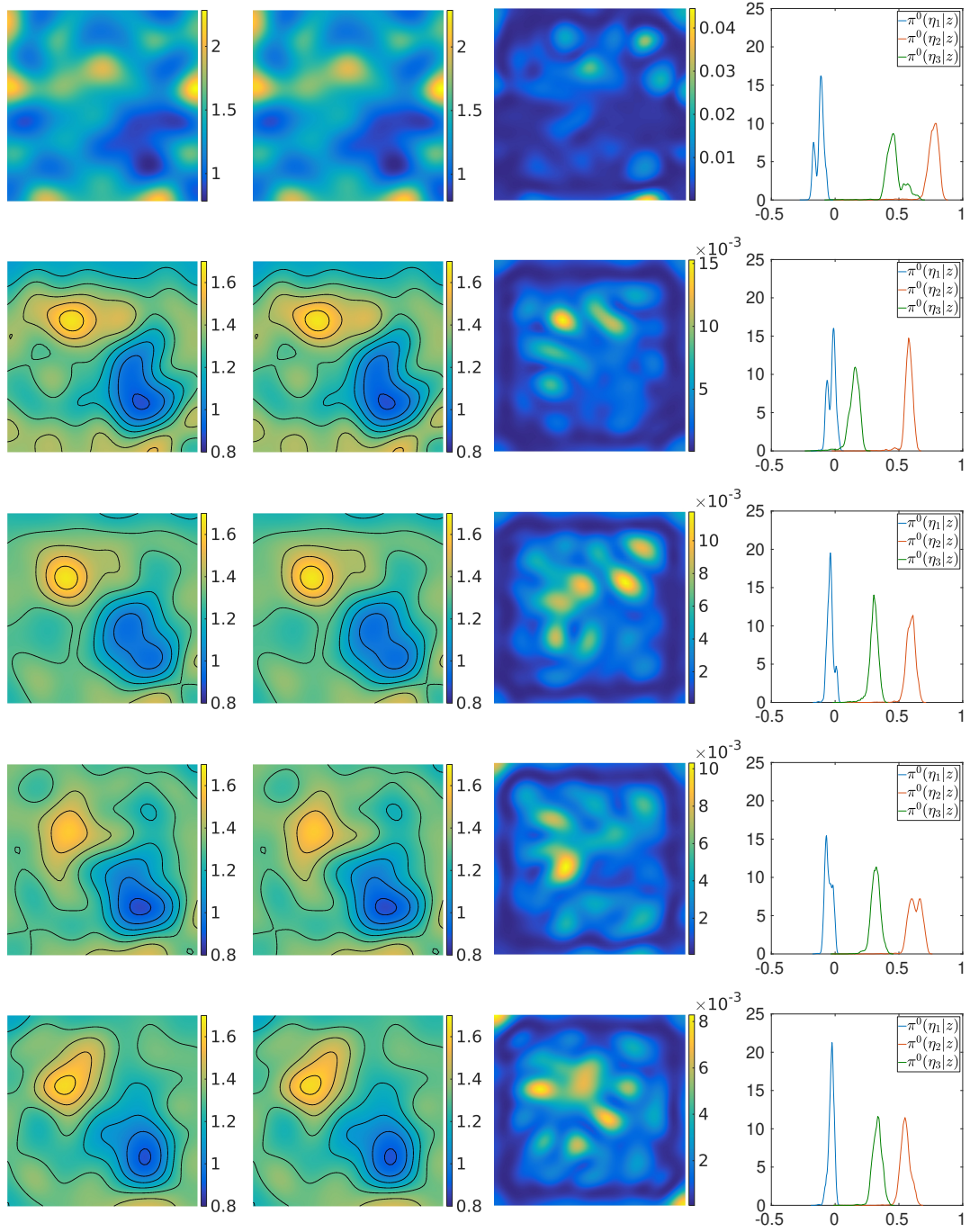
Figure 4.4: Comparison of numerical approximations of the posterior density for the problem considered in Section 4.5.2, obtained with different values of ε. From left to right the plotted quantities are $P_1(\mathbb{E}[\theta^{H,K}])$, $\mathbb{E}[P_1(\theta^{H,K})]$, $\mathrm{Var}[P_1(\theta^{H,K})]$, and the posterior density of the three first coefficients of the truncated Karhunen-Loève expansion, corresponding to $\varepsilon = \{1/4, 1/8, 1/16, 1/32, 1/64\}$. The length scale ε decreases from the top to the bottom. The other parameters are $H = 1/64$, $L = 6$, $K = 60$.
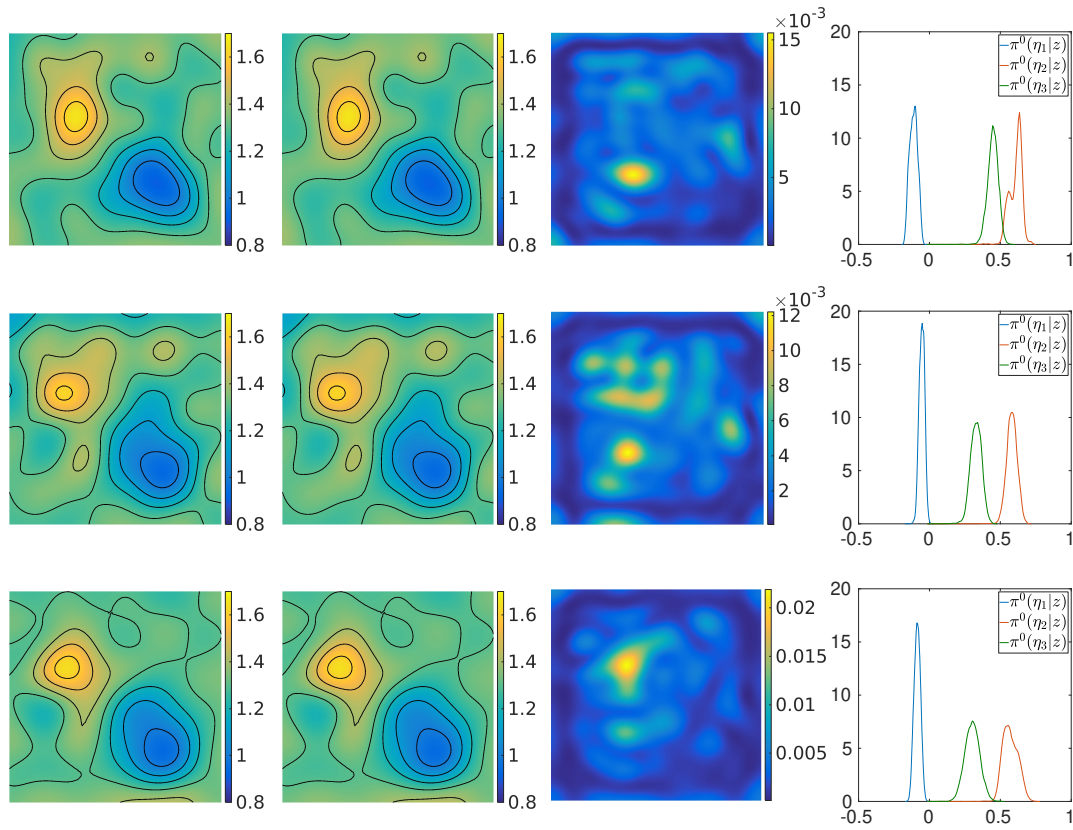
Figure 4.5: Comparison of numerical approximations of the posterior density for the problem considered in Section 4.5.2 obtained with $\varepsilon = 1/4$, for different values of M, the sample size used to approximate the homogenization error distribution. From left to right the plotted quantities are $P_1(\mathbb{E}[\theta^{H,K}])$, $\mathbb{E}[P_1(\theta^{H,K})]$, $\mathrm{Var}[P_1(\theta^{H,K})]$, and the posterior density of the three first coefficients of the truncated Karhunen-Loève expansion. The value of M is 5 in the first row, 10 in the second one, and 20 in the third row. The other parameters are $H = 1/64$, $L = 6$, $K = 60$.

Figure 4.6: Comparison of numerical approximations of the posterior density for the problem considered in Section 4.5.2 obtained for different values of L, the number of Dirichlet data. From left to right the plotted quantities are $P_1(\mathbb{E}[\theta^{H,K}])$, $\mathbb{E}[P_1(\theta^{H,K})]$, $\mathrm{Var}[P_1(\theta^{H,K})]$, and the posterior density of the three first coefficients of the truncated Karhunen-Loève expansion. In the first row $L = 2$, in the second one $L = 4$. For $L = 6$ see last row in Figure 4.4. The other parameters are $H = 1/64$, $\varepsilon = 1/64$, $K = 60$.
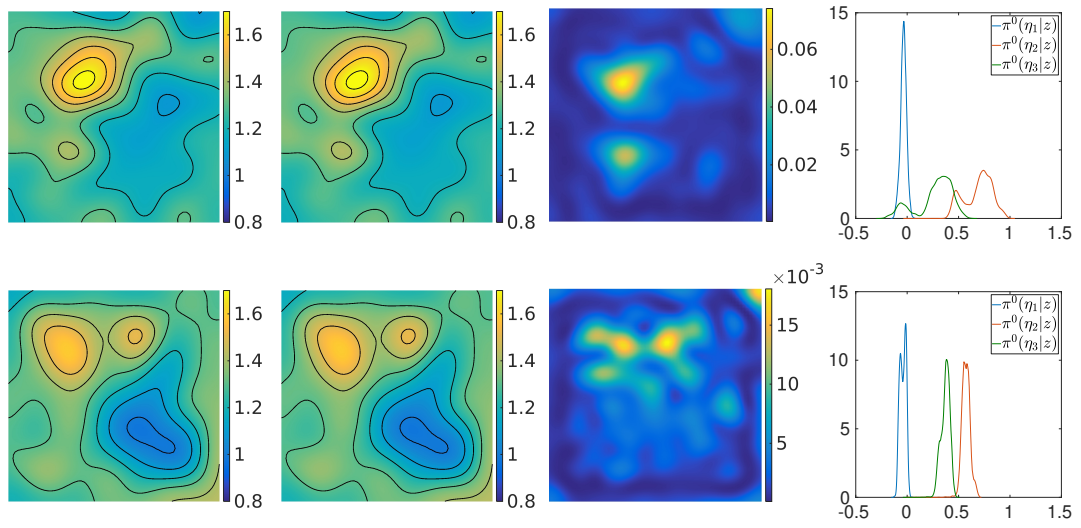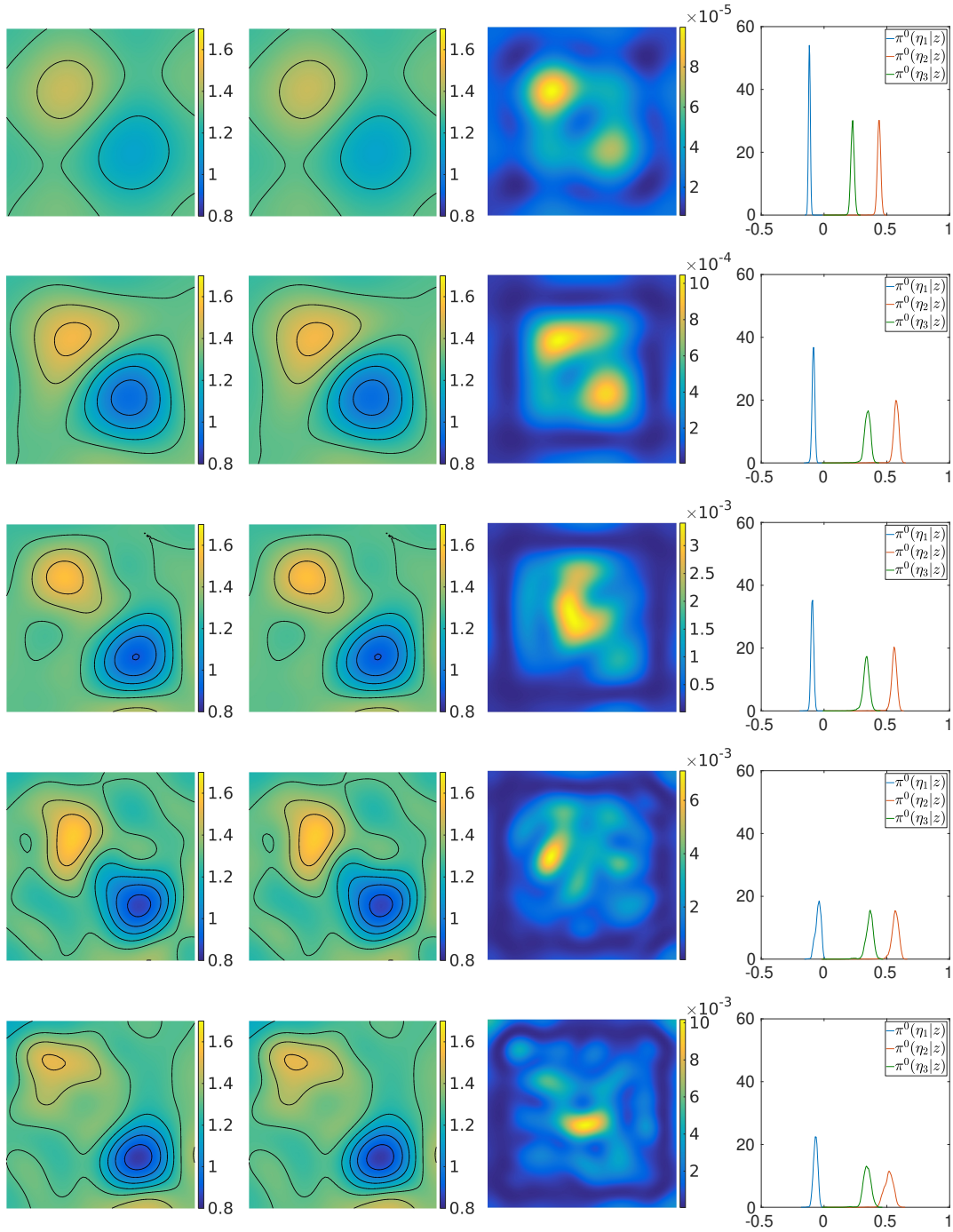
Figure 4.7: Comparison of numerical approximations of the posterior density for the problem considered in Section 4.5.2 obtained for different values of K, the number of coefficients in the truncated Karhunen-Loève expansion. From left to right the plotted quantities are $P_1(\mathbb{E}[\theta^{H,K}])$, $\mathbb{E}[P_1(\theta^{H,K})]$, $\mathrm{Var}[P_1(\theta^{H,K})]$, and the posterior density of the three first coefficients of the truncated Karhunen-Loève expansion, corresponding to $K = \{10, 20, 30, 40, 50\}$. The parameter K increases from the top to the bottom. For $K = 60$ see last row in Figure 4.4. The other parameters are $H = 1/64$, $\varepsilon = 1/64$, $L = 6$.

4.5.3   A 2D non-affinely parameterized tensor (orientation of micro oscillations)

Now we consider the case where the function σ^* controls the angle of the oscillations which characterize the full tensor $A_{\sigma^*}^\varepsilon$. The tensor is defined as

$$
\begin{aligned}
A_{11}(\sigma^*(x), x/\varepsilon) &= \sin\left(\frac{4\pi \mathbf{e}^{1\top} Q x}{\varepsilon}\right) + 1.5\,, \\
A_{22}(\sigma^*(x), x/\varepsilon) &= \cos^2\left(\frac{2\pi \mathbf{e}^{2\top} Q x}{\varepsilon}\right) + 1\,, \\
A_{12}(\sigma^*(x), x/\varepsilon) &= A_{21}(\sigma^*(x), x/\varepsilon) = 0\,,
\end{aligned}
\tag{4.34}
$$

where $Q = Q(\sigma^*(x))$ is a rotation matrix depending on $\sigma^* : D \to \mathbb{R}$

$$
Q(\sigma^*(x)) = \begin{pmatrix} \cos(2\pi\sigma^*(x)) & \sin(2\pi\sigma^*(x)) \\ -\sin(2\pi\sigma^*(x)) & \cos(2\pi\sigma^*(x)) \end{pmatrix}\,,
\tag{4.35}
$$

and

$$
\sigma^*(x) = a + b\mathbb{1}_{\widetilde{D}}\,, \quad \widetilde{D} \subset D, a, b \in \mathbb{R}\,.
$$

We consider the case where $\widetilde{D}$ is the circle defined as

$$
\widetilde{D} = \left\{ x = (x_1, x_2) : (x_1 - 1/3)^2 + (x_2 - 1/3)^2 \le 0.05 \right\}\,.
$$

In Figure 4.8 we show the function σ^* and the first component of the tensor A_{11}^ε. From (4.34),

σ^*. $A_{11}^\varepsilon, \varepsilon = 1/64.$
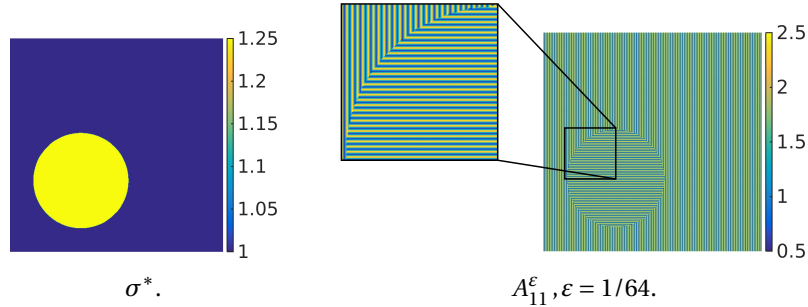
Figure 4.8: Representation of the true spatial field σ^* and the first component of the highly oscillating tensor for the non-affine case considered in Section 4.5.3 (orientation of oscillations).

(4.35) it can be observed that different values of a and b for σ^* can lead to the same rotation of the oscillations, and in general to the same tensor $A_{\sigma^*}^\varepsilon$. To ensure uniqueness we assume to know a priori the values of a and b. We take $a = 1$ and $b = 0.25$. Our task is thus to recover the region $\widetilde{D} \subset D$. To do so, we consider a level set prior for the unknown, defined using the function $P_2 : C^0(\overline{D}) \to U$ introduced in Section 4.2. The prior measure on $C^0(\overline{D})$ is defined as in (4.33) with $\theta_{\mathrm{pr}} = 1$, $\gamma = 0.025$, and $\lambda = 0.5$. Hence, we apply the map P_2 to each draw from

μ_{pr} to obtain a level set sample, i.e.,

$$P_2(\theta) = 1\mathbb{1}_{D_1} + 1.25\mathbb{1}_{D_2},$$

where

$$D_1 = \{x \in D : -\infty < \theta(x) \le 1\}, \quad D_2 = \{x \in D : 1 < \theta(x) < \infty\},$$

so that $\overline{D} = D_1 \cup D_2$, $D_1 \cap D_2 = \varnothing$. Four examples of draws from the level set prior are reported in Figure 4.9. We obtain data for $\varepsilon = 1/64$ and we approximate the homogenization error
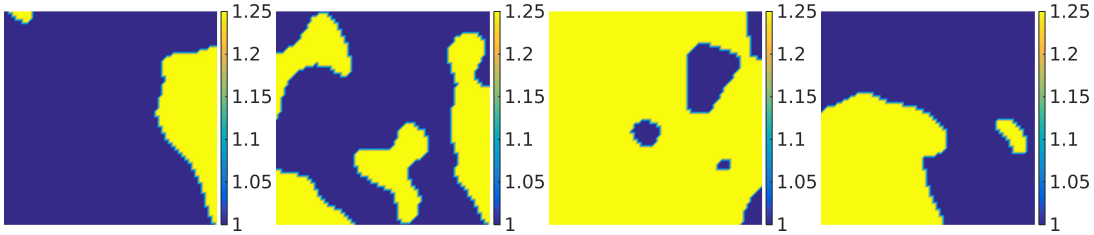

Figure 4.9: Four samples from the level set prior used in the problem considered in Section 4.5.3.

distribution as described in Section 4.2.2 using $M = 20$. The parameters K and L are set to 60 and 6 respectively. Then, we approximate the posterior by using the MH algorithm by drawing 4×10^5 samples using $s = 0.02$. For this choice of the parameters, we get an acceptance ratio during the sampling of about 73%. In Figure 4.10 we plot the quantities $P_2(\mathbb{E}[\theta^{H,K}])$, $\mathbb{E}[P_2(\theta^{H,K})]$, and $\mathrm{Var}[P_2(\theta^{H,K})]$. In particular $P_2(\mathbb{E}[\theta^{H,K}])$ preserves the binary field property of the admissible set, while the estimate $\mathbb{E}[P_2(\theta^{H,K})]$ gives a better understanding of the uncertainty across the interface where the discontinuity takes place. This uncertainty is also reflected by the plot of the variance $\mathrm{Var}[P_2(\theta^{H,K})]$. The numerical results show good agreement with Figure 4.8.
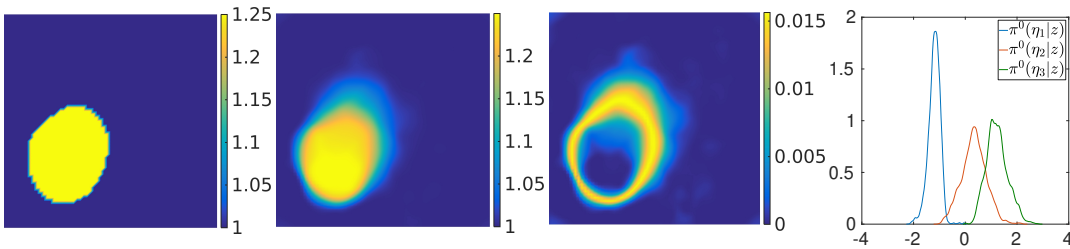
Figure 4.10: Numerical results for the non-affine parameterization considered in Section 4.5.3 (orientation of oscillations). From left to right the plotted quantities are $P_2(\mathbb{E}[\theta^{H,K}])$, $\mathbb{E}[P_2(\theta^{H,K})]$, $\mathrm{Var}[P_2(\theta^{H,K})]$, and the posterior density of the three first coefficients of the truncated Karhunen-Loève expansion. The values of the parameters are $H = 1/64$, $\varepsilon = 1/64$, $M = 20$, $L = 6$, $K = 60$.

4.5.4   A 2D non-affinely parameterized tensor (volume fraction of two phase layered material)

We conclude the numerical experiments by considering the case where $A_{\sigma^*}^{\varepsilon}$ represents the conductivity of a hypothetical two phase layered material. In this case the macroscopic function $\sigma^* : D \to [0,1]$ determines the volume fraction of each component. Then tensor is defined as

$$A_{11}(\sigma^*(x), x/\varepsilon) = A_{22}(\sigma^*(x), x/\varepsilon) = \begin{cases} 2 \text{ if } 0 \le (x_2 \bmod \varepsilon)/\varepsilon < \sigma^*(x) \\ 1 \text{ if } \sigma^*(x) \le (x_2 \bmod \varepsilon)/\varepsilon < 1, \end{cases} \quad (4.36)$$

$$A_{12}(\sigma^*(x), x/\varepsilon) = A_{21}(\sigma^*(x), x/\varepsilon) = 0.$$

We consider the case where σ^* is defined as

$$\sigma^*(x) = \sum_{i=1}^{n} c_i \mathbb{1}_{\widetilde{D}_i}, \quad \widetilde{D}_i \subset D, c_i \in [0,1],$$

$\widetilde{D}_i \cap \widetilde{D}_j = \varnothing$ for $i \ne j$, $\cup_{i=1}^{n} \widetilde{D}_i = D$. Again, we assume to know a priori the values $\{c_i\}_{i=1}^{n}$ that the function σ^* can take, and our goal is to recover the different regions $\{\widetilde{D}_i\}_{i=1}^{n}$. We note that knowing the range of possible values for σ^* allows us to efficiently use the RB method and in particular the EIM algorithm. For our problem we set $n = 4$, $c_1 = 0.8$, $c_2 = 0.6$, $c_3 = 0.4$, $c_4 = 0.2$, and we make the following choice for the sets $\{\widetilde{D}_i\}_{i=1}^{4}$:

$$\widetilde{D}_1 = \{x = (x_1, x_2) : 0 \le x_1 \le 0.25\},$$
$$\widetilde{D}_2 = \{x = (x_1, x_2) : 0.25 < x_1 \le 0.5\},$$
$$\widetilde{D}_3 = \{x = (x_1, x_2) : 0.5 < x_1 \le 0.75\},$$
$$\widetilde{D}_4 = \{x = (x_1, x_2) : 0.75 < x_1 \le 1\}.$$

The true field σ^* and the first component of the multiscale tensor are shown in Figure 4.11. We

$$\sigma^*. \qquad\qquad A_{11}^{\varepsilon}, \varepsilon = 1/64.$$

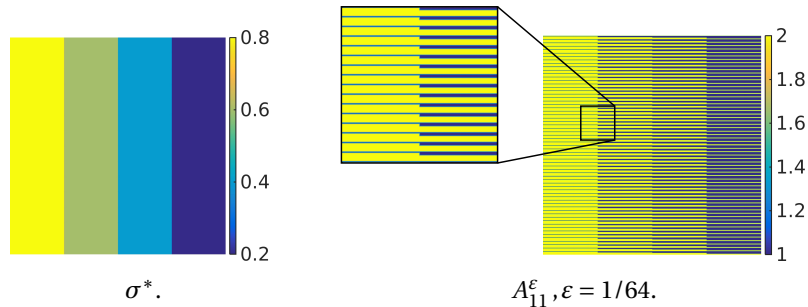Figure 4.11: Representation of the true spatial field σ^* and the first component of the highly oscillating tensor for the non-affine case considered in Section 4.5.4 (volume fraction).

consider for this last numerical experiment a macro discretization with mesh size $H = 1/32$, and a level set prior. The Gaussian prior measure μ_{pr} on $C^0(\overline{D})$ is the same used in the

previous numerical tests, with $\theta_{\mathrm{pr}} = 0.5$, $\gamma = 0.05$, $\lambda = 0.5$. The function $P_2 : C^0(\overline{D}) \to U$, is instead defined as

$$P_2(\theta) = c_1 \mathbb{1}_{D_1} + c_2 \mathbb{1}_{D_2} + c_3 \mathbb{1}_{D_3} + c_4 \mathbb{1}_{D_4},$$

where

$$D_1 = \{x \in D : 0.6 < \theta(x) < \infty\},$$
$$D_2 = \{x \in D : 0.4 < \theta(x) \le 0.6\},$$
$$D_3 = \{x \in D : 0.2 < \theta(x) \le 0.4\},$$
$$D_4 = \{x \in D : -\infty < \theta(x) \le 0.2\}.$$

Four samples from the considered level set prior are shown in Figure 4.12. To solve the
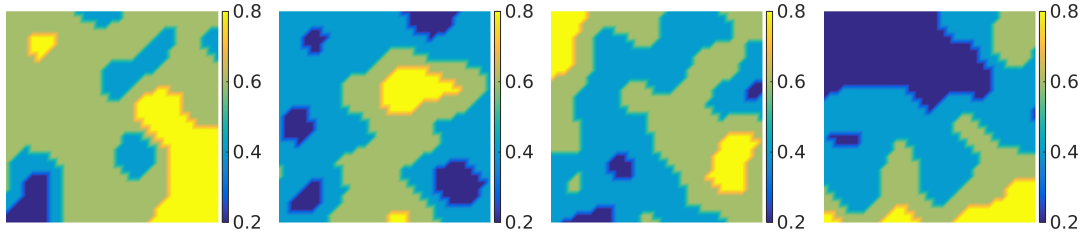
Figure 4.12: Four samples from the level set prior used in the problem considered in Section 4.5.4.

problem the observations are obtained for $\varepsilon = 1/64$. The homogenization error distribution is approximated offline as described in Section 4.2.2 using $M = 20$. The parameter K and L are set to 60 and 6 respectively. We draw 4×10^5 samples from the posterior distribution using the MH algorithm with $s = 0.01$, which leads to an acceptance ratio of 44%. The numerical results are shown in Figure 4.13, and are in good agreement with Figure 4.11.
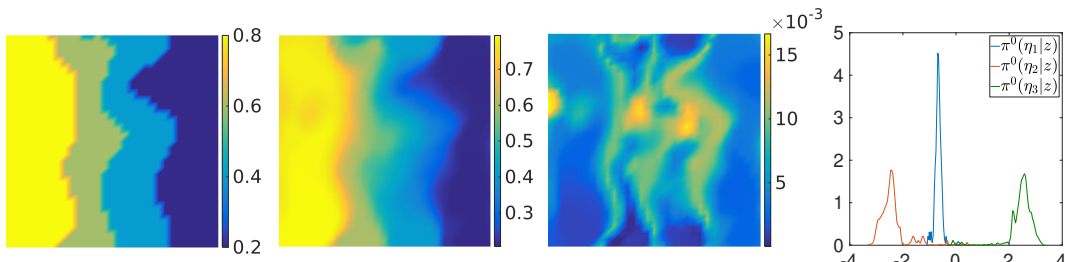
Figure 4.13: Numerical results for the non-affine parameterization considered in Section 4.5.4 (volume fraction). From left to right the plotted quantities are $P_2(\mathbb{E}[\theta^{H,K}])$, $\mathbb{E}[P_2(\theta^{H,K})]$, $\mathrm{Var}[P_2(\theta^{H,K})]$, and the posterior density of the three first coefficients of the truncated Karhunen-Loève expansion. $H = 1/32$, $\varepsilon = 1/64$, $M = 20$, $L = 6$, $K = 60$

5 Homogenization and multiscale methods for linear elasticity problems in random perforated domains

In this chapter we consider homogenization in linear elasticity with random porous media. We review the theory of homogenization in the context of linear elasticity with random perforated domains, and we give a rigorous formulation of the RB-FE-HMM in this setting, providing a priori error estimates. Extension and analysis of the FE-HMM in the context of linear elasticity appeared first in [2], while in [49] some numerical experiments are presented in order to verify numerically the theoretical findings given in [2]. In both [2] and [49] only problems in linear elasticity with multiscale periodic tensors are considered, while problems in perforated domains are not addressed. Extension of the FE-HMM for scalar valued elliptic problems in periodic perforated domains is presented in [61], while in [5] the use of the RB-FE-HMM for solving the Stokes problem in periodic porous media is described. Hence, to the best of our knowledge, studies on the use of the FE-HMM for solving linear elasticity problems in perforated (periodic and random) domains are not available in the literature, and are presented in this chapter. In addition, we combine the FE-HMM with reduced basis techniques to speed up the overall computational time. Finally, let us point out that we adopt the Einstein summation convention, i.e., we sum over repeated indices.

Outline.   The outline of the chapter is as follows. In Section 5.1 we start by recalling some preliminary definitions and results on homogenization of random tensors in linear elasticity. In Section 5.2 we define random perforated domains in $\mathbb{R}^d$, and we provide practical examples. We derive then homogenization results in linear elasticity with random perforated domains, and explain how in practice the coefficients of the effective tensor are approximated. In Section 5.3 we describe the FE-HMM and the RB-FE-HMM in the context of linear elasticity with random perforated domains. We derive stability results and provide a priori error estimates for the numerical methods. Finally, in Section 5.4 we conclude with some numerical experiments to assert our theoretical findings. The contents of this chapter are essentially taken from [8].

5.1 Homogenization in random linear elasticity

Homogenization of elliptic operators in perforated random domains is related to the theory of homogenization of elliptic operators with random coefficients. The literature treating homogenization of random structures is vast. Some foundational works can be found in [67, 76, 89, 63]. Let D be an open bounded set in $\mathbb{R}^d$, $d \leq 3$. Let $\Gamma_1 \subset \partial D$ and $\Gamma_2 \subset \partial D$ be two disjoint sets with positive measure such that $\Gamma_1 \cup \Gamma_2 = \partial D$, and consider the problem of finding $\mathbf{u}^\varepsilon = (u_1^\varepsilon, \dots, u_d^\varepsilon)$ such that, given $\mathbf{f} \in (L^2(D))^d$ and $\mathbf{h} \in (L^2(\Gamma_2))^d$, it satisfies

$$
\begin{aligned}
-\frac{\partial}{\partial x_j}\left(A_{ijlm}^\varepsilon \frac{\partial u_l^\varepsilon}{\partial x_m}\right) &= f_i & &\text{in } D, \\
\mathbf{u}^\varepsilon &= \mathbf{0} & &\text{on } \Gamma_1, \\
A_{ijlm}^\varepsilon \frac{\partial u_l^\varepsilon}{\partial x_m} \nu_j &= h_i & &\text{on } \Gamma_2,
\end{aligned}
\tag{5.1}
$$

for $i = 1, \dots, d$, where $\boldsymbol{\nu} = (\nu_1, \dots, \nu_d)$ is the unit outward normal at the boundary. We assume that the fourth-order tensor $A^\varepsilon(x) = \{A_{ijlm}^\varepsilon(x)\}_{1 \leq i,j,l,m \leq d}$, $A_{ijlm}^\varepsilon \in L^\infty(D)$, $A^\varepsilon(x) = A(x/\varepsilon) = A(y)$, $y = x/\varepsilon$, is statistically stationary with respect to the spatial variable $y \in \mathbb{R}^d$, or equivalently that it is a particular realization of a stationary random field. Moreover it is assumed that

$$
A_{ijlm}^\varepsilon = A_{jilm}^\varepsilon = A_{lmij}^\varepsilon \quad \text{for any } i, j, l, m = 1, \dots, d, \tag{5.2}
$$

$$
\alpha \|m\|_{\mathrm{F}}^2 \leq A^\varepsilon m \cdot m \quad \text{for any symmetric } d \times d \text{ matrix } m, \tag{5.3}
$$

$$
\|A^\varepsilon m\|_{\mathrm{F}} \leq \beta \|m\|_{\mathrm{F}} \quad \text{for any symmetric } d \times d \text{ matrix } m, \tag{5.4}
$$

where $\alpha, \beta > 0$ and for any $d \times d$ symmetric matrices $m, \widetilde{m}$ we have that

$$
A^\varepsilon m = \{(A_{ijlm}^\varepsilon m_{lm})_{ij}\}_{1 \leq i,j \leq d}, \quad A^\varepsilon m : \widetilde{m} = A_{ijlm}^\varepsilon m_{lm} \widetilde{m}_{ij}.
$$

We introduce the strain tensor e and the stress tensor σ defined as

$$
e(\mathbf{u}^\varepsilon) = \{e_{ij}(\mathbf{u}^\varepsilon)\}_{1 \leq i,j \leq d}, \quad e_{ij}(\mathbf{u}^\varepsilon) = \frac{1}{2}\left(\frac{\partial u_i^\varepsilon}{\partial x_j} + \frac{\partial u_j^\varepsilon}{\partial x_i}\right),
$$

$$
\sigma(\mathbf{u}^\varepsilon) = \{\sigma_{ij}(\mathbf{u}^\varepsilon)\}_{1 \leq i,j \leq d}, \quad \sigma_{ij}(\mathbf{u}^\varepsilon) = A_{ijlm}^\varepsilon \frac{\partial u_l^\varepsilon}{\partial x_m}.
$$

The space of admissible weak solutions for the problem (5.1) is represented by $(H_{\Gamma_1}^1(D))^d$, which is a Hilbert space for the norm

$$
\|\mathbf{v}\|_{H^1(D)} = \left(\sum_{i,j=1}^d \int_D \left(\frac{\partial v_i}{\partial x_j}\right)^2 \mathrm{d}x + \sum_{i=1}^d \int_D v_i^2 \,\mathrm{d}x\right)^{1/2}.
$$

The weak formulation of problem (5.1) reads: find $\mathbf{u}^\varepsilon \in (H^1_{\Gamma_1}(D))^d$ such that

$$B_\varepsilon(\mathbf{u}^\varepsilon, \mathbf{v}) = F(\mathbf{v}) \quad \forall \mathbf{v} \in (H^1_{\Gamma_1}(D))^d \, , \tag{5.5}$$

where

$$B_\varepsilon(\mathbf{v}, \mathbf{w}) = \int_D A^\varepsilon(x) e(\mathbf{v}) : e(\mathbf{w}) \, \mathrm{d}x \, ,$$

and

$$F(\mathbf{v}) = \int_D \mathbf{f} \cdot \mathbf{v} \, \mathrm{d}x + \int_{\Gamma_2} \mathbf{h} \cdot \mathbf{v} \, \mathrm{d}s \, .$$

From the Korn's inequality

$$\|\nabla \mathbf{v}\|_{L^2(D)} \leq C \left(\int_D |e(\mathbf{v})|^2 \, \mathrm{d}x \right)^{1/2} \, ,$$

which holds $\forall \mathbf{v} \in (H^1_{\Gamma_1}(D))^d$, and Lax-Milgram theorem we obtain existence and uniqueness of the solution of (5.5) and the a priori estimate

$$\|\mathbf{u}^\varepsilon\|_{H^1(D)} \leq C(\|\mathbf{f}\|_{L^2(D)} + \|\mathbf{h}\|_{L^2(\Gamma_2)}) \, .$$

For a complete review of homogenization in linear elasticity with tensors with random coefficients we mention [63]. Hence, we briefly report some notions presented in [63], before considering the case of perforated random domains.

5.1.1 Ergodic theory and G-convergence of random tensors

As mentioned, we assume that $A^\varepsilon(x) = A(x/\varepsilon) = A(y)$, $y = x/\varepsilon$, is statistically stationary with respect to the spatial variable $y \in \mathbb{R}^d$. We start by defining stationary random fields. Let (Ω, Σ, μ) be a probability space. Assume that for each $x \in \mathbb{R}^d$ a random variable $w(x)$ is given. Then the family of random variables $w(x) = w(x, \omega)$, $\omega \in \Omega$, assumed to be defined on the same probability space (Ω, Σ, μ), defines a random process on $\mathbb{R}^d$ which is called a random field. The random field is said to be stationary if, for any set of points $\{x_1, \dots, x_k\}$ and any $h \in \mathbb{R}^d$, the distribution of the vector $\{w(x_1 + h), \dots, w(x_k + h)\}$ does not depend on h. For an arbitrary random variable $v(\omega)$, we define $w(x, \omega) = v(T_x(\omega))$, where $T_x : \Omega \to \Omega$ is a map parameterized by $x \in \mathbb{R}^d$ which preserves the measure μ on Ω. Then it follows that $w(x, \omega)$ is a stationary random field.

Dynamical systems on probability spaces. We define $T_x : \Omega \to \Omega$, $x \in \mathbb{R}^d$, as a dynamical system possessing the following properties.

99

1. $T_0 = \mathrm{Id}$, $T_{x_1+x_2} = T_{x_1}\,T_{x_2}$, $\forall x_1, x_2 \in \mathbb{R}^d$.

2. The mapping $T_x : \Omega \to \Omega$ preserves the measure μ on Ω, i.e. $\mu(T_x(\mathscr{F})) = \mu(\mathscr{F})$, $\forall x \in \mathbb{R}^d$, $\forall \mathscr{F} \in \Sigma$.

3. For any measurable function $f(\omega)$, $\omega \in \Omega$, the function $f(T_x(\omega))$ defined on $\Omega \times \mathbb{R}^d$ is also measurable.

Given the dynamical system $T_x : \Omega \to \Omega$, we can introduce a wide class of random fields. Let f a measurable function defined on Ω. For a fixed $\omega \in \Omega$ we say that the function $f(T_x(\omega))$ of argument $x \in \mathbb{R}^d$ is a realization of f.

Ergodic theory. Next, we introduce the concept of ergodicity. A measurable function f is said invariant under T_x if $f(T_x(\omega)) = f(\omega)$ for any $x \in \mathbb{R}^d$ almost everywhere in Ω. Then, the dynamical system T_x is said ergodic if all the invariant functions under T_x are constant almost everywhere in Ω. An equivalent definition is that T_x is ergodic if for any invariant subset $\mathscr{F} \in \Sigma$ under T_x, we have $\mu(\mathscr{F}) = 1$ or $\mu(\mathscr{F}) = 0$, where $\mathscr{F}$ is invariant under T_x if $\mathscr{F} = T_x(\mathscr{F})$ for any $x \in \mathbb{R}^d$. Let us emphasize that homogenization results remain valid for non-ergodic maps. The ergodicity assumption on T_x allows to simplify the calculations, and therefore in what follows we will always assume T_x to be an ergodic dynamical system.

An important tool of ergodic theory is the Birkhoff's ergodic theorem, which, for a measurable function f on Ω, establishes the equivalence between the average of f computed on the events space Ω, and the average of a particular realization $f(T_x(\omega))$ computed on the space $\mathbb{R}^d$, while $\omega \in \Omega$ is fixed. In order to give a rigorous formulation of the theorem, let us introduce the notion of mean value for a function defined in $\mathbb{R}^d$. Let $f \in L^1_{\mathrm{loc}}(\mathbb{R}^d)$. We denote the mean value of f as $M(f)$ which is given by

$$\lim_{\varepsilon \to 0} \int_K f(x/\varepsilon)\,\mathrm{d}x = |K| M(f), \tag{5.6}$$

for any Lebesgue measurable set $K \subset \mathbb{R}^d$. Under some additional assumptions, the mean value of a function can be also expressed in terms of weak convergence. It suffices to take a family of functions $f(x/\varepsilon)$ which is bounded in $L^p_{\mathrm{loc}}(\mathbb{R}^d)$, $p \geq 1$. Hence, from the definition of weak convergence we have that as $\varepsilon \to 0$

$$f(x/\varepsilon) \rightharpoonup M(f) \quad \text{weakly in } L^p_{\mathrm{loc}}(\mathbb{R}^d) \tag{5.7}$$

if and only if

$$\lim_{\varepsilon \to 0} \int_{\mathbb{R}^d} f(x/\varepsilon)\varphi\,\mathrm{d}x = \int_{\mathbb{R}^d} M(f)\varphi\,\mathrm{d}x \quad \forall \varphi \in L^{p'}_{\mathrm{loc}}(\mathbb{R}^d),$$

where $1/p' = 1 - 1/p$. The result follows from (5.6) and the fact that linear combinations of characteristic functions of the sets $K \subset \mathbb{R}^d$ are dense in $L^{p'}_{\mathrm{loc}}(\mathbb{R}^d)$. We can now state the

Birkhoff's ergodic theorem. For more details see for example [45].

Theorem 5.1.1 (Birkhoff's ergodic theorem)**.** *Let $f \in L^p(\Omega)$, $p \geq 1$. Then for almost all $\omega \in \Omega$ the realization $f(T_x(\omega))$ possesses a mean value in the sense of (5.7), i.e.,*

$$f(T_{x/\varepsilon}(\omega)) \rightharpoonup M(f) \quad \text{weakly in } L^p_{\text{loc}}(\mathbb{R}^d).$$

Moreover, the mean value $M(f(T_x(\omega))$, considered as a function of ω, is invariant under T_x, i.e.,

$$\int_\Omega f(\omega) \, \mathrm{d}\mu = \int_\Omega M(f(T_x(\omega)) \, \mathrm{d}\mu.$$

In particular, if the dynamical system T_x is ergodic, then

$$M(f(T_x(\omega))) = \int_\Omega f(\omega) \, \mathrm{d}\mu \quad \text{for almost all } \omega \in \Omega.$$

Homogenization with random tensors. In order to formulate homogenization results in linear elasticity with random tensors, we introduce some spaces of functions defined on the probability space (Ω, Σ, μ). We say that a symmetric tensor field $v(x) = \{v_{ij}(x)\}_{1 \leq i,j \leq d}$, $v \in (L^2_{\text{loc}}(\mathbb{R}^d))^{d \times d}$, is a potential tensor field if it admits a representation of the form $v = e(\mathbf{u})$, for some vector field $\mathbf{u} \in (H^1_{\text{loc}}(\mathbb{R}^d))^d$. On the other hand, a symmetric tensor field v is said to be a solenoidal if

$$\int_{\mathbb{R}^d} v : e(\boldsymbol{\varphi}) \, \mathrm{d}x = 0 \quad \forall \boldsymbol{\varphi} \in (C_0^\infty(\mathbb{R}^d))^d, \tag{5.8}$$

where $(C_0^\infty(\mathbb{R}^d))^d$ is the space of vector fields which are infinitely differentiable and which have compact support in $\mathbb{R}^d$. Note that (5.8) is equivalent to the condition

$$\frac{\partial}{\partial x_j} v_{ij} = 0 \quad \forall i = 1, \ldots, d.$$

Now, a symmetric random tensor $v(\omega) = \{v_{ij}(\omega)\}_{1 \leq i,j \leq d}$, $v \in (L^2(\Omega))^{d \times d}$, is said to be potential (resp. solenoidal), if almost all its realizations $v(T_x(\omega))$ are potential (resp. solenoidal) tensor fields on $\mathbb{R}^d$. We denote by $V^2_{\text{pot}}(\Omega)$ (resp. $V^2_{\text{sol}}(\Omega)$) the space of all potential (resp. solenoidal) symmetric matrices having zero mean value. The two spaces are complete and mutually orthogonal. It can be shown [63] that the space $L^2(\Omega, \text{Sym}_d)$ consisting of $d \times d$ real valued symmetric matrix functions can be decomposed as

$$L^2(\Omega, \text{Sym}_d) = V^2_{\text{pot}}(\Omega) \oplus V^2_{\text{sol}}(\Omega) \oplus \text{Sym}_d,$$

where Sym_d denotes the class of $d \times d$ real valued symmetric matrices.

Chapter 5. Homogenization and multiscale methods for linear elasticity problems in random perforated domains

G-convergence in linear elasticity.   Theory of G-convergence in linear elasticity is similar to the one for elliptic scalar PDEs. Here we recall the definition of G-convergence for fourth-order tensor valued functions.

Definition 5.1.2. Let A^ε and A^0 be two tensors satisfying (5.2), (5.3), (5.4) in a domain $D \subset \mathbb{R}^d$. We say that the sequence $\{A^\varepsilon\}_{\varepsilon>0}$ G-converges to the tensor A^0 in D if and only if for any $\mathbf{f} \in (H^{-1}(D))^d$ and any $\mathbf{g} \in (H^{1/2}(\partial D))^d$ the solution $\mathbf{u}^\varepsilon$ of

$$-\frac{\partial}{\partial x_j}\left(A^\varepsilon_{ijlm}\frac{\partial u^\varepsilon_l}{\partial x_m}\right) = f_i \qquad \text{in } D,$$
$$\mathbf{u}^\varepsilon = \mathbf{g} \qquad \qquad \text{on } \partial D,$$

$\forall i = 1, \dots, d$, is such that

$$\mathbf{u}^\varepsilon \rightharpoonup \mathbf{u}^0 \quad \text{weakly in } (H^1(D))^d,$$

where $\mathbf{u}^0$ is the unique solution of

$$-\frac{\partial}{\partial x_j}\left(A^0_{ijlm}\frac{\partial u^0_l}{\partial x_m}\right) = f_i \qquad \text{in } D,$$
$$\mathbf{u}^0 = \mathbf{g} \qquad \qquad \text{on } \partial D,$$

$\forall i = 1, \dots, d$. A consequence of G-convergence is the weak convergence of the stresses

$$\sigma(\mathbf{u}^\varepsilon) = A^\varepsilon e(\mathbf{u}^\varepsilon) \rightharpoonup \sigma(\mathbf{u}^0) = A^0 e(\mathbf{u}^0) \quad \text{weakly in } (L^2(D))^{d \times d}.$$

Properties such as uniqueness of the G-limit, locality and compactness results we mentioned for elliptic scalar PDEs in Chapter 2 extend also to the case of linear elasticity problems. The following theorem is proved in [63].

Theorem 5.1.3. *Let $A = A(\omega)$ be a measurable tensor valued function defined in Ω and satisfying* (5.2), (5.3), (5.4). *Set*

$$A^\varepsilon(x) = A(x/\varepsilon) = A(y), \quad A(y) = A(T_y(\omega)).$$

Then there exists a tensor A^0, independent of x and ω, such that A^ε G-converges to A^0 in any domain $D \subset \mathbb{R}^d$. For any $m \in \mathrm{Sym}_d$, the tensor A^0 is defined by

$$m : A^0 m = \inf_{v \in V^2_{\mathrm{pot}}(\Omega)} \int_\Omega (m+v) : A(m+v) \, d\mu.$$

Remark 5.1.4. The same results of convergence can also be extended to the case of sequences of locally periodic tensors. We refer to [75] for a complete review on homogenization in elasticity problems.

5.2 The case of random perforated domains

Let (Ω, Σ, μ) be a probability space and $T_x : \Omega \to \Omega$, $x \in \mathbb{R}^d$, a dynamical system as defined in Section 5.1. Let us fix a measurable set $\mathscr{F} \in \Sigma$ and $\omega \in \Omega$. The random stationary set $Q = Q(\omega) \subset \mathbb{R}^d$ is obtained from $\mathscr{F}$ and it is given by

$$Q(\omega) = \left\{ x \in \mathbb{R}^d : T_x(\omega) \in \mathscr{F} \right\}.$$

Its density or concentration is defined as the mean value of its characteristic function. Theorem 5.1.1 shows that the density of Q exists for almost all $\omega \in \Omega$ and it is equal to $\mu(\mathscr{F})$. Let D be an open bounded set in $\mathbb{R}^d$. We define the set Q^ε homothetic to Q with ratio ε as

$$Q^\varepsilon = \left\{ x \in \mathbb{R}^d : x/\varepsilon \in Q \right\}.$$

By removing the set $D \cap Q^\varepsilon$ from D we obtain a perforated domain which we call D^ε, whose degree of fineness is inversely proportional to ε. Note that, as it is defined, D^ε could be not connected. Moreover, it could exhibit a fine grained boundary. Hence, in what follows we make the additional assumptions that D^ε is connected and that $\partial D \subset \partial D^\varepsilon$. Let $\Gamma_1 \subset \partial D$ and $\Gamma_2 \subset \partial D$ be two disjoint sets with positive measure such that $\Gamma_1 \cup \Gamma_2 = \partial D$. The goal of this section is to provide homogenization results for the problem of finding the weak solution $\mathbf{u}^\varepsilon = (u_1^\varepsilon, \dots, u_d^\varepsilon) \in (H^1_{\Gamma_1}(D^\varepsilon))^d$ such that, given $\mathbf{f} \in (L^2(D))^d$ and $\mathbf{h} \in (L^2(\Gamma_2))^d$, it satisfies

$$
\begin{aligned}
-\frac{\partial}{\partial x_j} \left(A_{ijlm} \frac{\partial u_l^\varepsilon}{\partial x_m} \right) = f_i && \text{in } D^\varepsilon, \\
\mathbf{u}^\varepsilon = \mathbf{0} && \text{on } \Gamma_1, \\
A_{ijlm} \frac{\partial u_l^\varepsilon}{\partial x_m} \nu_j = h_i && \text{on } \Gamma_2, \\
A_{ijlm} \frac{\partial u_l^\varepsilon}{\partial x_m} \nu_j = 0 && \text{on } \partial D^\varepsilon \backslash \partial D,
\end{aligned}
\tag{5.9}
$$

for $i = 1, \dots, d$, where $\boldsymbol{\nu} = (\nu_1, \dots, \nu_d)$ is the unit outward normal at the boundary, and $A(x) = \{A_{ijlm}(x)\}_{1 \le i,j,l,m \le d}$ is a fourth-order tensor. We assume $A_{ijlm} \in L^\infty(D)$ and that it satisfies (5.2), (5.3), (5.4). Note that in the definition of problem (5.9) we assume to have homogeneous Neumann boundary conditions on the boundary delimited by the inner holes. The problem of homogenization for PDEs in perforated domains (periodic and random) has been studied by several authors and for different types of boundary conditions on the inner holes. Some foundational works can be found in [35, 34, 37, 29, 32, 89].

5.2.1 Definition of random perforated domains and examples

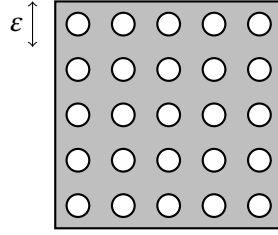In what follows, using ideas from [17], some practical examples of random sets in $\mathbb{R}^d$ are provided.

Figure 5.1: Set D^ε with periodic spherical holes of constant radius.

Example 1: periodic spheres in $\mathbb{R}^d$. As first example we consider the simple periodic set of spherical holes with constant radius, as depicted in Figure 5.1. We set the probability space as

$$(\Omega, \Sigma, \mu) = (Y, B(Y), \mathrm{Leb}),$$

where $Y = (0,1)^d$, $B(Y)$ is the Borel σ-algebra on Y, and Leb is the Lebesgue measure. We define the dynamical system $T_x : \Omega \to \Omega$, $x \in \mathbb{R}^d$ as

$$T_x(\omega) = x + \omega - \lfloor x + \omega \rfloor,$$

where for any $x \in \mathbb{R}^d$, $\lfloor x \rfloor$ is the vector whose elements are the greatest integers less or equal to the corresponding elements of x. It is easy to observe that T_x satisfies the three properties characterizing the dynamical system defined in Section 5.1. Given a radius $r > 0$, chosen so that the ball centered in Y is contained in Y, i.e. $0 < r < 1/2$, let us define the function $f : \Omega \to \mathbb{R}$,

$$f(\omega) = |\omega - 1/2\mathbf{e}|/r,$$

where $\mathbf{e} = (1, \ldots, 1)^\top \in \mathbb{R}^d$. Hence we define the subset $\mathscr{F} \in \Sigma$ as

$$\mathscr{F} = \left\{ \omega \in \Omega : f(\omega) \leq 1 \right\}.$$

Therefore given $\omega \in \Omega$ we obtain the set $Q = Q(\omega)$ as

$$Q(\omega) = \left\{ x \in \mathbb{R}^d : T_x(\omega) \in \mathscr{F} \right\},$$

consisting of Y-periodic and disjoint spherical sets, whose radius is r. In Figure 5.1 we plot the domain $D^\varepsilon = D \setminus (D \cap Q^\varepsilon)$, where

$$Q^\varepsilon = \left\{ x \in \mathbb{R}^d : x/\varepsilon \in Q \right\},$$

obtained for $D = (0,1)^2$, $r = 1/4$, $\varepsilon = 1/5$.

Example 2: ellipses in $\mathbb{R}^2$ with random axes and angle of rotation. In this second example we consider the random set depicted in Figure 5.2, consisting of ellipses in $\mathbb{R}^2$, whose minor

and major axes and angle of rotation are random variables. We denote by $I_a = [a^-, a^+] \subset \mathbb{R}$ the
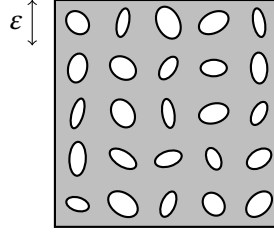

Figure 5.2: Set D^ε with ellipses whose axes and angle of rotation are random.

set of admissible values for the minor axis, $I_b = [b^-, b^+] \subset \mathbb{R}$ the set of admissible values for the major axis, and $I_\theta = [0, \theta] \subset \mathbb{R}$ the set of rotation angles. Then, we introduce three probability spaces defined as

$$(I_a, B(I_a), \mathscr{U}(I_a)),$$
$$(I_b, B(I_b), \mathscr{U}(I_b)),$$
$$(I_\theta, B(I_\theta), \mathscr{U}(I_\theta)),$$

where $B(I_a)$ (resp. $B(I_b)$, $B(I_\theta)$) is the Borel σ-algebra on I_a (resp. I_b, I_θ), and $\mathscr{U}(I_a)$ (resp. $\mathscr{U}(I_b)$, $\mathscr{U}(I_\theta)$) the uniform probability measure on I_a (resp. I_b, I_θ). Let us then define the space

$$(S, \Sigma_s, \mu_s) = \otimes_{z \in \mathbb{Z}^2} (I_a \times I_b \times I_\theta, B(I_a) \otimes B(I_b) \otimes B(I_\theta), \mathscr{U}(I_a) \times \mathscr{U}(I_b) \times \mathscr{U}(I_\theta)),$$

where Σ_s is the product σ-algebra, and μ_s is the product measure. Finally we define the space (Ω, Σ, μ) as

$$(\Omega, \Sigma, \mu) = (S, \Sigma_s, \mu_s) \otimes (Y, B(Y), \text{Leb}),$$

where $Y = (0, 1)^2$. Then each element $\omega \in \Omega$ is defined as

$$\omega = (s, y) = (\{s_z\}_{z \in \mathbb{Z}^2}, y), \quad s_z = (a_z, b_z, \theta_z)^\top \in I_a \times I_b \times I_\theta, y \in Y.$$

We define the dynamical system $T_x : \Omega \to \Omega$ as

$$\begin{aligned} T_x(\omega) &= T_x(s, y) \\ &= T_x(\{s_z\}_{z \in \mathbb{Z}^2}, y) \\ &= (\{s_{z + \lfloor x + y \rfloor}\}_{z \in \mathbb{Z}^2}, x + y - \lfloor x + y \rfloor). \end{aligned}$$

We remark that T_x satisfies the three properties characterizing a dynamical system defined in Section 5.1. Let us define the function $\widetilde{f} : I_a \times I_b \times I_\theta \times Y \to \mathbb{R}$ as

$$\widetilde{f}(s_z, y) = \frac{((y_1 - 1/2)\cos(\theta_z) - (y_2 - 1/2)\sin(\theta_z))^2}{a_z^2} + \frac{((y_1 - 1/2)\sin(\theta_z) + (y_2 - 1/2)\cos(\theta_z))^2}{b_z^2}.$$

Hence we define the function $f : \Omega \to \mathbb{R}$ as

$$f(\omega) = \widetilde{f}(s_0, y), \quad \text{for } \omega = (s, y) = (\{s_z\}_{z \in \mathbb{Z}^2}, y),$$

so that

$$
\begin{aligned}
f(T_x(\omega)) &= f(T_x(s, y)) \\
&= f(\{s_{z + \lfloor x + y \rfloor}\}_{z \in \mathbb{Z}^2}, x + y - \lfloor x + y \rfloor) \\
&= \widetilde{f}(s_{\lfloor x + y \rfloor}, x + y - \lfloor x + y \rfloor).
\end{aligned}
$$

Then we define the subset $\mathscr{F} \in \Sigma$ as

$$\mathscr{F} = \left\{ \omega \in \Omega : f(\omega) \leq 1 \right\}.$$

Finally given $\omega \in \Omega$ we obtain the set $Q = Q(\omega)$ as

$$Q(\omega) = \left\{ x \in \mathbb{R}^2 : T_x(\omega) \in \mathscr{F} \right\},$$

consisting of disjoint ellipses in $\mathbb{R}^2$, whose axes and angle of rotation are randomly defined. In Figure 5.2 we plot the domain D^ε obtained for $D = (0,1)^d$, $I_a = I_b = [1/8, 3/8]$, $I_\theta = [0, \pi]$, $\varepsilon = 1/5$.

5.2.2 Homogenization results

We can now illustrate homogenization results for the problem (5.9). In what follows we will assume the fourth-order tensor to be constant, i.e., $A = \{A_{ijlm}\}_{1 \leq i,j,l,m \leq d}$, $A_{ijlm} \in \mathbb{R}$. Extension to the case where A is a tensor valued function with $A_{ijlm} \in L^\infty(D)$, can be obtained using two-scale convergence techniques for example [18]. The proof of the homogenization results is done following the lines of the proof of Theroem 8.1 in [63], where homogenization of the Poisson's equation in random perforated domains is considered. We consider the problem

$$
\begin{aligned}
-\frac{\partial}{\partial x_j} \left(A^\rho_{ijlm} \frac{\partial u^\varepsilon_l}{\partial x_m} \right) &= f_i & &\text{in } D, \\
\mathbf{u}^\varepsilon &= \mathbf{0} & &\text{on } \Gamma_1, \\
A^\rho_{ijlm} \frac{\partial u^\varepsilon_l}{\partial x_m} \nu_j &= h_i & &\text{on } \Gamma_2,
\end{aligned}
\tag{5.10}
$$

for $i = 1, \ldots, d$, where the fourth-order tensor A^ρ is defined as

$$
A^\rho(x) = \begin{cases} A & x \in \mathbb{R}^d \setminus Q^\varepsilon, \\ \rho \mathbf{I} & x \in Q^\varepsilon, \end{cases}
$$

where $\rho > 0$, $\mathbf{I} = \delta_{il}\delta_{jm}\mathbf{e}^i \otimes \mathbf{e}^j \otimes \mathbf{e}^l \otimes \mathbf{e}^m$ is the fourth-order identity tensor, so that $\mathbf{I}m = m$, $m \in \text{Sym}_d$. Note that problem (5.10) is related to (5.9) in the sense that it is dependent of

the random stationary set Q^ε. However, (5.10) corresponds to a linear elasticity problem with random coefficients defined on the whole domain D (which is not perforated) and can therefore be treated using the theory illustrated in Section 5.1. Let us denote by $A^{0,\rho}$ the homogenized tensor corresponding to A^ρ. From Theorem 5.1.3 for any $m \in \mathrm{Sym}_d$ we have that

$$
\begin{aligned}
m : A^{0,\rho} m &= \inf_{v \in V^2_{\mathrm{pot}}(\Omega)} \int_\Omega (m+v) : A^\rho (m+v) \, \mathrm{d}\mu \\
&= \inf_{v \in V^2_{\mathrm{pot}}(\Omega)} \left(\int_{\Omega \backslash \mathscr{F}} (m+v) : A(m+v) \, \mathrm{d}\mu + \rho \int_\mathscr{F} |m+v|^2 \, \mathrm{d}\mu \right).
\end{aligned}
$$

If we consider the sequence $\{A^{0,\rho}\}_{\rho>0}$, we can verify that the limit $\lim_{\rho\to 0} A^{0,\rho}$ exists and it is given by

$$
\lim_{\rho \to 0} A^{0,\rho} = A^0, \tag{5.11}
$$

where A^0 satisfies

$$
m : A^0 m = \inf_{v \in V^2_{\mathrm{pot}}(\Omega)} \int_{\Omega \backslash \mathscr{F}} (m+v) : A(m+v) \, \mathrm{d}\mu. \tag{5.12}
$$

Indeed we have that

$$
\begin{aligned}
m : A^{0,\rho} m &= \inf_{v \in V^2_{\mathrm{pot}}(\Omega)} \left(\int_{\Omega \backslash \mathscr{F}} (m+v) : A(m+v) \, \mathrm{d}\mu + \rho \int_\mathscr{F} |m+v|^2 \, \mathrm{d}\mu \right) \\
&\geq \inf_{v \in V^2_{\mathrm{pot}}(\Omega)} \int_{\Omega \backslash \mathscr{F}} (m+v) : A(m+v) \, \mathrm{d}\mu + \inf_{v \in V^2_{\mathrm{pot}}(\Omega)} \rho \int_\mathscr{F} |m+v|^2 \, \mathrm{d}\mu \\
&\geq m : A^0 m + C_1 \rho,
\end{aligned}
$$

hence

$$
\liminf_{\rho \to 0} \left(m : A^{0,\rho} m \right) \geq m : A^0 m. \tag{5.13}
$$

On the other hand, by taking $v \in V^2_{\mathrm{pot}}(\Omega)$ in (5.12) such that the infimum is attained within $\tau > 0$, we have that

$$
\begin{aligned}
m : A^{0,\rho} m &\leq \int_{\Omega \backslash \mathscr{F}} (m+v) : A(m+v) \, \mathrm{d}\mu + \rho \int_\mathscr{F} |m+v|^2 \, \mathrm{d}\mu \\
&\leq \inf_{v \in V^2_{\mathrm{pot}}(\Omega)} \int_{\Omega \backslash \mathscr{F}} (m+v) : A(m+v) \, \mathrm{d}\mu + \tau + C_2 \rho \\
&= m : A^0 m + \tau + C_2 \rho.
\end{aligned}
$$

Hence,

$$\limsup_{\rho \to 0} \left(m : A^{0,\rho} m \right) \le m : A^0 m + \tau .$$

Since τ can be chosen arbitrarily small, and in view of (5.13), we have that (5.11) and (5.12) hold.

Hence, we can state the main theorem which defines the weak limit of the solution to problem (5.9). Let us recall that for a probability space (Ω, Σ, μ) we denote by $\mathscr{F}$ an element of Σ, and as $T_x : \Omega \to \Omega$, $x \in \mathbb{R}^d$, a dynamical system. Moreover, we denote by $Q = Q(\omega) \subset \mathbb{R}^d$ the random stationary set obtained from $\mathscr{F}$ as

$$Q(\omega) = \left\{ x \in \mathbb{R}^d : T_x(\omega) \in \mathscr{F} \right\},$$

and as Q^ε its homothetic transformation with ratio ε. We assume that

$$\theta = \mu(\Omega \backslash \mathscr{F}) > 0,$$

$$\mathbb{R}^d \backslash Q(\omega) \quad \text{is open and connected for almost all } \omega \in \Omega.$$

We note also that from Theorem 5.1.1 we have that

$$\mathbb{1}_{\mathbb{R}^d \backslash Q^\varepsilon} \rightharpoonup \int_\Omega \mathbb{1}_{\Omega \backslash \mathscr{F}} \, \mathrm{d}\mu = \mu(\Omega \backslash \mathscr{F}) = \theta \quad \text{weakly in } L^2_{\mathrm{loc}}(\mathbb{R}^d), \tag{5.14}$$

where $\mathbb{1}_{\mathbb{R}^d \backslash Q^\varepsilon}$ is the characteristic function of the set $\mathbb{R}^d \backslash Q^\varepsilon$. Finally, if D is an open bounded set in $\mathbb{R}^d$, we define $D^\varepsilon = D \backslash (D \cap Q^\varepsilon)$ to be the random perforated domain obtained from D. In what follows we will need this lemma given in [63].

Lemma 5.2.1. *Let $v = v(\omega)$ be a function such that*

$$v \in L^2(\Omega), \quad v|_{\mathscr{F}} = 0, \quad \int_\Omega v(\omega) \, \mathrm{d}\mu = 0 .$$

Let $v^\varepsilon(x) = v(T_y(\omega))$, where $y = x/\varepsilon$, and assume that $\{\varphi^\varepsilon\}_{\varepsilon > 0}$ is a sequence of functions such that $\varphi^\varepsilon \in C_0^\infty(D)$ and

$$\limsup_{\varepsilon \to 0} \|\varphi^\varepsilon\|_{H^1(D^\varepsilon)} < \infty .$$

Then

$$\lim_{\varepsilon \to 0} \int_D v^\varepsilon \varphi^\varepsilon \, \mathrm{d}x = 0 .$$

Theorem 5.2.2. *Let* $\{\hat{\mathbf{u}}^\varepsilon\}_{\varepsilon>0}$, $\hat{\mathbf{u}}^\varepsilon \in (C^\infty(\overline{D}))^d$, *be a sequence of functions such that*

$$\{\mathbb{1}_{\mathbb{R}^d \setminus Q^\varepsilon} \hat{\mathbf{u}}^\varepsilon\}_{\varepsilon>0}, \quad \{\mathbb{1}_{\mathbb{R}^d \setminus Q^\varepsilon} Ae(\hat{\mathbf{u}}^\varepsilon)\}_{\varepsilon>0},$$

are bounded in $(L^2(D))^d$ *and* $(L^2(D))^{d \times d}$ *respectively, where* $\mathbb{1}_{\mathbb{R}^d \setminus Q^\varepsilon}$ *is the characteristic function of the set* $\mathbb{R}^d \setminus Q^\varepsilon$, *and* $A = \{A_{ijlm}\}_{1 \le i,j,l,m \le d}$, $A_{ijlm} \in \mathbb{R}$, *satisfies* (5.2), (5.3), (5.4). *Let* $\Gamma_1 \subset \partial D$ *and* $\Gamma_2 \subset \partial D$ *be two disjoint sets with positive measure such that* $\Gamma_1 \cup \Gamma_2 = \partial D$. *Given* $\mathbf{f} \in (L^2(D))^d$, $\mathbf{h} \in (L^2(\Gamma_2))^d$, *assume that* $\hat{\mathbf{u}}^\varepsilon$ *satisfies*

$$B_\varepsilon(\hat{\mathbf{u}}^\varepsilon, \mathbf{v}) = F_\varepsilon(\mathbf{v}) \quad \forall \mathbf{v} \in (C^\infty_{\Gamma_1}(D))^d, \tag{5.15}$$

where

$$B_\varepsilon(\mathbf{v}, \mathbf{w}) = \int_{D^\varepsilon} Ae(\mathbf{v}) : e(\mathbf{w}) \, \mathrm{d}x,$$

and

$$F_\varepsilon(\mathbf{v}) = \int_{D^\varepsilon} \mathbf{f} \cdot \mathbf{v} \, \mathrm{d}x + \int_{\Gamma_2} \mathbf{h} \cdot \mathbf{v} \, \mathrm{d}s,$$

and $(C^\infty_{\Gamma_1}(D))^d$ *is the space of infinitely differentiable functions from* D *to* $\mathbb{R}^d$ *which vanish on* Γ_1. *Let us denote the weak limit of* $\{\mathbb{1}_{\mathbb{R}^d \setminus Q^\varepsilon} \hat{\mathbf{u}}^\varepsilon\}_{\varepsilon>0}$ *in* $(L^2(D))^d$ *as* $\theta \mathbf{u}^0$, *and the weak limit of* $\{\mathbb{1}_{\mathbb{R}^d \setminus Q^\varepsilon} Ae(\hat{\mathbf{u}}^\varepsilon)\}_{\varepsilon>0}$ *in* $(L^2(D))^{d \times d}$ *as* p^0. *Then we have that* $p^0 = A^0 e(\mathbf{u}^0)$, *where* A^0 *is independent of* x *and* ω *and given by* (5.12), *and* $\mathbf{u}^0$ *is the unique solution in* $(H^1(D))^d$ *which satisfies*

$$
\begin{aligned}
-\frac{\partial}{\partial x_j}\left(A^0_{ijlm} \frac{\partial u^0_l}{\partial x_m}\right) &= \theta f_i && \text{in } D, \\
\mathbf{u}^0 &= \mathbf{0} && \text{on } \Gamma_1, \\
A^0_{ijlm} \frac{\partial u^0_l}{\partial x_m} \nu_j &= h_i && \text{on } \Gamma_2,
\end{aligned}
\tag{5.16}
$$

for $i = 1, \ldots, d$, *where* $\theta = \mu(\Omega \setminus \mathscr{F})$.

Proof. The proof is adapted from the proof of Theorem 8.1 in [63], where a similar convergence result is established for the Poisson's equation. We first write (5.12) as

$$m : A^0 m = \inf_{v \in X} \int_{\Omega \setminus \mathscr{F}} (m + v) : A(m + v) \, \mathrm{d}\mu, \tag{5.17}$$

where X denotes the closure in $L^2(\Omega \setminus \mathscr{F})$ of $V^2_{\mathrm{pot}}(\Omega)$ and $m \in \mathrm{Sym}_d$. The solution of the variational problem (5.17) is unique and satisfies the problem of finding $v \in X$ such that

$$\int_{\Omega \setminus \mathscr{F}} A(m + v) : w \, \mathrm{d}\mu = 0 \quad \forall w \in V^2_{\mathrm{pot}}(\Omega). \tag{5.18}$$

109

From (5.8) this implies that the matrix

$$q = A(m+v)' \in (L^2_{\mathrm{sol}}(\Omega))^{d\times d},$$

where $(m+v)'$ denotes the zero extension of $m+v$ to the whole domain Ω. Let $v \in X$ be the solution to the problem (5.18). We have that

$$
\begin{aligned}
m : A^0 m &= \int_{\Omega\backslash\mathscr{F}} (m+v) : A(m+v)\,\mathrm{d}\mu \\
&= \int_{\Omega\backslash\mathscr{F}} m : A(m+v)\,\mathrm{d}\mu + \int_{\Omega\backslash\mathscr{F}} v : A(m+v)\,\mathrm{d}\mu \\
&= \int_{\Omega} m : q\,\mathrm{d}\mu + 0 \\
&= m : \int_{\Omega} q\,\mathrm{d}\mu,
\end{aligned}
$$

and then

$$A^0 m = \int_{\Omega} q\,\mathrm{d}\mu.$$

From the definition of the space X we have that for each $v \in X$ there exists a sequence $\{v^\delta\}_{\delta>0}$ in $V^2_{\mathrm{pot}}(\Omega)$ such that

$$\lim_{\delta\to 0} \int_{\Omega\backslash\mathscr{F}} |v - v^\delta|^2\,\mathrm{d}\mu = 0.$$

For a typical point $\omega \in \Omega$, let us set

$$
\begin{aligned}
v^\varepsilon(x) &= v(T_y(\omega)), \\
v^{\varepsilon,\delta}(x) &= v^\delta(T_y(\omega)), \\
q^\varepsilon(x) &= A(m + v(T_y(\omega)))',
\end{aligned}
$$

where we have used the change of variable $y = x/\varepsilon$. Note that v^ε is defined only on $\mathbb{R}^d \backslash Q^\varepsilon$, since v is the solution of (5.17). By construction we have that

$$\nabla \times v^{\varepsilon,\delta} = 0, \quad \lim_{\delta\to 0}\lim_{\varepsilon\to 0} \int_{D^\varepsilon} |v^\varepsilon - v^{\varepsilon,\delta}|^2\,\mathrm{d}x = 0, \tag{5.19}$$

$$q^\varepsilon|_{Q^\varepsilon} = 0, \quad \frac{\partial}{\partial x_j} q^\varepsilon_{ij} = 0 \quad \text{in } \mathbb{R}^d, \forall i = 1,\ldots,d, \tag{5.20}$$

$$q^\varepsilon \rightharpoonup \int_{\Omega} q\,\mathrm{d}\mu = A^0 m \quad \text{weakly in } (L^2(D))^{d\times d}.$$

Let $p^\varepsilon = \mathbb{1}_{\mathbb{R}^d \setminus Q^\varepsilon} Ae(\hat{\mathbf{u}}^\varepsilon)$ so that (5.15) can be rewritten as

$$\int_D p^\varepsilon : e(\mathbf{v}) \, dx = \int_D \mathbb{1}_{\mathbb{R}^d \setminus Q^\varepsilon} \mathbf{f} \cdot \mathbf{v} \, dx + \int_{\Gamma_2} \mathbf{h} \cdot \mathbf{v} \, ds \quad \forall \mathbf{v} \in (C_{\Gamma_1}^\infty(D))^d. \tag{5.21}$$

Taking the limit $\varepsilon \to 0$ in (5.21) and using (5.14) we obtain

$$\int_D p^0 : e(\mathbf{v}) \, dx = \int_D \theta \mathbf{f} \cdot \mathbf{v} \, dx + \int_{\Gamma_2} \mathbf{h} \cdot \mathbf{v} \, ds \quad \forall \mathbf{v} \in (C_{\Gamma_1}^\infty(D))^d.$$

In order to obtain (5.16), it remains to show that $p^0 = A^0 e(\mathbf{u}^0)$. To do so let us define

$$z^\varepsilon = p^\varepsilon : (m + v^\varepsilon)',$$

where $(m + v^\varepsilon)'$ is the zero extension of $m + v^\varepsilon$ to the whole $\mathbb{R}^d$. Note that due to the symmetry of A we have that

$$\begin{aligned} z^\varepsilon &= p^\varepsilon : (m + v^\varepsilon)' \\ &= \mathbb{1}_{\mathbb{R}^d \setminus Q^\varepsilon} Ae(\hat{\mathbf{u}}^\varepsilon) : (m + v^\varepsilon)' \\ &= \mathbb{1}_{\mathbb{R}^d \setminus Q^\varepsilon} e(\hat{\mathbf{u}}^\varepsilon) : \mathbb{1}_{\mathbb{R}^d \setminus Q^\varepsilon} A(m + v^\varepsilon)' \\ &= \mathbb{1}_{\mathbb{R}^d \setminus Q^\varepsilon} e(\hat{\mathbf{u}}^\varepsilon) : q^\varepsilon. \end{aligned} \tag{5.22}$$

In what follows we prove that

$$\lim_{\varepsilon \to 0} \int_D \varphi z^\varepsilon \, dx = \int_D \varphi p^0 : m \, dx = \int_D \varphi A^0 e(\mathbf{u}^0) : m \, dx \quad \forall \varphi \in C_0^\infty(D), \tag{5.23}$$

where $C_0^\infty(D)$ is the space of functions which are infinitely differentiable and have compact support in D. Since $C_0^\infty(D)$ is dense in $L^2(D)$ and any matrix function in $L^2(D, \mathrm{Sym}_d)$ can be represented as a linear combination of matrix functions ϕm, $\phi \in L^2(D)$, $m \in \mathrm{Sym}_d$, the two identities in (5.23) imply the assertion of Theorem 5.2.2. Let us start by noticing that

$$\int_D \varphi z^\varepsilon \, dx = I_1^\varepsilon + I_2^\varepsilon + I_3^\varepsilon,$$

where

$$I_1^\varepsilon = \int_D \varphi p^\varepsilon : m \, dx,$$

$$I_2^\varepsilon = \int_D \varphi p^\varepsilon : v^{\varepsilon, \delta} \, dx,$$

$$I_3^\varepsilon = \int_D \varphi p^\varepsilon : ((v^\varepsilon)' - v^{\varepsilon, \delta}) \, dx,$$

and $(v^\varepsilon)'$ is the zero extension of v^ε to the whole D. Since $p^\varepsilon \rightharpoonup p^0$ weakly in $(L^2(D))^{d \times d}$ we have that

$$\lim_{\varepsilon \to 0} I_1^\varepsilon = \int_D \varphi p^0 : m \, dx.$$

Let us consider $v^{\varepsilon,\delta}$ for a fixed $\delta > 0$. Let us recall that $v^{\varepsilon,\delta}(x) = v^\delta(T_y(\omega))$, $y = x/\varepsilon$, for a typical point $\omega \in \Omega$, and that $v^\delta \in V_{\text{pot}}^2(\Omega)$. Therefore $v^{\varepsilon,\delta}$ is a potential tensor field in $\mathbb{R}^d$, and by Theorem 5.1.1

$$v^{\varepsilon,\delta} \rightharpoonup \int_\Omega v^\delta \, d\mu = 0 \quad \text{weakly in } (L^2_{\text{loc}}(\mathbb{R}^d))^{d \times d}.$$

Since $v^{\varepsilon,\delta}$ is a potential tensor field, there exists a vector field $\mathbf{w}^\varepsilon$ such that $v^{\varepsilon,\delta} = e(\mathbf{w}^\varepsilon)$. In particular, we can choose $\mathbf{w}^\varepsilon$ such that

$$\int_{\widetilde{D}} \mathbf{w}^\varepsilon \, dx = 0,$$

where $\widetilde{D}$ is a set containing D. Then from Poincaré inequality and Korn's inequality we obtain that

$$\|\mathbf{w}^\varepsilon\|_{L^2(\widetilde{D})} \le C \|\nabla \mathbf{w}^\varepsilon\|_{L^2(\widetilde{D})} \le C \|e(\mathbf{w}^\varepsilon)\|_{L^2(\widetilde{D})},$$

and hence the sequence $\{\mathbf{w}^\varepsilon\}_{\varepsilon > 0}$ is bounded in $(H^1(\widetilde{D}))^d$. By definition $\mathbf{w}^\varepsilon \rightharpoonup 0$ weakly in $(H^1(\widetilde{D}))^d$, and hence by Sobolev embedding theorem

$$\lim_{\varepsilon \to 0} \|\mathbf{w}^\varepsilon\|_{L^2(\widetilde{D})} = 0. \tag{5.24}$$

Thus

$$
\begin{aligned}
I_2^\varepsilon &= \int_D \varphi p^\varepsilon : e(\mathbf{w}^\varepsilon) \, dx \\
&= \int_D p^\varepsilon : e(\varphi \mathbf{w}^\varepsilon) \, dx - \frac{1}{2} \int_D p^\varepsilon : (\mathbf{w}^\varepsilon (\nabla \varphi)^\top + \nabla \varphi (\mathbf{w}^\varepsilon)^\top) \, dx \\
&= \int_D \mathbf{f} \cdot \varphi \mathbf{w}^\varepsilon \, dx + \int_{\Gamma_2} \mathbf{h} \cdot \varphi \mathbf{w}^\varepsilon \, ds - \frac{1}{2} \int_D p^\varepsilon : (\mathbf{w}^\varepsilon (\nabla \varphi)^\top + \nabla \varphi (\mathbf{w}^\varepsilon)^\top) \, dx,
\end{aligned}
$$

which, because of (5.24), converges to zero as $\varepsilon \to 0$. Finally we have that

$$
\begin{aligned}
I_3^\varepsilon &= \int_{D^\varepsilon} \varphi p^\varepsilon : (v^\varepsilon - v^{\varepsilon,\delta}) \, dx \\
&\le \|\varphi\|_{L^\infty(D^\varepsilon)} \|p^\varepsilon\|_{L^2(D^\varepsilon)} \|v^\varepsilon - v^{\varepsilon,\delta}\|_{L^2(D^\varepsilon)} \\
&\le C \|v^\varepsilon - v^{\varepsilon,\delta}\|_{L^2(D^\varepsilon)},
\end{aligned}
$$

and thus by (5.19)

$$\lim_{\delta \to 0} \lim_{\varepsilon \to 0} I_3^\varepsilon = 0 \,.$$

Hence, the first identity in (5.23) is proved. Note that from (5.22) we have that

$$\int_D \varphi z^\varepsilon \, \mathrm{d}x = \int_D \varphi \mathbb{1}_{\mathbb{R}^d \setminus Q^\varepsilon} \, e(\hat{\mathbf{u}}^\varepsilon) : q^\varepsilon \, \mathrm{d}x$$

$$= \int_{D^\varepsilon} \varphi \, e(\hat{\mathbf{u}}^\varepsilon) : q^\varepsilon \, \mathrm{d}x \,.$$

Using integration by parts, by (5.20) and the fact that $\varphi = 0$ on ∂D, we have that

$$\int_D \varphi z^\varepsilon \, \mathrm{d}x = -\int_{D^\varepsilon} q^\varepsilon \hat{\mathbf{u}}^\varepsilon \cdot \nabla \varphi \, \mathrm{d}x$$

$$= -\int_D q^\varepsilon \mathbb{1}_{\mathbb{R}^d \setminus Q^\varepsilon} \hat{\mathbf{u}}^\varepsilon \cdot \nabla \varphi \, \mathrm{d}x \,,$$

for any $\varphi \in C_0^\infty(D)$. Hence we have

$$-\int_D q^\varepsilon \mathbb{1}_{\mathbb{R}^d \setminus Q^\varepsilon} \hat{\mathbf{u}}^\varepsilon \cdot \nabla \varphi \, \mathrm{d}x = -\int_D \theta^{-1} A^0 m \, \mathbb{1}_{\mathbb{R}^d \setminus Q^\varepsilon} \hat{\mathbf{u}}^\varepsilon \cdot \nabla \varphi \, \mathrm{d}x - \int_D (q^\varepsilon - \theta^{-1} A^0 m) \mathbb{1}_{\mathbb{R}^d \setminus Q^\varepsilon} \hat{\mathbf{u}}^\varepsilon \cdot \nabla \varphi \, \mathrm{d}x \,.$$

Passing to the limit as $\varepsilon \to 0$, we get

$$\lim_{\varepsilon \to 0} \int_D \varphi z^\varepsilon \, \mathrm{d}x = -\int_D A^0 m \, \mathbf{u}^0 \cdot \nabla \varphi \, \mathrm{d}x - \lim_{\varepsilon \to 0} \int_D \mathbb{1}_{\mathbb{R}^d \setminus Q^\varepsilon} (q^\varepsilon - \theta^{-1} A^0 m) \hat{\mathbf{u}}^\varepsilon \cdot \nabla \varphi \, \mathrm{d}x \,.$$

By assumption,

$$\hat{u}_i^\varepsilon \frac{\partial \varphi}{\partial x_j} \in C_0^\infty(D) \,, \quad \forall i, j = 1, \dots, d \,.$$

Moreover by noticing that $\mathbb{1}_{\Omega \setminus \mathscr{F}} q = q$, from Theorem 5.1.1 we have that

$$\int_\Omega \mathbb{1}_{\Omega \setminus \mathscr{F}} (q(\omega) - \theta^{-1} A^0 m) \, \mathrm{d}\mu = 0 \,.$$

Therefore, by Lemma 5.2.1 we can conclude that

$$\lim_{\varepsilon \to 0} \int_D \mathbb{1}_{\mathbb{R}^d \setminus Q^\varepsilon} (q^\varepsilon - \theta^{-1} A^0 m) \hat{\mathbf{u}}^\varepsilon \cdot \nabla \varphi \, \mathrm{d}x = 0 \,.$$

Hence, we have obtained that

$$
\begin{aligned}
\int_D \varphi p^0 : m \, dx &= - \int_D A^0 m \mathbf{u}^0 \cdot \nabla \varphi \, dx \\
&= \int_D \varphi e(\mathbf{u}^0) : A^0 m \, dx \\
&= \int_D \varphi A^0 e(\mathbf{u}^0) : m \, dx,
\end{aligned}
$$

which concludes the proof. $\qquad\qquad\square$

Remark 5.2.3. In case of more complex boundary conditions, as non-homogeneous Dirichlet or periodic, the assertion of Theorem 5.2.2 is still valid. For example if $\hat{\mathbf{u}}^\varepsilon = \mathbf{g}$ on Γ_1, $\mathbf{g} \in (H^{1/2}(\Gamma_1))^d$, then Theorem 5.2.2 still holds and $\mathbf{u}^0 = \mathbf{g}$ on Γ_1. See [63] for example.

Remark 5.2.4. It is possible to verify that the assumptions of Theorem 5.2.2 hold for the problem (5.9) using Korn's inequality and a method based on extension properties [51, 63, 35]. Using extension properties we obtain that the weak solution $\mathbf{u}^\varepsilon$ to (5.9) is bounded in the norm $\|\cdot\|_{H^1(D^\varepsilon)}$ uniformly with respect to ε, and that there exists an extension $\hat{\mathbf{u}}^\varepsilon$ such that

$$
\|\hat{\mathbf{u}}^\varepsilon\|_{H^1(D)} \le C,
$$

where C is independent of ε. Hence we can extract a subsequence $\{\hat{\mathbf{u}}^\varepsilon\}_{\varepsilon>0}$ which admits a weak limit in $(H^1(D))^d$. Note that the sequence of extensions $\{\mathbb{1}_{\mathbb{R}^d \setminus Q^\varepsilon} \hat{\mathbf{u}}^\varepsilon\}_{\varepsilon>0}$ converges to $\theta \mathbf{u}^0$ weakly in $(L^2(D))^d$. Hence, given the sequence of weak solutions $\{\mathbf{u}^\varepsilon\}_{\varepsilon>0}$, we can conclude by straightforward calculations that there exists a sequence of extensions $\{\hat{\mathbf{u}}^\varepsilon\}_{\varepsilon>0}$ such that

$$
\hat{\mathbf{u}}^\varepsilon \rightharpoonup \mathbf{u}^0 \quad \text{weakly in } (H^1(D))^d.
$$

5.2.3 Computable approximation of the effective tensor

Theorem 5.2.2 establishes that the problem (5.9) admits an effective PDE which is given by (5.16), where the homogenized tensor is defined by (5.12). However, (5.12) is stated in an abstract space and does not allow for a direct computational procedure. In [24] the authors deal with the problem of approximating the coefficients of a homogenized tensor corresponding to a multiscale tensor with random coefficients. They use a cut-off technique, where the homogenized coefficients are computed by solving PDEs on bounded domains in $\mathbb{R}^d$ of size δ. Moreover, convergence of the approximation error as $\delta \to \infty$ is established for different types of boundary conditions. The goal of this section is to extend these results in the context of linear elasticity with multiscale random perforated domains.

Let us consider the problem (5.9). In what follows we come back to the initial hypothesis where A is a tensor valued function, i.e., $A(x) = \{A_{ijlm}(x)\}_{1 \le i,j,l,m \le d}$, $A_{ijlm} \in L^\infty(D)$. Given $x \in \mathbb{R}^d$, we are interested in finding an approximation of the homogenized tensor $A^0(x)$. We introduce

the two sets $X_\delta = (0,\delta)^d$, and $X_\delta^\varepsilon = X_\delta \setminus (X_\delta \cap Q^\varepsilon)$. Note that $X_\delta^\varepsilon \subset \mathbb{R}^d \setminus Q^\varepsilon$ is a random perforated domain of size δ, whose degree of fineness is inversely proportional to ε. We assume that X_δ^ε is connected and does not exhibit a fine grained boundary, i.e., $\partial X_\delta \subset \partial X_\delta^\varepsilon$. Let $Y = (0,1)^d$. We map X_δ into Y through the change of variable $x = \delta y$. We denote by Y^δ the transformation of X_δ^ε through the same change of variable, i.e.

$$Y^\delta = \left\{ y \in Y : \delta y \in X_\delta^\varepsilon \right\}.$$

Let us introduce the functions space $(W(Y^\delta))^d$ which, in case of periodic coupling, is defined as

$$(W(Y^\delta))^d = (W_{\mathrm{per}}^1(Y^\delta))^d = \left\{ \mathbf{z} \in (H_{\mathrm{per}}^1(Y^\delta))^d : \int_{Y^\delta} z_i \, \mathrm{d}y = 0, i = 1,\dots,d \right\},$$

where $(H_{\mathrm{per}}^1(Y^\delta))^d$ is the closure of $(C_{\mathrm{per}}^\infty(Y))^d$ for the $H^1(Y^\delta)$-norm. We recall that the quantity

$$\|\mathbf{z}\|_{W_{\mathrm{per}}^1(Y^\delta)} = \left(\int_{Y^\delta} |e(\mathbf{z})|^2 \, \mathrm{d}y \right)^{1/2}$$

defines a norm for $(W_{\mathrm{per}}^1(Y^\delta))^d$. Otherwise in case of Dirichlet coupling we set

$$(W(Y^\delta))^d = (H_{\partial Y}^1(Y^\delta))^d,$$

where $(H_{\partial Y}^1(Y^\delta))^d$ denotes the space of functions in $(H^1(Y^\delta))^d$ which vanish on ∂Y but not necessarily on the boundary of the interior holes. Let $\chi^{\delta,lm}(x,\cdot) \in (W(Y^\delta))^d$ be the unique solution to

$$\int_{Y^\delta} A(x) e_y(\chi^{\delta,lm}) : e_y(\mathbf{z}) \, \mathrm{d}y = - \int_{Y^\delta} A(x) e_y(I^{lm}) : e_y(\mathbf{z}) \, \mathrm{d}y \quad \forall \mathbf{z} \in (W(Y^\delta))^d, \qquad (5.25)$$

where $I^{lm} = \{I_p^{lm}\}_{1 \le p \le d}$ is a function given by

$$I_p^{lm} = y_m \delta_{pl}, \quad \delta_{pl} \text{ is the Kronecker symbol}.$$

Note that problem (5.25) is well-posed. Well-posedness is obtained by using extension properties (see Remark 5.2.4), Lax-Milgram theorem and Korn's inequality, i.e.,

$$\|\nabla \mathbf{z}\|_{L^2(Y^\delta)} \le C \left(\int_{Y^\delta} |e_y(\mathbf{z})|^2 \, \mathrm{d}y \right)^{1/2}.$$

We approximate the coefficients of the homogenized tensor as

$$\widetilde{A}^0_{ijlm}(x) = \int\limits_{Y^\delta} A(x) e_y(\chi^{\delta,lm} + I^{lm}) : e_y(I^{ij}) \, dy. \tag{5.26}$$

Let $w^{\delta,lm} = \chi^{\delta,lm} + I^{lm}$, hence

$$\widetilde{A}^0_{ijlm}(x) = \int\limits_{Y^\delta} A(x) e_y(w^{\delta,lm}) : e_y(I^{ij}) \, dy.$$

Note that $w^{\delta,lm}$ satisfies $w^{\delta,lm} - I^{lm} \in (W(Y^\delta))^d$,

$$\int\limits_{Y^\delta} A(x) e_y(w^{\delta,lm}) : e_y(\mathbf{z}) \, dy = 0 \quad \forall \mathbf{z} \in (W(Y^\delta))^d.$$

Theorem 5.2.5. *Consider an open bounded domain $D \subset \mathbb{R}^d$, $d \le 3$. Consider the problem* (5.9), *where $A(x) = \{A_{ijlm}(x)\}_{1 \le i,j,l,m \le d}$, $A_{ijlm} \in L^\infty(D)$, and A satisfies* (5.2), (5.3), (5.4). *Let $x \in D$, and consider the tensor $\widetilde{A}^0(x)$ defined by* (5.26). *Then $\widetilde{A}^0(x) \to A^0(x)$ a.s. as $\delta \to \infty$, where $A^0(x)$ is the value in x of the homogenized tensor associated to problem* (5.9).

Proof. Let us consider the case where $(W(Y^\delta))^d = (W^1_{\text{per}}(Y^\delta))^d$. The problems (5.25) are well-posed and the solutions $\chi^{\delta,lm}$ are bounded in $(H^1(Y^\delta))^d$ independently of δ for almost all $\omega \in \Omega$, and so are the functions $w^{\delta,lm}$. Let us denote by $(w^{\delta,lm})'$ and $(e_y(w^{\delta,lm}))'$ the zero extensions in Y of $w^{\delta,lm}$ and $e_y(w^{\delta,lm})$ respectively. Hence the sequences $\{(w^{\delta,lm})'\}_{\delta>0}$ and $\{A(e_y(w^{\delta,lm}))'\}_{\delta>0}$ are bounded in $(L^2(Y))^d$ and $(L^2(Y))^{d \times d}$ respectively, and therefore admit a.s. a weak limit. Let us denote by $\theta w^{\infty,lm}$ and p^∞ their weak limits. From Theorem 5.2.2 we have that $p^\infty = A^0(x) e_y(w^{\infty,lm})$ where $w^{\infty,lm}$ satisfies the problem: find $w^{\infty,lm}$ such that $w^{\infty,lm} - I^{lm} \in (W^1_{\text{per}}(Y))^d$ and

$$\int\limits_Y A^0(x) e_y(w^{\infty,lm}) : e_y(\mathbf{z}) \, dy = 0 \quad \forall \mathbf{z} \in (W^1_{\text{per}}(Y))^d. \tag{5.27}$$

Note that (5.27) is equivalent in finding $\chi^{\infty,lm} \in (W^1_{\text{per}}(Y))^d$ such that

$$\int\limits_Y A^0(x) e_y(\chi^{\infty,lm}) : e_y(\mathbf{z}) \, dy = -\int\limits_Y A^0(x) e_y(I^{lm}) : e_y(\mathbf{z}) \, dy \quad \forall \mathbf{z} \in (W^1_{\text{per}}(Y))^d. \tag{5.28}$$

The problem (5.28) is well-posed, and the solution $\chi^{\infty,lm}$ is unique. In particular, the only

$\chi^{\infty,lm} \in (W^1_{\text{per}}(Y))^d$ such that (5.28) is satisfied is $\chi^{\infty,lm} = \mathbf{0}$. We have then that

$$
\begin{aligned}
\lim_{\delta\to\infty} \widetilde{A}^0_{ijlm}(x) &= \lim_{\delta\to\infty} \int_{Y^\delta} A(x) e_y(w^{\delta,lm}) : e_y(I^{ij}) \, dy \\
&= \lim_{\delta\to\infty} \int_Y A(x) (e_y(w^{\delta,lm}))' : e_y(I^{ij}) \, dy \\
&= \int_Y A^0(x) e_y(w^{\infty,lm}) : e_y(I^{ij}) \, dy \\
&= \int_Y A^0(x) e_y(\chi^{\infty,lm} + I^{lm}) : e_y(I^{ij}) \, dy \\
&= A^0_{ijlm}(x).
\end{aligned}
$$

This complete the proof in the case where $(W(Y^\delta))^d = (W^1_{\text{per}}(Y^\delta))^d$. The assertion of Theorem 5.2.5 in the case of Dirichlet coupling can be proved in a similar way. $\qquad\square$

5.3 Numerical homogenization of multiscale linear elasticity problems in random perforated domains

This section is devoted to illustrating the numerical procedure to approximate the solution of problem (5.16) by relying only on data defining the fine scale problem. We recall that the analysis of the HMM in periodic perforated domains has been addressed in [61]. We extend the FE-HMM defined in Chapter 2 to the context of linear elasticity with random perforated domains. This is carried out in the first part of this section. Later we will apply model order reduction to speed up the computational procedure. In what follows we will take (5.9) as a model problem and hence we will describe and analyze the numerical method for mixed boundary conditions.

5.3.1 FE-HMM in linear elasticity with random perforated domains

To describe the FE-HMM and the RB-FE-HMM in the context of linear elasticity we follow the framework introduced in Chapter 2. Let us consider the problem (5.9) and assume that D is a convex polygon. Let us define the macro finite element space

$$
S^l_{\Gamma_1}(D, \mathcal{T}_H) = \left\{ \mathbf{v}^H \in (H^1_{\Gamma_1}(D))^d : \mathbf{v}^H|_K \in (\mathscr{P}^l(K))^d, \forall K \in \mathcal{T}_H \right\},
$$

where $\mathcal{T}_H$ is a partition of D in simplicial or quadrilateral elements K of diameter H_K, and $(\mathscr{P}^l(K))^d$ is the space of polynomial vector fields on K of total degree at most l if K is a simplicial element. Otherwise, if K is a quadrilateral element, $(\mathscr{P}^l(K))^d$ is the space of polynomial

vector fields of degree at most l in each variable. For a given $\mathscr{T}_H$ we define

$$H = \max_{K \in \mathscr{T}_H} H_K,$$

and we allow H_K to be much larger than ε. As for the scalar elliptic case, we assume $\mathscr{T}_H$ to be admissible and shape regular. Assume that on each macro element $K \in \mathscr{T}_H$ a quadrature formula $\{x_{K_j}, \omega_{K_j}\}_{j=1}^{J}$ satisfying (2.8) is given. In order to evaluate the effective tensor, which is unknown at the macro quadrature points x_{K_j}, the solution of micro problems is required. For each macro element $K \in \mathscr{T}_H$, and for each macro quadrature point x_{K_j}, we define a micro domain $K_{\delta_j}^{\varepsilon} = K_{\delta_j} \backslash (K_{\delta_j} \cap Q^{\varepsilon})$, where $K_{\delta_j} = x_{K_j} + (-\delta/2, \delta/2)^d$, and $\delta \geq \varepsilon$. As usual, we assume that for each $K \in \mathscr{T}_H$ and for each x_{K_j}, $K_{\delta_j}^{\varepsilon}$ is connected and does not exhibit a fine grained boundary. Hence for a micro domain $K_{\delta_j}^{\varepsilon}$ we consider the micro finite element space

$$S^q(K_{\delta_j}^{\varepsilon}, \mathscr{T}_h) = \left\{ \mathbf{z}^h \in (W(K_{\delta_j}^{\varepsilon}))^d : \mathbf{z}^h|_T \in (\mathscr{P}^q(T))^d, \forall T \in \mathscr{T}_h \right\},$$

where

$$(W(K_{\delta_j}^{\varepsilon}))^d = (W_{\text{per}}^1(K_{\delta_j}^{\varepsilon}))^d$$

in case of periodic coupling, or

$$(W(K_{\delta_j}^{\varepsilon}))^d = (H_{\partial K_{\delta_j}}^1(K_{\delta_j}^{\varepsilon}))^d$$

for Dirichlet coupling. We introduce the bilinear form

$$B_H(\mathbf{v}^H, \mathbf{w}^H) = \sum_{K \in \mathscr{T}_H} \sum_{j=1}^{J} \frac{\omega_{K_j}}{|K_{\delta_j}|} \int_{K_{\delta_j}^{\varepsilon}} A(x) e(\mathbf{v}_{K_j}^h) : e(\mathbf{w}_{K_j}^h) \, dx, \qquad (5.29)$$

where $\mathbf{v}_{K_j}^h$ (respectively $\mathbf{w}_{K_j}^h$) denotes the solution to the micro problem: find $\mathbf{v}_{K_j}^h$ such that $\mathbf{v}_{K_j}^h - \mathbf{v}_{\text{lin},j}^H \in S^q(K_{\delta_j}^{\varepsilon}, \mathscr{T}_h)$ and

$$\int_{K_{\delta_j}^{\varepsilon}} A(x) e(\mathbf{v}_{K_j}^h) : e(\mathbf{z}^h) \, dx = 0 \quad \forall \mathbf{z}^h \in S^q(K_{\delta_j}^{\varepsilon}, \mathscr{T}_h),$$

where $\mathbf{v}_{\text{lin},j}^H(x) = \mathbf{v}^H(x_{K_j}) + (x - x_{K_j}) e(\mathbf{v}^H)_{K_j}$, where $e(\mathbf{v}^H)_{K_j} = e(\mathbf{v}^H)(x_{K_j})$. Finally, the FE-HMM solution to problem (5.9) is given by $\mathbf{u}^H \in S_{\Gamma_1}^l(D, \mathscr{T}_H)$ such that

$$B_H(\mathbf{u}^H, \mathbf{v}^H) = F(\mathbf{v}^H) \quad \forall \mathbf{v}^H \in S_{\Gamma_1}^l(D, \mathscr{T}_H),$$

where

$$F(\mathbf{v}^H) = \int\limits_D \theta \mathbf{f} \cdot \mathbf{v}^H \, \mathrm{d}x + \int\limits_{\Gamma_2} \mathbf{h} \cdot \mathbf{v}^H \, \mathrm{d}s.$$

Reformulation of the FE-HMM. As for the scalar elliptic problem, we can think of computing the values of the homogenized tensor during the assembly process. For each $K \in \mathscr{T}_H$ and each x_{K_j}, we consider the micro problem of finding $\hat{\chi}_{K_j}^{lm,h} \in S^q(K_{\delta_j}^\varepsilon, \mathscr{T}_h)$ such that

$$\int\limits_{K_{\delta_j}^\varepsilon} A(x) e(\hat{\chi}_{K_j}^{lm,h}) : e(\mathbf{z}^h) \, \mathrm{d}x = - \int\limits_{K_{\delta_j}^\varepsilon} A(x) e(I^{lm}) : e(\mathbf{z}^h) \, \mathrm{d}x \quad \forall \mathbf{z}^h \in S^q(K_{\delta_j}^\varepsilon, \mathscr{T}_h), \tag{5.30}$$

where $I_p^{lm} = x_m \delta_{pl}$ and δ_{pl} is the Kronecker symbol. By solving (5.30) we can then approximate the coefficients of the homogenized tensor as

$$A_{ijlm}^{0,h}(x_{K_j}) = \frac{1}{|K_{\delta_j}|} \int\limits_{K_{\delta_j}^\varepsilon} A(x) e(\hat{\chi}_{K_j}^{lm,h} + I^{lm}) : e(I^{ij}) \, \mathrm{d}x. \tag{5.31}$$

Thus, we have an equivalent expression for (5.29) which reads

$$B_H(\mathbf{v}^H, \mathbf{w}^H) = \sum_{K \in \mathscr{T}_H} \sum_{j=1}^J \omega_{K_j} A^{0,h}(x_{K_j}) e(\mathbf{v}^H)_{K_j} : e(\mathbf{w}^H)_{K_j}.$$

Having to solve (5.30) for each $K \in \mathscr{T}_H$, and for each x_{K_j}, represents the bottleneck for the FE-HMM. To speed up the algorithm, as for the elliptic scalar problem, we employ model order reduction techniques to build a reduced space of micro functions which allows for fast solutions of (5.30). The procedure is similar to the one described in Section 2.3, and is illustrated in the next section.

5.3.2 RB-FE-HMM in linear elasticity with random perforated domains

We can note from (5.30) that each micro solution is parameterized by the macro quadrature point x_{K_j} and the indices l, m, $1 \le l, m \le d$. In particular, the micro problem (5.30) is defined so that for each x_{K_j} a different micro domain $K_{\delta_j}^\varepsilon$ is considered. Hence, (5.30) does not allow directly for model order reduction, since in our case to build a reduced space of solutions it is necessary that the micro functions are defined on the same domain. Hence, we consider a generic reference perforated random domain $K_\delta^\varepsilon = K_\delta \backslash (K_\delta \cap Q^\varepsilon)$, where for example $K_\delta = (-\delta/2, \delta/2)^d$. We give then a different formulation of the FE-HMM based on the bilinear form

$$\overline{B}_H(\mathbf{v}^H, \mathbf{w}^H) = \sum_{K \in \mathscr{T}_H} \sum_{j=1}^J \omega_{K_j} \overline{A}^{0,h}(x_{K_j}) e(\mathbf{v}^H)_{K_j} : e(\mathbf{w}^H)_{K_j}, \tag{5.32}$$

where

$$\overline{A}_{ijlm}^{0,h}(x_{K_j}) = \frac{1}{|K_\delta|} \int\limits_{K_\delta^\epsilon} A(x_{K_j} + x) e(\overline{\chi}_{K_j}^{lm,h} + I^{lm}) : e(I^{ij}) \, dx, \tag{5.33}$$

and $\overline{\chi}_{K_j}^{lm,h} \in S^q(K_\delta^\epsilon, \mathcal{T}_h)$ solves

$$\int\limits_{K_\delta^\epsilon} A(x_{K_j} + x) e(\overline{\chi}_{K_j}^{lm,h}) : e(\mathbf{z}^h) \, dx = - \int\limits_{K_\delta^\epsilon} A(x_{K_j} + x) e(I^{lm}) : e(\mathbf{z}^h) \, dx \quad \forall \mathbf{z}^h \in S^q(K_\delta^\epsilon, \mathcal{T}_h). \tag{5.34}$$

Note that Theorem 5.2.5 implies that (5.31) and (5.33) converge to the same value as $\delta \to \infty$. We denote by $\overline{\mathbf{u}}^H \in S_{\Gamma_1}^l(D, \mathcal{T}_H)$ the solution to

$$\overline{B}_H(\overline{\mathbf{u}}^H, \mathbf{v}^H) = F(\mathbf{v}^H) \quad \forall \mathbf{v}^H \in S_{\Gamma_1}^l(D, \mathcal{T}_H).$$

Note that by (5.34) all the micro problems are defined on the same micro domain. However, each solution depends on the macro quadrature point x_{K_j}, so the solution of multiple micro problems is still required.

Parameterized micro problems. We map K_δ into $Y = (0,1)^d$ through the change of variable $x = \delta(y - 1/2)$. We denote by Y^δ the transformation of K_δ^ϵ under the same change of variable. Hence, for each $K \in \mathcal{T}_H$ and each x_{K_j}, we consider the problem of finding $\chi_{K_j}^{lm,\hat{h}} \in S^q(Y^\delta, \mathcal{T}_{\hat{h}})$ such that

$$\int\limits_{Y^\delta} A_{x_{K_j}}(y) e(\chi_{K_j}^{lm,\hat{h}}) : e(\mathbf{z}^{\hat{h}}) \, dy = - \int\limits_{Y^\delta} A_{x_{K_j}}(y) e(I^{lm}) : e(\mathbf{z}^{\hat{h}}) \, dy \quad \forall \mathbf{z}^{\hat{h}} \in S^q(Y^\delta, \mathcal{T}_{\hat{h}}), \tag{5.35}$$

where $I_p^{lm} = y_m \delta_{pl}$, δ_{pl} is the Kronecker symbol and $\hat{h} = h/\delta$. Note that we have used the notation $A_{x_{K_j}}(y) = A(G_{x_{K_j}}(y))$, $x = G_{x_{K_j}}(y) = x_{K_j} + \delta(y - 1/2)$. Consequently we approximate the coefficients of the homogenized tensor as

$$\overline{A}_{ijlm}^{0,h}(x_{K_j}) = \int\limits_{Y^\delta} A_{x_{K_j}}(y) e(\chi_{K_j}^{lm,\hat{h}} + I^{lm}) : e(I^{ij}) \, dy.$$

We assemble a reduced space of micro functions by using a greedy procedure. We define the space of parameters $\Xi = D \times \{1, \ldots, d\}^2$. Given an element $\xi = (x, l, m) \in \Xi$, we denote the corresponding micro function as $\chi_\xi^{\hat{h}}$ which satisfies the weak problem of finding $\chi_\xi^{\hat{h}} \in S^q(Y^\delta, \mathcal{T}_{\hat{h}})$ such that

$$b_\delta(\chi_\xi^{\hat{h}}, \mathbf{z}^{\hat{h}}; \xi) = f_\delta(\mathbf{z}^{\hat{h}}; \xi) \quad \forall \mathbf{z}^{\hat{h}} \in S^q(Y^\delta, \mathcal{T}_{\hat{h}}), \tag{5.36}$$

where

$$b_\delta(\mathbf{z}^{\hat{h}}, \mathbf{w}^{\hat{h}}; \xi) = \int_{Y^\delta} A_x(y) e(\mathbf{z}^{\hat{h}}) : e(\mathbf{w}^{\hat{h}}) \, dy,$$

and

$$f_\delta(\mathbf{z}^{\hat{h}}; \xi) = -b_\delta(I^{lm}, \mathbf{z}^{\hat{h}}; \xi).$$

Offline stage. In the offline stage we build the reduced space of micro functions

$$S^N(Y^\delta) = \mathrm{span}\left\{\psi_1^{\hat{h}}, \dots, \psi_N^{\hat{h}}\right\},$$

where $N \ll \dim(S^q(Y^\delta, \mathcal{T}_{\hat{h}}))$. Hence, given the reduced space $S^N(Y^\delta)$ and a $\xi \in \Xi$ we can obtain a RB approximation of the problem (5.36) by finding $\chi_\xi^N \in S^N(Y^\delta)$ such that

$$b_\delta(\chi_\xi^N, \psi_i^{\hat{h}}; \xi) = f_\delta(\psi_i^{\hat{h}}; \xi) \quad \forall i = 1, \dots, N. \tag{5.37}$$

As in Section 2.3, we remark that an affine representation of the tensor $A_x(y)$ such as

$$A_x(y) = \sum_{q=1}^{Q} \Theta^q(x) A^q(y) \quad \forall y \in Y,$$

where $\Theta^q : D \to \mathbb{R}$, is necessary for the efficiency of the method, otherwise we can appeal to the empirical interpolation method (EIM). Indeed, thanks to the affine representation of $A_x(y)$, it is possible to perform fast estimations of the a posteriori error. For a given $\xi \in \Xi$, let us define the error

$$\hat{e}_\xi^N = \chi_\xi^N - \chi_\xi^{\hat{h}},$$

where χ_ξ^N is the solution of (5.37), and $\chi_\xi^{\hat{h}}$ is the solution of (5.36). From (5.36) we have that

$$b_\delta(\hat{e}_\xi^N, \mathbf{z}^{\hat{h}}; \xi) = b_\delta(\chi_\xi^N, \mathbf{z}^{\hat{h}}; \xi) + f_\delta(\mathbf{z}^{\hat{h}}; \xi) \quad \forall \mathbf{z}^{\hat{h}} \in S^q(Y^\delta, \mathcal{T}_{\hat{h}}),$$

and hence by Riesz's theorem we know the existence of a unique $\overline{e}_\xi^N \in S^q(Y^\delta, \mathcal{T}_{\hat{h}})$ such that

$$\langle \overline{e}_\xi^N, \mathbf{z}^{\hat{h}} \rangle_{W(Y^\delta)} = b_\delta(\hat{e}_\xi^N, \mathbf{z}^{\hat{h}}; \xi) \quad \forall \mathbf{z}^{\hat{h}} \in S^q(Y^\delta, \mathcal{T}_{\hat{h}}), \tag{5.38}$$

where $\langle \cdot, \cdot \rangle_{W(Y^\delta)}$, defined as

$$\langle \mathbf{z}, \mathbf{w} \rangle_{W(Y^\delta)} = \int_{Y^\delta} e(\mathbf{z}) : e(\mathbf{w}) \, dy,$$

denotes the inner product in the space $(W(Y^\delta))^d$. We remark that the error estimate $\overline{e}_\xi^N$ can be computed very efficiently, since the affine representation of the tensor $A_x(y)$ allows to decompose the right hand side of (5.38) into several parameter independent bilinear forms, which can be precomputed. Finally, the a posteriori error estimate is defined as

$$\Delta_\xi^N = \frac{\|\overline{e}_\xi^N\|_{W(Y^\delta)}}{\sqrt{\alpha_{\mathrm{LB}}}},$$

where α_{LB} is a lower bound for the coercivity constant of the bilinear form $b_\delta(\cdot,\cdot;\cdot)$.

Next, we summarize the list of operations to perform the greedy offline stage. Input parameters are N_{Train} (the size of the training set), tol_{RB} (a prescribed tolerance used as stopping criterion), and N_{RB} (the maximum number of reduced basis functions allowed).

1. Randomly define (by a Monte Carlo method for example) the training set $\Xi_{\mathrm{Train}} \subset \Xi$

$$\Xi_{\mathrm{Train}} = \{\xi_i = (x_i, l_i, m_i) : 1 \le i \le N_{\mathrm{Train}}, x_i \in D, 1 \le l_i, m_i \le d\}.$$

2. Select randomly one element from Ξ_{Train}, i.e. ξ_1, and compute $\chi_{\xi_1}^{\hat{h}}$ such that

$$b_\delta(\chi_{\xi_1}^{\hat{h}}, \mathbf{z}^{\hat{h}}; \xi_1) = -f_\delta(\mathbf{z}^{\hat{h}}; \xi_1) \quad \forall \mathbf{z}^{\hat{h}} \in S^q(Y^\delta, \mathcal{T}_{\hat{h}}).$$

   Set

$$\psi_1^{\hat{h}} = \frac{\chi_{\xi_1}^{\hat{h}}}{\|\chi_{\xi_1}^{\hat{h}}\|_{W(Y^\delta)}},$$

   and initialize the space as $S^1(Y^\delta) = \mathrm{span}\left\{\psi_1^{\hat{h}}\right\}$.

3. For $2 \le j \le N_{\mathrm{RB}}$ perform the following steps.
   (a) For each $\xi_i \in \Xi_{\mathrm{Train}}$ compute the corresponding micro function $\chi_{\xi_i}^{j-1} \in S^{j-1}(Y^\delta)$ by solving

$$b_\delta(\chi_{\xi_i}^{j-1}, \psi_k^{\hat{h}}; \xi_i) = -f_\delta(\psi_k^{\hat{h}}; \xi_i) \quad \forall k = 1,\ldots, j-1,$$

   and the corresponding residual $\Delta_{\xi_i}^{j-1}$.
   (b) Select the new reduced basis by choosing

$$\xi_j = \max_{\xi_i \in \Xi_{\mathrm{Train}}} \Delta_{\xi_i}^{j-1}.$$

   (c) If $(\Delta_{\xi_j}^{j-1})^2 < tol_{\mathrm{RB}}$ the algorithm ends, otherwise compute $\chi_{\xi_j}^{\hat{h}}$ such that

$$b_\delta(\chi_{\xi_j}^{\hat{h}}, \mathbf{z}^{\hat{h}}; \xi_j) = -f_\delta(\mathbf{z}^{\hat{h}}; \xi_j) \quad \forall \mathbf{z}^{\hat{h}} \in S^q(Y^\delta, \mathcal{T}_{\hat{h}}).$$

Set

$$\psi_j^{\hat{h}} = \frac{R_j^{\hat{h}}}{\|R_j^{\hat{h}}\|_{W(Y^\delta)}},$$

where

$$R_j^{\hat{h}} = \chi_{\xi_j}^{\hat{h}} - \sum_{k=1}^{j-1} \langle \chi_{\xi_j}^{\hat{h}}, \psi_k^{\hat{h}} \rangle_{W(Y^\delta)} \psi_k^{\hat{h}}.$$

(d) $S^j(Y^\delta) = S^{j-1}(Y^\delta) \cup \text{span}\left\{\psi_j^{\hat{h}}\right\}.$

Online stage. Based on the reduced space $S^N(Y^\delta)$, we define the new macro bilinear form

$$B_{H,\text{RB}}(\mathbf{v}^H, \mathbf{w}^H) = \sum_{K \in \mathcal{T}_H} \sum_{j=1}^{J} \omega_{K_j} A^{0,N}(x_{K_j}) e(\mathbf{v}^H)_{K_j} : e(\mathbf{w}^H)_{K_j}, \tag{5.39}$$

where

$$A_{ijlm}^{0,N} = \int_{Y^\delta} A_{x_{K_j}}(y) e(\chi_{K_j}^{lm,N} + I^{lm}) : e(I^{ij}) \, \mathrm{d}y,$$

and $\chi_{K_j}^{lm,N}$ is the solution of (5.35) computed in the reduced space $S^N(Y^\delta)$. In particular given $\xi = (x, l, m) \in \Xi$, we look for $\chi_\xi^N \in S^N(Y^\delta)$ such that

$$\int_{Y^\delta} A_x(y) e(\chi_\xi^N) : e(\psi_i^{\hat{h}}) \, \mathrm{d}y = -\int_{Y^\delta} A_x(y) e(I^{lm}) : e(\psi_i^{\hat{h}}) \, \mathrm{d}y \quad \forall i = 1, \dots, N. \tag{5.40}$$

Note that χ_ξ^N can be represented as

$$\chi_\xi^N = \sum_{i=1}^{N} a_i \psi_i^{\hat{h}},$$

where $a_i \in \mathbb{R}$, $1 \le i \le N$. Thanks to the affine representation of the tensor $A_x(y)$, solving (5.40) is equal to finding $(a_1, \dots, a_N)^\top \in \mathbb{R}^N$ such that

$$\sum_{q=1}^{Q} \sum_{i=1}^{N} \Theta^q(x) a_i \int_{Y^\delta} A^q(y) e(\psi_i^{\hat{h}}) : e(\psi_{i'}^{\hat{h}}) \, \mathrm{d}y = -\sum_{q=1}^{Q} \int_{Y^\delta} A^q(y) e(I^{lm}) : e(\psi_{i'}^{\hat{h}}) \, \mathrm{d}y \quad \forall i' = 1, \dots, N,$$

$$\tag{5.41}$$

where the integrals in (5.41) are parameter independent and then can be precomputed. Finally, we retrieve the macro solution by finding $\mathbf{u}^{H,\mathrm{RB}} \in S_{\Gamma_1}^l(D,\mathcal{T}_H)$ such that

$$B_{H,\mathrm{RB}}(\mathbf{u}^{H,\mathrm{RB}},\mathbf{v}^H) = F(\mathbf{v}^H) \quad \forall \mathbf{v}^H \in S_{\Gamma_1}^l(D,\mathcal{T}_H).$$

A priori error analysis. We give a priori error estimates for the error between the exact homogenized solution to (5.16), i.e. $\mathbf{u}^0$, and its numerical approximation $\mathbf{u}^{H,\mathrm{RB}}$ obtained by means of the RB-FE-HMM. We decompose the global error into four different parts, and we consider each source of error separately. Let us consider $\mathbf{u}^{0,H}$ which is the FEM approximation of problem (5.16), under the assumption that we know the exact homogenized tensor. The FEM approximation is defined as the unique $\mathbf{u}^{0,H} \in S_{\Gamma_1}^l(D,\mathcal{T}_H)$ such that

$$B_{0,H}(\mathbf{u}^{0,H},\mathbf{v}^H) = F(\mathbf{v}^H) \quad \forall \mathbf{v}^H \in S_{\Gamma_1}^l(D,\mathcal{T}_H),$$

where

$$B_{0,H}(\mathbf{v}^H,\mathbf{w}^H) = \sum_{K\in\mathcal{T}_H}\sum_{j=1}^J \omega_{K_j} A^0(x_{K_j}) e(\mathbf{v}^H)_{K_j} : e(\mathbf{w}^H)_{K_j}. \tag{5.42}$$

Let us introduce also the bilinear form

$$\widetilde{B}_H(\mathbf{v}^H,\mathbf{w}^H) = \sum_{K\in\mathcal{T}_H}\sum_{j=1}^J \omega_{K_j} \widetilde{A}^0(x_{K_j}) e(\mathbf{v}^H)_{K_j} : e(\mathbf{w}^H)_{K_j}, \tag{5.43}$$

where the coefficients of $\widetilde{A}^0$ are computed as in (5.33) with the difference that the micro functions $\overline{\chi}_{K_j}^{lm,h}$ solving (5.34) are replaced by the exact solutions $\overline{\chi}_{K_j}^{lm} \in (W(K_\delta^\varepsilon))^d$. The corresponding macro solution is $\widetilde{\mathbf{u}}^H \in S_{\Gamma_1}^l(D,\mathcal{T}_H)$ such that

$$\widetilde{B}_H(\widetilde{\mathbf{u}}^H,\mathbf{v}^H) = F(\mathbf{v}^H) \quad \forall \mathbf{v}^H \in S_{\Gamma_1}^l(D,\mathcal{T}_H).$$

Using the triangle inequality we split the global error as

$$\|\mathbf{u}^0 - \mathbf{u}^{H,\mathrm{RB}}\|_{H^1(D)} \le \|e_{\mathrm{mac}}\|_{H^1(D)} + \|e_{\mathrm{mod}}\|_{H^1(D)} + \|e_{\mathrm{mic}}\|_{H^1(D)} + \|e_{\mathrm{RB}}\|_{H^1(D)},$$

where

$$e_{\mathrm{mac}} = \mathbf{u}^0 - \mathbf{u}^{0,H}, \quad e_{\mathrm{mod}} = \mathbf{u}^{0,H} - \widetilde{\mathbf{u}}^H, \quad e_{\mathrm{mic}} = \widetilde{\mathbf{u}}^H - \overline{\mathbf{u}}^H, \quad e_{\mathrm{RB}} = \overline{\mathbf{u}}^H - \mathbf{u}^{H,\mathrm{RB}}.$$

The macro error e_{mac} can be bounded using standard FEM error estimates. By assuming $\mathbf{u}^0 \in (H^{l+1}(D))^d$ and $A_{ijlm}^0 \in W^{l+1,\infty}(D)$, $1 \le i,j,l,m \le d$, we obtain that

$$\|\mathbf{u}^0 - \mathbf{u}^{H,\mathrm{RB}}\|_{H^1(D)} \le CH^l + \|e_{\mathrm{mod}}\|_{H^1(D)} + \|e_{\mathrm{mic}}\|_{H^1(D)} + \|e_{\mathrm{RB}}\|_{H^1(D)},$$

where C is a generic constant independent of H, h, ε and δ. Moreover from (5.32), (5.39), (5.42), (5.43) and the well-posedness of problem (5.16), we obtain the following bounds for e_{mod}, e_{mic}, and e_{RB}:

$$\|e_{\text{mod}}\|_{H^1(D)} \leq C \sup_{K \in \mathcal{T}_H} \sup_{1 \leq j \leq J} \sup_{1 \leq l,m,s,t \leq d} |A^0_{lmst}(x_{K_j}) - \widetilde{A}^0_{lmst}(x_{K_j})|,$$

$$\|e_{\text{mic}}\|_{H^1(D)} \leq C \sup_{K \in \mathcal{T}_H} \sup_{1 \leq j \leq J} \sup_{1 \leq l,m,s,t \leq d} |\widetilde{A}^0_{lmst}(x_{K_j}) - \overline{A}^{0,h}_{lmst}(x_{K_j})|,$$

$$\|e_{\text{RB}}\|_{H^1(D)} \leq C \sup_{K \in \mathcal{T}_H} \sup_{1 \leq j \leq J} \sup_{1 \leq l,m,s,t \leq d} |\overline{A}^{0,h}_{lmst}(x_{K_j}) - A^{0,N}_{lmst}(x_{K_j})|.$$

To estimate e_{mic} some sufficient regularity of the micro solutions $\overline{\chi}^{lm}_{K_j}$ is required. In particular we assume that $\overline{\chi}^{lm}_{K_j} \in (H^{q+1}(K^\varepsilon_\delta))^d$ and that

$$|\overline{\chi}^{lm}_{K_j}|_{H^{q+1}(K^\varepsilon_\delta)} \leq C\varepsilon^{-q}\sqrt{|K_\delta|},$$

where C is independent of K, j, ε and δ (see Remark 4.6 in [11] for a justification of this assumption). Then, for both periodic and Dirichlet coupling it can be proved that

$$\|e_{\text{mic}}\|_{H^1(D)} \leq C\left(\frac{h}{\varepsilon}\right)^{2q}.$$

The quantity e_{RB} can be bounded by the decay of the Kolmogorov N-width of $\mathcal{M}(Y^\delta, \mathcal{T}_{\hat{h}})$ (see Section 2.3.2). A priori error estimates of the Kolmogorov N-with of the micro solutions manifold are not available in general. However, exponential decay is often observed in practice. For what concerns the modeling error e_{mod}, if the perforated domain is periodic and the slow variable of the tensor A is collocated at the macro quadrature points, following [1, 48] we get

$$\|e_{\text{mod}}\|_{H^1(D)} = 0 \quad \text{if } (W(K^\varepsilon_\delta))^d = (W^1_{\text{per}}(K^\varepsilon_\delta))^d \text{ and } \frac{\delta}{\varepsilon} \in \mathbb{N},$$

$$\|e_{\text{mod}}\|_{H^1(D)} \leq C\frac{\varepsilon}{\delta} \quad \text{if } (W(K^\varepsilon_\delta))^d = (H^1_{\partial K_\delta}(K^\varepsilon_\delta))^d \text{ and } \delta > \varepsilon.$$

On the other hand, explicit error estimates for the case of random perforated domains are not available. However, we can rely on Theorem 5.2.5 to conclude that, if we collocate the slow variable of the tensor at the macro quadrature points, we have that

$$\|e_{\text{mod}}\|_{H^1(D)} \to 0 \quad \text{a.s.} \quad \text{as} \quad \delta \to \infty.$$

5.4 Numerical experiments

In this last section we present some numerical experiments to verify the theoretical findings about our proposed numerical method and demonstrate its efficiency. We consider a three dimensional beam with length $l_1 = 500\,\text{mm}$, height $l_2 = 100\,\text{mm}$, and thickness $l_2 = 10\,\text{mm}$. We assume the material under plane stress condition, so that a two dimensional model is
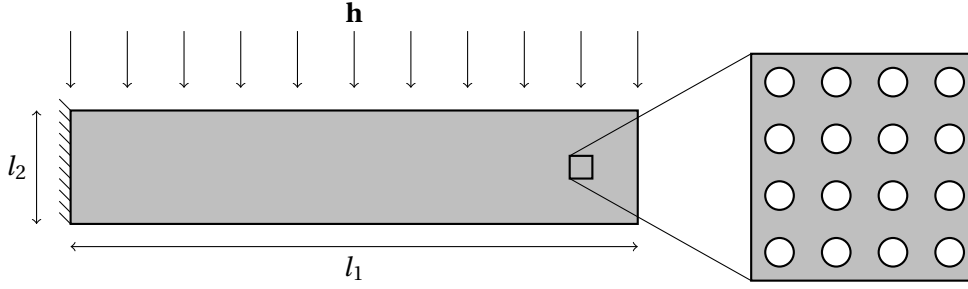
Figure 5.3: Geometry and boundary conditions for the numerical experiment.

considered. We apply a vertical load on the upper edge equal to $\mathbf{h} = (0, -50)\,\mathrm{N/mm^2}$, while the displacement on left edge of the beam is constrained to zero, as sketched in Figure 5.3. We consider an orthotropic fourth-order tensor, so that

$$A_{1111} = \frac{E_1}{1 - v_{12}v_{21}},$$

$$A_{1122} = \frac{E_1 v_{21}}{1 - v_{12}v_{21}},$$

$$A_{2222} = \frac{E_2}{1 - v_{12}v_{21}},$$

$$A_{1212} = G_{12},$$

$$A_{1112} = A_{2212} = 0,$$

where E_i is the Young's modulus along the axis i, v_{ij} is the Poisson's ratio that corresponds to a contraction in direction j when an extension is applied in direction i, and G_{ij} is the shear modulus in direction j on the plane whose normal is in direction i. We let these elastic properties vary with respect to the space variable x as

$$E_1(x) = 100000 + \frac{1}{2}x_1^2 + 50x_2\,[\mathrm{N/mm^2}],$$

$$E_2(x) = 40000 + 2x_2^2 + \frac{1}{2}x_1 x_2\,[\mathrm{N/mm^2}],$$

$$v_{12}(x) = 0.3,$$

$$v_{21}(x) = \frac{E_2(x)}{E_1(x)}v_{12}(x),$$

$$G_{12}(x) = 50000 + \frac{1}{2}x_1 x_2\,[\mathrm{N/mm^2}].$$

5.4.1 The periodic case

We start by considering the case where the beam exhibits circular holes which appear periodically in the medium, as sketched in Figure 5.3. The set $Q = Q(\omega)$ is obtained by following the description of the first example of random set given in Section 5.2.1 by using as radius $r = 1/4$.
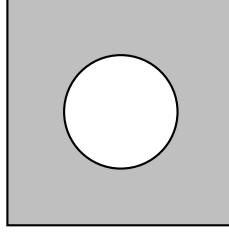
Figure 5.4: Micro reference cell for the periodic perforated domain.

Hence the multiscale random set is obtained by considering the homothetic transformation of Q with ratio ε. The perforated reference cell looks like the one depicted in Figure 5.4. We fix $\delta = \varepsilon$. Note that for this choice of δ the modeling error vanishes, since we are considering a periodic medium and we collocate the tensor at the macro quadrature points. We perform some numerical experiments to observe how the error behaves accordingly to the macro and the micro discretization considered, and the number of reduced basis functions used in the online stage. In particular, we use piecewise linear simplicial elements for both macro and micro finite element spaces. The numerical error can be decomposed as

$$\|\mathbf{u}^0 - \mathbf{u}^{H,\mathrm{RB}}\|_{H^1(D)} \le \|e_{\mathrm{mac}}\|_{H^1(D)} + \|e_{\mathrm{mic}}\|_{H^1(D)} + \|e_{\mathrm{RB}}\|_{H^1(D)},$$

where

$$e_{\mathrm{mac}} = \mathbf{u}^0 - \mathbf{u}^{0,H},$$
$$e_{\mathrm{mic}} = \mathbf{u}^{0,H} - \overline{\mathbf{u}}^H,$$
$$e_{\mathrm{RB}} = \overline{\mathbf{u}}^H - \mathbf{u}^{H,\mathrm{RB}}.$$

Since we do not dispose of the functions $\mathbf{u}^0$, $\mathbf{u}^{0,H}$, $\overline{\mathbf{u}}^H$, we approximate them as follows (see also Table 5.1 for a summary).

1. $\overline{\mathbf{u}}^H$ is approximated using the RB-FE-HMM with the complete reduced space $S^{N_{\max}}(Y^\delta)$, where $N_{\max} = 52$, but with the same macro and micro mesh used to compute $\mathbf{u}^{H,\mathrm{RB}}$.

2. $\mathbf{u}^{0,H}$ is approximated using the RB-FE-HMM with the complete reduced space $S^{N_{\max}}(Y^\delta)$, where $N_{\max} = 52$, the finest micro mesh containing approximately 10000 micro elements, but with the same macro mesh used to compute $\mathbf{u}^{H,\mathrm{RB}}$.

3. $\mathbf{u}^0$ is approximated using the RB-FE-HMM with the complete reduced space $S^{N_{\max}}(Y^\delta)$, where $N_{\max} = 52$, the finest micro mesh containing approximately 10000 micro elements, and the finest macro mesh containing 40960 macro elements.

Periodic case: coarse micro mesh and small RB space. We perform a first experiment where we compute the solution $\mathbf{u}^{H,\mathrm{RB}}$ for four different macro discretizations, which are structured triangulations of the geometry depicted in Figure 5.3, possessing respectively 160, 640, 2560, and 10240 macro elements, while we adopt as micro mesh the one depicted in

$\mathbf{u}^{H,\mathrm{RB}}$	$\mathbf{u}^0$	$\mathbf{u}^{0,H}$	$\overline{\mathbf{u}}^H$
Els_{mac}	$(Els_{\mathrm{mac}})_{\max}$	Els_{mac}	Els_{mac}
Els_{mic}	$(Els_{\mathrm{mic}})_{\max}$	$(Els_{\mathrm{mic}})_{\max}$	Els_{mic}
N	$N_{\max}$	$N_{\max}$	$N_{\max}$

Table 5.1: Details about how the different functions $\mathbf{u}^0$, $\mathbf{u}^{0,H}$, $\mathbf{u}^H$ are computed. Given a macro (resp. micro) discretization we denote by Els_{mac} (resp. Els_{mic}) the corresponding number of macro (resp. micro) elements. In particular $(Els_{\mathrm{mac}})_{\max} = 40960$, $(Els_{\mathrm{mic}})_{\max} \approx 10000$, $N_{\max} = 52$.

Figure 5.5, which possesses approximately 150 micro elements. The micro problems are solved online by using a reduced space consisting of only $N = 5$ basis functions. In Figure 5.5 we show the decay of the a posteriori error estimate as we increase N. The relative errors for both $L^2(D)$-norm and $H^1(D)$-seminorm are shown in Figure 5.6. We can observe how the micro error becomes soon dominant, while the one due to the reduced basis approach is already small, even with only $N = 5$ basis function.
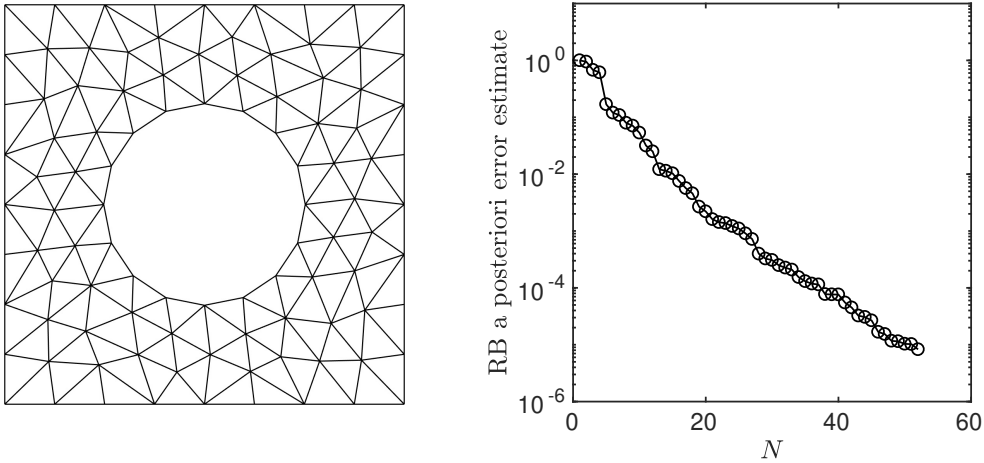

Figure 5.5: Micro triangulation used for the first numerical experiment, and decay of the a posteriori error estimate.

Periodic case: refined micro mesh and small RB space. We perform the same numerical experiment, but this time we use a finer micro discretization, which possesses approximately 600 micro elements, depicted in Figure 5.7 together with the decay of the a posteriori error estimate due to the reduced basis approach. In particular we can observe that the decay of the reduced basis error is not affected by the finer discretization. The number of reduced basis functions used in the online stage is still equal to 5. Numerical errors are shown in Figure 5.8. We can observe that the micro error decreases, but is still the main reason for saturation of the global error.
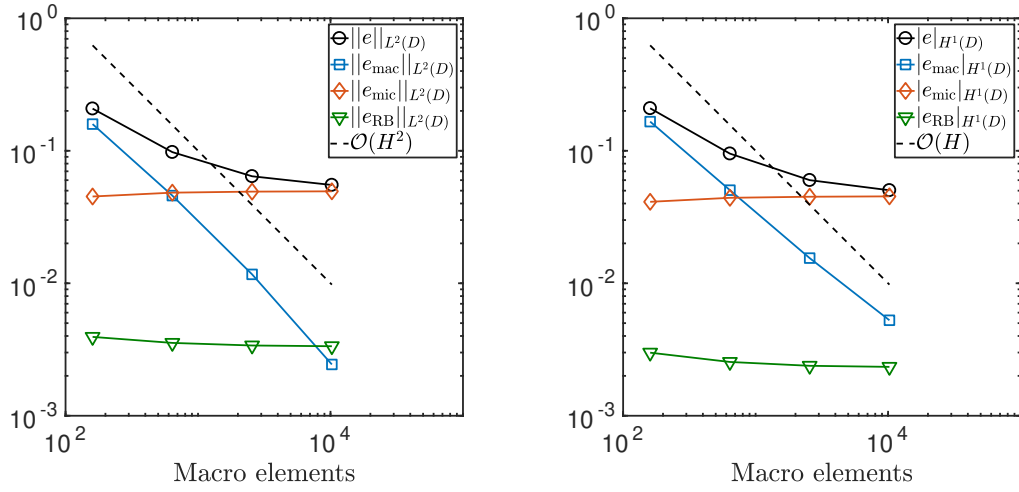
Figure 5.6: $L^2(D)$-norm and $H^1(D)$-seminorm of relative errors for $Els_{\mathrm{mic}} \approx 150$ and $N = 5$.
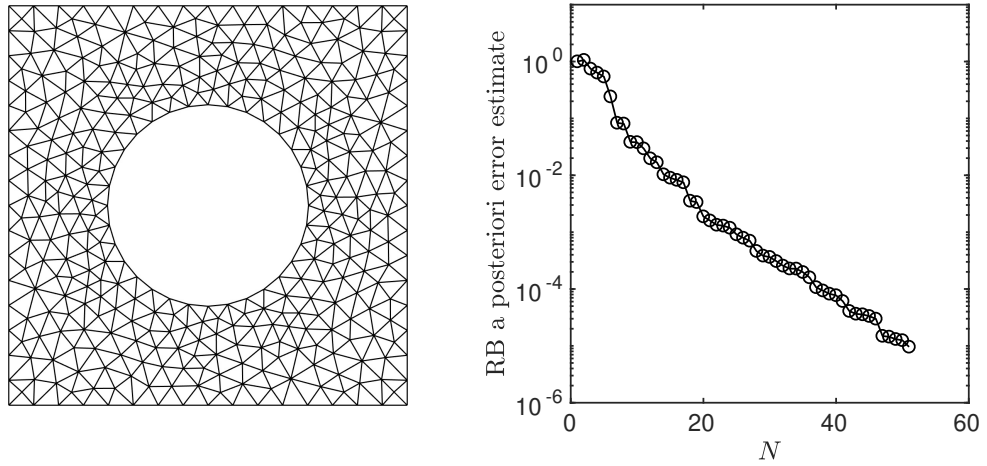

Figure 5.7: Micro triangulation used for the second numerical experiment, and decay of the a posteriori error estimate.

Periodic case: highly refined micro mesh and small RB space. We refine further the micro discretization, so composed now by approximately 2500 triangles, as depicted in Figure 5.9. For $N = 5$ reduced basis for the online computation, we can observe in Figure 5.10 how now the micro error has a magnitude comparable to the one associated to the reduced basis error. In particular, we have no saturation of the global error. Finally, in Figure 5.11 we show the horizontal and the vertical displacement obtained by means of the RB-FE-HMM, using the finest macro and micro meshes (40960 macro elements and approximately 10000 micro elements), and a reduced space consisting of 52 basis functions. In Figure 5.12 instead we show the stresses σ_{11}, σ_{22}, σ_{12} together with the deformed geometry.
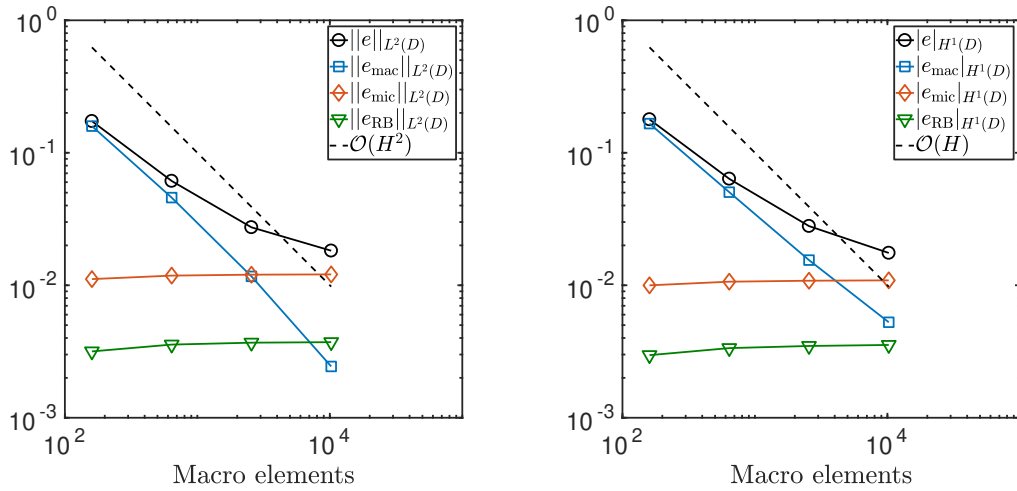
Figure 5.8: $L^2(D)$-norm and $H^1(D)$-seminorm of the relative errors for $Els_{\mathrm{mic}} \approx 600$ and $N = 5$.
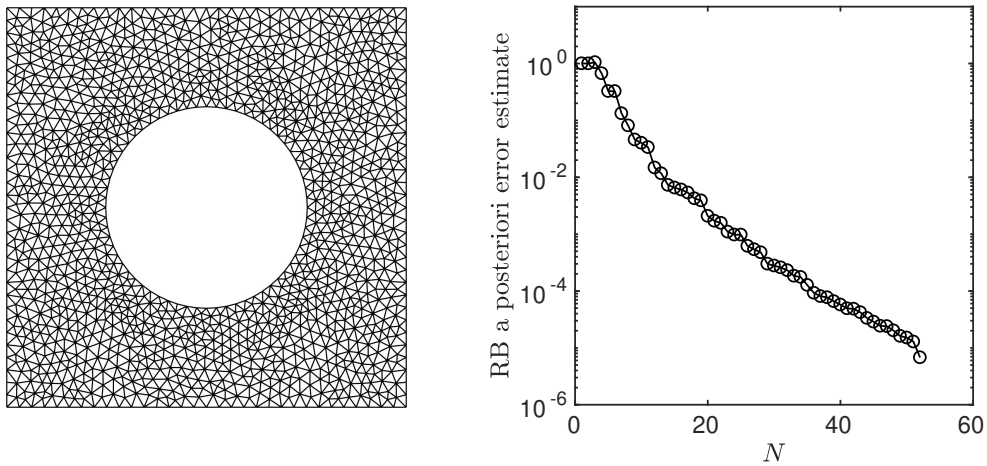

Figure 5.9: Micro triangulation used for the third numerical experiment, and decay of the a posteriori error estimate.

5.4.2   The random case

Now we consider the case of random perforated domains. We assume that the holes are ellipses in $\mathbb{R}^2$, whose axes and angle of rotation are random variables. The construction of the random domain $Q(\omega)$ is described in the second example of Section 5.2.1. In particular, we assume the major and the minor axes are uniformly distributed in the interval $[1/8, 3/8]$, while each ellipse can rotate of an angle uniformly distributed between 0 and π. Once Q is assembled we consider its homothetic transformation with ratio ε to define the multiscale medium. Since we are no more in the periodic framework, we have to deal with an additional source of error when approximating the homogenized solution $\mathbf{u}^0$. We have described in Section 5.2.3 how to approximate the homogenized tensor for perforated random domains, and we have
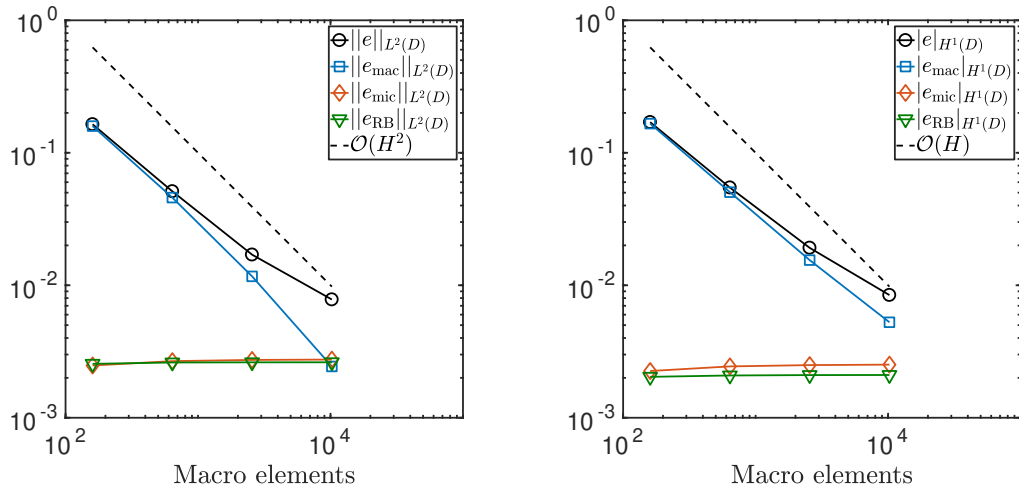
Figure 5.10: $L^2(D)$-norm and $H^1(D)$-seminorm of the relative errors for $Els_{\text{mic}} \approx 2500$ and $N = 5$.
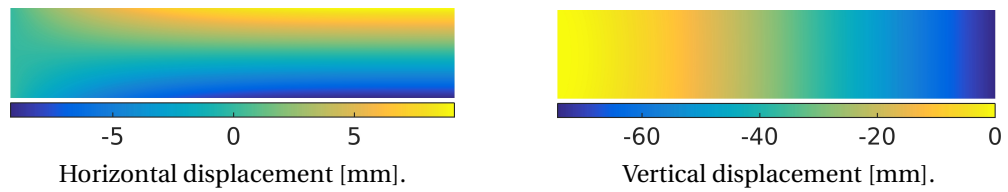

Figure 5.11: Displacement $\mathbf{u}^{H,\text{RB}}$ obtained with the finest macro and micro meshes, and reduced space of 52 basis functions.
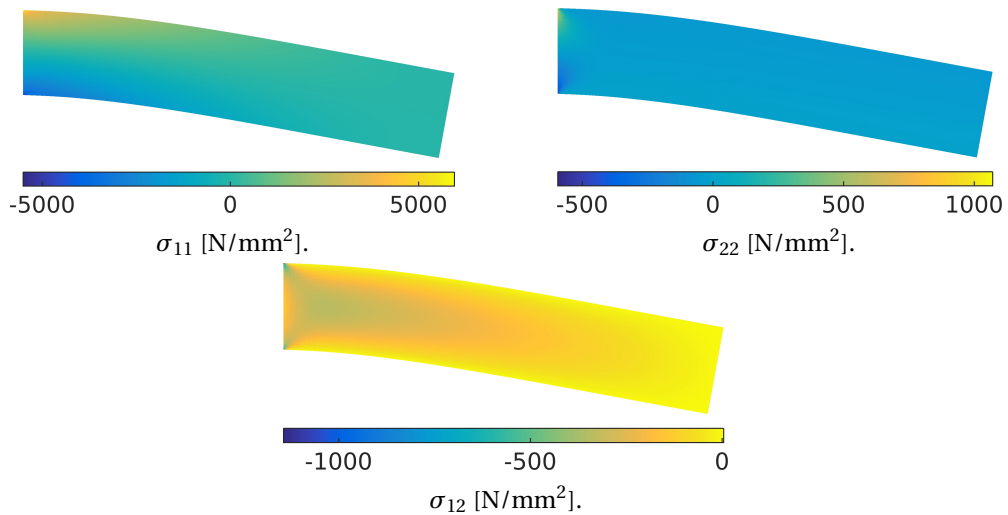

Figure 5.12: Stresses σ_{ij} obtained with the finest macro and micro meshes, and reduced space of 52 basis functions.
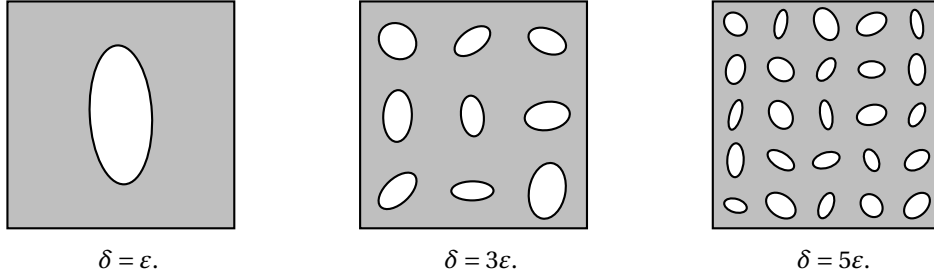
$\delta = \varepsilon.$ $\delta = 3\varepsilon.$ $\delta = 5\varepsilon.$

Figure 5.13: Sample of micro domains for different values of δ.

proved that the approximation improves as the micro cell's size $\delta \to \infty$. We consider then three different micro reference cells for $\delta = \{\varepsilon, 3\varepsilon, 5\varepsilon\}$, and we observe how the numerical error behaves as δ increases. To this end, we will consider a relatively fine micro mesh, and a large number of reduced basis functions, so that the dominant numerical error will be the modeling error proportional to δ. Let us denote by $\mathbf{u}^{H,\mathrm{RB}}$ the approximated homogenized solution obtained by means of the RB-FE-HMM. The global error can be decomposed as

$$\|\mathbf{u}^0 - \mathbf{u}^{H,\mathrm{RB}}\|_{H^1(D)} \leq \|e_{\mathrm{mac}}\|_{H^1(D)} + \|e_{\mathrm{mod}}\|_{H^1(D)} + \|e_{\mathrm{mic}}\|_{H^1(D)} + \|e_{\mathrm{RB}}\|_{H^1(D)},$$

where

$$e_{\mathrm{mac}} = \mathbf{u}^0 - \mathbf{u}^{0,H},$$
$$e_{\mathrm{mod}} = \mathbf{u}^{0,H} - \widetilde{\mathbf{u}}^H,$$
$$e_{\mathrm{mic}} = \widetilde{\mathbf{u}}^H - \overline{\mathbf{u}}^H,$$
$$e_{\mathrm{RB}} = \overline{\mathbf{u}}^H - \mathbf{u}^{H,\mathrm{RB}}.$$

From Section 5.2.3 we know that $\|e_{\mathrm{mod}}\|_{H^1(D)}$ should converge to zero a.s. as $\delta \to \infty$. In Figure 5.13 are shown three samples of micro domains for $\delta = \{\varepsilon, 3\varepsilon, 5\varepsilon\}$.

Since we do not dispose of the functions $\mathbf{u}^0$, $\mathbf{u}^{0,H}$, $\widetilde{\mathbf{u}}^H$, $\overline{\mathbf{u}}^H$ we approximate them as follows (see also Table 5.2 for a summary).

1. $\overline{\mathbf{u}}^H$ is approximated using the RB-FE-HMM with the same δ used to compute $\mathbf{u}^{H,\mathrm{RB}}$. The complete reduced space $S^{N_{\mathrm{max}}}(Y^\delta)$ for the particular choice of δ is used, while the same macro and micro meshes used to compute $\mathbf{u}^{H,\mathrm{RB}}$ are employed.

2. $\widetilde{\mathbf{u}}^H$ is approximated using the RB-FE-HMM with the same δ used to compute $\mathbf{u}^{H,\mathrm{RB}}$. The complete reduced space $S^{N_{\mathrm{max}}}(Y^\delta)$ for the particular choice of δ is used, while the same macro mesh used to compute $\mathbf{u}^{H,\mathrm{RB}}$ is employed. The micro discretization is given by the finest mesh for the particular choice of δ, i.e., the micro mesh possesses the highest ratio (approximately equal to 5000) between the number of micro elements and $(\delta/\varepsilon)^2$.

3. $\mathbf{u}^{0,H}$ is approximated using the RB-FE-HMM with the highest δ ($\delta_{\mathrm{max}} = 7\varepsilon$). The complete reduced space $S^{N_{\mathrm{max}}}(Y^\delta)$ for the choice $\delta = \delta_{\mathrm{max}}$ is used, while the same macro

mesh used to compute $\mathbf{u}^{H,\text{RB}}$ is employed. The micro discretization is given by the finest mesh for the choice $\delta = \delta_{\max}$, i.e., the micro mesh possesses the highest ratio (approximately equal to 5000) between the number of micro elements and $(\delta/\varepsilon)^2$.

4. $\mathbf{u}^0$ is approximated using the RB-FE-HMM with the highest δ ($\delta_{\max} = 7\varepsilon$). The complete reduced space $S^{N_{\max}}(Y^\delta)$ for the choice $\delta = \delta_{\max}$ is used. The finest macro mesh containing 40960 macro elements is employed. The micro discretization is given by the finest mesh for the choice $\delta = \delta_{\max}$, i.e., the micro mesh possesses the highest ratio (approximately equal to 5000) between the number of micro elements and $(\delta/\varepsilon)^2$.

$\mathbf{u}^{H,\text{RB}}$	$\mathbf{u}^0$	$\mathbf{u}^{0,H}$	$\widetilde{\mathbf{u}}^H$	$\overline{\mathbf{u}}^H$
Els_{mac}	$(Els_{\text{mac}})_{\max}$	Els_{mac}	Els_{mac}	Els_{mac}
δ	$\delta_{\max}$	$\delta_{\max}$	δ	δ
$\left(\dfrac{Els_{\text{mic}}}{(\delta/\varepsilon)^2}\right)$	$\left(\dfrac{Els_{\text{mic}}}{(\delta/\varepsilon)^2}\right)_{\max}$	$\left(\dfrac{Els_{\text{mic}}}{(\delta/\varepsilon)^2}\right)_{\max}$	$\left(\dfrac{Els_{\text{mic}}}{(\delta/\varepsilon)^2}\right)_{\max}$	$\left(\dfrac{Els_{\text{mic}}}{(\delta/\varepsilon)^2}\right)$
N	$N_{\max}$	$N_{\max}$	$N_{\max}$	$N_{\max}$

Table 5.2: Details about how the different functions $\mathbf{u}^0$, $\mathbf{u}^{0,H}$, $\widetilde{\mathbf{u}}^H$, $\overline{\mathbf{u}}^H$ are computed. Given a macro (resp. micro) discretization we denote by Els_{mac} (resp. Els_{mic}) the corresponding number of macro (resp. micro) elements. In particular $(Els_{\text{mac}})_{\max} = 40960$, $\delta_{\max} = 7\varepsilon$, $(Els_{\text{mic}}/(\delta/\varepsilon)^2)_{\max} \approx 5000$, $56 \leq N_{\max} \leq 59$ depending on δ.

Fine micro mesh, large RB space, $\delta = \varepsilon$. We start by setting $\delta = \varepsilon$. We solve the problem for different macro discretizations. In particular the same structured grids used in the preceding periodic case are considered. On the other side, the number of micro elements and the number of reduced basis functions are fixed. In Figure 5.14 we show the micro mesh used for this numerical test and the decay of the a posteriori reduced basis error estimate computed during the offline stage. The micro mesh possesses about 1000 micro elements, while the number of reduced basis is fixed to 25. The numerical errors are reported in Figure 5.15 for both the $L^2(D)$-norm and the $H^1(D)$-seminorm. We can observe that $\delta = \varepsilon$ does not represent a good choice. The value of e_{mod} is too large, and we do not get convergence as we increase the number of macro elements.

Fine micro mesh, large RB space, $\delta = 3\varepsilon$. We redo the experiment with $\delta = 3\varepsilon$. The ratio between the number of micro elements and $(\delta/\varepsilon)^2$ is approximately the same as the one used for $\delta = \varepsilon$, so that the contribution of the micro error to the global error is comparable to the one obtained in the preceding experiment. The number of reduced basis is still equal to 25. In Figure 5.16 we show the micro mesh and the decay of the a posteriori reduced basis error estimate. The numerical errors are reported in Figure 5.17 for both the $L^2(D)$-norm and the $H^1(D)$-seminorm. This time we can observe convergence of the global error as we increase the number of macro elements. The modeling error is indeed lower than the one observed for $\delta = 3\varepsilon$. However, it is still the main reason for the saturation of the global error.
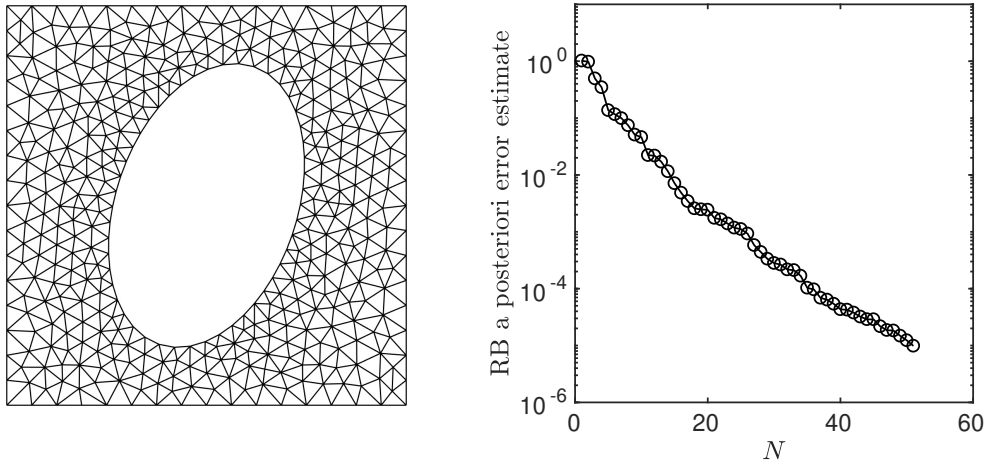
Figure 5.14: Micro triangulation used for the numerical experiment with random perforated domain ($\delta = \varepsilon$), and decay of the a posteriori error estimate.

Figure 5.15: $L^2(D)$-norm and $H^1(D)$-seminorm of the relative errors for $\delta = \varepsilon$.

Fine micro mesh, large RB space, $\delta = 5\varepsilon$.   Finally, we select $\delta = 5\varepsilon$. In Figure 5.18 we show the micro mesh and the decay of the a posteriori reduced basis error estimate. Again the ratio between the number of micro elements and $(\delta/\varepsilon)^2$ is approximately the same as the one used in the previous numerical tests, and the number of reduced basis function is set to 25. The numerical errors are reported in Figure 5.19 for both the $L^2(D)$-norm and the $H^1(D)$-seminorm. We now observe that the error due to δ is not anymore the main cause for saturation of the global error since its magnitude is smaller than the micro error.

Figure 5.16: Micro triangulation used for the numerical experiment with random perforated domain ($\delta = 3\varepsilon$), and decay of the a posteriori error estimate.

Figure 5.17: $L^2(D)$-norm and $H^1(D)$-seminorm of the relative errors for $\delta = 3\varepsilon$.

Figure 5.18: Micro triangulation used for the numerical experiment with random perforated domain ($\delta = 5\varepsilon$), and decay of the a posteriori error estimate.
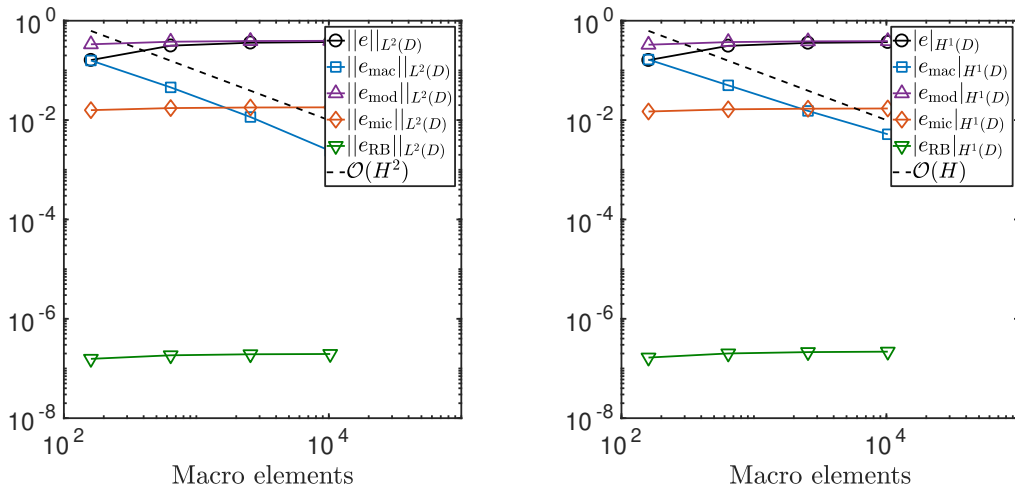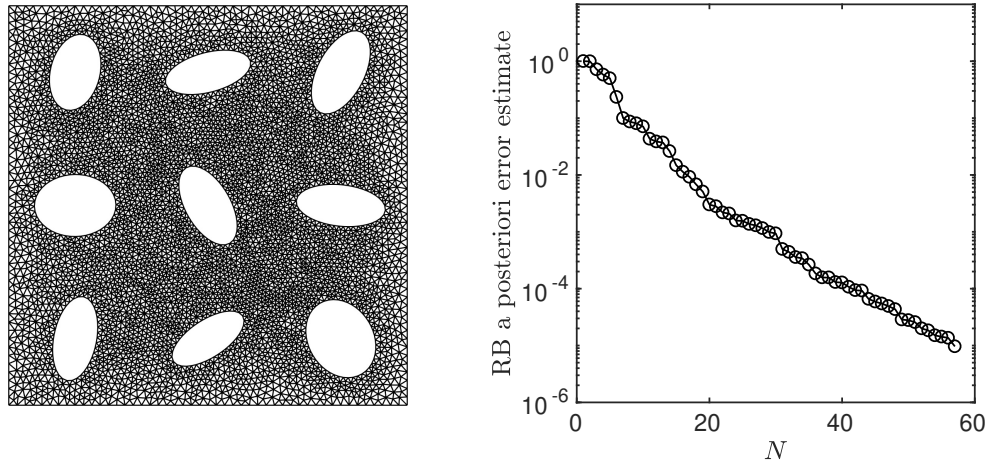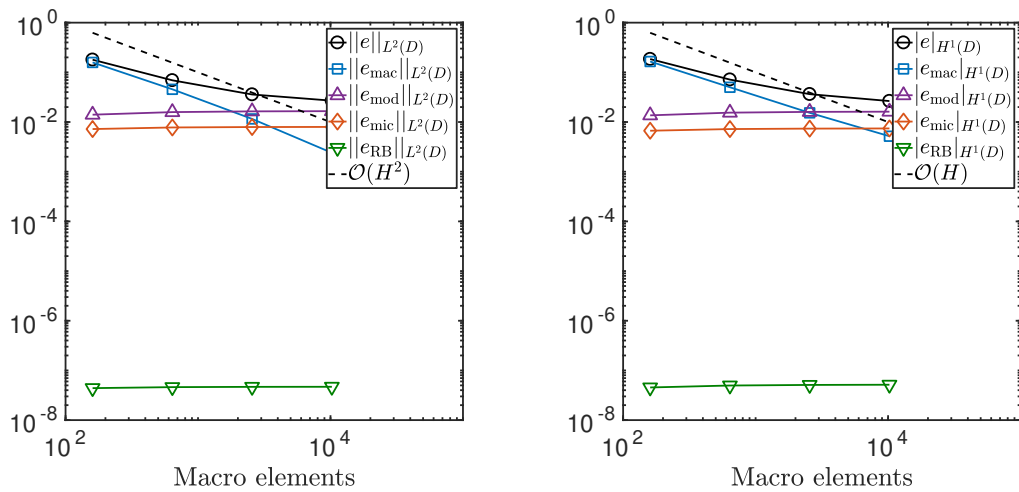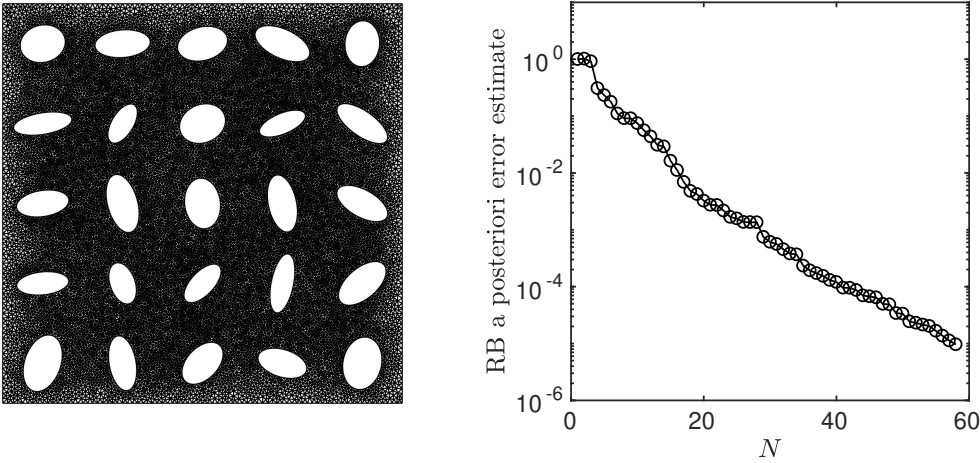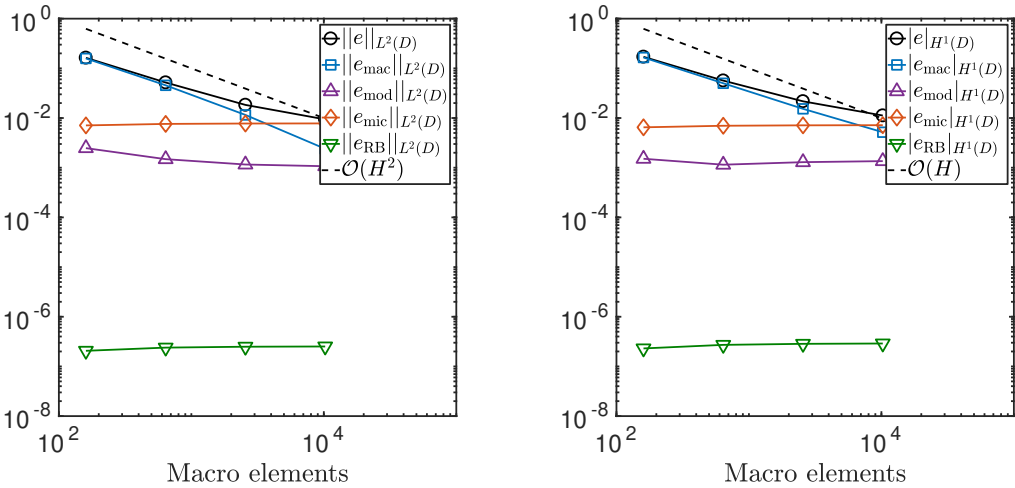

Figure 5.19: $L^2(D)$-norm and $H^1(D)$-seminorm of the relative errors for $\delta = 5\varepsilon$.

136

6 Uncertainty quantification for inverse linear elastic problems in random perforated domains

In this chapter we consider the problem of determining elastic properties of materials which exhibit high heterogeneity. In particular we look at random multiscale perforated domains, and we want to recover the elastic properties characterizing the material from measurements of the displacement $\mathbf{u}^{\varepsilon}$, by using an efficient and coarse graining approach based on Bayesian analysis, homogenization and model order reduction. In the preceding chapter we have described how different sources of error affect our forward model: the geometry discretization, the number of reduced basis functions, the size of the micro sampling domains. All these errors converge asymptotically to zero as we refine the forward model. However, when solving inverse problems, one typically needs multiple evaluations of the forward model, and therefore highly accurate models are usually not appropriate for this scope. On the other hand, the numerical errors propagate into the numerical posterior, and if relatively large they can lead to overconfident or misleading predictions. In what follows we are mostly concerned with the effect of the size of the micro sampling domain, i.e., the modeling error. We develop a probabilistic numerical method which allows us to account for the impact of the error in the forward solver, and gives rise to a posterior distribution which is more robust to numerical errors and reveals the uncertainty in the approximate solution due to the numerical method. Moreover, asymptotic convergence with respect to the size of the micro domain is preserved. Finally, let us point out that we adopt the Einstein summation convention, i.e., we sum over repeated indices.

Outline.   The outline of the chapter is as follows. In Section 6.1 we describe the setting of the inverse elastic problem that we will consider through the chapter. Section 6.2 is devoted to studying the validity of our approach. We prove existence and well-posedness of the probabilistc effective posterior probability measure, and we provide convergence results. In Section 6.3 we describe the numerical algorithm used to solve the inverse problem. In Section 6.4 we illustrate through some numerical tests the efficiency of the suggested probabilistic approach. The content of this chapter is essentially taken from [6].

6.1 Setting of the Bayesian linear elastic inverse problem

Model problem. Let us recall the definition of multiscale random perforated domains in $\mathbb{R}^d$. Let (Ω, Σ, μ) a probability space and $T_x : \Omega \to \Omega$, $x \in \mathbb{R}^d$, a dynamical system satisfying the following properties.

1. $T_0 = \text{Id}$, $T_{x_1+x_2} = T_{x_1} T_{x_2}$, $\forall x_1, x_2 \in \mathbb{R}^d$.

2. The mapping $T_x : \Omega \to \Omega$ preserves the measure μ on Ω, i.e. $\mu(T_x(\mathscr{F})) = \mu(\mathscr{F})$, $\forall x \in \mathbb{R}^d$, $\forall \mathscr{F} \in \Sigma$.

3. For any measurable function $f(\omega)$, $\omega \in \Omega$, the function $f(T_x(\omega))$ defined on $\Omega \times \mathbb{R}^d$ is also measurable.

Let us fix a measurable set $\mathscr{F} \in \Sigma$ and $\omega \in \Omega$. We obtain a random stationary set $Q(\omega) \subset \mathbb{R}^d$ from $\mathscr{F}$ by setting

$$Q(\omega) = \left\{ x \in \mathbb{R}^d : T_x(\omega) \in \mathscr{F} \right\}.$$

We then define the set Q^ε homothetic to Q with ratio ε as

$$Q^\varepsilon = \left\{ x \in \mathbb{R}^d : x/\varepsilon \in Q \right\}.$$

Given $D \subset \mathbb{R}^d$, we set $D^\varepsilon = D \setminus (D \cap Q^\varepsilon)$, and we assume that D^ε is connected for almost all $\omega \in \Omega$ and such that $\partial D \subset \partial D^\varepsilon$. Let $\Gamma_1 \subset \partial D$, $\Gamma_2 \subset \partial D$, such that $|\Gamma_1|, |\Gamma_2| > 0$, $\Gamma_1 \cap \Gamma_2 = \emptyset$, $\Gamma_1 \cup \Gamma_2 = \partial D$. Given $\mathbf{h} \in L^2(\Gamma_2)$, consider the linear elasticity problem

$$
\begin{aligned}
-\frac{\partial}{\partial x_j} \left(A_{ijlm} \frac{\partial u_l^\varepsilon}{\partial x_m} \right) = 0 & \qquad \text{in } D^\varepsilon, \\
\mathbf{u}^\varepsilon = \mathbf{0} & \qquad \text{on } \Gamma_1, \\
A_{ijlm} \frac{\partial u_l^\varepsilon}{\partial x_m} v_j = h_i & \qquad \text{on } \Gamma_2, \\
A_{ijlm} \frac{\partial u_l^\varepsilon}{\partial x_m} v_j = 0 & \qquad \text{on } \partial D^\varepsilon \setminus \partial D,
\end{aligned}
\tag{6.1}
$$

for $i = 1, \dots, d$, where $\boldsymbol{v}$ is the unit outward normal at the boundary, and $A = \{A_{ijlm}\}_{1 \le i,j,l,m \le d}$, $A_{ijlm} \in \mathbb{R}$, is a constant fourth-order tensor which satisfies

$$A_{ijlm} = A_{jilm} = A_{lmij} \quad \text{for any } i, j, l, m = 1, \dots, d. \tag{6.2}$$

Based on observations of the displacement $\mathbf{u}^\varepsilon$, our goal is to retrieve A. Throughout this chapter we will assume that the considered material is isotropic. Hence the coefficients of A can be characterized as function of only two scalar parameters, e.g. the Young's modulus E

and the Poisson's ratio v, as follows:

$$A_{ijlm}(E,v) = \frac{E(1-v)}{(1+v)(1-2v)}, \qquad i = j = l = m,$$
$$A_{ijlm}(E,v) = \frac{Ev}{(1+v)(1-2v)}, \quad i = j, l = m, i \neq l, \tag{6.3}$$
$$A_{ijlm}(E,v) = \frac{E}{2(1+v)}, \qquad i = l, j = m, i \neq j.$$

All the other coefficients are zero. In what follows, we will denote by $\boldsymbol{\eta}$ the vector of unknown parameters we want to determine, e.g. $\boldsymbol{\eta} = (E,v)$ for our setting. Moreover, $\boldsymbol{\eta}^* = (E^*,v^*)$ will denote the exact value of the unknown parameters. Let us note that for any $\boldsymbol{\eta} = (E,v)$ such that $0 < E$ and $-1 < v < 0.5$, we have that there exist two positive constants $\alpha_{\boldsymbol{\eta}}$ and $\beta_{\boldsymbol{\eta}}$ such that the following two conditions hold:

$$\alpha_{\boldsymbol{\eta}} \|m\|_F^2 \leq A(\boldsymbol{\eta})m : m \quad \forall m \in \mathrm{Sym}_d, \tag{6.4}$$
$$\|A(\boldsymbol{\eta})m\|_F \leq \beta_{\boldsymbol{\eta}} \|m\|_F \quad \forall m \in \mathrm{Sym}_d, \tag{6.5}$$

where for any $d \times d$ symmetric matrices m, $\widetilde{m}$ we have that

$$Am = \{(A_{ijlm} m_{lm})_{ij}\}_{1 \leq i,j \leq d}, \quad Am : \widetilde{m} = A_{ijlm} m_{lm} \widetilde{m}_{ij}.$$

The admissible set of parameters is hence defined as a subset of $\mathbb{R}^2$ given by

$$U = \left\{ \boldsymbol{\eta} = (E,v) \in \mathbb{R}^2 : 0 < E, v^- \leq v \leq v^+ \right\}, \tag{6.6}$$

with $-1 < v^- < v^+ < 0.5$. Let us remark that all the theoretical arguments and algorithms we will present throughout this chapter can be extended to the case of more complex situations, e.g. orthotropic or anisotropic materials, or to the case where the unknown A is varying in space. Let us introduce the strain tensor e and the stress tensor σ defined as

$$e(\mathbf{u}^\varepsilon) = \{e_{ij}(\mathbf{u}^\varepsilon)\}_{1 \leq i,j \leq d}, \quad e_{ij}(\mathbf{u}^\varepsilon) = \frac{1}{2}\left(\frac{\partial u_i^\varepsilon}{\partial x_j} + \frac{\partial u_j^\varepsilon}{\partial x_i}\right),$$
$$\sigma(\mathbf{u}^\varepsilon) = \{\sigma_{ij}(\mathbf{u}^\varepsilon)\}_{1 \leq i,j \leq d}, \quad \sigma_{ij}(\mathbf{u}^\varepsilon) = A_{ijlm} \frac{\partial u_l^\varepsilon}{\partial x_m}.$$

For any $\boldsymbol{\eta} \in U$ the parameterized problem (6.1) admits an unique weak solution $\mathbf{u}^\varepsilon \in (H^1_{\Gamma_1}(D^\varepsilon))^d$ which satisfies

$$B_\varepsilon(\mathbf{u}^\varepsilon, \mathbf{v}; \boldsymbol{\eta}) = F(\mathbf{v}) \quad \forall \mathbf{v} \in (H^1_{\Gamma_1}(D^\varepsilon))^d, \tag{6.7}$$

where

$$B_\varepsilon(\mathbf{v}, \mathbf{w}; \boldsymbol{\eta}) = \int_{D^\varepsilon} A(\boldsymbol{\eta}) e(\mathbf{v}) : e(\mathbf{w}) \, dx,$$

and

$$F(\mathbf{v}) = \int\limits_{\Gamma_2} \mathbf{h} \cdot \mathbf{v} \, ds.$$

Bayesian setting. According to the Bayesian approach, let us introduce the prior probability density π_{pr} which reflects our prior knowledge about the two parameters of interest. Since $E > 0$ and $v \in [v^-, v^+]$, we consider the case where the prior probability measure, denoted as μ_{pr}, is given by the combination of a log-Gaussian distribution for the Young's modulus E, and a uniform distribution for the Poisson's ratio v. In particular, we take the unknown vector to be $\boldsymbol{\theta} = (k, v) \in V$, with $k \sim \mathcal{N}(\overline{k}, \sigma_k)$, $v \sim \mathcal{U}([v^-, v^+])$, and $E = \exp(k)$. Hence we denote the map $(k, v) \in V \mapsto (\exp(k), v) \in U$ as P, and we write $\boldsymbol{\eta} = P(\boldsymbol{\theta})$. The probability density for the random variable $\boldsymbol{\theta} = (k, v)$ reads

$$\pi_{\mathrm{pr}}(\boldsymbol{\theta}) = \frac{1}{\sigma_k \sqrt{2\pi}} \exp\left(-\frac{(k - \overline{k})^2}{2\sigma_k^2} \right) \frac{1}{v^+ - v^-} \mathbb{1}_{[v^-, v^+]}(v). \tag{6.8}$$

Moreover by noticing that

$$\exp(-|k|) \le \exp(k) \le \exp(|k|) \quad \forall k \in \mathbb{R},$$

and using the fact that any admissible v is uniformly bounded, we have that for any $\boldsymbol{\eta} = (\exp(k), v)$ there exists a constant c such that

$$\alpha_{\boldsymbol{\eta}} \le c^{-1} \exp(-|k|), \quad \beta_{\boldsymbol{\eta}} \le c \exp(|k|). \tag{6.9}$$

We take as observations the average displacement measured at $J \in \mathbb{N}$ different locations along Γ_2. Then we may introduce the forward operator $G^\varepsilon : V \to \mathbb{R}^{Jd}$ defined as

$$G^\varepsilon(\boldsymbol{\theta}) = \mathrm{vec}(\{g_{ij}^\varepsilon(\boldsymbol{\theta})\}_{\substack{1 \le i \le d \\ 1 \le j \le J}}), \tag{6.10}$$

with

$$g_{ij}^\varepsilon(\boldsymbol{\theta}) = \int\limits_{S_j} u_i^\varepsilon(P(\boldsymbol{\theta})) \, ds,$$

where $u_i^\varepsilon(P(\boldsymbol{\theta}))$ is the i component of the solution to (6.7) with $\boldsymbol{\eta} = P(\boldsymbol{\theta})$, and $S_j \subset \Gamma_2$, $S_i \cap S_j = \emptyset$ if $i \ne j$. In the following setting we denote the measurements as z and, according to the Bayesian approach to inverse problems, we assume that they are corrupted by some Gaussian noise, so that

$$z = G^\varepsilon(\boldsymbol{\theta}^*) + \zeta, \quad \zeta \sim \mathcal{N}(0, C_\zeta), \tag{6.11}$$

where $\boldsymbol{\theta}^* = (\log(E^*), \nu^*)$, and C_ζ is the covariance matrix of the multivariate normal distribution of the noise. We denote by $\Phi^\varepsilon : V \times \mathbb{R}^{Jd} \to \mathbb{R}$ the potential or likelihood function which measures the distance between the measured values and the values produced by the forward model defined for any $\boldsymbol{\theta} \in V$, as

$$
\begin{aligned}
\Phi^\varepsilon(\boldsymbol{\theta}, z) &= \frac{1}{2} \| z - G^\varepsilon(\boldsymbol{\theta}) \|_{C_\zeta}^2 \\
&= \frac{1}{2} \langle z - G^\varepsilon(\boldsymbol{\theta}), z - G^\varepsilon(\boldsymbol{\theta}) \rangle_{C_\zeta}, \\
&= \frac{1}{2} (z - G^\varepsilon(\boldsymbol{\theta}))^\top C_\zeta^{-1} (z - G^\varepsilon(\boldsymbol{\theta})).
\end{aligned}
$$

Bayes' theorem yields the posterior probability density of $\boldsymbol{\theta}$ given the measurements z, which reads

$$
\pi^\varepsilon(\boldsymbol{\theta}|z) = \frac{1}{C^\varepsilon(z)} \exp(-\Phi^\varepsilon(\boldsymbol{\theta}, z)) \pi_{\text{pr}}(\boldsymbol{\theta}), \tag{6.12}
$$

where $C^\varepsilon(z)$ is the normalization constant and is given by

$$
C^\varepsilon(z) = \int_{\mathbb{R}^2} \exp(-\Phi^\varepsilon(\boldsymbol{\theta}, z)) \mu_{\text{pr}}(\mathrm{d}\boldsymbol{\theta}).
$$

Classical results in Bayesian analysis ensure that the posterior distribution $\pi^\varepsilon(\boldsymbol{\theta}|z)$ converges to the Dirac distribution $\delta(\boldsymbol{\theta} - \boldsymbol{\theta}^*)$ in the small noise limit [84]. Note that the relation (6.12) can be rewritten also in terms of probability measures using the Radon-Nikodym derivative

$$
\frac{\mathrm{d}\mu^\varepsilon(\boldsymbol{\theta}|z)}{\mathrm{d}\mu_{\text{pr}}(\boldsymbol{\theta})} = \frac{1}{C^\varepsilon(z)} \exp(-\Phi^\varepsilon(\boldsymbol{\theta}, z)). \tag{6.13}
$$

In general, the posterior distribution is not available in closed form, hence it is necessary to approximate it using sampling techniques such as Markov chain Monte Carlo (MCMC) methods. To do so, with the help of a numerical solver, the forward model G^ε has to be evaluated multiple times for different realizations of the parameters of interest, and the results have to be compared with the observed data to determine which values are the more plausible. We can then see that standard numerical techniques such as the finite element methods (FEMs) are not suited for our problem, since they require mesh resolution at the smallest scale ε and their computational cost becomes prohibitive in the limit $\varepsilon \to 0$. To overcome this issue, an alternative way of approximating G^ε is required. Let $\mathbf{u}^\varepsilon$ be the weak solution of (6.1) with $A = A(\boldsymbol{\eta})$, for some $\boldsymbol{\eta} \in U$. From homogenization theory [63, 35] (see also Theorem 5.2.2 and Remark 5.2.4) we know that there exists an extension of $\mathbf{u}^\varepsilon$ in the whole domain D that admits a.s. a weak limit $\mathbf{u}^0 \in (H_{\Gamma_1}^1(D))^d$ which solves the problem

$$
B_0(\mathbf{u}^0, \mathbf{v}; \boldsymbol{\eta}) = F(\mathbf{v}) \quad \forall \mathbf{v} \in (H_{\Gamma_1}^1(D))^d,
$$

where

$$B_0(\mathbf{v}, \mathbf{w}; \boldsymbol{\eta}) = \int_D A^0(\boldsymbol{\eta}) e(\mathbf{v}) : e(\mathbf{w}) \, dx,$$

and $A^0(\boldsymbol{\eta})$, the effective or homogenized tensor corresponding to $A(\boldsymbol{\eta})$, has constant coefficients, is positive definite, and is non-random. Hence we may introduce the homogenized forward operator $G^0 : V \rightarrow \mathbb{R}^{Jd}$,

$$G^0(\boldsymbol{\theta}) = \text{vec}(\{g_{ij}^0(\boldsymbol{\theta})\}_{\substack{1 \le i \le d \\ 1 \le j \le J}}), \tag{6.14}$$

with

$$g_{ij}^0(\boldsymbol{\theta}) = \int_{S_j} u_i^0(P(\boldsymbol{\theta})) \, ds.$$

Hence a new potential function $\Phi^0 : V \times \mathbb{R}^{Jd} \rightarrow \mathbb{R}$ can be defined as

$$\Phi^0(\boldsymbol{\theta}, z) = \frac{1}{2} \| z - G^0(\boldsymbol{\theta}) \|_{C_\zeta}^2.$$

Finally, as for the full fine scale model, using the Bayes' formula we can define the effective posterior probability density $\pi^0(\boldsymbol{\theta}|z)$ which is given by

$$\pi^0(\boldsymbol{\theta}|z) = \frac{1}{C^0(z)} \exp(-\Phi^0(\boldsymbol{\theta}, z)) \pi_{\text{pr}}(\boldsymbol{\theta}), \tag{6.15}$$

with

$$C^0(z) = \int_{\mathbb{R}^2} \exp(-\Phi^0(\boldsymbol{\theta}, z)) \mu_{\text{pr}}(d\boldsymbol{\theta}).$$

Also in this case it is possible to rewrite (6.15) in terms of probability measures as

$$\frac{d\mu^0(\boldsymbol{\theta}|z)}{d\mu_{\text{pr}}(\boldsymbol{\theta})} = \frac{1}{C^0(z)} \exp(-\Phi^0(\boldsymbol{\theta}, z)). \tag{6.16}$$

This new posterior is much more easier to explore via sampling techniques since the homogenized problem can be approximated numerically at a cost independent of ε. However, in practice it is difficult to deal directly with the effective posterior (6.15) since the homogenized tensor is usually not known and has to be approximated. Following Chapter 5 we can approximate its coefficients by solving micro problems on a bounded domain $X_\delta \subset \mathbb{R}^d$ of size $\delta \ge \varepsilon$. We define $X_\delta = (0, \delta)^d$ and $X_\delta^\varepsilon(\omega) = X_\delta \setminus (X_\delta \cap Q^\varepsilon(\omega))$, and we assume that X_δ^ε is connected and that $\partial X_\delta \subset X_\delta^\varepsilon$. Using the change of variable $x = \delta y$, we map X_δ and X_δ^ε into $Y = (0, 1)^d$ and $Y^\delta(\omega) \subset Y$ respectively. Let us introduce the functions space $(W(Y^\delta))^d$ which, in case of

periodic coupling, is defined as

$$(W(Y^\delta))^d = (W^1_{\text{per}}(Y^\delta))^d = \left\{ \mathbf{z} \in (H^1_{\text{per}}(Y^\delta))^d : \int_{Y^\delta} z_i \, dy = 0 \; i = 1,\ldots,d \right\},$$

where $(H^1_{\text{per}}(Y^\delta))^d$ is the closure of $(C^\infty_{\text{per}}(Y))^d$ for the $H^1(Y^\delta)$-norm. Otherwise in case of Dirichlet coupling we set

$$(W(Y^\delta))^d = (H^1_{\partial Y}(Y^\delta))^d.$$

Hence we look for $\chi^{\delta,lm} \in (W(Y^\delta))^d$ which is the unique solution to

$$\int_{Y^\delta} A(\boldsymbol{\eta}) e(\chi^{\delta,lm}) : e(\mathbf{z}) \, dy = - \int_{Y^\delta} A(\boldsymbol{\eta}) e(I^{lm}) : e(\mathbf{z}) \, dy \quad \forall \mathbf{z} \in (W(Y^\delta))^d, \tag{6.17}$$

where $I^{lm} = \{I^{lm}_p\}_{1 \le p \le d}$ is a function given by

$$I^{lm}_p = y_m \delta_{pl}, \quad \delta_{pl} \text{ is the Kronecker symbol}.$$

The problem (6.17) admits an unique solution bounded in $(H^1(Y^\delta))^d$ uniformly with respect to δ for almost all $\omega \in \Omega$ (we refer to [63] for a complete overview on homogenization in perforated random domains). Then we approximate the coefficients of the homogenized tensor as

$$\widetilde{A}^0_{ijlm}(\boldsymbol{\eta}) = \int_{Y^\delta} A(\boldsymbol{\eta}) e(\chi^{\delta,lm} + I^{lm}) : e(I^{ij}) \, dy. \tag{6.18}$$

In the previous chapter we have shown that $\widetilde{A}^0(\boldsymbol{\eta})$ converges to $A^0(\boldsymbol{\eta})$ a.s. as $\delta \to \infty$. The tensor $\widetilde{A}^0$ is positive definite and satisfies (6.2), (6.4), (6.5). However its value, in contrast to A^0, is not deterministic but is a random variable depending on the particular realization of X^ε_δ (or equivalently Y^δ). Given (6.18) we define the forward operator

$$\widetilde{G}^{0,\delta}(\boldsymbol{\theta}) = \text{vec}(\{\widetilde{g}^{0,\delta}_{ij}(\boldsymbol{\theta})\}_{\substack{1 \le i \le d \\ 1 \le j \le J}}), \tag{6.19}$$

with

$$\widetilde{g}^{0,\delta}_{ij}(\boldsymbol{\theta}) = \int_{S_j} \widetilde{u}^0_i(P(\boldsymbol{\theta})) \, ds,$$

where $\widetilde{\mathbf{u}}^0 \in (H^1_{\Gamma_1}(D))^d$ denotes the unique solution to

$$\widetilde{B}_0(\widetilde{\mathbf{u}}^0, \mathbf{v}; \boldsymbol{\eta}) = F(\mathbf{v}) \quad \forall \mathbf{v} \in (H^1_{\Gamma_1}(D))^d, \tag{6.20}$$

143

where $\boldsymbol{\eta} = P(\boldsymbol{\theta})$ and

$$\widetilde{B}_0(\mathbf{v}, \mathbf{w}; \boldsymbol{\eta}) = \int_D \widetilde{A}^0(\boldsymbol{\eta}) e(\mathbf{v}) : e(\mathbf{w}) \, dx.$$

The corresponding potential function is denoted by $\widetilde{\Phi}^{0,\delta}$ and it is defined as

$$\widetilde{\Phi}^{0,\delta}(\boldsymbol{\theta}, z) = \frac{1}{2} \| z - \widetilde{G}^{0,\delta}(\boldsymbol{\theta}) \|^2_{C_\zeta}. \tag{6.21}$$

Finally, as for the full fine scale model, using the Bayes' formula, we can define an effective posterior probability density $\widetilde{\pi}^{0,\delta}(\boldsymbol{\theta}|z)$ which is given by

$$\widetilde{\pi}^{0,\delta}(\boldsymbol{\theta}|z) = \frac{1}{\widetilde{C}^{0,\delta}(z)} \exp(-\widetilde{\Phi}^{0,\delta}(\boldsymbol{\theta}, z)) \pi_{\mathrm{pr}}(\boldsymbol{\theta}), \tag{6.22}$$

where $\widetilde{C}^{0,\delta}(z)$ is the normalization constant and is given by

$$\widetilde{C}^{0,\delta}(z) = \int_{\mathbb{R}^2} \exp(-\widetilde{\Phi}^{0,\delta}(\boldsymbol{\theta}, z)) \mu_{\mathrm{pr}}(d\boldsymbol{\theta}).$$

Note that the relation (6.22) can be rewritten also in terms of probability measures as

$$\frac{d\widetilde{\mu}^{0,\delta}(\boldsymbol{\theta}|z)}{d\mu_{\mathrm{pr}}(\boldsymbol{\theta})} = \frac{1}{\widetilde{C}^{0,\delta}(z)} \exp(-\widetilde{\Phi}^{0,\delta}(\boldsymbol{\theta}, z)). \tag{6.23}$$

We remark that since $\widetilde{A}^0$ is a random variable (it depends on the realization of $X_\delta^\varepsilon(\omega)$), also the forward operator $\widetilde{G}^{0,\delta}$ is random, as well as the functional $\widetilde{\Phi}^{0,\delta}$, and consequently the measure $\widetilde{\mu}^{0,\delta}$ too. Hence in what follows we will refer sometimes to $\widetilde{\mu}^{0,\delta}$ as a random measure.

6.2 Well-posedness and convergence of the effective posterior measure

In this section we discuss existence and well-posedness of the effective posterior measure (6.23). Existence and well-posedness are determined from continuity properties of the likelihood function as established by the following theorem which is an adaptation of Theorem 4.2.2 to our problem.

Theorem 6.2.1 (See [84] or [41])**.** *Assume that μ_{pr} is a measure on V such that $\mu_{\mathrm{pr}}(V) = 1$. In addition, assume that the random function $\widetilde{\Phi}^{0,\delta} : V \times \mathbb{R}^{Jd} \to \mathbb{R}$ and the probability measure μ_{pr} satisfy the following properties for almost all $\omega \in \Omega$ and $\forall \delta > 0$:*

1. *For every $r > 0$ there is a $K = K(r)$ such that for all $\boldsymbol{\theta} \in V$ and for all $z \in \mathbb{R}^{Jd}$ such that $\max\{\|\boldsymbol{\theta}\|_2, \|z\|_{C_\zeta}\} < r$*

$$0 \le \widetilde{\Phi}^{0,\delta}(\boldsymbol{\theta}, z) \le K.$$

2. *For any fixed $z \in \mathbb{R}^{Jd}$ the function $\widetilde{\Phi}^{0,\delta}(\cdot, z) : V \to \mathbb{R}$ is continuous μ_{pr}-almost surely.*

3. *For $z_1, z_2 \in \mathbb{R}^{Jd}$ with $\max\{\|z_1\|_{C_\zeta}, \|z_2\|_{C_\zeta}\} < r$ and for every $\boldsymbol{\theta} \in V$, there exists $M = M(r, \|\boldsymbol{\theta}\|_2)$, $M : \mathbb{R}^+ \times \mathbb{R}^+ \to \mathbb{R}^+$, monotonic non-decreasing, such that*

$$|\widetilde{\Phi}^{0,\delta}(\boldsymbol{\theta}, z_1) - \widetilde{\Phi}^{0,\delta}(\boldsymbol{\theta}, z_2)| \leq M(r, \|\boldsymbol{\theta}\|_2)\|z_1 - z_2\|_{C_\zeta}.$$

Then the posterior measure $\widetilde{\mu}^{0,\delta}$ given by (6.23) is a well-defined probability measure for almost all $\omega \in \Omega$ and $\forall \delta > 0$.

4. *Moreover, if*

$$M(r, \|\cdot\|_2) \in L^2_{\mu_{\mathrm{pr}}}(V),$$

then $\widetilde{\mu}^{0,\delta}$ is Lipschitz in the data z, with respect to the Hellinger distance, for almost all $\omega \in \Omega$ and $\forall \delta > 0$: if $\widetilde{\mu}^{0,\delta}(\boldsymbol{\theta}|z_1)$ and $\widetilde{\mu}^{0,\delta}(\boldsymbol{\theta}|z_2)$ are two measures corresponding to data z_1 and z_2, then there is a constant $C = C(r) > 0$ such that, for all z_1, z_2 with $\max\{\|z_1\|_{C_\zeta}, \|z\|_{C_\zeta}\} < r$,

$$d_{\mathrm{Hell}}(\widetilde{\mu}^{0,\delta}(\boldsymbol{\theta}|z_1), \widetilde{\mu}^{0,\delta}(\boldsymbol{\theta}|z_2)) \leq C\|z_1 - z_2\|_{C_\zeta}.$$

6.2.1 Well-posedness of the effective posterior measure

Consider a fourth-order tensor A which depends on a parameter $t \in \mathbb{R}$ (the parameter t could represent the Young's modulus E or the Poisson's ratio v). The following lemma establishes a regularity result for the solutions of the cell problems (6.17) with respect to the variable t. It is an extension of Lemma 3.2.2 to the context of linear elasticity.

Lemma 6.2.2. *Let $t \mapsto A(t)$ be of class $C^1(T)$, where T is a subset of $\mathbb{R}$, and assume that $A(t)$ satisfies (6.2), (6.4), (6.5), $\forall t \in T$. Consider the micro functions $\chi_t^{\delta,lm}$ unique solutions of: find $\chi_t^{\delta,lm} \in (W(Y^\delta))^d$ such that*

$$\int_{Y^\delta} A(t)e(\chi_t^{\delta,lm}) : e(\mathbf{z}) \, \mathrm{d}y = -\int_{Y^\delta} A(t)e(I^{lm}) : e(\mathbf{z}) \, \mathrm{d}y \quad \forall \mathbf{z} \in (W(Y^\delta))^d. \qquad (6.24)$$

Then the map $t \in T \mapsto \chi_t^{\delta,lm} \in (W(Y^\delta))^d$ is of class $C^1(T)$ and satisfies

$$\partial_t \chi_t^{\delta,lm} = \phi_t^{\delta,lm}, \quad \partial_t e(\chi_t^{\delta,lm}) = e(\phi_t^{\delta,lm}) \qquad (6.25)$$

where $\phi_t^{\delta,lm} \in (W(Y^\delta))^d$ satisfies

$$\int_{Y^\delta} A(t)e(\phi_t^{\delta,lm}) : e(\mathbf{z}) \, \mathrm{d}y = -\int_{Y^\delta} \partial_t A(t)e(\chi_t^{\delta,lm} + I^{lm}) : e(\mathbf{z}) \, \mathrm{d}y \quad \forall \mathbf{z} \in (W(Y^\delta))^d. \qquad (6.26)$$

Proof. Consider the problem (6.24) for the tensors $A(t)$ and $A(t + \Delta t)$, and denote the corre-

sponding solutions as $\chi_t^{\delta,lm}$ and $\chi_{t+\Delta t}^{\delta,lm}$. We have that $\forall \mathbf{z} \in (W^1(Y^\delta))^d$

$$\int_{Y^\delta} A(t)e(\chi_{t+\Delta t}^{\delta,lm} - \chi_t^{\delta,lm}) : e(\mathbf{z})\,dy = \int_{Y^\delta} (A(t) - A(t+\Delta t))e(\chi_{t+\Delta t}^{\delta,lm} + I^{lm}) : e(\mathbf{z})\,dy. \qquad (6.27)$$

Using Korn's inequality and the fact that $t \mapsto A(t)$ is of class $C^1(T)$, we obtain that $\|\chi_{t+\Delta t}^{\delta,lm} - \chi_t^{\delta,lm}\|_{H^1(Y^\delta)} \to 0$ as $\Delta t \to 0$. Now consider the identity (6.27), divide it by Δt, and subtract equation (6.26). We obtain

$$\frac{1}{\Delta t} \int_{Y^\delta} A(t)e(\chi_{t+\Delta t}^{\delta,lm} - \chi_t^{\delta,lm}) : e(\mathbf{z})\,dy - \int_{Y^\delta} A(t)e(\phi_t^{\delta,lm}) : e(\mathbf{z})\,dy$$

$$= \frac{1}{\Delta t} \int_{Y^\delta} (A(t) - A(t+\Delta t))e(\chi_{t+\Delta t}^{\delta,lm} + I^{lm}) : e(\mathbf{z})\,dy + \int_{Y^\delta} \partial_t A(t)e(\chi_t^{\delta,lm} + I^{lm}) : e(\mathbf{z})\,dy.$$

By taking the limit $\Delta t \to 0$ we deduce (6.25). $\qquad \square$

Lemma 6.2.3. *Let $t \mapsto A(t)$ be of class $C^1(T)$, where T is a subset of $\mathbb{R}$. Let $s \in T$ and assume that there exist two positive constants α_s and β_s such that*

$$\alpha_s \|m\|_F^2 \le A(s)m : m \quad \forall m \in \mathrm{Sym}_d,$$

$$\|A(s)m\|_F \le \beta_s \|m\|_F \quad \forall m \in \mathrm{Sym}_d.$$

Then for almost all $\omega \in \Omega$ and $\forall \delta > 0$

$$\alpha_s \|m\|_F^2 \le \widetilde{A}^{0,\delta}(s)m : m \quad \forall m \in \mathrm{Sym}_d, \qquad (6.28)$$

$$\|\widetilde{A}^{0,\delta}(s)m\|_F \le \beta_s \|m\|_F \quad \forall m \in \mathrm{Sym}_d,, \qquad (6.29)$$

and there exists a constant $\gamma_s > 0$ such that

$$\|\widetilde{A}^{0,\delta}(s)\|_F + \|\partial_t \widetilde{A}^{0,\delta}(s)\|_F \le \gamma_s. \qquad (6.30)$$

Proof. The conditions (6.28) and (6.29) are classical results in homogenization theory (see [33] for example). The components of the approximated homogenized tensor satisfy

$$\widetilde{A}_{ijlm}^0(s) = \int_{Y^\delta} A(s)e(\chi_s^{\delta,lm} + I^{lm}) : e(\chi_s^{\delta,ij} + I^{ij})\,dy. \qquad (6.31)$$

The functions $\chi_s^{\delta,lm}$ solve (6.24) with $t = s$ and are bounded in $(H^1(Y^\delta))^d$ uniformly with respect to δ for almost all $\omega \in \Omega$. Moreover, differentiating with respect to t, and using (6.26) we have that

$$\partial_t \widetilde{A}_{ijlm}^0(s) = \int_{Y^\delta} \partial_t A(s)e(\chi_s^{\delta,lm} + I^{lm}) : e(\chi_s^{\delta,ij} + I^{ij})\,dy,$$

and therefore (6.30) follows. $\qquad\qquad\square$

We can next state the following corollary which establishes an analogous result to the one given in Lemma 6.2.3, but which is adapted to our particular case of interest.

Corollary 6.2.4. *Let $\boldsymbol{\eta} = (E, \nu) \in U$, where U is defined as in* (6.6). *Let $A(\boldsymbol{\eta})$ be defined as in* (6.3). *Then there exist $\alpha_{\boldsymbol{\eta}}$, $\beta_{\boldsymbol{\eta}}$, $\gamma_{\boldsymbol{\eta}}$ such that the tensor $\widetilde{A}^0(\boldsymbol{\eta})$ defined in* (6.18) *satisfies for almost all $\omega \in \Omega$ and $\forall \delta > 0$*

$$\alpha_{\boldsymbol{\eta}} \|m\|_{\mathrm{F}}^2 \leq \widetilde{A}^{0,\delta}(\boldsymbol{\eta}) m : m \quad \forall m \in \mathrm{Sym}_d,$$
$$\|\widetilde{A}^{0,\delta}(\boldsymbol{\eta}) m\|_{\mathrm{F}} \leq \beta_{\boldsymbol{\eta}} \|m\|_{\mathrm{F}} \quad \forall m \in \mathrm{Sym}_d,$$
$$\|\widetilde{A}^{0,\delta}(\boldsymbol{\eta})\|_{\mathrm{F}} + \|\partial_E \widetilde{A}^{0,\delta}(\boldsymbol{\eta})\|_{\mathrm{F}} + \|\partial_\nu \widetilde{A}^{0,\delta}(\boldsymbol{\eta})\|_{\mathrm{F}} \leq \gamma_{\boldsymbol{\eta}}.$$

The following Lemma provides a regularity result for the solution $\widetilde{\mathbf{u}}^0$ to problem (6.20) with respect to the parameter $\boldsymbol{\eta}$.

Lemma 6.2.5. *Let the assumptions of Corollary 6.2.4 be satisfied. Let $\{\boldsymbol{\eta}_n\}_{n>0} = \{(E_n, \nu_n)\}_{n>0}$ be a sequence in U such that converges to some $\boldsymbol{\eta} = (E, \nu) \in U$. Then for almost all $\omega \in \Omega$ and $\forall \delta > 0$ we have that the sequence $\{\widetilde{\mathbf{u}}^0(\boldsymbol{\eta}_n)\}_{n>0}$ converges to $\widetilde{\mathbf{u}}^0(\boldsymbol{\eta})$ in $H^1(D)$.*

Proof. From (6.20) we have that

$$\int_D \widetilde{A}^0(\boldsymbol{\eta}) e(\widetilde{\mathbf{u}}^0(\boldsymbol{\eta}) - \widetilde{\mathbf{u}}^0(\boldsymbol{\eta}_n)) : e(\mathbf{v}) \, \mathrm{d}x$$
$$= \int_D (\widetilde{A}^0(\boldsymbol{\eta}_n) - \widetilde{A}^0(\boldsymbol{\eta})) e(\widetilde{\mathbf{u}}^0(\boldsymbol{\eta}_n)) : e(\mathbf{v}) \, \mathrm{d}x$$

$\forall \mathbf{v} \in (H^1_{\Gamma_1}(D))^d$. Since $\boldsymbol{\eta}_n$ converges to $\boldsymbol{\eta}$, we have that for n sufficiently large the quantities $\alpha_{\boldsymbol{\eta}_n}$, $\beta_{\boldsymbol{\eta}_n}$, $\gamma_{\boldsymbol{\eta}_n}$ are uniformly bounded with respect to n. Hence we will denote such quantities simply as α, β and γ. Taking $\mathbf{v} = \widetilde{\mathbf{u}}^0(\boldsymbol{\eta}) - \widetilde{\mathbf{u}}^0(\boldsymbol{\eta}_n)$ and using Korn's inequality we obtain

$$\|\widetilde{\mathbf{u}}^0(\boldsymbol{\eta}) - \widetilde{\mathbf{u}}^0(\boldsymbol{\eta}_n)\|_{H^1(D)}$$
$$\leq \alpha^{-1} \|\widetilde{\mathbf{u}}^0(\boldsymbol{\eta}_n)\|_{H^1(D)} \|\widetilde{A}^0(\boldsymbol{\eta}_n) - \widetilde{A}^0(\boldsymbol{\eta})\|_{\mathrm{F}}.$$

Let $\{\overline{\boldsymbol{\eta}}_n\}_{n>0} = \{(E, \nu_n)\}_{n>0}$. We then obtain using Corollary 6.2.4

$$\|\widetilde{\mathbf{u}}^0(\boldsymbol{\eta}) - \widetilde{\mathbf{u}}^0(\boldsymbol{\eta}_n)\|_{H^1(D)}$$
$$\leq \alpha^{-1} \|\widetilde{\mathbf{u}}^0(\boldsymbol{\eta}_n)\|_{H^1(D)} \|\widetilde{A}^0(\boldsymbol{\eta}_n) - \widetilde{A}^0(\overline{\boldsymbol{\eta}}) + \widetilde{A}^0(\overline{\boldsymbol{\eta}}) - \widetilde{A}^0(\boldsymbol{\eta})\|_{\mathrm{F}}$$
$$\leq C\alpha^{-2} (\|\widetilde{A}^0(\boldsymbol{\eta}_n) - \widetilde{A}^0(\overline{\boldsymbol{\eta}})\|_{\mathrm{F}} + \|\widetilde{A}^0(\overline{\boldsymbol{\eta}}) - \widetilde{A}^0(\boldsymbol{\eta})\|_{\mathrm{F}})$$
$$\leq C\alpha^{-2} \gamma (|E_1 - E_2| + |\nu_1 - \nu_2|)$$
$$\leq C\alpha^{-2} \gamma \|\boldsymbol{\eta} - \boldsymbol{\eta}_n\|_2, \tag{6.32}$$

and the desired result follows. $\qquad\qquad\qquad\qquad\qquad\qquad\qquad\qquad\qquad\qquad\qquad$ $\square$

Finally, we can now prove that the likelihood function $\widetilde{\Phi}^{0,\delta} : V \times \mathbb{R}^{Jd} \to \mathbb{R}$ given in (6.21) and the probability measure μ_{pr} associated to the density (6.8) satisfy the conditions of Theorem 6.2.1.

Lemma 6.2.6. *Let the assumptions of Corollary 6.2.4 be satisfied. Let μ_{pr} be the prior probability measure associated to the probability density* (6.8)*. Then function $\widetilde{\Phi}^{0,\delta} : V \times \mathbb{R}^{Jd} \to \mathbb{R}$ defined in* (6.21) *satisfies for almost all $\omega \in \Omega$ and $\forall \delta > 0$ the assumptions 1-4 of Theorem 6.2.1.*

Proof. For any $\boldsymbol{\eta} = P(\boldsymbol{\theta}) \in U$ we have that

$$
\begin{aligned}
\|\widetilde{G}^{0,\delta}(\boldsymbol{\theta})\|_{C_\zeta} &\le C \sum_{j=1}^{J} \sum_{i=1}^{d} \int_{S_j} |\widetilde{u}_i^0(P(\boldsymbol{\theta}))| \, \mathrm{d}s \\
&\le C \|\widetilde{\mathbf{u}}^0(\boldsymbol{\eta})\|_{L^2(\partial D)} \\
&\le C \alpha_{\boldsymbol{\eta}}^{-1} \\
&\le C \exp(\|\boldsymbol{\theta}\|_2),
\end{aligned}
$$

where we have used (6.9) and the fact that $|k| \le \|\boldsymbol{\theta}\|_2$ for any $\boldsymbol{\theta} = (k, v) \in V$. From the triangle inequality we have that

$$
\widetilde{\Phi}^{0,\delta}(\boldsymbol{\theta}, z) \le \frac{1}{2} (\|z\|_{C_\zeta}^2 + \|\widetilde{G}^{0,\delta}(\boldsymbol{\theta})\|_{C_\zeta}^2),
$$

and therefore the first assumption of Theorem 6.2.1 is satisfied. The second assumption of Theorem 6.2.1 can be verified by using Lemma 6.2.5. Indeed for any $\boldsymbol{\theta}_1 \in V$ and $\boldsymbol{\theta}_2 \in V$ we have that

$$
|\widetilde{\Phi}^{0,\delta}(\boldsymbol{\theta}_1, z) - \widetilde{\Phi}^{0,\delta}(\boldsymbol{\theta}_2, z)| = \frac{1}{2} |\langle \widetilde{G}^{0,\delta}(\boldsymbol{\theta}_1) + \widetilde{G}^{0,\delta}(\boldsymbol{\theta}_2) - 2z, \widetilde{G}^{0,\delta}(\boldsymbol{\theta}_1) - \widetilde{G}^{0,\delta}(\boldsymbol{\theta}_2) \rangle_{C_\zeta}|
$$

and assumption 2 follows from continuity of $\widetilde{G}^{0,\delta}$ at $\boldsymbol{\theta} \in V$. Finally, given two measurements $z_1, z_2 \in \mathbb{R}^{Jd}$, we have that

$$
\begin{aligned}
|\widetilde{\Phi}^{0,\delta}(\boldsymbol{\theta}, z_1) - \widetilde{\Phi}^{0,\delta}(\boldsymbol{\theta}, z_2)| &= \frac{1}{2} |\langle z_1 + z_2 - 2\widetilde{G}^{0,\delta}(\boldsymbol{\theta}), z_1 - z_2 \rangle_{C_\zeta}| \\
&\le C(\|z_1\|_{C_\zeta} + \|z_2\|_{C_\zeta} + 2\widetilde{G}^{0,\delta}(\boldsymbol{\theta}))\|z_1 - z_2\|_{C_\zeta}.
\end{aligned}
$$

Let r such that $\max\{\|z_1\|_{C_\zeta}, \|z_2\|_{C_\zeta}\} < r$. Hence we obtain

$$
\begin{aligned}
|\widetilde{\Phi}^{0,\delta}(\boldsymbol{\theta}, z_1) - \widetilde{\Phi}^{0,\delta}(\boldsymbol{\theta}, z_2)| &\le C(2r + 2\widetilde{G}^{0,\delta}(\boldsymbol{\theta}))\|z_1 - z_2\|_{C_\zeta} \\
&\le M(r, \|\boldsymbol{\theta}\|_2)\|z_1 - z_2\|_{C_\zeta},
\end{aligned}
$$

with

$$
M(r, \|\boldsymbol{\theta}\|_2) = C(2r + 2\exp(\|\boldsymbol{\theta}\|_2)).
$$

We note that $M(r, \|\boldsymbol{\theta}\|_2)$ is positive, monotonic non-decreasing, and satisfies $M(r, \|\cdot\|_2) \in L^2_{\mu_{\mathrm{pr}}}(V)$, hence assumptions 3 and 4 of Theorem 6.2.1 follow. $\qquad\square$

Remark 6.2.7. Using similar arguments as in the proof of Lemma 6.2.6 it can be shown that the posterior measures μ^ε and μ^0, based on the potential functions Φ^ε and Φ^0 respectively, are also well-defined and Lipschitz in the data.

6.2.2 Convergence of the effective posterior measure towards the fine scale posterior

We note that the observations (6.11) can be rewritten as

$$z = \widetilde{G}^{0,\delta}(\boldsymbol{\theta}^*) + \zeta^\varepsilon(\boldsymbol{\theta}^*) + \zeta^\delta(\boldsymbol{\theta}^*) + \zeta,$$

where

$$\zeta \sim \mathcal{N}(0, C_\zeta), \quad \zeta^\varepsilon(\boldsymbol{\theta}^*) = G^\varepsilon(\boldsymbol{\theta}^*) - G^0(\boldsymbol{\theta}^*), \quad \zeta^\delta(\boldsymbol{\theta}^*) = G^0(\boldsymbol{\theta}^*) - \widetilde{G}^{0,\delta}(\boldsymbol{\theta}^*).$$

The quantity ζ^ε represents the error due to the mismatch between the full multiscale model and the homogenized one. The quantity ζ^δ quantifies the error between the homogenized model and its approximation obtained by homogenization on a sampling domain of size δ. For both errors we can show that they converge to zero when $\varepsilon \to 0$ and $\delta \to \infty$ respectively.

Lemma 6.2.8. *Let $G^\varepsilon : U \to \mathbb{R}^{Jd}$ and $G^0 : U \to \mathbb{R}^{Jd}$ be defined as in* (6.10) *and* (6.14)*, respectively. Let $\zeta^\varepsilon(\boldsymbol{\theta}) = G^\varepsilon(\boldsymbol{\theta}) - G^0(\boldsymbol{\theta})$. Then we have*

$$\lim_{\varepsilon \to 0} \|\zeta^\varepsilon(\boldsymbol{\theta})\|_{C_\zeta} = 0 \quad a.s. \quad \forall \boldsymbol{\theta} \in U.$$

Proof. For any $\boldsymbol{\theta} \in V$ we have that

$$\|\zeta^\varepsilon(\boldsymbol{\theta})\|_{C_\zeta} \leq C \sum_{j=1}^{J} \sum_{i=1}^{d} \int_{S_j} |u_i^\varepsilon(P(\boldsymbol{\theta})) - u_i^0(P(\boldsymbol{\theta}))| \, \mathrm{d}s$$

$$\leq C \|\mathbf{u}^\varepsilon(P(\boldsymbol{\theta})) - \mathbf{u}^0(P(\boldsymbol{\theta}))\|_{L^2(\partial D)}.$$

From homogenization theory [63, 35] we know that there exists an extension $\hat{\mathbf{u}}^\varepsilon$ of $\mathbf{u}^\varepsilon$ into D such that

$$\hat{\mathbf{u}}^\varepsilon \rightharpoonup \mathbf{u}^0 \quad \text{a.s. weakly in } (H^1(D))^d \quad \forall P(\boldsymbol{\theta}) \in U.$$

Therefore by compactness we have that

$$\hat{\mathbf{u}}^\varepsilon \to \mathbf{u}^0 \quad \text{a.s. strongly in } (L^2(\partial D))^d \quad \forall \boldsymbol{\eta} \in U.$$

Since $\hat{\mathbf{u}}^\varepsilon = \mathbf{u}^\varepsilon$ on ∂D, the result follows. $\qquad\square$

Lemma 6.2.9. *Let $G^0 : V \to \mathbb{R}^{Jd}$ and $\widetilde{G}^{0,\delta} : V \to \mathbb{R}^{Jd}$ defined as in (6.14) and (6.19), respectively. Let $\zeta^\delta(\boldsymbol{\theta}) = G^0(\boldsymbol{\theta}) - \widetilde{G}^{0,\delta}(\boldsymbol{\theta})$. Then we have*

$$\lim_{\delta \to \infty} \|\zeta^\delta(\boldsymbol{\theta})\|_{C_\zeta} = 0 \quad a.s. \quad \forall \boldsymbol{\theta} \in U.$$

Proof. For any $\boldsymbol{\theta} \in V$ we have that

$$
\begin{aligned}
\|\zeta^\delta(\boldsymbol{\theta})\|_{C_\zeta} &\leq C \sum_{j=1}^{J} \sum_{i=1}^{d} \int_{S_j} |u_i^0(P(\boldsymbol{\theta})) - \tilde{u}_i^0(P(\boldsymbol{\theta}))| \, \mathrm{d}s \\
&\leq C \|\mathbf{u}^0(P(\boldsymbol{\theta})) - \widetilde{\mathbf{u}}^0(P(\boldsymbol{\theta}))\|_{L^2(\partial D)} \\
&\leq C \|\mathbf{u}^0(P(\boldsymbol{\theta})) - \widetilde{\mathbf{u}}^0(P(\boldsymbol{\theta}))\|_{H^1(D)}.
\end{aligned}
$$

We know that $\widetilde{A}^0(P(\boldsymbol{\theta})) \to A^0(P(\boldsymbol{\theta}))$ a.s. as $\delta \to \infty$. This implies that $\widetilde{\mathbf{u}}^0(P(\boldsymbol{\theta})) \to \mathbf{u}^0(P(\boldsymbol{\theta}))$ strongly in $(H^1(D))^d$ a.s. as $\delta \to \infty$, and hence the desired result follows. $\qquad\square$

Lemma 6.2.10. *Let μ^ε and μ^0 be defined as in (6.13) and (6.16), respectively. Let the assumptions of Lemma 6.2.6 be satisfied. Then we have*

$$\lim_{\varepsilon \to 0} d_{\mathrm{Hell}}(\mu^\varepsilon, \mu^0) = 0 \quad a.s.$$

Proof. From the definition of the Hellinger distance we have that

$$
\begin{aligned}
2d_{\mathrm{Hell}}^2(\mu^\varepsilon, \mu^0) &= \int_{\mathbb{R}^2} \left(\sqrt{\frac{\mathrm{d}\mu^\varepsilon}{\mathrm{d}\mu_{\mathrm{pr}}}} - \sqrt{\frac{\mathrm{d}\mu^0}{\mathrm{d}\mu_{\mathrm{pr}}}} \right)^2 \mu_{\mathrm{pr}}(\mathrm{d}\boldsymbol{\theta}) \\
&= \int_{\mathbb{R}^2} \left(\frac{1}{\sqrt{C^\varepsilon}} \exp\left(-\frac{1}{2}\Phi^\varepsilon(\boldsymbol{\theta}, z)\right) - \frac{1}{\sqrt{C^0}} \exp\left(-\frac{1}{2}\Phi^0(\boldsymbol{\theta}, z)\right) \right)^2 \mu_{\mathrm{pr}}(\mathrm{d}\boldsymbol{\theta}),
\end{aligned}
$$
(6.33)

where C^ε and C^0 are the two normalization constants such that $\mu^\varepsilon(\boldsymbol{\theta}|z)$ and $\mu^0(\boldsymbol{\theta}|z)$ are probability measures, i.e.,

$$C^\varepsilon = \int_{\mathbb{R}^2} \exp(-\Phi^\varepsilon(\boldsymbol{\theta}, z)) \mu_{\mathrm{pr}}(\mathrm{d}\boldsymbol{\theta}), \quad C^0 = \int_{\mathbb{R}^2} \exp(-\Phi^0(\boldsymbol{\theta}, z)) \mu_{\mathrm{pr}}(\mathrm{d}\boldsymbol{\theta}).$$

Let us notice that

$$
\begin{aligned}
|C^\varepsilon - C^0| &\leq \int_{\mathbb{R}^2} \left| \exp(-\Phi^\varepsilon(\boldsymbol{\theta}, z)) - \exp(-\Phi^0(\boldsymbol{\theta}, z)) \right| \mu_{\mathrm{pr}}(\mathrm{d}\boldsymbol{\theta}) \\
&\leq \int_{\mathbb{R}^2} \left| \Phi^\varepsilon(\boldsymbol{\theta}, z) - \Phi^0(\boldsymbol{\theta}, z) \right| \mu_{\mathrm{pr}}(\mathrm{d}\boldsymbol{\theta}).
\end{aligned}
$$
(6.34)

From (6.33) we get that

$$2d_{\mathrm{Hell}}^2(\mu^\varepsilon, \mu^0) \le I_1 + I_2\,,$$

where

$$I_1 = \frac{1}{C^0} \int_{\mathbb{R}^2} \left(\exp\left(-\frac{1}{2}\Phi^\varepsilon(\boldsymbol{\theta}, z) \right) - \exp\left(-\frac{1}{2}\Phi^0(\boldsymbol{\theta}, z) \right) \right)^2 \mu_{\mathrm{pr}}(\mathrm{d}\boldsymbol{\theta})\,,$$

$$I_2 = \left(\frac{1}{\sqrt{C^\varepsilon}} - \frac{1}{\sqrt{C^0}} \right)^2 C^\varepsilon\,.$$

We have that

$$I_1 \le \frac{1}{4C^0} \int_{\mathbb{R}^2} (\Phi^\varepsilon(\boldsymbol{\theta}, z) - \Phi^0(\boldsymbol{\theta}, z))^2 \mu_{\mathrm{pr}}(\mathrm{d}\boldsymbol{\theta})\,,$$

and

$$I_2 \le \frac{1}{4} \max\left\{ (C^\varepsilon)^{-3}, (C^0)^{-3} \right\} (C^\varepsilon - C^0)^2$$

$$\le C \int_{\mathbb{R}^2} (\Phi^\varepsilon(\boldsymbol{\theta}, z) - \Phi^0(\boldsymbol{\theta}, z))^2 \mu_{\mathrm{pr}}(\mathrm{d}\boldsymbol{\theta})\,,$$

where we have used (6.34). Using the definition of Φ^ε and Φ^0 we find

$$2d_{\mathrm{Hell}}^2(\mu^\varepsilon, \mu^0) \le C \int_{\mathbb{R}^2} (\Phi^\varepsilon(\boldsymbol{\theta}, z) - \Phi^0(\boldsymbol{\theta}, z))^2 \mu_{\mathrm{pr}}(\mathrm{d}\boldsymbol{\theta})$$

$$\le C \int_{\mathbb{R}^2} (2\|z\|_{C_\zeta} + \|G^0(\boldsymbol{\theta})\|_{C_\zeta} + \|G^\varepsilon(\boldsymbol{\theta})\|_{C_\zeta})^2 \|G^\varepsilon(\boldsymbol{\theta}) - G^0(\boldsymbol{\theta})\|_{C_\zeta}^2 \mu_{\mathrm{pr}}(\mathrm{d}\boldsymbol{\theta})\,.$$

From Lemma 6.2.8 we have that a.s. $\lim_{\varepsilon \to 0} \|G^\varepsilon(\boldsymbol{\theta}) - G^0(\boldsymbol{\theta})\|_{C_\zeta} = 0$. We also have (see Lemma 6.2.6 and Remark 6.2.7) that for any $\boldsymbol{\theta} \in V$ both $\|G^0(\boldsymbol{\theta})\|_{C_\zeta}$ and $\|G^\varepsilon(\boldsymbol{\theta})\|_{C_\zeta}$ are bounded by some scalar multiple of $\exp(\|\boldsymbol{\theta}\|_2)$. Since $\exp(\|\cdot\|_2) \in L_{\mu_{\mathrm{pr}}}^2(V)$, by the Lebesgue's dominated convergence theorem, it follows that $d_{\mathrm{Hell}}(\mu^\varepsilon, \mu^0) \to 0$ a.s. as $\varepsilon \to 0$. $\qquad\square$

The following lemma establishes the convergence between μ^0 and the random measure $\widetilde{\mu}^{0,\delta}$.

Lemma 6.2.11. *Let μ^0 and $\widetilde{\mu}^{0,\delta}$ be defined as in* (6.16) *and* (6.23)*, respectively. Let the assumptions of Lemma 6.2.6 be satisfied. Then we have*

$$\lim_{\delta \to \infty} d_{\mathrm{Hell}}(\mu^0, \widetilde{\mu}^{0,\delta}) = 0 \quad a.s.$$

Proof. From the definition of the Hellinger distance we have that

$$2d_{\text{Hell}}^2(\mu^0, \widetilde{\mu}^{0,\delta}) = \int_{\mathbb{R}^2} \left(\sqrt{\frac{d\mu^0}{d\mu_{\text{pr}}}} - \sqrt{\frac{d\widetilde{\mu}^{0,\delta}}{d\mu_{\text{pr}}}} \right)^2 \mu_{\text{pr}}(d\boldsymbol{\theta})$$

$$= \int_{\mathbb{R}^2} \left(\frac{1}{\sqrt{C^0}} \exp\left(-\frac{1}{2}\Phi^0(\boldsymbol{\theta}, z)\right) - \frac{1}{\sqrt{\widetilde{C}^{0,\delta}}} \exp\left(-\frac{1}{2}\widetilde{\Phi}^{0,\delta}(\boldsymbol{\theta}, z)\right) \right)^2 \mu_{\text{pr}}(d\boldsymbol{\theta}),$$

where C^0 and $\widetilde{C}^{0,\delta}$ are the two normalization constants such that $\mu^0(\boldsymbol{\theta}|z)$ and $\widetilde{\mu}^{0,\delta}(\boldsymbol{\theta}|z)$ are probability measures. Using arguments similar to the ones employed in the proof of Lemma 6.2.10 we obtain that

$$2d_{\text{Hell}}^2(\mu^0, \widetilde{\mu}^{0,\delta}) \le C \int_{\mathbb{R}^2} (2\|z\|_{C_\zeta} + \|\widetilde{G}^{0,\delta}(\boldsymbol{\theta})\|_{C_\zeta} + \|G^0(\boldsymbol{\theta})\|_{C_\zeta})^2 \|G^0(\boldsymbol{\theta}) - \widetilde{G}^{0,\delta}(\boldsymbol{\theta})\|_{C_\zeta}^2 \mu_{\text{pr}}(d\boldsymbol{\theta}).$$

From Lemma 6.2.9 we have that $\lim_{\delta\to\infty} \|G^0(\boldsymbol{\theta}) - \widetilde{G}^{0,\delta}(\boldsymbol{\theta})\|_{C_\zeta} = 0$ a.s. We also have (see Lemma 6.2.6 and Remark 6.2.7) that for any $\boldsymbol{\theta} \in V$ both $\|G^0(\boldsymbol{\theta})\|_{C_\zeta}$ and $\|\widetilde{G}^{0,\delta}(\boldsymbol{\theta})\|_{C_\zeta}$ are bounded by some scalar multiple of $\exp(\|\boldsymbol{\theta}\|_2)$. Since $\exp(\|\cdot\|_2) \in L_{\mu_{\text{pr}}}^2(V)$, by the Lebesgue's dominated convergence theorem, it follows that $d_{\text{Hell}}(\mu^0, \widetilde{\mu}^{0,\delta}) \to 0$ a.s. as $\delta \to \infty$. $\qquad\square$

Finally, we can establish convergence between the fine scale posterior μ^ε and the random measure $\widetilde{\mu}^{0,\delta}$.

Theorem 6.2.12. *Let μ^ε and $\widetilde{\mu}^{0,\delta}$ be defined as in* (6.13) *and* (6.23)*, respectively. Let the assumptions of Lemma 6.2.6 be satisfied. Then we have*

$$\lim_{\varepsilon\to0}\lim_{\delta\to\infty} d_{\text{Hell}}(\mu^\varepsilon, \widetilde{\mu}^{0,\delta}) = 0 \quad a.s.,$$

$$\lim_{\delta\to\infty}\lim_{\varepsilon\to0} d_{\text{Hell}}(\mu^\varepsilon, \widetilde{\mu}^{0,\delta}) = 0 \quad a.s.$$

Proof. Using the triangle inequality we get

$$\lim_{\varepsilon\to0}\lim_{\delta\to\infty} d_{\text{Hell}}(\mu^\varepsilon, \widetilde{\mu}^{0,\delta}) \le \lim_{\varepsilon\to0} d_{\text{Hell}}(\mu^\varepsilon, \mu^0) + \lim_{\delta\to\infty} d_{\text{Hell}}(\mu^0, \widetilde{\mu}^{0,\delta}).$$

Note that the same holds by changing the order of the limits of the left hand side, i.e.,

$$\lim_{\delta\to\infty}\lim_{\varepsilon\to0} d_{\text{Hell}}(\mu^\varepsilon, \widetilde{\mu}^{0,\delta}) \le \lim_{\varepsilon\to0} d_{\text{Hell}}(\mu^\varepsilon, \mu^0) + \lim_{\delta\to\infty} d_{\text{Hell}}(\mu^0, \widetilde{\mu}^{0,\delta}).$$

The assertion of the lemma follows from Lemma 6.2.10 and Lemma 6.2.11. $\qquad\square$

6.2.3 Convergence of the probabilistic effective posterior measure towards the fine scale posterior

We have proved that if we let $\delta \to \infty$ the random measure $\widetilde{\mu}^{0,\delta}$ concentrates towards the effective measure μ^0, which in turn is a good approximation of μ^ε when $\varepsilon \ll 1$. However, in practice it is infeasible to let $\delta \to \infty$ in numerical experiments. Indeed, trying to approximate the density $\widetilde{\mu}^{0,\delta}$ for large values of δ requires a computational cost comparable to the one needed for approximating the measure μ^ε. On the other hand, if δ is too small, our method could be biased due to the excessively large modeling error, and therefore lead to misleading predictions, as we will illustrate with some numerical experiments. To overcome this issue and account for the impact of the modeling error, we then propose a probabilistic numerical method which aims at approximating the expected probability density $\overline{\pi}^{0,\delta}$ with respect to the measure μ, where μ is the measure of the probability space (Ω, Σ, μ) used to construct the random set $Q^\varepsilon(\omega)$. The expected probability density $\overline{\pi}^{0,\delta}$ is defined as

$$\overline{\pi}^{0,\delta}(\boldsymbol{\theta}|z) = \mathbb{E}_\mu[\widetilde{\pi}^{0,\delta}(\boldsymbol{\theta}|z)]. \tag{6.35}$$

We denote the probability measure associated to $\overline{\pi}^{0,\delta}$ as $\overline{\mu}^{0,\delta}$ which satisfies

$$\frac{\mathrm{d}\overline{\mu}^{0,\delta}(\boldsymbol{\theta}|z)}{\mathrm{d}\mu_{\mathrm{pr}}(\boldsymbol{\theta})} = \mathbb{E}_\mu\left[\frac{1}{\widetilde{C}^{0,\delta}(z)}\exp(-\widetilde{\Phi}^{0,\delta}(\boldsymbol{\theta},z))\right]. \tag{6.36}$$

We remark that the expected measure $\overline{\mu}^{0,\delta}$ is not a random measure, but represents a deterministic approximation of the measure μ^0. Moreover, as we will illustrate in the numerical experiments, it allows to better quantify the uncertainty due to the intrinsic modeling error caused by the truncation of the micro domain. Finally, it is important to remark that convergence results established for the random measure $\widetilde{\mu}^{0,\delta}$ are valid also for the measure $\overline{\mu}^{0,\delta}$ as stated by what follows.

Lemma 6.2.13. *Let μ^0 and $\overline{\mu}^{0,\delta}$ be defined as in* (6.16) *and* (6.36), *respectively. Then we have*

$$\lim_{\delta \to \infty} d_{\mathrm{Hell}}(\mu^0, \overline{\mu}^{0,\delta}) = 0.$$

Proof. From the definition of the Hellinger distance, Jensen's inequality and Fubini's theorem

we have that

$$
\begin{aligned}
d_{\mathrm{Hell}}^2(\mu^0, \overline{\mu}^{0,\delta}) &= \int_{\mathbb{R}^2} \left(\sqrt{\pi^0} - \sqrt{\overline{\pi}^{0,\delta}} \right)^2 \mu_{\mathrm{pr}}(\mathrm{d}\boldsymbol{\theta}) \\
&= \int_{\mathbb{R}^2} \left(\sqrt{\pi^0} - \sqrt{\mathbb{E}_\mu[\widetilde{\pi}^{0,\delta}]} \right)^2 \mu_{\mathrm{pr}}(\mathrm{d}\boldsymbol{\theta}) \\
&\leq \int_{\mathbb{R}^2} \mathbb{E}_\mu \left[\left(\sqrt{\pi^0} - \sqrt{\widetilde{\pi}^{0,\delta}} \right)^2 \right] \mu_{\mathrm{pr}}(\mathrm{d}\boldsymbol{\theta}) \\
&= \mathbb{E}_\mu \left[\int_{\mathbb{R}^2} \left(\sqrt{\pi^0} - \sqrt{\widetilde{\pi}^{0,\delta}} \right)^2 \mu_{\mathrm{pr}}(\mathrm{d}\boldsymbol{\theta}) \right] \\
&= \mathbb{E}_\mu[d_{\mathrm{Hell}}^2(\mu^0, \widetilde{\mu}^{0,\delta})].
\end{aligned}
$$

We note that $d_{\mathrm{Hell}}(\mu^0, \widetilde{\mu}^{0,\delta})$ is itself a random variable depending on the particular realization of the random perforated micro domain X_δ^ε. As established in Lemma 6.2.11 the random variable $d_{\mathrm{Hell}}(\mu^0, \widetilde{\mu}^{0,\delta})$ converges to 0 a.s., and it is bounded by 1 by definition. Hence we also have that $\mathbb{E}_\mu[d_{\mathrm{Hell}}^2(\mu^0, \widetilde{\mu}^{0,\delta})] \to 0$ as $\delta \to \infty$, and the proof is complete. $\qquad\square$

We conclude this section with the following theorem which establishes the convergence between μ^ε and $\overline{\mu}^{0,\delta}$.

Theorem 6.2.14. *Let μ^ε and $\overline{\mu}^{0,\delta}$ be defined as in (6.13) and (6.36), respectively. Then we have*

$$
\lim_{\varepsilon \to 0} \lim_{\delta \to \infty} d_{\mathrm{Hell}}(\mu^\varepsilon, \overline{\mu}^{0,\delta}) = 0 \quad a.s.,
$$
$$
\lim_{\delta \to \infty} \lim_{\varepsilon \to 0} d_{\mathrm{Hell}}(\mu^\varepsilon, \overline{\mu}^{0,\delta}) = 0 \quad a.s.
$$

Proof. The result follows from Lemma 6.2.10, Lemma 6.2.13 and the triangle inequality. $\qquad\square$

6.3 Probabilistic numerical method for the solution of the Bayesian linear elastic inverse problem

In this section we discuss the numerical solution of a Bayesian linear elastic inverse problem in random perforated domains by means of a probabilistic numerical method. We approximate the density (6.35) by the Monte Carlo method, i.e.,

$$
\overline{\pi}_{\mathrm{MC}}^{0,\delta}(\boldsymbol{\theta}|z) = \frac{1}{R} \sum_{i=1}^{R} \widetilde{\pi}_i^{0,\delta}(\boldsymbol{\theta}|z), \tag{6.37}
$$

where each $\widetilde{\pi}_i^{0,\delta}$ is a probability density defined as in (6.22) for a typical realization of the micro random perforated domain $X_{\delta,i}^\varepsilon$, $i = 1, \dots, R$. We then combine all the samples together to obtain a representation of the density (6.35), as illustrated by the following algorithm. Inputs are

the target distribution $\overline{\pi}^{0,\delta}(\boldsymbol{\theta}|z)$, a starting point $\boldsymbol{\theta}^1 \in V$, a desired number of samples N_{sample} in the Metropolis-Hastings routine, the number R in the Monte Carlo approximation (6.37), and a symmetric proposal density $\mathcal{N}(0, s^2 I)$.

1. Draw R realizations of the sampling domain $\{X_{\delta,i}^\varepsilon\}_{i=1}^R$.

2. Set $\mathcal{S} = \emptyset$.

3. For $1 \le i \le R$ do the following.
   (a) Set $k = 1$, $\mathcal{S}_i = \boldsymbol{\theta}^1$.

   (b) For $2 \le k \le N_{\text{sample}}$ perform the following steps.
      i. $\boldsymbol{\theta} = \boldsymbol{\theta}^k + sw$, $w \sim \mathcal{N}(0, I)$.

      ii. $a(\boldsymbol{\theta}^k, \boldsymbol{\theta}) = \min\left\{1, \dfrac{\widetilde{\pi}_i^{0,\delta}(\boldsymbol{\theta}|z)}{\widetilde{\pi}_i^{0,\delta}(\boldsymbol{\theta}^k|z)}\right\}$.

      iii. Draw $u \sim \mathcal{U}([0,1])$, and if $a(\boldsymbol{\theta}^k, \boldsymbol{\theta}) > u$ accept $\boldsymbol{\theta}$ and set $\boldsymbol{\theta}^{k+1} = \boldsymbol{\theta}$. Otherwise reject the proposed step and set $\boldsymbol{\theta}^{k+1} = \boldsymbol{\theta}^k$.

      iv. $\mathcal{S}_i = \mathcal{S}_i \cup \boldsymbol{\theta}^{k+1}$.

   (c) $\mathcal{S} = \mathcal{S} \cup \mathcal{S}_i$.

4. Return $\mathcal{S}$.

Numerical approximation of the forward model. Given a typical realization of the micro domain $X_\delta^\varepsilon = X_\delta \setminus (X_\delta \cap Q^\varepsilon)$, $X_\delta = (0,\delta)^d$, to sample from the posterior density $\widetilde{\pi}^{0,\delta}$ we need an efficient numerical algorithm to evaluate the forward operator $\widetilde{G}^{0,\delta} : \mathbb{R}^2 \to \mathbb{R}^{Jd}$. Let us consider macro and micro finite element spaces involving only piecewise linear simplicial elements and periodic coupling. The macro finite element space is defined as

$$S_{\Gamma_1}^1 = \left\{\mathbf{v}^H \in (H_{\Gamma_1}^1(D))^d : \mathbf{v}^H|_K \in (\mathscr{P}^1(K))^d, \forall K \in \mathscr{T}_H\right\},$$

where $\mathscr{T}_H$ is a triangulation of the domain in simplicial elements K and $(\mathscr{P}^1(K))^d$ is the space of linear polynomial vector fields on K. Since we have assumed the tensor A to be constant on the whole domain, the corresponding homogenized tensor is constant too, and therefore its value does not have to be computed for all the macro quadrature points, but only once. Hence for the micro domain X_δ^ε we we consider the micro finite element space

$$S^1(X_\delta^\varepsilon, \mathscr{T}_h) = \left\{\mathbf{z}^h \in (W_{\text{per}}^1(X_\delta^\varepsilon))^d : \mathbf{z}^h \in (\mathscr{P}^1(T))^d, \forall T \in \mathscr{T}_h\right\}.$$

We map the domain X_δ^ε into $Y^\delta \subset (0,1)^d$ using the change of variable $x = \delta y$. Given $\boldsymbol{\theta} \in V$ we introduce the parameterized bilinear form

$$B_H(\mathbf{v}^H, \mathbf{w}^H; \boldsymbol{\eta}) = \sum_{K \in \mathscr{T}_H} |K| A^{0,h}(\boldsymbol{\eta}) e(\mathbf{v}^H)_K : e(\mathbf{w}^H)_K, \tag{6.38}$$

where $\boldsymbol{\eta} = P(\boldsymbol{\theta})$, and

$$A_{ijlm}^{0,h}(\boldsymbol{\eta}) = \int_{Y^\delta} A(\boldsymbol{\eta}) e(\chi_{\boldsymbol{\eta}}^{lm,\hat{h}} + I^{lm}) : e(I^{ij}) \, dy,$$

and $\chi_{\boldsymbol{\eta}}^{lm,\hat{h}} \in S^1(Y^\delta, \mathcal{T}_{\hat{h}})$, $\hat{h} = h/\delta$, is the solution of

$$\int_{Y^\delta} A(\boldsymbol{\eta}) e(\chi_{\boldsymbol{\eta}}^{lm,\hat{h}}) : e(\mathbf{z}^{\hat{h}}) \, dy = - \int_{Y^\delta} A(\boldsymbol{\eta}) e(I^{lm}) : e(\mathbf{z}^{\hat{h}}) \, dy \quad \forall \mathbf{z}^{\hat{h}} \in S^1(Y^\delta, \mathcal{T}_{\hat{h}}), \tag{6.39}$$

where $I_p^{lm} = y_m \delta_{pl}$, and δ_{pl} is the Kronecker symbol. Finally, we can evaluate the forward model by computing $\mathbf{u}^H \in S^1_{\Gamma_1}(D, \mathcal{T}_H)$ such that

$$B_H(\mathbf{u}^H, \mathbf{v}^H; \boldsymbol{\eta}) = F(\mathbf{v}^H) \quad \forall \mathbf{v}^H \in S^1_{\Gamma_1}(D, \mathcal{T}_H). \tag{6.40}$$

Model order reduction. The Metropolis-Hastings algorithm requires the solution of (6.40) multiple times for different values of $\boldsymbol{\eta}$. For every new value of $\boldsymbol{\eta}$ a new micro problem of type (6.39) has to be solved, whose computational cost increases as we refine the micro mesh and increase δ. Hence, despite being independent of ε, solving the inverse problem using (6.40) as forward model is still computationally very expensive. To speed up the algorithm we exploit the parametrization of the micro problems to build a reduced space of precomputed micro functions which enables us to perform fast evaluation of (6.40) at a cost which is independent of δ and h. We define the space of parameters $\Xi = U \times \{1, \ldots, d\}^2$, and for a given $\xi = (\boldsymbol{\eta}, l, m) \in \Xi$ we denote the corresponding micro solution as $\chi_\xi^{\hat{h}} \in S^1(Y^\delta, \mathcal{T}_{\hat{h}})$ which satisfies

$$b_\delta(\chi_\xi^{\hat{h}}, \mathbf{z}^{\hat{h}}; \xi) = f_\delta(\mathbf{z}^{\hat{h}}; \xi) \quad \forall \mathbf{z}^{\hat{h}} \in S^1(Y^\delta, \mathcal{T}_{\hat{h}}),$$

where

$$b_\delta(\mathbf{z}^{\hat{h}}, \hat{\mathbf{w}}^h; \xi) = \int_{Y^\delta} A(\boldsymbol{\eta}) e(\mathbf{z}^{\hat{h}}) : e(\hat{\mathbf{w}}^{\hat{h}}) \, dy,$$

and

$$f_\delta(\mathbf{z}^{\hat{h}}, \xi) = -b_\delta(I^{lm}, \mathbf{z}^{\hat{h}}; \xi).$$

Following the algorithm described in Chapter 5, we randomly define a training set

$$\Xi_{\text{Train}} = \left\{ \xi_n = (\boldsymbol{\eta}_n, l_n, m_n) : 1 \leq n \leq N_{\text{Train}}, \boldsymbol{\eta}_n \in U, 1 \leq l_n, m_n \leq d \right\},$$

and perform a greedy offline stage to build the reduced space

$$S^N(Y^\delta) = \text{span} \left\{ \psi_1^{\hat{h}}, \ldots, \psi_N^{\hat{h}} \right\}.$$

Thus we introduce the parameterized macro bilinear form defined upon the reduced space

$$B_{H,\mathrm{RB}}(\mathbf{v}^H, \mathbf{w}^H; \boldsymbol{\eta}) = \sum_{K \in \mathscr{T}_H} A^{0,N}(\boldsymbol{\eta}) e(\mathbf{v}^H)_K : e(\mathbf{w}^H)_K,$$

where

$$A^{0,N}_{ijlm}(\boldsymbol{\eta}) = \int\limits_{Y^\delta} A(\boldsymbol{\eta}) e(\chi^{lm,N}_{\boldsymbol{\eta}} + I^{lm}) : e(I^{ij}) \, dy, \tag{6.41}$$

and $\chi^{lm,N}_{\boldsymbol{\eta}}$ is the solution of (6.39) computed in the reduced space $S^N(Y^\delta)$. Hence we compute the solution $\mathbf{u}^{H,\mathrm{RB}} \in S^1_{\Gamma_1}(D, \mathscr{T}_H)$ by solving

$$B_{H,\mathrm{RB}}(\mathbf{u}^{H,\mathrm{RB}}, \mathbf{v}^H; \boldsymbol{\eta}) = F(\mathbf{v}^H) \quad \forall \mathbf{v}^H \in S^1_{\Gamma_1}(D, \mathscr{T}_H). \tag{6.42}$$

Summary of the probabilistic method. Given the noisy observation $z \in \mathbb{R}^{Jd}$, the probabilistic numerical method for solving the multiscale Bayesian linear elastic inverse problem in random perforated media can be summarized as follows.

1. Draw randomly (for example by using a Monte Carlo method) R realizations of the micro domains $\{X^\varepsilon_{\delta,i}\}_{i=1}^R$.

2. Set $\mathscr{S} = \varnothing$.

3. For $1 \le i \le R$ do the following.
    (a) Perform an offline stage to construct the reduced space $S^N(Y^\delta_i)$, where $Y^\delta_i \subset Y = (0,1)^d$ is the perforated reference domain corresponding to $X^\varepsilon_{\delta,i}$.

    (b) By using the Metropolis-Hastings algorithm draw the sample $\mathscr{S}_i$ from the posterior $\tilde{\pi}^{0,\delta}_i$ corresponding to the micro domain realization $X^\varepsilon_{\delta,i}$. In particular, given a new point $\boldsymbol{\theta} \in V$, to evaluate $\tilde{\pi}^{0,\delta}_i(\boldsymbol{\eta}|z)$, compute (6.41) and solve(6.42) with $\boldsymbol{\eta} = P(\boldsymbol{\theta})$.

    (c) $\mathscr{S} = \mathscr{S} \cup \mathscr{S}_i$.

4. Return $\mathscr{S}$.

6.4 Numerical experiments

In this section we present some numerical experiments to verify our theoretical findings and illustrate the efficiency of our proposed method. The domain D is the two dimensional unit square

$$D = \{x = (x_1, x_2) : 0 < x_1, x_2 < 1\}.$$

We define two different configurations of multiscale perforated domain. In particular, in the first test we consider a periodic perforated domain (no modeling error), and in the second

experiment a random perforated domain (presence of modeling error). The model problem reads

$$-\frac{\partial}{\partial x_j}\left(A_{ijlm}\frac{\partial u_l^\varepsilon}{\partial x_m}\right) = 0 \qquad \text{in } D^\varepsilon,$$

$$\mathbf{u}^\varepsilon = \mathbf{0} \qquad \text{on } \Gamma_1,$$

$$A_{ijlm}\frac{\partial u_l^\varepsilon}{\partial x_m}v_j = h_i \qquad \text{on } \Gamma_2, \qquad (6.43)$$

$$A_{ijlm}\frac{\partial u_l^\varepsilon}{\partial x_m}v_j = 0 \qquad \text{on } \partial D^\varepsilon \backslash \partial D,$$

for $i = 1, \dots, d$, where

$$\Gamma_1 = \left\{x = (x_1, x_2) \in \mathbb{R}^2 : x_2 = 0, 0 \le x_1 \le 1\right\},$$
$$\Gamma_2 = \partial D \backslash \Gamma_1,$$

and where the function $\mathbf{h}$ is defined as

$$\mathbf{h} = \begin{cases} (0, -1) & \text{if } 0 \le x_1 \le 1 \text{ and } x_2 = 1, \\ (0, 0) & \text{elsewhere}. \end{cases}$$

The exact value of the unknown is $\boldsymbol{\eta}^* = (E^*, \nu^*) = (7.3, 0.35)$. We define the observations according to (6.11), with $J = 30$ and $\{S_j\}_{j=1}^J$ equally spaced boundary portions on Γ_2, each of length 0.05, as depicted in Figure 6.1 and Figure 6.4. We compute synthetic observations by means of FEM, using a mesh size much smaller than ε. We then corrupt these observations with an additive source of zero-mean Gaussian noise $\zeta \sim \mathcal{N}(0, C_\zeta)$, where the covariance is defined as $C_\zeta = 10^{-8}I$ which leads to a mean error on the data of about 5% for the horizontal displacement, and of about 1% for the vertical displacement. The density of the prior is defined as in (6.8) with $\overline{k} = 0$, $\sigma_k = 1$, $\nu^- = 0$, $\nu^+ = 0.5$.

6.4.1 The periodic case

In this first numerical test we consider the case of multiscale periodic perforated domains. The holes are circles whose centers are distributed periodically with equal spacing ε, and whose radii are chosen so that $\pi r^2/\varepsilon^2 = 0.2$. The domain is depicted in Figure 6.1 for the choice $\varepsilon = 1/5$. Since the medium is periodic there is no modeling error due to the truncation of the micro domain and therefore there is no need to perform Monte Carlo iterations over the Metropolis-Hastings algorithm, i.e. no need for a probabilistic method. We approximate the homogenized model with a structured macro triangulation with mesh size $H = 1/64$ (4096 macro DOFs). The micro reference cell depicted in Figure 6.2 is discretized using a triangulation composed of 5209 micro DOFs. In the offline stage we compute the reduced space of micro functions by fixing 10^{-4} as tolerance for the control of the a posteriori error, which yields a reduced space consisting of 9 basis functions. The Bayesian inverse problem
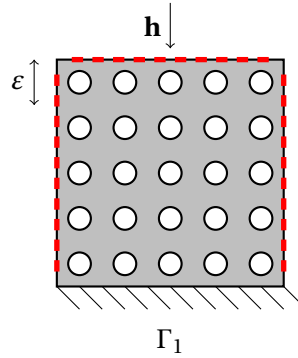
Figure 6.1: Scheme of the model problem from where the data are obtained (periodic case).
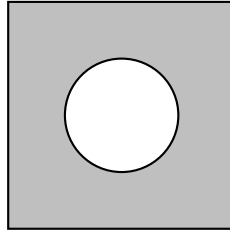

Figure 6.2: Micro reference cell for the periodic perforated domain.

is solved for different choices of ε, namely $\varepsilon = \{1/5, 1/10, 1/20, 1/50\}$, to verify the theoretical result given in Lemma 6.2.10. The effective posterior is approximated by drawing a sample of 10000 realizations using Metropolis-Hastings, where a Gaussian proposal with standard deviation equal to 0.001 is employed. Once samples from the effective posterior are collected we push them in U through $P : \boldsymbol{\theta} \mapsto \boldsymbol{\eta}$, in order to approximate the posterior for the unknown $\boldsymbol{\eta}$. Results are shown in Figure 6.3. It is possible to observe how, according to Lemma 6.2.10, the effective posterior moves towards the exact values of E and v as ε gets smaller.

Homogenization error. We recall that the observation can be rewritten as

$$z = \widetilde{G}^{0,\delta}(\boldsymbol{\theta}^*) + \zeta^\varepsilon(\boldsymbol{\theta}^*) + \zeta^\delta(\boldsymbol{\theta}^*) + \zeta,$$

where

$$\zeta \sim \mathcal{N}(0, C_\zeta), \quad \zeta^\varepsilon(\boldsymbol{\theta}^*) = G^\varepsilon(\boldsymbol{\theta}^*) - G^0(\boldsymbol{\theta}^*), \quad \zeta^\delta(\boldsymbol{\theta}^*) = G^0(\boldsymbol{\theta}^*) - \widetilde{G}^{0,\delta}(\boldsymbol{\theta}^*).$$

Let $\zeta^*(\boldsymbol{\theta}) = \zeta^\varepsilon(\boldsymbol{\theta}) + \zeta^\delta(\boldsymbol{\theta})$, $\boldsymbol{\theta} \in V$. At a fixed scale, if ε is relatively large, we can correct the posterior by including the distribution of the homogenization and the modeling error (see [28, 7]). Given the prior measure μ_{pr} and a sample size M, the numerical procedure is given by the following steps.

1. Draw from the prior measure a sample of realizations $S = \{\boldsymbol{\theta}_1, \dots, \boldsymbol{\theta}_M\}$.

2. For $1 \le i \le M$ compute

$$\zeta_i^* = G^\varepsilon(\boldsymbol{\theta}_i) - \widetilde{G}^{0,\delta}(\boldsymbol{\theta}_i).$$

3. $\overline{\zeta}^* = \dfrac{1}{M} \Sigma_{i=1}^M \zeta_i^*.$

4. $C_{\zeta^*} = \dfrac{1}{M} \Sigma_{i=1}^M (\overline{\zeta}^* - \zeta_i^*)(\overline{\zeta}^* - \zeta_i^*)^\top.$

Since the homogenized model G^0 is replaced by $\widetilde{G}^{0,\delta}$, this scheme actually approximates the mean and the covariance of an approximation error given by the combination of both the homogenization and the modeling error. However, in the periodic setting the modeling error vanishes, and thus the algorithm computes only the statistics corresponding to the homogenization error. We assume a Gaussian distribution for ζ^*, so that $\zeta^* \sim \mathcal{N}(\overline{\zeta}^*, C_{\zeta^*})$, for all $\boldsymbol{\theta} \in V$. Then, we may define the new likelihood as

$$\widetilde{\Phi}^{0,\delta}(\boldsymbol{\theta}, \overline{z}) = \frac{1}{2} \|\overline{z} - \widetilde{G}^{0,\delta}(\boldsymbol{\theta})\|_{C_\zeta + C_{\zeta^*}}^2 ,$$

where $\overline{z} = z - \overline{\zeta}^*$. Note that conclusions about existence and well-posedness of the posterior measure are still valid under this definition of the potential function. We remark that the cost of this offline stage depends on ε, and becomes prohibitive as $\varepsilon \to 0$. On the other hand, for small values of ε, the homogenization error vanishes (see Figure 6.3) and can be neglected. Let us finally remark that for relatively large values of ε, it would be possible to solve the inverse problem simply using FEM and reduced basis. Indeed, this approach would require an offline stage whose computational cost is comparable to the one needed to obtain the homogenization error distribution. However, this would be true only for this particular inverse problem, where the quantity of interest is represented by a few scalar parameters. In more complicated problems, where the quantity of interest is given for example by scalar fields, homogenization becomes necessary.

6.4.2 The random case

We consider now the case of random perforated domains, where we wish to observe how the size of the micro domains affects the solution of the inverse problem. In this experiment, holes are given by ellipses which are periodically distributed as the circles in the previous test, but whose axes and angle of rotation are random variables. Both axes are uniformly distributed in the interval $[r/2, 3r/2]$, where $\pi r^2/\varepsilon^2 = 0.2$, and the angle is uniformly distributed between 0 and π. An illustration of the resulting random set is depicted in Figure 6.4 for $\varepsilon = 1/5$. Let us start by fixing $\varepsilon = 1/50$. Due to the choice of ε, the homogenization error is negligible, and we study how different choices of δ, the size of the micro domain, can affect our predictions. The macro domain is discretized with the same degree of refinement as in the periodic case, i.e., with a structured triangulation of mesh size $H = 1/64$. We then consider three different values of δ, $\delta = \{\varepsilon, 3\varepsilon, 5\varepsilon\}$. For each value of δ we draw $R = 100$ realizations of the micro domain
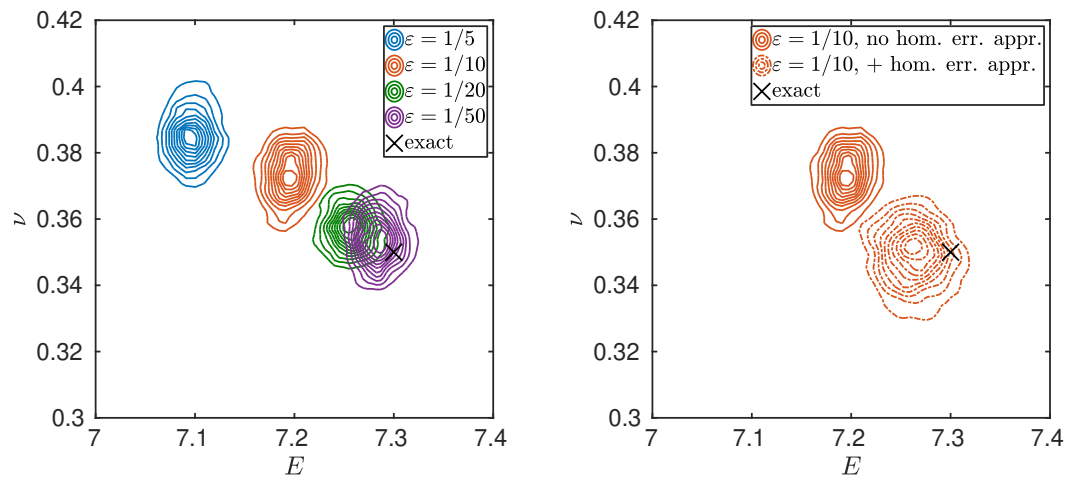
Figure 6.3: On the left, the convergence of the posterior distribution as $\varepsilon \to 0$ in the periodic setting is plotted. On the right, we compare the posterior distribution obtained for $\varepsilon = 1/10$, with and without the approximation of the homogenization error statistics. For approximating the homogenization error distribution the sample size M is set equal to 100.
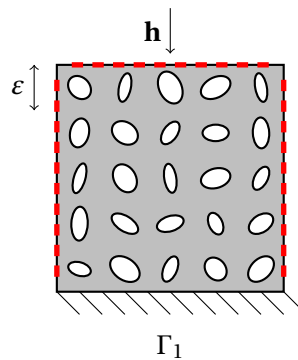

Figure 6.4: Scheme of the model problem from where the data are obtained (random case).
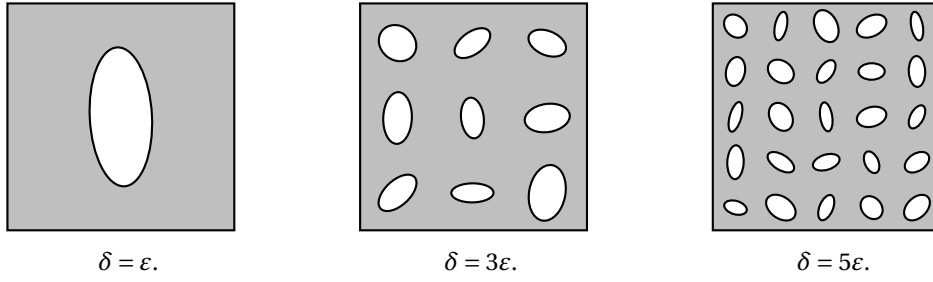
$$\delta = \varepsilon. \qquad\qquad \delta = 3\varepsilon. \qquad\qquad \delta = 5\varepsilon.$$

Figure 6.5: Three micro domains for different values of δ.

$\{X^\varepsilon_{\delta,i}\}^R_{i=1}$. Each micro domain is mapped to the corresponding reference micro domain Y^δ_i. In Figure 6.5 we show three typical realizations of the micro domain Y^δ_i, one for each value of δ. Each micro domain Y^δ_i is discretized with a triangulation composed of approximately $5000 \times (\delta/\varepsilon)^2$ micro DOFs. Each $X^\varepsilon_{\delta,i}$ yields a different posterior $\widetilde{\pi}^{0,\delta}_i$. We compare the results obtained using the probabilistic numerical method, which approximates the density $\overline{\pi}^{0,\delta}$ as

$$\overline{\pi}^{0,\delta}_{\mathrm{MC}}(\boldsymbol{\theta}|z) = \frac{1}{R}\sum_{i=1}^R \widetilde{\pi}^{0,\delta}_i(\boldsymbol{\theta}|z)\,,$$

with the results predicted by a single posterior $\widetilde{\pi}^{0,\delta}_i$ chosen at random. In the offline stage we assemble a reduced space of micro functions for each Y^δ_i, $\delta = \{\varepsilon, 3\varepsilon, 5\varepsilon\}$, $1 \le i \le R$, choosing the tolerance 10^{-4} for the stopping criterion. For each Y^δ_i we obtain a reduced space whose size is comprised between 9 and 12, independently of δ. In Figure 6.6 we show the results. We first sample from the random posterior $\widetilde{\pi}^{0,\delta}_i$ with $\delta = \{\varepsilon, 3\varepsilon, 5\varepsilon\}$ and $i = 1$. We draw 2000 samples employing the Metropolis-Hastings algorithm with a Gaussian proposal whose standard deviation is equal to 0.001. Hence, we push the samples into the space U to observe the random posterior of the unknown $\boldsymbol{\eta}$. From the left picture of Figure 6.6, we can observe that none of these densities manages to identify the exact values of the unknowns, as the modeling error is so large that the posterior distributions are overconfident on incorrect values. This is a common outcome when the mismatch between the model used to obtain the data and the forward model used to reproduce them is higher than the noise in the measurements. Moreover, also convergence with respect to δ is not clear. On the right picture of Figure 6.6 we show the results obtained using the probabilistic method. We sample from $\overline{\pi}^{0,\delta}_{\mathrm{MC}}$, by performing $R = 100$ independent parallel runs of the Metropolis-Hastings, each providing a sample of 2000 realizations. We note how the expected posterior densities better reflect the uncertainty due to the modeling error. Convergence with respect to δ is now clearly seen, since as δ increases the expected posterior concentrates on the exact values of the unknown parameters. Moreover, the posterior variances are larger than the ones obtained without using the probabilistic method, and provide a better quantification of the modeling error in the approximated forward model. Finally, using the same parameters, we repeat the same experiment for $\varepsilon = 1/10$. The results, depicted in Figure 6.7, are similar to the ones obtained for $\varepsilon = 1/50$ (compare with Figure 6.6). However, even though the posterior measure obtained with the probabilistic method reflects
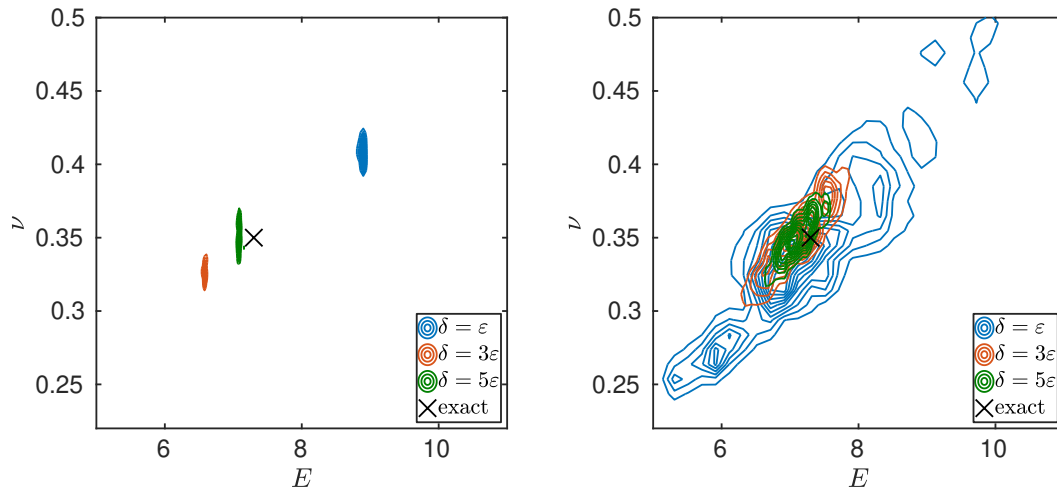
Figure 6.6: Comparison between the random effective posterior, which is obtained by performing a single run of the Metropolis-Hastings algorithm (left figure), and the expected effective posterior obtained with the probabilistic method (right figure). For this experiment $\varepsilon = 1/50$. The second distribution provides better quantification of the uncertainty due to the modeling error.

the uncertainty due to the modeling error, it seems to converge to a distribution which does not contain the exact value of the quantity of interest. This negative outcome may be due to the larger value of the homogenization error. The probabilistic method indeed accounts only for the modeling error which is intrinsic in the numerical approximation, but not for the homogenization error which is due to the discrepancy between the forward model and the data. Nevertheless, for the chosen value of ε, it may be preferable to approximate offline the approximation error distribution as described for the periodic setting, and perform only one run of the Metropolis-Hastings algorithm instead of using the probabilistic method. Results are shown in Figure 6.8. We see that the offline strategy is able to correct for both homogenization and modeling error. Let us emphasize that this type of correction becomes computationally expensive as $\varepsilon \to 0$.

Figure 6.7: Comparison between the random effective posterior, which is obtained by performing a single run of the Metropolis-Hastings algorithm (left figure), and the expected effective posterior obtained with the probabilistic method (right figure). For this experiment $\varepsilon = 1/10$. The second distribution provides better quantification of the uncertainty due to the modeling error.
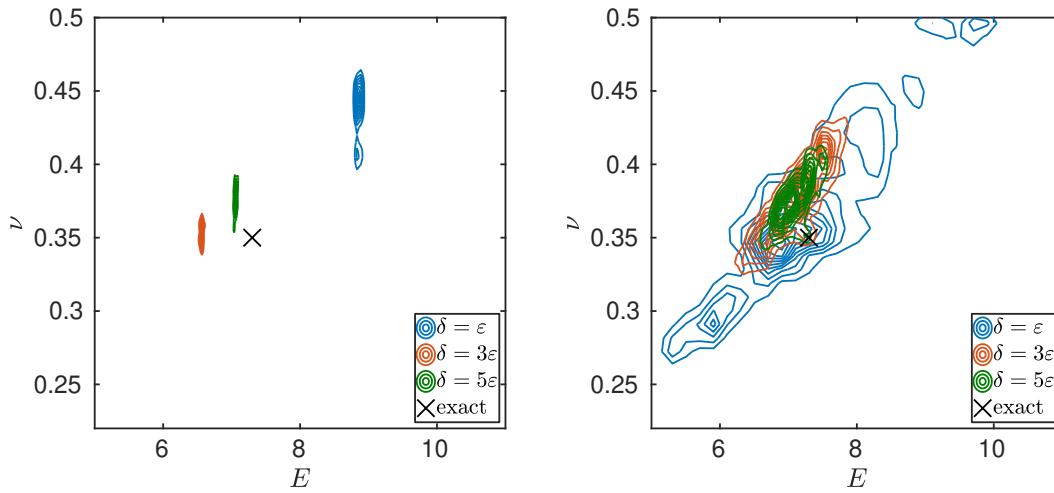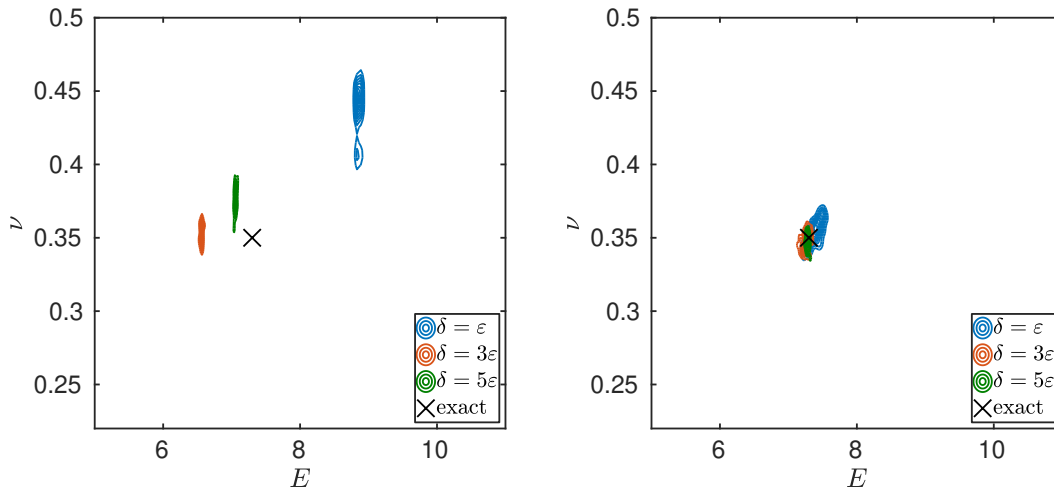

Figure 6.8: The random effective posterior, obtained by performing a single run of the Metropolis-Hastings algorithm, with (right figure) and without (left figure) the approximation of the homogenization error statistics. For this experiment $\varepsilon = 1/10$.

7 Conclusion and outlook

7.1   Conclusion

In this thesis we have considered inverse problems for multiscale elliptic partial differential equations. Since in this context classical forward solvers require mesh resolution at the finest scale, we suggested a coarse graining method based on homogenization which is independent of the small scale of the original model.

In the first part of the thesis, we considered elliptic scalar problems where our goal was to recover the full fine scale tensor under the assumption that its microscopic structure of the fine scale tensor is known to us but its macroscopic behavior is unknown. Practical examples include multi-phase media, whose constituents are known, but their respective volume fraction or macroscopic orientation are unknown. We considered the inverse conductivity problem as formulated by Calderón and we showed that if the fine scale problem is well-posed, then the effective inverse problem, with observed data consisting of the homogenized DtN map, is also well-posed. Considering finite measurements of the DtN map, we solved the problem by means of Tikhonov regularization and we established a convergence result of the solution of the effective inverse problem with multiscale observations by means of G-convergence. The numerical strategy we proposed is based on numerical homogenization and model order reduction. Finally, we illustrated with several numerical experiments the efficiency of our scheme.

In the second part of the thesis, we introduced a new numerical method based on Bayesian analysis and numerical homogenization. We proved the existence and well-posedness of the effective posterior measure obtained by homogenization of the forward operator. By means of G-convergence we showed that the fine scale posterior measure converges to the homogenized posterior measure. At fixed size of the microstructure, we discussed a procedure to account for the homogenization error. We also proposed an efficient algorithm to sample from the posterior measure combining numerical homogenization and reduced basis techniques. Several numerical examples illustrating the efficiency of the proposed method and confirming our theoretical findings were also given.

Finally, we considered multiscale inverse problems in linear elasticity. In this setting we assumed that the multiscale nature of the problem was determined by the domain's geometry rather than by the coefficients of the equation. Hence, we considered multiscale porous domains and we allowed for random perforations. We introduced a new forward solver for this problem based on numerical homogenization and reduced basis techniques, and we provided a priori error estimates. We solved the inverse problem following the Bayesian approach. We proved existence and well-posedness of the effective posterior measure, as well as its convergence in the fine scale limit by means of G-convergence. Moreover, we introduced a new probabilistic numerical method which allows to define a new posterior measure accounting for the modeling error due to the (random) approximation of the effective elastic tensor.

7.2 Outlook

The strategy we proposed for solving elliptic multiscale inverse problems, based on general theory of homogenization, can be seen as foundation for many possible extensions and interesting applications. We could consider for example to extend the method to parabolic problems, fluid dynamics or wave equations. Considering the wave equation would let us deal with applications in seismic analysis or medical imaging which are of crucial interest nowadays. We also mention possible extensions to problems defined on multiple scales, since not every application could fit in the two-scale framework. Last but not least a deeper investigation on the behavior of the model discrepancy between the fine scale model and homogenized model could be carried on, for a better understanding of how to account for approximation errors in the inversion process. It is likely that in certain cases, the assumption on the homogenization error being Gaussian could be proved to be true.

Bibliography

[1] A. ABDULLE, *On a priori error analysis of fully discrete heterogeneous multiscale FEM*, Multiscale Model. Simul., 4 (2005), pp. 447–459.

[2] ——, *Analysis of a heterogeneous multiscale FEM for problems in elasticity*, Math. Models Methods Appl. Sci., 16 (2006), pp. 615–635.

[3] ——, *The finite element heterogeneous multiscale method: a computational strategy for multiscale PDEs*, in Multiple scales problems in biomathematics, mechanics, physics and numerics, vol. 31 of GAKUTO Internat. Ser. Math. Sci. Appl., Gakkōtosho, Tokyo, 2009, pp. 133–181.

[4] A. ABDULLE AND Y. BAI, *Reduced basis finite element heterogeneous multiscale method for high-order discretizations of elliptic homogenization problems*, J. Comput. Phys., 231 (2012), pp. 7014–7036.

[5] A. ABDULLE AND O. BUDÁČ, *A reduced basis finite element heterogeneous multiscale method for Stokes flow in porous media*, Comp. Meth. Appl. Mech. Eng., 307 (2016), pp. 1–31.

[6] A. ABDULLE AND A. DI BLASIO, *Bayesian numerical homogenization and probabilistic methods for inverse problems in elastic porous media.* Preprint, 2018.

[7] ——, *A Bayesian numerical homogenization method for elliptic multiscale inverse problems.* Submitted to SIAM UQ, 2018.

[8] ——, *Homogenization and multiscale methods for linear elasticity in random perforated domains.* Preprint, 2018.

[9] ——, *Numerical homogenization and model order reduction for multiscale inverse problems.* Accepted in SIAM MMS, 2018.

[10] A. ABDULLE AND W. E, *Finite difference heterogeneous multi-scale method for homogenization problems*, J. Comput. Phys., 191 (2003), pp. 18–39.

[11] A. ABDULLE, W. E, B. ENGQUIST, AND E. VANDEN-EIJNDEN, *The heterogeneous multiscale method*, Acta Numer., 21 (2012), pp. 1–87.

Bibliography

[12] A. ABDULLE AND G. GAREGNANI, *Random time step probabilistic methods for uncertainty quantification in chaotic and geometric numerical integration.* arXiv preprint arXiv:1801.01340, 2018.

[13] A. ABDULLE AND M. J. GROTE, *Finite element heterogeneous multiscale method for the wave equation*, Multiscale Model. Simul., 9 (2011), pp. 766–792.

[14] A. ABDULLE AND C. SCHWAB, *Heterogeneous multiscale FEM for diffusion problems on rough surfaces*, Multiscale Model. Simul., 3 (2005), pp. 195–220.

[15] A. ABDULLE AND G. VILMART, *Analysis of the finite element heterogeneous multiscale method for quasilinear elliptic homogenization problems*, Math. Comp., 83 (2014), pp. 513–536.

[16] G. ALESSANDRINI AND R. GABURRO, *Determining conductivity with special anisotropy by boundary measurements*, SIAM J. Math. Anal., 33 (2001), pp. 153–171.

[17] A. ALEXANDERIAN, M. RATHINAM, AND R. ROSTAMIAN, *Homogenization, symmetry, and periodization in diffusive random media*, Acta Math. Sci. Ser. B (Engl. Ed.), 32 (2012), pp. 129–154.

[18] G. ALLAIRE, *Homogenization and two-scale convergence*, SIAM J. Math. Anal., 23 (1992), pp. 1482–1518.

[19] S. R. ARRIDGE, J. P. KAIPIO, V. KOLEHMAINEN, M. SCHWEIGER, E. SOMERSALO, T. TARVAINEN, AND M. VAUHKONEN, *Approximation errors and model reduction with an application in optical diffusion tomography*, Inverse Problems, 22 (2006), pp. 175–195.

[20] K. ASTALA AND L. PÄIVÄRINTA, *Calderón's inverse conductivity problem in the plane*, Ann. of Math. (2), 163 (2006), pp. 265–299.

[21] A. BENSOUSSAN, J.-L. LIONS, AND G. PAPANICOLAOU, *Asymptotic analysis for periodic structures*, North-Holland Publishing Co., Amsterdam, 1978.

[22] P. BINEV, A. COHEN, W. DAHMEN, R. DEVORE, G. PETROVA, AND P. WOJTASZCZYK, *Convergence rates for greedy algorithms in reduced basis methods*, SIAM J. Math. Anal., 43 (2011), pp. 1457–1472.

[23] V. I. BOGACHEV, *Measure theory. Vol. I, II*, Springer-Verlag, Berlin, 2007.

[24] A. BOURGEAT AND A. PIATNITSKI, *Approximations of effective coefficients in stochastic homogenization*, Ann. Inst. Henri Poincaré Probab. Stat., 40 (2004), pp. 153–165.

[25] R. H. BYRD, M. E. HRIBAR, AND J. NOCEDAL, *An interior point algorithm for large-scale nonlinear programming*, SIAM J. Optim., 9 (1999), pp. 877–900. Dedicated to John E. Dennis, Jr., on his 60th birthday.

[26] A.-P. CALDERÓN, *On an inverse boundary value problem*, in Seminar on Numerical Analysis and its Applications to Continuum Physics (Rio de Janeiro, 1980), Soc. Brasil. Mat., Rio de Janeiro, 1980, pp. 65–73.

[27] D. CALVETTI, M. DUNLOP, E. SOMERSALO, AND A. STUART, *Iterative updating of model error for Bayesian inversion*, Inverse Problems, 34 (2018), pp. 025008, 38.

[28] D. CALVETTI, O. ERNST, AND E. SOMERSALO, *Dynamic updating of numerical model discrepancy using sequential sampling*, Inverse Problems, 30 (2014), pp. 114019, 19.

[29] G. CARDONE, C. D'APICE, AND U. DE MAIO, *Homogenization in perforated domains with mixed conditions*, NoDEA Nonlinear Differential Equations Appl., 9 (2002), pp. 325–346.

[30] G. F. CAREY, S.-S. CHOW, AND M. K. SEAGER, *Approximate boundary-flux calculations*, Comput. Methods Appl. Mech. Engrg., 50 (1985), pp. 107–120.

[31] P. G. CIARLET, *The finite element method for elliptic problems*, vol. 4 of Studies in Mathematics and its Applications, North-Holland, 1978.

[32] D. CIORANESCU, A. DAMLAMIAN, AND G. GRISO, *Periodic unfolding and homogenization*, C. R. Math. Acad. Sci. Paris, 335 (2002), pp. 99–104.

[33] D. CIORANESCU AND P. DONATO, *An introduction to homogenization*, vol. 17 of Oxford Lecture Series in Mathematics and its Applications, Oxford University Press, New York, 1999.

[34] D. CIORANESCU AND F. MURAT, *Un terme étrange venu d'ailleurs. II*, in Nonlinear partial differential equations and their applications. Collège de France Seminar, Vol. III (Paris, 1980/1981), vol. 70 of Res. Notes in Math., Pitman, Boston, Mass.-London, 1982, pp. 154–178, 425–426.

[35] D. CIORANESCU AND J. S. J. PAULIN, *Homogenization in open sets with holes*, J. Math. Anal. Appl., 71 (1979), pp. 590–607.

[36] D. COLTON, H. ENGL, A. K. LOUIS, J. MCLAUGHIN, AND W. RUNDELL, *Surveys on Solution Methods for Inverse Problems*, Springer-Verlag, Wien, 2000.

[37] C. CONCA AND P. DONATO, *Nonhomogeneous Neumann problems in domains with small holes*, RAIRO Modél. Math. Anal. Numér., 22 (1988), pp. 561–607.

[38] P. R. CONRAD, M. GIROLAMI, S. SÄRKKÄ, A. STUART, AND K. ZYGALAKIS, *Statistical analysis of differential equations: introducing probability measures on numerical solutions*, Stat. Comput., 27 (2017), pp. 1065–1082.

[39] S. L. COTTER, M. DASHTI, AND A. M. STUART, *Approximation of Bayesian inverse problems for PDEs*, SIAM J. Numer. Anal., 48 (2010), pp. 322–345.

Bibliography

[40] M. DASHTI AND A. M. STUART, *Uncertainty quantification and weak approximation of an elliptic inverse problem*, SIAM J. Numer. Anal., 49 (2011), pp. 2524–2542.

[41] ——, *The Bayesian Approach to Inverse Problems*, in Handbook of Uncertainty Quantification, Springer, 2016, pp. 1–118.

[42] E. DE GIORGI AND S. SPAGNOLO, *Sulla convergenza degli integrali dell'energia per operatori ellittici del secondo ordine*, Boll. Un. Mat. Ital., 4 (1973), pp. 391–411.

[43] M. DESBRUN, R. D. DONALDSON, AND H. OWHADI, *Modeling across scales: discrete geometric structures in homogenization and inverse homogenization*, in Multiscale analysis and nonlinear dynamics, Rev. Nonlinear Dyn. Complex., Wiley-VCH, Weinheim, 2013, pp. 21–64.

[44] T. J. DODWELL, C. KETELSEN, R. SCHEICHL, AND A. L. TECKENTRUP, *A hierarchical multi-level Markov chain Monte Carlo algorithm with applications to uncertainty quantification in subsurface flow*, SIAM/ASA J. Uncertain. Quantif., 3 (2015), pp. 1075–1108.

[45] N. DUNFORD AND J. T. SCHWARTZ, *Linear operators. Part I*, Wiley Classics Library, John Wiley & Sons, Inc., New York, 1988. General theory, With the assistance of William G. Bade and Robert G. Bartle, Reprint of the 1958 original, A Wiley-Interscience Publication.

[46] M. M. DUNLOP AND A. M. STUART, *The Bayesian formulation of EIT: analysis and algorithms*, Inverse Probl. Imaging, 10 (2016), pp. 1007–1036.

[47] W. E AND B. ENGQUIST, *The heterogeneous multiscale methods*, Commun. Math. Sci., 1 (2003), pp. 87–132.

[48] W. E, P. MING, AND P. ZHANG, *Analysis of the heterogeneous multiscale method for elliptic homogenization problems*, J. Amer. Math. Soc., 18 (2005), pp. 121–156.

[49] B. EIDEL AND A. FISCHER, *The heterogeneous multiscale finite element method for the homogenization of linear elastic solids and a comparison with the* FE^2 *method*, Comput. Methods Appl. Mech. Engrg., 329 (2018), pp. 332–368.

[50] H. W. ENGL, M. HANKE, AND A. NEUBAUER, *Regularization of inverse problems*, vol. 375 of Mathematics and its Applications, Kluwer Academic Publishers Group, Dordrecht, 1996.

[51] L. C. EVANS, *Partial differential equations*, vol. 19 of Graduate Studies in Mathematics, American Mathematical Society, Providence, RI, second ed., 2010.

[52] L. C. EVANS AND R. F. GARIEPY, *Measure theory and fine properties of functions*, Studies in Advanced Mathematics, CRC Press, Boca Raton, FL, 1992.

[53] B. G. FITZPATRICK, *Bayesian analysis in inverse problems*, Inverse Problems, 7 (1991), pp. 675–702.

[54] C. FREDERICK AND B. ENGQUIST, *Numerical methods for multiscale inverse problems*, Commun. Math. Sci., 15 (2017), pp. 305–328.

[55] T. GALLOUËT AND A. MONIER, *On the regularity of solutions to elliptic equations*, Rend. Mat. Appl., 19 (2000), pp. 471–488.

[56] M. GEHRE, B. JIN, AND X. LU, *An analysis of finite element approximation in electrical impedance tomography*, Inverse Problems, 30 (2014), pp. 045013, 24.

[57] M. A. GREPL, Y. MADAY, N. C. NGUYEN, AND A. T. PATERA, *Efficient reduced-basis treatment of nonaffine and nonlinear partial differential equations*, ESAIM: Mathematical Modelling and Numerical Analysis-Modélisation Mathématique et Analyse Numérique, 41 (2007), pp. 575–605.

[58] P. C. HANSEN, *Analysis of discrete ill-posed problems by means of the L-curve*, SIAM Rev., 34 (1992), pp. 561–580.

[59] P. C. HANSEN AND D. P. O'LEARY, *The use of the L-curve in the regularization of discrete ill-posed problems*, SIAM J. Sci. Comput., 14 (1993), pp. 1487–1503.

[60] P. HENNIG, M. A. OSBORNE, AND M. GIROLAMI, *Probabilistic numerics and uncertainty in computations*, Proc. A., 471 (2015), pp. 20150142, 17.

[61] P. HENNING AND M. OHLBERGER, *The heterogeneous multiscale finite element method for elliptic homogenization problems in perforated domains*, Numer. Math., 113 (2009), pp. 601–629.

[62] M. A. IGLESIAS, Y. LU, AND A. STUART, *A Bayesian level set method for geometric inverse problems*, Interfaces Free Bound., 18 (2016), pp. 181–217.

[63] V. V. JIKOV, S. M. KOZLOV, AND O. A. OLEINIK, *Homogenization of differential operators and integral functionals*, Springer-Verlag, Berlin, Heidelberg, 1994.

[64] J. KAIPIO AND E. SOMERSALO, *Statistical and computational inverse problems*, vol. 160 of Applied Mathematical Sciences, Springer-Verlag, New York, 2005.

[65] A. C. KAK AND M. SLANEY, *Principles of computerized tomographic imaging*, vol. 33 of Classics in Applied Mathematics, Society for Industrial and Applied Mathematics (SIAM), Philadelphia, PA, 2001. Reprint of the 1988 original.

[66] R. KOHN AND M. VOGELIUS, *Determining conductivity by boundary measurements*, Comm. Pure Appl. Math., 37 (1984), pp. 289–298.

[67] S. M. KOZLOV, *The averaging of random operators*, Mat. Sb. (N.S.), 109(151) (1979), pp. 188–202, 327.

[68] H. C. LIE, T. J. SULLIVAN, AND A. L. TECKENTRUP, *Random Forward Models and Log-Likelihoods in Bayesian Inverse Problems*, SIAM/ASA J. Uncertain. Quantif., 6 (2018), pp. 1600–1629.

[69] N. G. MEYERS, *An L^p-estimate for the gradient of solutions of second order elliptic divergence equations*, Ann. Scuola Norm. Sup. Pisa, 17 (1963), pp. 189–206.

[70] F. MURAT AND L. TARTAR, *H-convergence*, in Topics in the mathematical modelling of composite materials, vol. 31 of Progr. Nonlinear Differential Equations Appl., Birkhäuser Boston, Boston, MA, 1997, pp. 21–43.

[71] A. I. NACHMAN, *Global uniqueness for a two-dimensional inverse boundary value problem*, Ann. of Math. (2), 143 (1996), pp. 71–96.

[72] F. NOBILE AND F. TESEI, *A multi level Monte Carlo method with control variate for elliptic PDEs with log-normal coefficients*, Stoch. Partial Differ. Equ. Anal. Comput., 3 (2015), pp. 398–444.

[73] J. NOLEN, G. A. PAVLIOTIS, AND A. M. STUART, *Multiscale modeling and inverse problems*, in Numerical analysis of multiscale problems, vol. 83 of Lect. Notes Comput. Sci. Eng., Springer, Heidelberg, 2012, pp. 1–34.

[74] M. OHLBERGER, *A posteriori error estimates for the heterogeneous multiscale finite element method for elliptic homogenization problems*, Multiscale Model. Simul., 4 (2005), pp. 88–114.

[75] O. A. OLEINIK, A. SHAMAEV, AND G. YOSIFIAN, *Mathematical Problems in Elasticity and homogenization*, North-Holland, Amsterdam, 1992.

[76] G. C. PAPANICOLAOU AND S. R. S. VARADHAN, *Boundary value problems with rapidly oscillating random coefficients*, Random fields, 1 (1979), pp. 835–873.

[77] G. A. PAVLIOTIS AND A. M. STUART, *Multiscale methods*, vol. 53 of Texts in Applied Mathematics, Springer, New York, 2008. Averaging and homogenization.

[78] A. I. PEHLIVANOV, R. D. LAZAROV, G. F. CAREY, AND S.-S. CHOW, *Superconvergence analysis of approximate boundary-flux calculations*, Numer. Math., 63 (1992), pp. 483–501.

[79] A. QUARTERONI, G. ROZZA, AND A. MANZONI, *Certified reduced basis approximation for parametrized partial differential equations and applications*, Journal of Mathematics in Industry, 1 (2011), pp. 1–49.

[80] G. ROZZA, D. B. P. HUYNH, AND A. T. PATERA, *Reduced basis approximation and a posteriori error estimation for affinely parametrized elliptic coercive partial differential equations*, Arch. Comput. Methods. Eng., 15 (2008), pp. 229–275.

[81] E. SÁNCHEZ-PALENCIA, *Nonhomogeneous media and vibration theory*, vol. 127 of Lecture Notes in Phys., Springer-Verlag, Berlin-New York, 1980.

[82] O. SCHERZER, *The use of Morozov's discrepancy principle for Tikhonov regularization for solving nonlinear ill-posed problems*, Computing, 51 (1993), pp. 45–60.

[83] S. SPAGNOLO, *Sulla convergenza di soluzioni di equazioni paraboliche ed ellittiche*, Ann. Sc. Norm. Super. Pisa Cl. Sci., 22 (1968), pp. 571–597.

[84] A. M. STUART, *Inverse problems: a Bayesian perspective*, Acta Numer., 19 (2010), pp. 451–559.

[85] J. SYLVESTER AND G. UHLMANN, *A global uniqueness theorem for an inverse boundary value problem*, Ann. of Math. (2), 125 (1987), pp. 153–169.

[86] A. TARANTOLA, *Inverse problem theory and methods for model parameter estimation*, Society for Industrial and Applied Mathematics (SIAM), Philadelphia, PA, 2005.

[87] L. TARTAR, *The general theory of homogenization*, vol. 7 of Lecture Notes of the Unione Matematica Italiana, Springer-Verlag, Berlin; UMI, Bologna, 2009. A personalized introduction.

[88] A. N. TIKHONOV, *On the solution of ill-posed problems and the method of regularization*, Dokl. Akad. Nauk SSSR, 151 (1963), pp. 501–504.

[89] V. V. ZHIKOV, *Averaging in punctured random domains of general type*, Mat. Zametki, 53 (1993), pp. 41–58.

Curriculum Vitae

Personal data

Name	Andrea Di Blasio
Date of birth	August 9, 1990
Nationality	Italy

Education

2014 - 2018   **PhD in Mathematics**
École Polytechnique Fédérale de Lausanne, Switzerland.
Thesis advisor: Prof. A. Abdulle.

2012 - 2014   **Master of Science in Computational Science and Engineering**
École Polytechnique Fédérale de Lausanne, Switzerland.
Thesis advisor: Prof. A. Quarteroni.

2009 - 2012   **Bachelor of Science in Mathematical Engineering**
Politecnico di Milano, Italy.
Thesis advisor: Prof. M. Grasselli.

PhD publications

[1] A. ABDULLE AND A. DI BLASIO, *Numerical homogenization and model order reduction for multiscale inverse problems.* Accepted in SIAM MMS, 2018.

[2] ——, *A Bayesian numerical homogenization method for elliptic multiscale inverse problems.* Submitted to SIAM UQ, 2018.

[3] ——, *Homogenization and multiscale methods for linear elasticity in random perforated domains.* Preprint, 2018.

[4] ——, *Bayesian numerical homogenization and probabilistic methods for inverse problems in elastic porous media.* Preprint, 2018.

Presentations

- THE SWISS NUMERICS COLLOQUIUM (Fribourg, Switzerland, 22 April 2016);
  Poster: *A reduced basis method for multiscale inverse problems.*

- MATHICSE Retreat (Leysin, Switzerland, 27–29 June 2016);
  Talk: *A reduced basis method for multiscale inverse problems.*

- The Swiss Numerics Colloquium (Basel, Switzerland, 28 April 2017);
  Talk: *Solving elliptic multiscale inverse problems using Bayesian techniques and numerical homogenization.*

- MATHICSE Retreat (Leysin, Switzerland, 14–16 June 2017);
  Talk: *Using numerical homogenization for solving elliptic multiscale inverse problems.*

- Equadiff 2017 (Bratislava, Slovakia, 24–28 July 2017);
  Talk: *Numerical homogenization and Bayesian techniques for multiscale inverse problems.*

- COMPLAS 2017 (Barcelona, Spain, 5–7 September 2017);
  Talk: *Model order reduction and Bayesian techniques for multiscale inverse problems.*

- ECCM - ECFD 2018 (Glasgow, UK, 11–15 June 2018);
  Talk: *Numerical homogenization and model order reduction for solving linear elasticity problems in perforated domains.*

- MATHICSE Retreat (Sainte-Croix, Switzerland, 19–21 June 2018);
  Talk: *Numerical methods for solving Bayesian multiscale inverse problems.*

- EUROMECH Colloquium 597 (Bad-Herrenalb, Germany, 28–31 August 2018);
  Talk: *Model order reduction and numerical homogenization for solving Bayesian multiscale inverse problems.*